

UNIVERSITY OF
BIRMINGHAM

Characterization and Reduction of Leakiness in Melamine Formaldehyde Microcapsules

Yue Long

A thesis submitted to The University of Birmingham for the degree of DOCTOR OF PHILOSOPHY

Submitted to School of Chemistry
The University of Birmingham

UNIVERSITY OF
BIRMINGHAM

University of Birmingham Research Archive

e-theses repository

This unpublished thesis/dissertation is copyright of the author and/or third parties. The intellectual property rights of the author or third parties in respect of this work are as defined by The Copyright Designs and Patents Act 1988 or as modified by any successor legislation.

Any use made of information contained in this thesis/dissertation must be in accordance with that legislation and must be properly acknowledged. Further distribution or reproduction in any format is prohibited without the permission of the copyright holder.

Abstract

This thesis is concerned with tackling three major challenges of melamine formaldehyde (MF) microcapsules for delivering of core materials: reducing the formaldehyde content in the formulation, modulate the mechanical properties and reducing the leakage of the core material through the microcapsules.

Thus, to reduce the formaldehyde content in the microcapsules, a low formaldehyde to melamine (F/M) molar ratio (0.20-0.49) compared to the conventional literature formulations (2.30-5.50) was used to produce the MF microcapsules in this study. It was found that there is a relatively small window of F/M molar ratio between 0.20 and 0.49 in which the wall thickness and nominal rupture stress of the microcapsules can be modulated significantly. Above 0.49 increases in F/M molar ratios only increase these properties marginally.

Furthermore, to reduce the leakage of the microcapsules, organic/inorganic double shell composite microcapsules with MF/copolymer as the inner shell, and ripened $CaCO_3$ nanoparticles as the outer shell were produced. A ~20 fold reduction in leakage was observed between the double shell composite microcapsules and the MF microcapsules by the end of 24 hours, and it was also found that the mechanical properties of these double shell composite microcapsules are dominated by the $CaCO_3$ nanoparticles outer wall.

Finally, calcium shellac matrix containing MF microcapsules and unripened $CaCO_3$ nanoparticulate microcapsules (complex capsules) were also produced to reduce the leakage. A ~37 fold leakage reduction between calcium shellac matrix containing MF microcapsules and MF microcapsules alone by the end of 20 days was observed, and a ~14 fold reduction was found between calcium shellac containing unripened $CaCO_3$ nanoparticulate microcapsules and the unripened $CaCO_3$ nanoparticulate microcapsules alone.

Acknowledgements

I would like to express my deepest gratitude and appreciation to all supervisors: Prof. Jon Preece, Prof. Zhibing Zhang, and Prof. David York for their supervision, invaluable guidance and support thought the PhD, without which this work would not have been possible.

I would also like to thank Graham Burns for his generous help with GC; Ming Chu, Paul Stanley and Theresa Morris for their technical support on SEM and TEM; to members of NMR and Mass spectrometry departments for their technical support.

I would like to convey my deepest thanks to the past and present members of Prof. Preece's and Zhang's research group for their help, encouragement and companionship throughout the PhD.

I would like to thank School of Chemistry and School of Chemical Engineering, University of Birmingham for funding, administrative support and laboratory facilities, as well as Overseas Research Scholarship (ORS) and Proctor and Gamble for the financial support.

Finally, I would like to dedicate this opportunity to express my immense love for my parents for their constant support, love and understanding in every aspect of my life.

CONTENTS

Chapter 1. Introduction: Microencapsulation and Perfumes 1

Abstract 1

1.1 Perfume in Consumer Products 1

1.1.1 The Role of Perfume in Consumer Products 1

1.1.2 Behaviour of Perfume Oils in Consumer Products 2

1.1.3 Challenges for Perfumes in Consumer Products 2

***1.1.3.1 Evaporation* 3**

***1.1.3.2 Water Insolubility* 4**

***1.1.3.3 pH Effect-hydrolysis* 4**

***1.1.3.4 Oxidation* 4**

1.1.4 Perfume Oil in Microcapsules 4

1.2 Microencapsulation 6

1.3 Encapsulation Methods 7

1.3.1 *In Situ* Polymerization 8

***1.3.1.1 Melamine Formaldehyde (MF) Microcapsules* 10**

1.3.1.1.1 Chemical Structures of MF Microcapsules Wall 10

1.3.1.1.2 Effect of Formaldehyde to Melamine Molar Ratio 13

1.3.1.1.3 Surface Morphology 14

1.3.1.1.4 Size 15

1.3.1.1.5 Wall Thickness 16

1.3.2 Interfacial Polymerization 16

1.3.3 Layer-by-layer 18

1.3.4 Recent Developments 20

***1.3.4.1 Double Shell Microcapsules* 20**

***1.3.4.2 Microcapsules with Nanoparticles* 22**

1.4 Applications of Microencapsulation 26

1.4.1 Microcapsules in Cosmetic and Household Products 26

1.4.2 Microcapsules in Food 27

1.4.3 Cell Microencapsulation 28

1.4.4 Microencapsulation of Phase Change Materials (PCM) 28

1.4.5 Microencapsulation of Self-healing Materials **29**

1.5 Release Mechanism of Microcapsules **30**

1.5.1 Rupture **31**

1.5.2 Diffusion **32**

1.5.3 Dissolution **33**

1.6 Characterization of Microcapsules **34**

1.6.1 Mechanical Properties **34**

1.6.1.1 Mechanical Properties of Ensembles of Microcapsules ***34***

1.6.1.1.1 Compressing between Two Plates *35*

1.6.1.1.2 Osmotic Pressure *35*

1.6.1.2 Mechanical Properties of Single Microcapsules ***36***

1.6.1.2.1 Micropipette Aspiration *36*

1.6.1.2.2 Atomic force Microscope (AFM) *36*

1.6.1.2.3 Texture Analyser *36*

1.6.1.2.4 Micromanipulation *36*

1.6.2 Particle Size and Size Distribution **38**

1.6.3 Morphology **38**

1.6.4 Wall Structure and Thickness **39**

1.6.5 Release Rate **39**

1.7 Conclusions **40**

1.8 Objectives **42**

1.8.1 The Challenge **42**

1.8.2 Proposed Solution **42**

1.9 Overview of Thesis **44**

Chapter 2. Introduction of the Experimental Techniques **47**

Abstract **47**

2.1 Gas Chromatography (GC) **47**

2.1.1 Carrier Gas **48**

2.1.2 Columns **48**

2.1.3 Sample Injection Port **49**

2.1.4 Flame Ionization Detector (FID) **50**

2.1.5 Output **50**

2.2 Micromanipulation **51**

2.2.1 Compressing A Single Microcapsule **51**

2.2.2 Preparation of Transducer Probes **53**

2.2.3 Output **53**

2.3 Static Light Scattering (SLS) **54**

2.3.1 Output **56**

2.4 Scanning Electron Microscopy (SEM) **57**

2.5 Environmental Scanning Electron Microscope (ESEM) **59**

2.5.1 Output **60**

2.6 Transmission Electron Microscopy (TEM) **61**

2.6.1 Output **63**

2.7 Focused Ion Beam (FIB) **63**

2.7.1 Output **64**

Chapter 3. Microcapsules with Low Content of Formaldehyde: Preparation and Characterization **66**

Abstract **66**

3.1 Introduction **67**

3.2 Experimental **68**

3.2.1 Materials **68**

3.2.2 Preparation of Microcapsules **69**

3.2.2.1 Microcapsule A ***69***

3.2.2.2 Microcapsule B, C, D and E ***69***

3.2.3 Gas Chromatography **70**

3.2.3.1 Calibration ***70***

3.2.4 Encapsulation Efficiency Measurement **72**

3.2.5 Leakage Measurement **74**

3.2.6 Size Analysis **74**

3.2.7 Transmission Electron Microscopy (TEM) **74**

3.2.7.1 Sampling by Ultra-microtome ***75***

3.2.8 Environmental Scanning Electron Microscopy (ESEM) **76**

3.2.9 Micromanipulation **76**

3.3 Results and Discussion **77**

3.3.1 Synthesis **77**

3.3.2 Encapsulation Efficiency **77**

3.3.3 Morphology **78**

3.3.4 Particle Diameter and Distribution **80**

3.3.5 Wall Thickness **81**

3.3.6 Mechanical Properties **82**

3.3.7 Oil leakage and kinetics **89**

3.4 Conclusions **92**

Chapter 4. A New Dual Strategy for Controlling the Leakage of Microcapsules: Organic/inorganic Composite Microcapsules from MF/$CaCO_3$ nanoparticles **93**

Abstract **93**

4.1 Introduction **94**

4.2 Experimental **95**

4.2.1 Materials **95**

4.2.2 Preparation of Microcapsules **95**

4.2.2.1 Preparation of MF Microcapsules (Microcapsule A, Scheme 1, Step 1, 2, 3) ***95***

4.2.2.2 Preparation of Ripened Double Shell Composite Microcapsules (Microcapsule F, Scheme 1, Step 4) ***98***

4.2.2.3 Preparation of Unripened Double Shell Composite Microcapsules (Microcapsule G, Scheme 1, Step 5) ***98***

4.2.2.4 Preparation of Ripened Single Shell Nanoparticulate $CaCO_3$ Microcapsules (Microcapsule H, Scheme 1, Step 6 and 7) ***98***

4.2.2.5 Preparation of Ripened Double Shell Composite Microcapsules (Microcapsule I, Scheme 1, Step 8) ***99***

4.2.3 Gas Chromatography (GC) **99**

4.2.4 Encapsulation Efficiency Measurement **99**

4.2.5 Leakage Measurement 100

4.2.6 Size Analysis 100

4.2.7 Transmission Electron Microscopy (TEM) 101

4.2.8 Environmental Scanning Electron Microscopy (ESEM) 101

4.2.9 Calculation of the Degree of the Wall Formation Formed by the Unripened or Ripened Nanoparticulate $CaCO_3$ Nanoparticles from TEM Images 101

4.2.10 Micromanipulation 101

4.2.11 Solubility Test for $CaCO_3$ Nanoparticles 102

4.3 Results and Discussion 102

4.3.1 Synthesis 102

4.3.2 Encapsulation Efficiency 103

4.3.3 Particle Diameter and Distribution 104

4.3.4 Morphology 107

4.3.5 Wall Structure and Thickness 108

4.3.6 Degree of Wall Formation of the Unripened or Ripened $CaCO_3$ Nanoparticles 113

4.3.7 Mechanical Properties 114

4.3.8 Oil leakage and kinetics 119

4.4 Conclusions 124

Chapter 5. Engineering the Mechanical and Physical Properties of Organic/inorganic Composite Microcapsules 126

Abstract 126

5.1 Introduction 127

5.2 Experimental 129

5.2.1 Materials 129

5.2.2 Preparation of Ripened Double Shell Composite Microcapsules (Microcapsules $I_{6.0}$, J, K, L and M) 130

5.2.3 Gas Chromatography (GC) 131

5.2.4 Encapsulation Efficiency Measurement 131

5.2.5 Leakage Measurement 132

5.2.6 Size Analysis 132

5.2.7 Transmission Electron Microscopy (TEM) 133

5.2.8 Environmental Scanning Electron Microscopy (ESEM) 133

5.2.9 Calculation of the Degree of the Wall Formation Formed by the Ripened Nanoparticulate $CaCO_3$ Nanoparticles from TEM Images 133

5.2.10 Micromanipulation 133

5.3 Results and Discussion 134

5.3.1 Synthesis 134

5.3.2 Encapsulation Efficiency 135

5.3.3 Wall Thickness and Degree of Wall Completeness 135

5.3.4 Average Particle Diameter and Distribution 139

5.3.5 Mechanical Properties 140

5.3.6 Oil leakage 143

5.4 Conclusions 144

Chapter 6. Preparation and Characterization of Calcium Shellac Matrix with Microcapsules Embedded (Complex Microcapsules) 146

Abstract 146

6.1 Introduction 146

6.2 Experimental 148

6.2.1 Material 148

6.2.2 Formation of Microcapsules 148

6.2.2.1 Formation of MF Microcapsules (A) *148*

6.2.2.2 Formation of Unripened $CaCO_3$ Nanoparticles Stabilised Microcapsules (F) *149*

6.2.2.3 Formation of Calcium Shellac MatrixContaining MF Microcapsules (A) or Unripened $CaCO_3$ Nanoparticles Microcapsules stabilised (F) (Complex Capsules) *149*

6.2.2.4 Formation of Calcium Shellac Microparticles *150*

6.2.3 Freeze Drying 151

6.2.4 Encapsulation Efficiency of Primary Microcapsules 151

6.2.5 Environmental Scanning Electron Microscopy (ESEM) 152
6.2.6 Focused Ion Beam (FIB) and SEM 152
6.2.7 Optical Microscope 152
6.2.8 Size Analysis (SLS) 152
6.2.9 Micromanipulation 153
6.2.10 Leakage Measurement 153
6.2.11 Gas Chromatography (GC) 154
6.3 Results and Discussion 154
6.3.1 Synthesis 154
6.3.2 Encapsulation Efficiency of Primary Microcapsules 155
6.3.3 Microcapsules Structure 156
6.3.4 Average Particle Size and Distribution 158
6.3.5 Surface Morphology and Storage Stability 160
6.3.6 Inner Structure 162
6.3.7 Mechanical Strength 163
6.3.8 Leakage 166
6.4 Conclusions 169

Chapter 7. Overall Conclusions and Future Work 171
7.1 Overall Conclusions 171
7.1.1 Microcapsules with low content of formaldehyde (Chapter 3, microcapsules A-E) 174
7.1.2 Organic/inorganic composite double shell microcapsules (Chapter 4 and 5, microcapsules F, G, H, $I_{4.5}$, $I_{5.5}$, $I_{6.0}$, $I_{7.0}$, J, K, L and M) 174
7.1.3 Calcium shellac matrix with microcapsules embedded (complex microcapsules) (Chapter 6, calcium shellac microparticles, calcium shellac matrix containing A, and calcium shellac matrix containing F) 176
7.1.4 Overall comparison of the mechanical properties of the microcapsules 177
7.1.5 Overall comparison of the leakage of the microcapsules 178
7.1.6 Overall discussion of the relation between leakage and mechanical stress 179
7.2 Future work 180

References 182

Appendix 189

A1. GC Traces for Calibration 189

A2. Area vs. Oil Concentration for Calibration 193

List of figures

CHAPTER 1

Figure 1. Chemical structure of MF precondensate (tri-methylolmelamine) 10

Figure 2. SEM images of surface morphology of microcapsules synthesized at different dropping rates (a: 2.08 ml min^{-1}, b: 0.27 ml min^{-1}) 15

Figure 3. a) TEM images and b) SEM images of the SiO_2/TiO_2 hybrid spheres 21

Figure 4. SEM image of the silica-lipid microcapsules 23

Figure 5. Confocal microscope image of biocompatible microcapsules labelled with red- emitting CdTe nanocrystals 25

Figure 6. SEM photographs of fragrant cotton fabric treated with the microcapsules after laundry 26

Figure 7. Schematic representation of MF microcapsule 44

Figure 8. Schematic representation of double shell composite microcapsule 45

Figure 9. Schematic representation of calcium shellac matrix containing MF microcapsules or unripened nanoparticulate $CaCO_3$ microcapsules 46

CHAPTER 2

Figure 1. Schematic representation of gas chromatography 48

Figure 2. Schematic representation of sample injection port 49

Figure 3. Schematic representation of a flame ionization detector 50

Figure 4. A typical GC trace and data of a mixture of 22 components (perfume oil) 51

Figure 5. a) Schematic diagram of the micromanipulation rig, b) Glass probe for compression of single microcapsules 52

Figure 6. Force vs. probe moving distance for compressing single microcapsules to rupture 54

Figure 7. Light scattered by particles 55

Figure 8. Schematic representation of dynamic light scattering 56

Figure 9. A typical size distribution curve obtained from SLS measurement 57

Figure 10. Schematic representation of scanning electron microscope 58

Figure 11. Schematic representation of the interaction between the electron beam and the sample 59

Figure 12. Schematic representation of the Environmental Secondary Detector 60

Figure 13. A typical ESEM image of microcapsules 61

Figure 14. Schematic representation of transmission electron microscope 62

Figure 15. A TEM image of the ultra-microtome section of the microcapsules 63

Figure 16. Schematic representation of FIB 64

Figure 17. A single microcapsule is cut by FIB over a predefined area 65

CHAPTER 3

Figure 1. GC trace for perfume oil in hexane at a concentration of 0.6 mg/ml 71

Figure 2. Calibration curves for GC analysis with a rention time of 9.03 min 72

Figure 3. GC data of sample taken from the aqueous layer in the encapsulation efficiency test 73

Figure 4. ESEM images of microcapsules **A**-**E** (LHS), and TEM images of ultra thin sections for microcapule **A**-**E** (RHS) 79

Figure 5. A microscopic image of microcapsules **D** dispersed in water (microcapsules **A**, **B**, **C** and **E** all look similar to **D** (not aggregated) when dispersed in aqueous) 80

Figure 6. (a) Size distribution chart for oil droplets in the o/w emulsions for preparing microcapsules **A-E** (DLS), b) Size distribution chart for microcapsules **A**-**E** in aqueous dispersion (DLS) 81

Figure 7. A plot of microcapsule diameter and wall thickness vs. F/M molar ratio 82

Figure 8. (a-d) Force vs. probe moving distance for compressing single microcapsules to rupture for microcapsules **B**-**E**, (e) schematic diagram of the probe compressing a single microcapsule to rupture 84

Figure 9. Mechanical property parameters vs. F/M molar ratio (average value of 3 size ranges) for microcapsules **B**-**E**. (a) Deformation at rupture, (b) Rupture force, (c) Nominal rupture stress 87

Figure 10. Mechanical property parameters vs. diameter for microcapsules **B-E**. (a) Displacement at rupture, (b) Rupture force, (c) Nominal rupture stress 88

Figure 11. Leakiness vs. time of microcapsules **A**-**E** over 20 days 890

Figure 12. The experimental leakage curve and the Korsmeyer-Peppas model for microcapsules **A**-**E** 91

CHAPTER 4

Figure 1. Encapsulation efficiencies of microcapsules **A**, **G**, **H**, $\mathbf{I_{4.5}}$, $\mathbf{I_{5.0}}$, $\mathbf{I_{5.5}}$, $\mathbf{I_{6.0}}$ and $\mathbf{I_{7.0}}$ 104

Figure 2. a) Average particle size for microcapsules **A**, **G**, **H**, $\mathbf{I_{7.0}}$ and $\mathbf{I_{6.0}}$,b) Average particles size for microcapsules **H** and **I** at pH 4.5, 5.0, 5.5, 6.0 and 7.0 106

Figure 3. ESEM images of morphology of microcapsules **A**, **G**, **H** and $\mathbf{I_{6.0}}$ 108

Figure 4. TEM images of microcapsule walls; a) microcapsules **A**, b) microcapsules **G**, c) microcapsules **H**, d) microcapsules $\mathbf{I_{5.5}}$, e) microcapsule $\mathbf{I_{6.0}}$ 111

Figure 5. a) Enlarged TEM image of the double shell composite microcapsules. b-d) EDX analysis of the ultramicrotome section of the double shell composite microcapsules 113

Figure 6. a) Force vs. probe moving distance for compressing single microcapsules $\mathbf{I_{6.0}}$ to rupture, b) force vs. probe moving distance for compressing single microcapsules $\mathbf{I_{5.5}}$ 115

Figure 7. a) and b) Optical microscopic images of microcapsules $\mathbf{I_{4.5}}$ and $\mathbf{I_{5.5}}$ in aqueous, c) and d) side view optical microscopic images of microcapsules $\mathbf{I_{4.5}}$ and $\mathbf{I_{5.5}}$ on a glass substrate for the macromanipulation measurement 116

Figure 8. Nominal rupture stress and deformation at rupture of microcapsules **A**, **G**, **H**, $\mathbf{I_{7.0}}$ and $\mathbf{I_{6.0}}$ 117

Figure 9. Displacement at rupture, rupture force and nominal stress at rupture for microcapsule $\mathbf{I_{6.0}}$ as a function of diameter 119

Figure 10. Leakage for microcapsules **A**, **G**, **H**, $\mathbf{I_{4.5}}$, $\mathbf{I_{5.0}}$, $\mathbf{I_{5.5}}$, $\mathbf{I_{6.0}}$ and $\mathbf{I_{7.0}}$ 120

Figure 11. Leakage kinetics of microcapsules **A**, **G**, **H**, $\mathbf{I_{6.0}}$ and $\mathbf{I_{7.0}}$ 123

CHAPTER 5

Figure 1. Wall thicknesses and the degree of wall completeness of the ripened double shell composite microcapsules $\mathbf{I_{6.0}}$, **J**, **K**, **L** and **M** 136

Figure 2. Average diameter and size distribution of the ripened double shell composite microcapsules (microcapsules $\mathbf{I_{6.0}}$, **J**, **K**, **L** and **M**) 139

Figure 3. Average diameter and size distribution of the ripened double shell composite microcapsules (microcapsules $\mathbf{I_{6.0}}$, **J**, **K**, **L** and **M**) 140

Figure 4. Typical force vs. probe moving distance curve obtained by compressing one of the microcapsules in $\mathbf{I_{6.0}}$ 141

Figure 5. Displacement at rupture vs. diameter, rupture force vs. diameter, and nominal stress at rupture vs. diameter for the ripened double shell composite microcapsules **M** 143

Figure 6. Leakiness of the ripened double shell composite microcapsules $\mathbf{I_{6.0}}$, **J**, **K**, **L** and **M** 144

CHAPTER 6

Figure 1. Optical microscope images of a) microcapsules **A**, b) microcapsules **F**, c) calcium shellac microparticles, d) calcium shellac matrix containing microcapsules **A**, e)calcium shellac matrix containing microcapsules **F** 157

Figure 2. Static light scattering measurement of a) size distribution for calcium shellac microparticles, b) size distribution for microcapsules **A** and calcium shellac matrix containing microcapsules **A**, c) size distribution for microcapsules **F** and calcium shellac matrix containing microcapsules **F** 159

Figure 3. SEM images of a) calcium shellac matrix containing microcapsules **A** (1 day), b) calcium shellac matrix containing microcapsules **A (**25 days), c) calcium Shellac matrix containing microcapsules **F** (1 day), d) calcium shellac matrix containing microcapsules **F** (25 days), e) calcium shellac microparticles (1 day), f) calcium shellac microparticles (25days) 161

Figure 4. SEM images of microcapsules cut by a FIB; a) cross sectional image of calcium shellac microparticles, b) cross sectional image of calcium shellac matrix containing microcapsules **F** 163

Figure 5. Force vs. probe moving distance for compressing single microcapsules (calcium shellac matrix containing microcapsules **A**) to rupture 164

Figure 6. Mechanical properties of a) deformation at rupture of microcapsules **A** and **F**, calcium shellac matrix containing microcapsules **A** and **F** and Calcium shellac microparticles, b) nominal rupture stress of microcapsules **A** and **F**, calcium shellac matrix containing microcapsules **A** and **F** and calcium shellac microparticles 166

Figure 7. Leakage profile of a) microcapsules **A** and **F**, and calcium shellac matrix containing microcapsules **A** and **F** over 20 days, b) linear plots for calculation of D_{eff} for microcapsules **A** and **F**, and calcium shellac matrix containing microcapsules **A** and **F** 169

List of schemes

CHAPTER 1

Scheme 1. Challenges of perfumes in consumer products 3

Scheme 2. Schematic representation of the polymerization process in *in situ* polymerization 8

Scheme 3. Schematic representation of the formation of microcapsules using an *in situ* polymerization process 9

Scheme 4. Mechanism of the MF precondensate converted to its conjugated acid form 11

Scheme 5. Formation of the methylene linkage 11

Scheme 6. Formation of the ether linkage 12

Scheme 7. Reaction mechanism between MF precondensate and copolymer 13

Scheme 8. Schematic representation of the polymerization process in interfacial polymerization 17

Scheme 9. Schematic representation of the formation of microcapsules using interfacial polymerization 18

Scheme 10. Schematic representation of the formation of multilayer assemblies by theconsecutive adsorption of counterpolyions and of the subsequent core removal 19

Scheme 11. Schematic representation of silica-lipid hybrid microcapsules 23

Scheme 12. Schematic representation of phase changing process 28

Scheme 13. Schematic representation of the self-healing process by microencapsulated Material, a) crack occurs, b) microcapsules containinghealing agenruptured, c) healing agent releases and filled the crack 30

Scheme 14. Schematic representation of the microencapsulated dye in carbonless copy paper 32

Scheme 15. Schematic representation for characterizing the mechanical properties of microcapsules by compression 35

Scheme 16. Schematic representation of the side view of compressing one single microcapsule using micromanipulation, a) probe moving in the

air before it has made contact with the microcapsule, b) probe touches the microcapsule, c) probe compresses the microcapsule, d) the microcapsule ruptured, e) the microcapsule has been completely squashed and the probe touches the glass slide 37

Scheme 17. Schematic representation of core oil leaking through the microcapsules wall 42

Scheme 18. Schematic representation of the difference approaches for reducing the leakingof the oil from the microcapsules 43

CHAPTER 3

Scheme 1. Schematic presentation of microcapsule formation by *in situ* polymerization 77

CHAPTER 4

Scheme 1. Schematic representation of the formation of microcapsules **F**, **G**, **H**, $\mathbf{I_{4.5}}$, $\mathbf{I_{5.0}}$, $\mathbf{I_{5.5}}$, $\mathbf{I_{6.0}}$ and $\mathbf{I_{7.0}}$ 97

Scheme 2. A schematic representation of the pH effect on the particle size of the microcapsules **H** at pH 4.5, 5.0 and 5.5 107

Scheme 3. Schematic representation of the MF inner wall formation of the double shell composite microcapsules 112

CHAPTER 5

Scheme 1. Schematic diagram of the formation of the double shell composite Microcapsules 129

Scheme 2. Schematic diagram of the possible wall structure of the microcapsules wall from increase the volume of aqueous $CaCl_2$ and Na_2CO_3 (**step 3**) 138

CHAPTER 6

Scheme 1. Schematic representation of the formation of calcium shellac matrix containing microcapsules **A** and **F** 150

List of tables

CHAPTER 5

Table 1. Encapsulation efficiency of microcapsules $\mathbf{I_{6.0}}$, **J**, **K**, **L** and **M** 131

CHAPTER 7

Table 1. Summary of encapsulation efficiency, physical and mechanical properties and leakage data of microcapsules 173

Chapter 1

Introduction: Microencapsulation and Perfumes

Abstract

The objective of this chapter is to understand the functionalities and release mechanism of melamine formaldehyde (MF) microcapsules containing perfume oils used in consumer products, and to analyse possible ways to reduce the leakage. Therefore, properties of perfume oils and the possible interactions between the oil and the capsules are reviewed. Various microencapsulation methods and characteristics of microcapsules are identified and discussed in details. The release mechanisms and the release kinetics of the microcapsules are then reviewed to gain a fundamental understanding of the factors involved that affect the leakage.

1.1 Perfume in Consumer Products

1.1.1 The Role of Perfume in Consumer Products

Perfume is a mixture of natural extracts and synthetic essential oils,[1] which can contain several hundred different ingredients ranging from aliphatic hydrocarbons, alcohols and aldehydes to terpenes.[1-3] Perfumes are in scented products such as fabric conditioners,[4] facial creams,[5] and laundry soaps,[6] to make them appealing to the customer.[7] Hence, perfume plays an important role in supporting brand image and market position of the product. Unfortunately, perfumes are costly and hence formulation strategies are required that maximise the aesthetic nature of perfumes to reduce costs of manufacture.

1.1.2 Behaviour of Perfume Oils in Consumer Products

The interaction between fragrances in products can be divided into three stages of the product life cycle.

- The first stage is the blending stage.[8] In products that contain multiple phases (*i.e.* gas, liquid and solid), it is the time when the fragrance mixes with the product and the subsequent period in which the odorant molecules migrate through the products' various phases.[9]

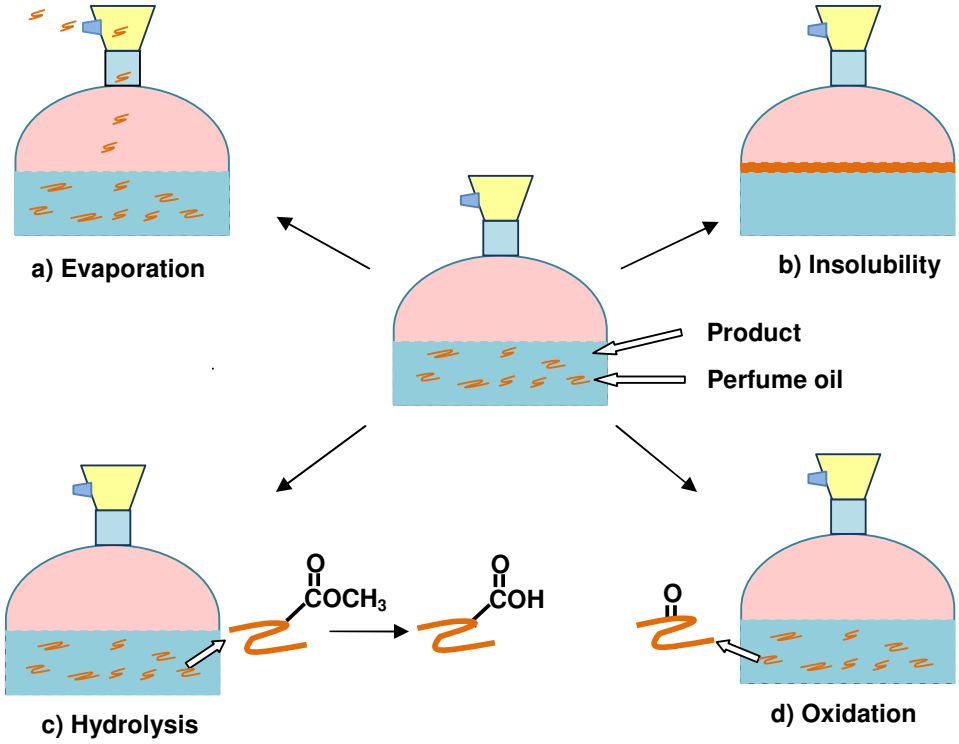
- The second stage is the latent stage,[8] in which the product remains in its closed container. This stage ranges from the storage of the product at the manufactures to the customers opening the product. The fragrance should remain both chemically and physically unchanged during this stage, and it must not cause any undesirable changes of the product.

- The final stage is called the active stage, [8] in which the fragrance fulfils its purpose perceived by the consumer, *i.e.* meeting the odour intensity quickly, and retaining a consistent release of the scent till the product is used up.

1.1.3 Challenges for Perfumes in Consumer Products

Challenges that need to be considered and overcome for incorporating perfumes in the consumer products including (**Scheme 1**):

- Evaporation
- Water insolubility
- pH Effects – hydrolysis
- Oxidation



Scheme 1. Challenges of perfumes in consumer products.

1.1.3.1 Evaporation (Scheme 1a)

Perfume oil is a mixture of many different components that evaporate at different rates, which may lead to undesirable production problems and product quality issues as the starting fragrance may be different from the final product fragrance.[8]

1.1.3.2 Water Insolubility (Scheme 1b)

Water insolubility of the perfume is one of the major problems in water based products. It may manifest itself by spoiling the appearance of the product, which could severely damage the branding.[5] Solubility issues arise due to a decrease in ambient temperature during storage, which reduces the perfume solubility, and hence precipitation or temperature increases leading to the formation of insoluble materials by polymerization.[10] Thus, storage management is a particular issue.

1.1.3.3 pH Effects – Hydrolysis (Scheme 1c)

Some products in which perfumes are used require acidic or alkaline conditions that may lead to degradation of some of the components of the perfume. As water is the medium used for most perfumery application ester hydrolysis[11] could be induced when perfumes are stored under acidic (*i.e.* fabric softeners, body lotions and shampoos) or alkaline (*i.e.* detergent or soup) conditions.[12]

1.1.3.4 Oxidation (Scheme 1d)

Some perfume components, notably aldehydes and unsaturated hydrocarbons, may undergo oxidation[13] in air. Oxidation is very likely to occur where the contact surface area is very large. The oxidation is accelerated by heat and induces odour changes, colour changes and the formation of precipitates.

1.1.4 Perfume Oil in Microcapsules

With the challenges faced in using perfumes in consumer products, actions were taken by the manufacturers to overcome them, such as choosing less volatile component for the perfume

oils to prevent or minimise the evaporation,[7, 8] mixing the perfume oil with a suitable surface-active agent to prevent insolubility,[8] changing the formulation of the perfume oil to avoid chemical reactions occurring during processing and storing,[14] and eliminating the factors that promote the oxidation which is enhanced by heat and air.[2] However, these methods either impact on the quality of the final product, as a result of sacrificing some of the key components of the perfume, or greatly increase the cost due to the extra expense in the formulation process.[15] Hence, research that protects the perfume from the product ingredients whilst retaining the perfume for release until the products is used is now a major research area.

Perfume oil encapsulation is a technique which fulfils the above criteria.[16] Encapsulating the perfume oil into micron-sized packages provides the possibility of:

(i) mixing the, usually hydrophobic, perfume oil with water based products,
(ii) reducing the heavy losses of fragrances during the storage, and
(iii) delivering the perfume in a longer lasting and controlled way.

Therefore, manufacturers are seeking ways to incorporate encapsulated perfume oils into their products. However, encapsulation is a generic methodology and hence it has attracted academic interests in areas such as food,[17] pharmaceuticals,[18] and cosmetics.[9] Numerous ways have been successfully developed for microencapsulation such as spray drying,[19] coacervation,[20] *in situ* polymerization[21] and interfacial polymerization,[22] and are described in the next section.

1.2 Microencapsulation

Microencapsulation is the formation of micron sized particles with a core/shell structure, where the core is a liquid, a solid/liquid dispersion, or a gas, and the shell is an organic polymer or inorganic matrix.[23] The concept of microencapsulation first achieved significant recognition[23] in 1954 when carbonless copy paper was introduced by the National Cash Register Company (NCR), Dayton, Ohio.

For the past 60 years, microencapsulation has been researched and developed by scientists around the world in an amazingly diverse number of fields.[23] The main drive for this field of research is the functionality that microencapsulation can bestow, such as:

- protection of the active component in a single mixture,[24]
- mixing of immiscible and incompatible materials,[24]
- increased environmental stability,[25]
- conversion of liquids or tacky solids to free flowing powders,[25] and
- targeting of active ingredients to specific sites.[26]

Thus, the initial idea of developing a convenient way of making copying paper has become a life saving aspect of drug delivery,[27, 28] and live cell encapsulation,[29] as well as having uses in more everyday items such as fabric conditioners,[30] textiles,[31, 32] toothpaste,[33] and food.[34, 35]

1.3 Encapsulation methods

The first commercialised microcapsules were made by complex coacervation.[36] Since then, many other methods for preparing microcapsules have been developed. Microencapsulation methods can be classified into three types: chemical, mechanical and physical-chemical methods (shown in **Table 1**).[23]

Table 1. Classification of microencapsulation methods.

Chemical	Mechanical	Physical-chemical
• *In situ* polymerization • Interfacial polymerization • Rapid insolubilization of polymer	• Extrusion • Coating • Spraying • Electrostatic aerosol	• Solvent evaporation • Coacervation • Suspension crosslinking • Phase separation • Layer-by-layer

The selection of the encapsulation methods is dependent on several factors:

- Size of the microcapsules,
- Release mechanism of the microcapsules,
- Properties of the core and/or wall material,
- Stability of the microcapsules,
- Cost, and
- Application of the products.

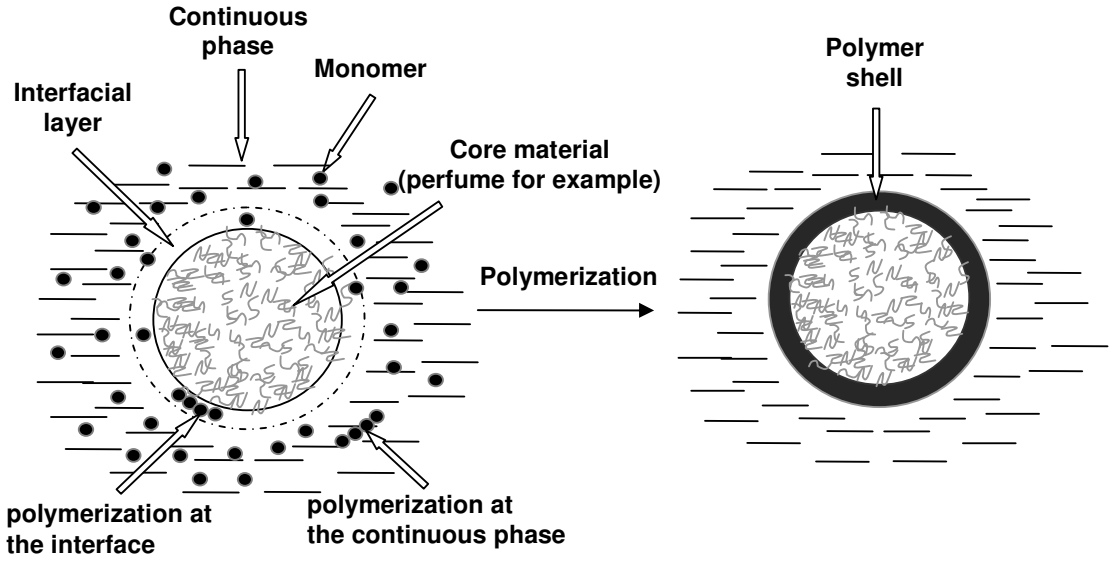
Among these encapsulation methods, *in situ* polymerization, interfacial polymerization and layer by layer deposition are discussed in details.

1.3.1 *In Situ* Polymerization

In situ polymerization is an encapsulation process in which shell formation is primarily due to polymerization of shell reactants at interfaces.[26] Shell formation in *in situ* polymerization occurs:

- exclusively at the continuous side of the interface, or
- by a combination of reactions at the continuous side of the interface, and at the continuous phase away from the interface (**Scheme 2**).[37]

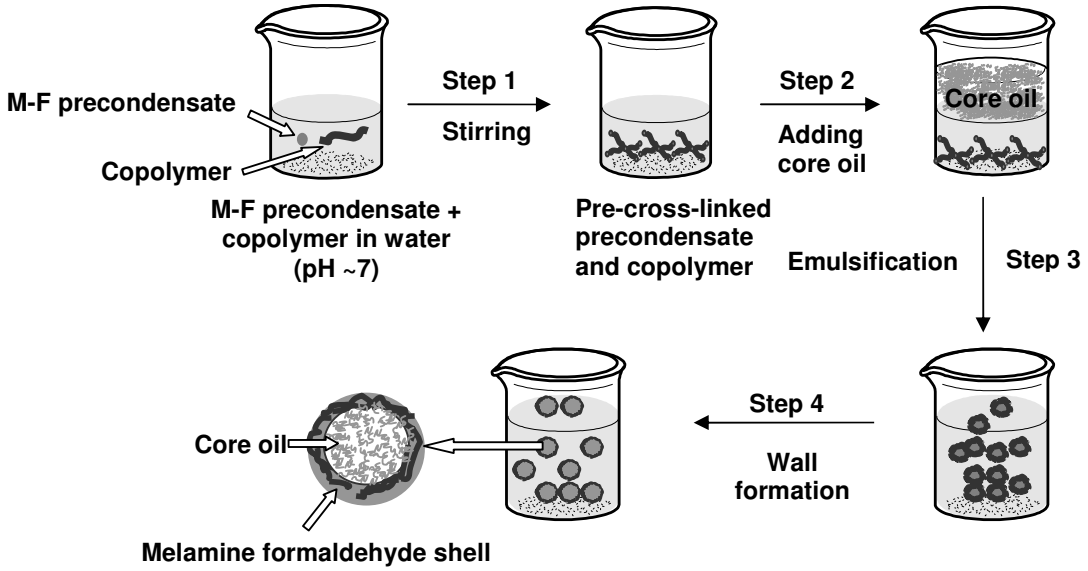
In situ polymerization protocols are typically carried out at liquid/liquid, solid/liquid, or solid/gas interfaces, and it is ideal for encapsulating hydrophobic materials.[23]



Scheme 2. Schematic representation of the polymerization process in *in situ* polymerization.

In situ polymerization has many benefits over some other microencapsulation processes. It is simple, and the wall formation step is quick and straight forward. Moreover, the polymer wall is highly cross-linked and compact,[38] which makes it a strong candidate for encapsulation of small molecules.

In situ polymerization involves several steps. **Scheme 3** shows a typical formulation process for preparing a liquid core and solid wall microcapsules using an *in situ* polymerization method. In this process, a monomer and copolymer are firstly dissolved in the aqueous (continuous) phase and stirred to form the wall solution (**step 1**). The core oil is added (**step 2**) to the resulting solution to form an oil in water (o/w) emulsion by agitation (**step 3**). Finally, the wall material is cross-linked on the oil droplet surface to form the microcapsules (**step 4**).[39]



Scheme 3. Schematic representation of the formation of microcapsules using an *in situ* polymerization process.

1.3.1.1 Melamine Formaldehyde (MF) Microcapsules

The most commonly used material for producing microcapsules using *in situ* polymerization are amino containing resins such as melamine or urea formaldehyde polymers.[23] The popularity of these materials is that the microcapsules wall has excellent acid and alkaline resistance,[40] good mechanical strength[41] and low cost.[23] The wall formation step in the amino resin microcapsules is always triggered by lowering the pH to below 5 and/or raising the temperature.[40, 42]

1.3.1.1.1 Chemical Structures of MF Microcapsules Wall

For MF microcapsules, MF precondensate is usually used as the monomer to form the wall, following copolymerizetion with a copolymer. It is a commercially available product prepared by the reaction of melamine and formaldehyde. However, the molar ratio between formaldehyde and melamine in different products/suppliers is different. **Figure 1** shows the chemical structure of a typical MF precondensate in which the formaldehyde to melamine (F/M) molar ratio is 3.

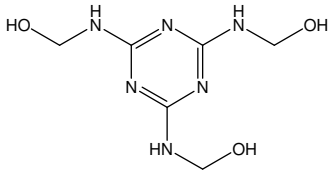
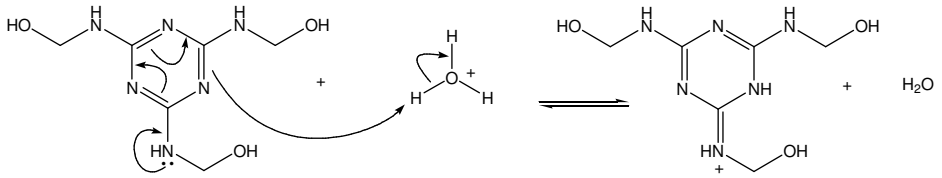


Figure 1. Chemical structure of MF precondensate (tri-methylolmelamine).

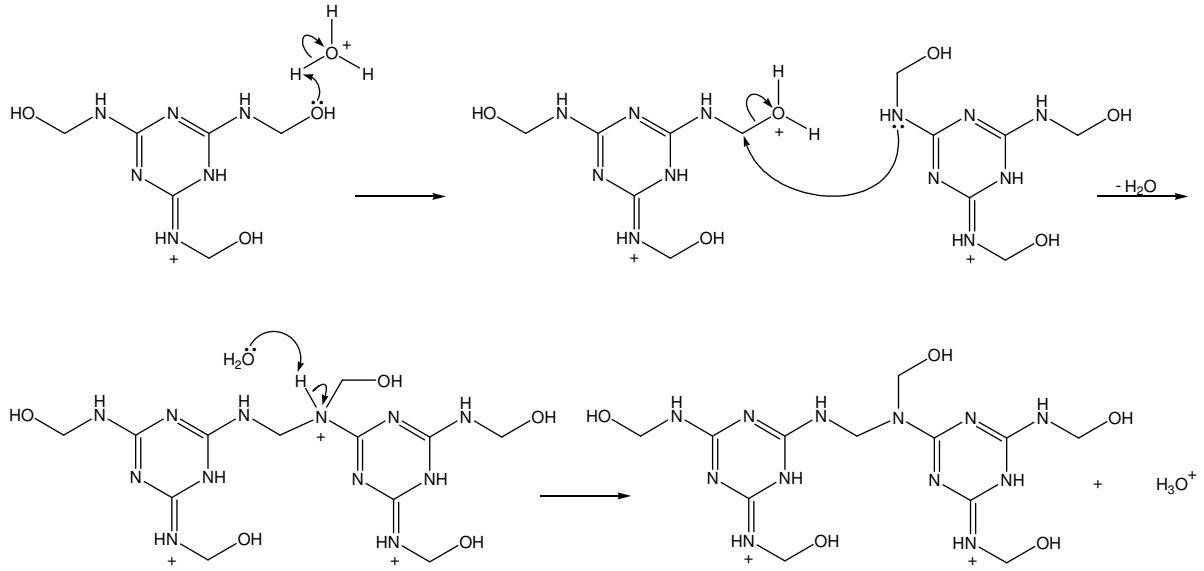
The MF polymer wall is formed by the polycondensation reaction which occurs between the MF precondensate. The rate of reaction increases upon the addition of acid. Based on the kinetic study by Sato *et. al.*[43], the condensation reaction has the highest reaction rate at pH ~4.5.

In acid conditions, MF precondensate is converted into its conjugated acid form (**Scheme 4**).[43]



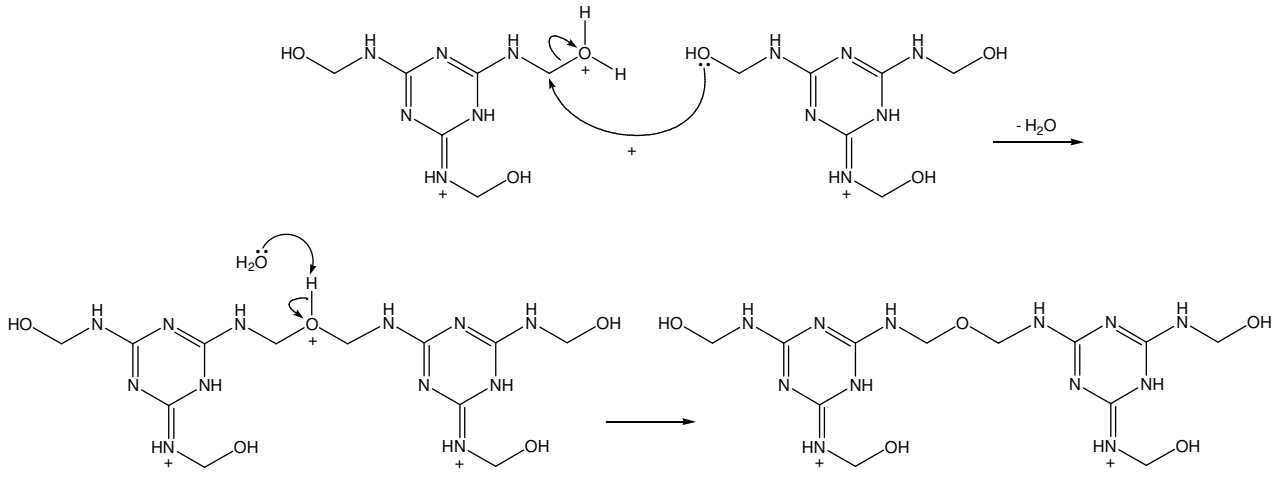
Scheme 4. Mechanism of the MF precondensate converted to its conjugated acid form.

Polycondensation reaction occurs between the two conjugate acids. Resulting in two different types of linkages. As shown in **Scheme 5**, a diamino methylene linkage is formed by further protonation of the hydroxyl group on the conjugate acid to form H_2O^+ as a leaving group that can be displaced by an amino functionality from another conjugate acid. Formation of the methylene linkage is favoured at pH 4.5.[44]



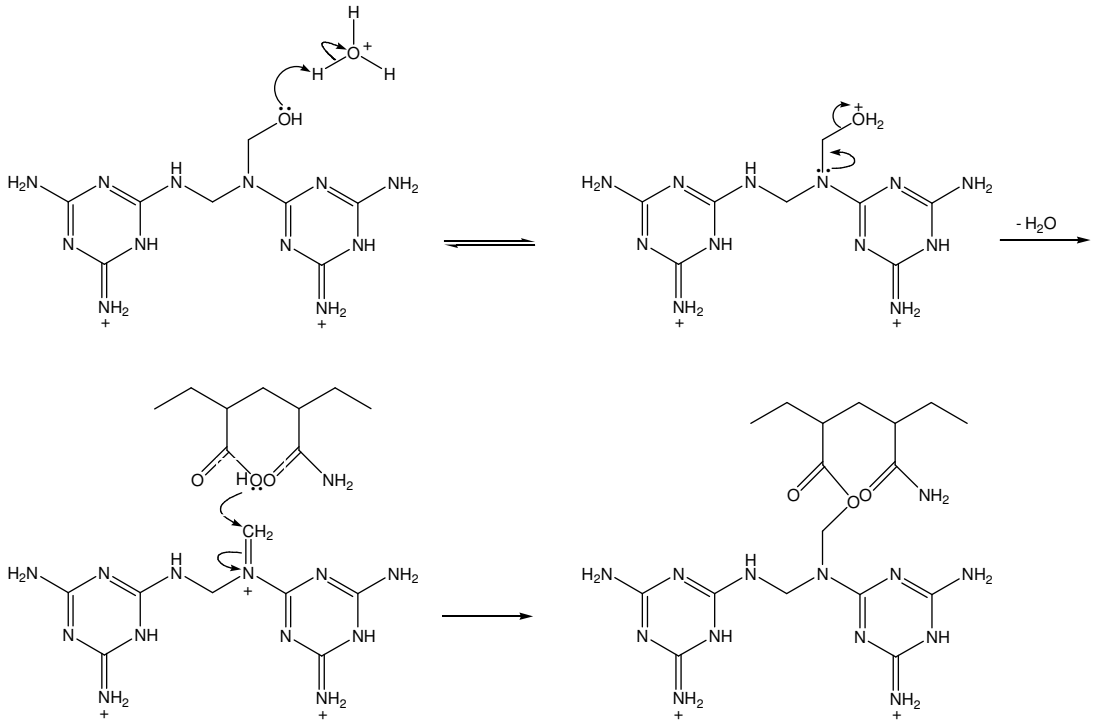
Scheme 5. Formation of the methylene linkage.

The second type of link is an ether formed through the condensation reaction between the protonated conjugate acid and the hydroxyl methyl group from another conjugate acid (**Scheme 6**).[45] It is reported that ether bridges can be formed more easily in a high F/M molar ratio than in a low F/M molar ratio.[44]



Scheme 6. Formation of the ether linkage.

Copolymers and emulsifiers are normally added into the formulation to cross-link with MF precondensate in the aqueous phase to assist the emulsification step by stabilising the oil in water emulsion. A typical copolymer used in the formation of MF microcapsules is poly(acrylamide-acrylic acid, sodium salt), and the reaction is showing below in **Scheme 7**.[46]



Scheme 7. Reaction mechanism between MF precondensate and copolymer.

A large number of oligomeric derivatives and a cross-linked network are formed during the polycondensation reaction forming the polymer wall of the microcapsules.[30]

The properties of the amino resin microcapsules such as the mean particle size, size distribution, morphology, wall thickness, mechanical strength and loading efficiency can be affected by many parameters such as stirring time, stirring speed, emulsifier type, emulsifier

concentration, the viscosities of the core/wall materials, and the feed rate of adding the wall material.[47-49]

1.3.1.1.2 Effect of Formaldehyde to Melamine Molar Ratio

From the previous literature reports, formaldehyde to melamine molar ratio used in the preparation of MF microcapsules ranges between 2.3 to 5.5.[30, 50, 51] It was suggested that F/M molar ratio is a key factor that determines the mechanical properties of the microcapsules. High F/M molar ratio gives high flexibility, and strong walls.[30]

In the reaction between melamine and formaldehyde, the residual formaldehyde content was monitored vs. reaction time at different F/M molar ratios. [30] It was found that as the F/M molar ratio increased, content of the residual formaldehyde increased and the reaction reached an equilibrium state earlier. This unreacted residual formaldehyde tends to react with the methylolmelamine and precipitates as small particles, which deposits onto the melamine formaldehyde wall, resulting in a relatively rough surface morphology of the microcapsules.[52]

Despite the benefits of producing highly deformable and stronger walls at higher F/M ratios, a considerable amount of unreacted formaldehyde remaining in the microcapsule slurry, which has raised concerns due to its toxicity.[53] In order to reduce this residual formaldehyde content, several methods have been used. Urea[54] or ammonium chloride[53] can be added after the microencapsulation process to react with the excess amount of formaldehyde. Another way of lowering the formaldehyde content is reacting the excess formaldehyde with urea after the microcapsules are formed to form urea-formaldehyde polymer, so that the remnant formaldehyde content can be significantly reduced.[55] However, none of them have totally eliminated or effectively reduced the free formaldehyde from the products. Hence,

significantly reducing the formaldehyde content in the formulation process is highly desired (see **Chapter 3**).

1.3.1.1.3 Surface Morphology

Apart from the F/M molar ratio mentioned above, there are a few other factors which influence the morphology of the MF microcapsules. Feed rate during the addition of the MF precondensate is one of the important elements.[55] A slow feed rate reduces flocculation of the microcapsules and the microcapsules wall surface becomes smoother. In addition, the precondensate can concentrate on the surface of emulsion droplets allowing condensation to take place, as shown in **Figure 2** at feed rate at 2.08 ml min^{-1} (**Figure 2a**) and 0.27 ml min^{-1} (**Figure 2b**).[55] Furthermore, the stirring speed is considered to affect the surface morphology.[56] The surface of the microcapsule becomes smoother with an increase in stirring speed.[56] Other experimental parameters which affect the surface morphology include the type of emulsifiers used and the core materials been encapsulated.[57]

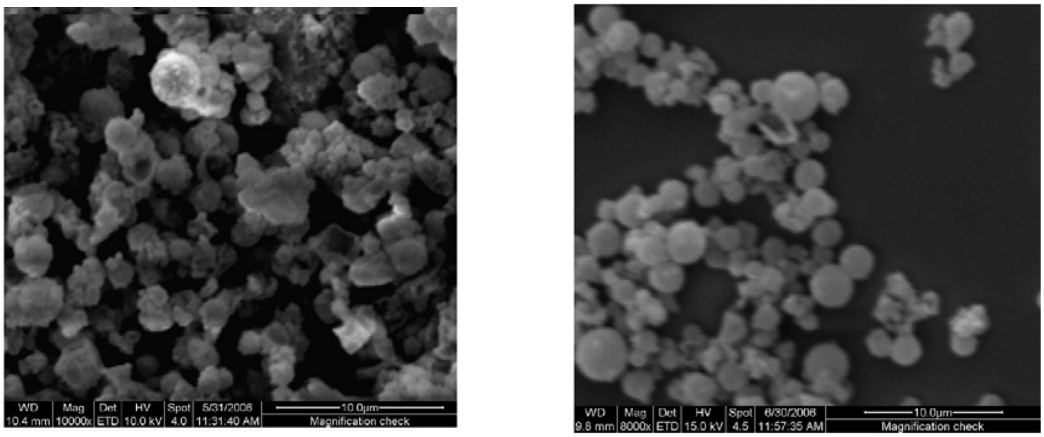


Figure 2. SEM images of surface morphology of microcapsules synthesized at different dropping rates (a: 2.08 ml min^{-1}, b: 0.27 ml min^{-1}).[55]

1.3.1.1.4 Size

Size of the MF microcapsules produced by *in situ* polymerization process is governed by several factors, and one which influences the most is the stirring speed. Increasing the stirring speed results in decreasing the diameter of the microcapsules,[24] as there is higher shear force and turbulence breaking the emulsion droplets into smaller droplets. The size change of microcapsules can also be attributed to the viscosity of the solution.[58] It was observed that average diameter of the microcapsules decreased with viscosity of the dispersed solution, as lower shear force was needed to break the droplets.[59] Addition of a stabiliser appeared to reduce the particle size as well.[21] The average diameter is inversely proportional to the concentration of the emulsifier. However, broad size distribution curves were observed if a high concentration of the emulsifier is used.[21]

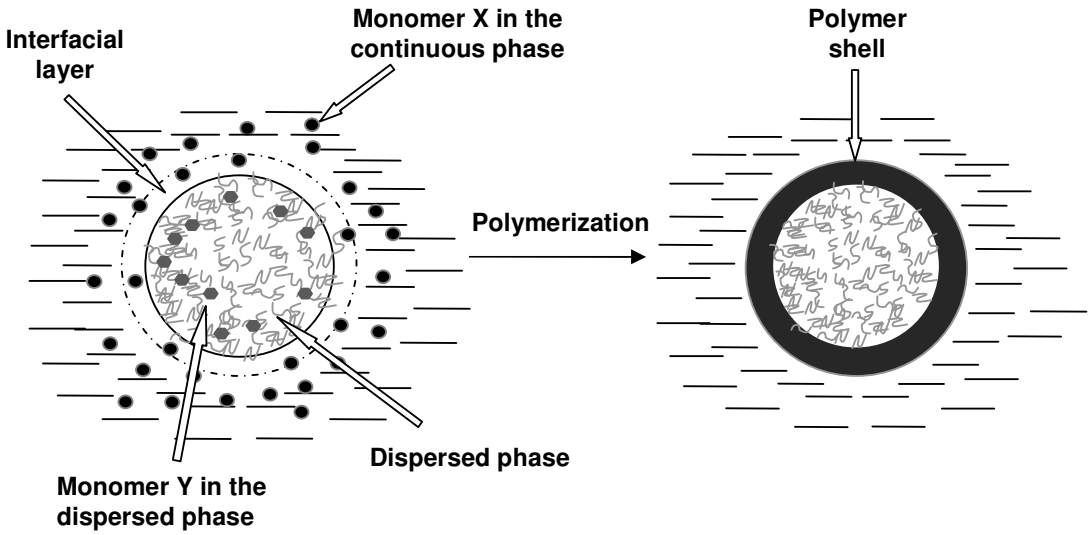
1.3.1.1.5 Wall Thickness

The wall thickness of MF microcapsules is predominantly governed by the amount of wall material (MF precondensate) used in the preparation stage.[60] It was found that the shell thickness increases linearly with the wall material concentration. However, at higher concentrations there is a plateau effect and additional resin precipitates in the solution.[61] In addition, it was found that the thickness of the MF microcapsules wall increased with the polymerization time.[60]

Melamine formaldehyde microcapsules produced by *in situ* polymerization process has been widely used in numerous areas and products containing electrophoretic particles,[62, 63] flame retardants,[58, 64] and fragrant oils[63]. Recent developments include the incorporation of these microcapsules in self-healing,[65] and phase changing[66, 67] products.

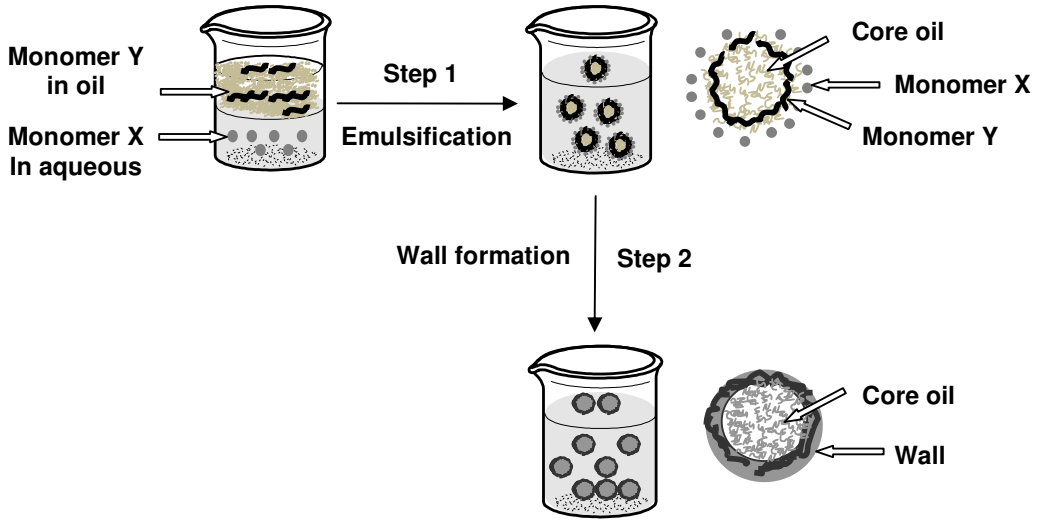
1.3.2 Interfacial Polymerization

Unlike *in situ* polymerization, in the interfacial polymerization process the reactants (monomers) involved in shell formation initially are located in both dispersed and continuous phases, and the polymerization of two monomers occurs at the interface of the two immiscible phases to form the microcapsule wall (**Scheme 8**).



Scheme 8. Schematic representation of the polymerization process in interfacial polymerization.

This process requires the two monomers (X and Y) to have relatively large differences in their partition coefficients. A schematic diagram for synthesising the microcapsules using interfacial polymerization process is illustrated in **Scheme 9**. Monomer X dissolves in the aqueous phase and monomer Y dissolves in the oil phase. Monomers X and Y diffuse to the dispersed/continuous phase interface where they react and thereby form the microcapsules wall.



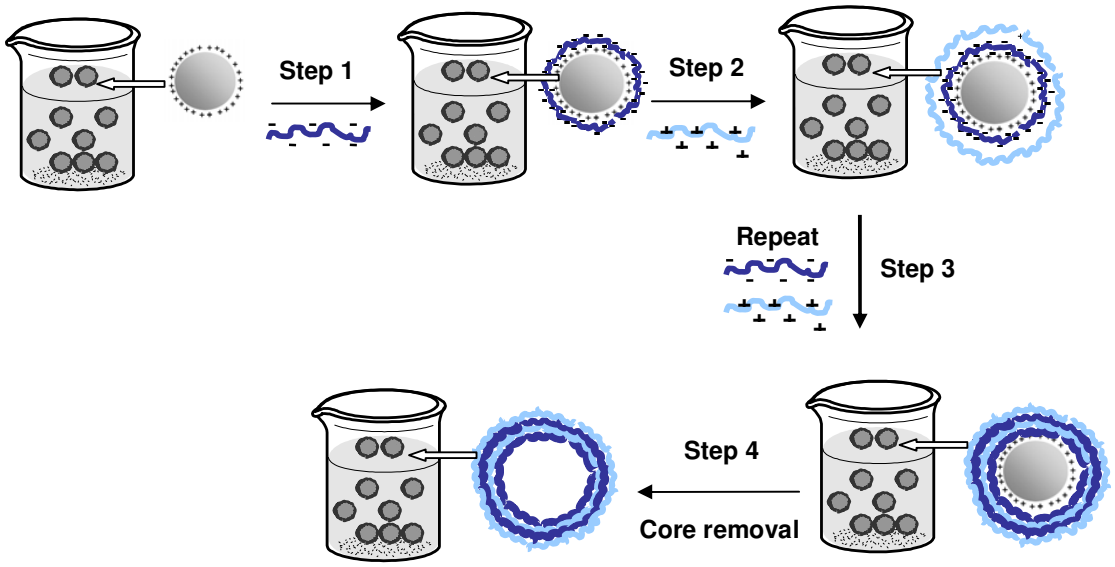
Scheme 9. Schematic representation of the formation of microcapsules using interfacial polymerization.

Monomer X typically is an oil-soluble bis-acid chloride or isocyanate. Higher molecular weight acid chloride such as terephthaloyl[68, 69] and sebacoyl chloride [70, 71] are normally chosen to prepare the microcapsule wall. They are stable and highly resistant to hydrolysis. Monomer Y tends to be a tris or tetratris amine or hydroxyl compound to achieve cross-linking.

1.3.3 Layer-by-layer

The LbL approach pioneered by Decher[72] to create homogeneous ultrathin films on solid supports based on electrostatic attraction between opposite charges. This LbL technique was then utilised to produce microcapsules.[73] It has been used not only for coating colloidal particles, but also been used to produce hollow microspheres as drug delivery vehicles.[74] In the later case, a solid core (template) has been employed in the initial state to allow the deposition of the polyanions and polycations, after the formation of the polymer films, the core is removed subsequently (**Scheme 10**).

Layer-by-layer (LbL) encapsulation utilizes electrostatic interactions and complex formation between oppositely charged polyelectrolyte species.[75] Multilayers are formed by successive alternate polyionic polyelectrolyte deposition *via* a charge overcompensation of the previous layer.[74, 75]



Scheme 10. Schematic representation of the formation of multilayer assemblies by the consecutive adsorption of counterpolyions and of the subsequent core removal.

LbL technique has attracted substantial interest due to the ability for producing highly tailored polymer thin films. The film thickness and the deposited amount of polyelectrolytes increase typically linearly with the number of deposited layers.[72, 76, 77] Improvements to this technique have been reported by Elbert *et al.* [78] and Picart *et al.*[79, 80] where precise control of wall thickness has been achieved by an exponential growth of both the mass and the thickness of the film with the number of deposition steps.[81]

The LbL technique has been used most extensively in biological and pharmaceutical industries for encapsulating large molecules. However, the relatively porous wall limits its application in coating small molecules such as perfume oil or flavour additives.

1.3.4 Recent Developments

1.3.4.1 Double Shell Microcapsules

In order to solve the problem of thin walls and have poor mechanical properties for some microcapsules, another shell can be coated on their original wall.[82] In the case of gelatine gum arabic microcapsules containing electronic ink, urea-formaldehyde polymer was coated on top of the gelatine gum arabic inner shell to produce double shell microcapsules, and results show that both the hermetization property and compactness of the microcapsules were improved.[82]

The advantages of double shell microcapsules including reduced permeability and improved mechanical properties of the wall,[48, 83] as well as multi-step releasing of the core material.[81] Conventionally used microcapsules for drug delivery are normally porous. Hence, the need for well-controlled drug delivery carriers remains a problem. A double shell microcapsules system with a biodegradable polymer shell surrounded by another polymeric shell offers the opportunity to control the drug release rate, particle diameter and the thickness of the polymer shell.[81] Another way to improve the controlled release of the microcapsules is described by Shum *et al.*[84] utilising a double emulsion system for the assembly of amphiphilic diblock copolymers into vesicle structures. These double shell microcapsules were prepared and used to encapsulate small hydrophilic solutes.

To enhance the cross-linking of the microcapsule shell, MF double shell microcapsules were produced by using a two step feeding method, *i.e.* MF precondensate was added twice during the shell forming stage to form a more compacted wall.[85] This two steps addition of the MF precondensate may be attributed to the reduction in defects in the wall structure and the increased cross-linking density. Similar work for producing the double shell MF microcapsules by using the two step feeding method was also reported by Luo *et al.*[86] However, the second MF precondensate used was hexamethylolmelamine instead of trimehylolmelamine that was initially added.

Some other double shell microcapsules were also produced to improve their original properties depending on the purpose of the formulation.[87, 88] Silica/Titania hybrid double shell microspheres with polystyrene as the core are prepared *via* sol-gel process to improve the titania photocatalytic activity (**Figure 3**).[88]

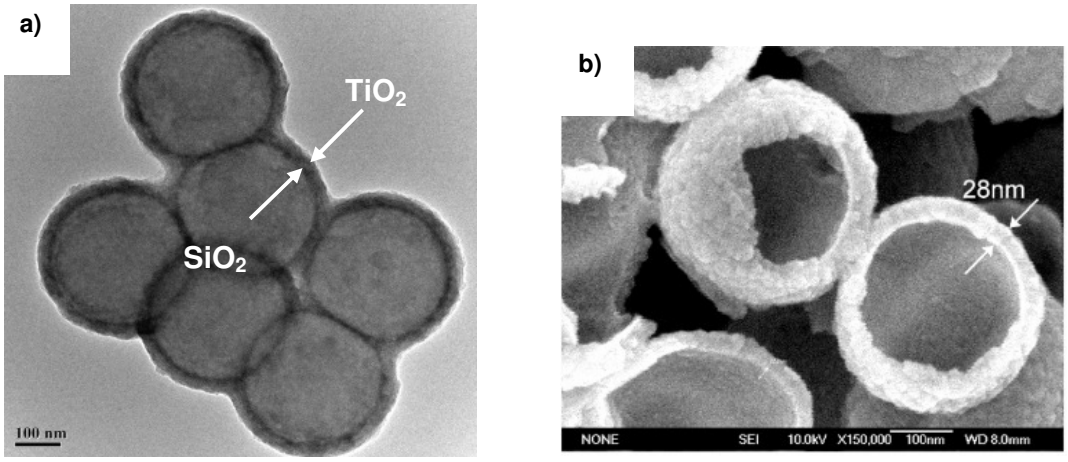


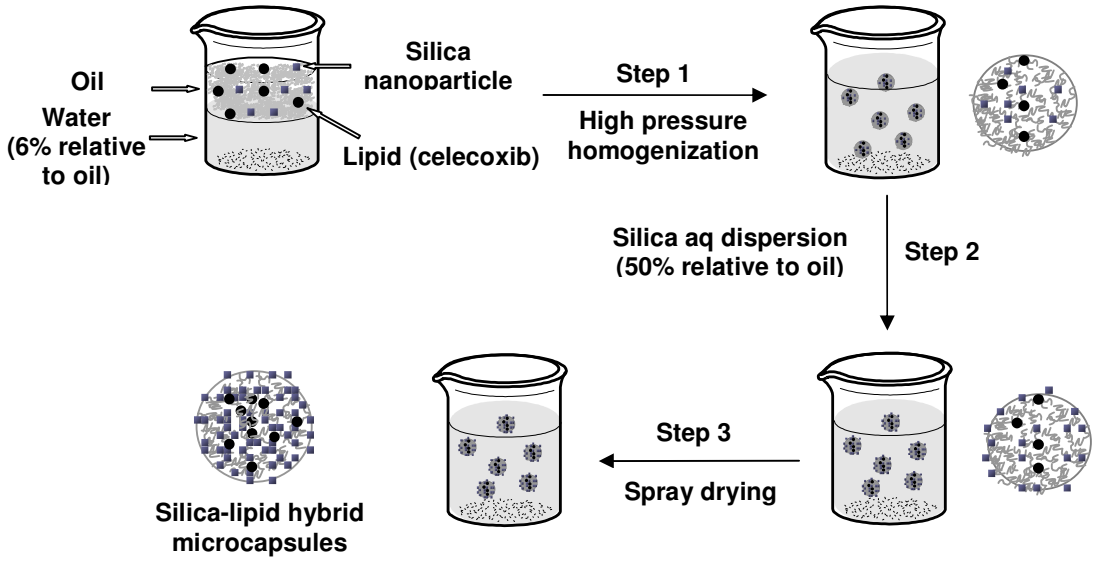
Figure 3. a) TEM images and b) SEM images of the SiO_2/TiO_2 hybrid spheres.[88]

1.3.4.2 Microcapsules with Nanoparticles

Previous work has demonstrated that incorporating nanoparticles into the microcapsule shell has very beneficial impacts on:

- improving the stiffness and resistance to deformation of microcapsules,[89]
- preventing heat-shrinking during the encapsulation process,[90] and
- improving thermal behaviour of microcapsules.[91]

Therefore, combining nanoparticles with wall materials has proved very beneficial in many applications. Silica-lipid hybrid microcapsules[92] are one of the examples to encapsulate poorly soluble drugs. It combined the solubilising effect of lipids and the stabilising effect of silica nanoparticles to enhance the dissolution kinetics of the carrier compounds used in drug delivery. As shown in **Scheme 11** the microcapsules were prepared *via* a two step process, *i.e.* homogenization followed by spray-drying of the silica-stabilised emulsions.



Scheme 11. Schematic representation of silica-lipid hybrid microcapsules.[92]

An SEM image of the silica-lipid hybrid microcapsule is shown in **Figure 4**.

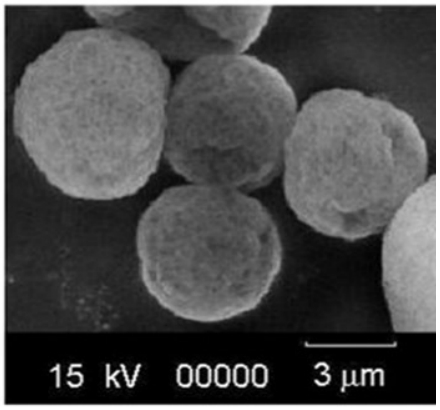


Figure 4. SEM image of the silica-lipid microcapsules.[92]

Incorporating nanoparticles in the microcapsules could also help to achieve controlled release of the core content of the microcapsules.[93] Ag nanoparticles provide the possibility of achieving remote release of an encapsulated material from polyelectrolyte capsules based on laser light illumination. The capsules containing Ag nanoparticles were deformed or cut when under laser illumination,[93] hence remote release of the core content could be accomplished.

Multifunctional microcapsules have also been reported by introducing different types of nanoparticles to the microcapsules. By incorporating luminescent colloidal semiconductor nanocrystals like CdTe and CdSe quantum dots, the capsules can be easily detected by measuring their fluorescence signal with noninvasive optical techniques (**Figure 5**).[94] The labelling of the microcapsules by quantum dots can be achieved when the majority of the nanocrystals are incorporated into the capsule wall, because of the electrostatic interactions of their capping ligands with the oppositely charged polymers.[94]

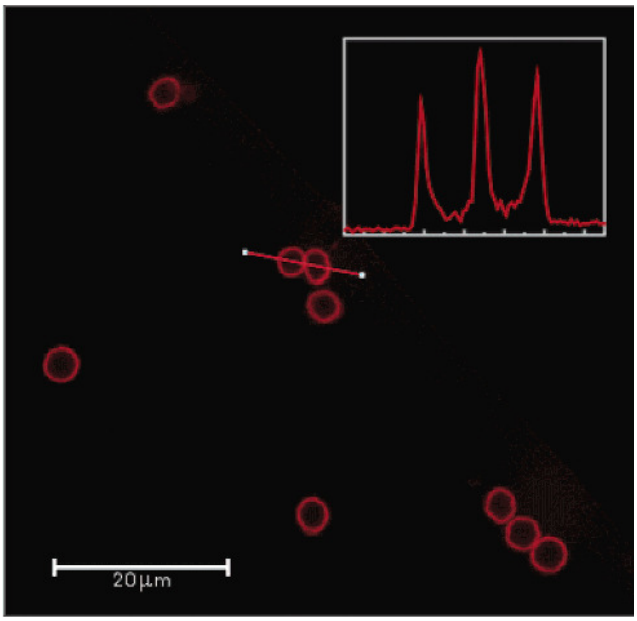


Figure 5. Confocal microscope image of biocompatible microcapsules labelled with red-emitting CdTe nanocrystals.[94]

The incorporation of magnetic nanoparticles into microcapsules for drug delivery has also been studies recently. The magnetic property of the nanoparticles allows the possibility of manipulating the drug delivering process externally by a magnetic field.[95] When magnetic nanoparticles such as Fe_3O_4 were embedded into the capsule wall, the movement of capsules in a desired direction can be controlled by applying an external magnetic field gradient.[96]

The novelty of these microcapsules as a carrier lies in the possibility of combining all these different strategies into one single material, and thus provides true multifunctionality.[90]

1.4 Applications of Microencapsulation

Microencapsulated products[23] impinge on many parts of our daily life. It provides a new product concept that improves its performance through controlled-release and reinforcing the image of innovation of the product. Numerous companies are engaged in encapsulation of a variety of functional molecules.

1.4.1 Microcapsules in Cosmetic and Household Products

In terms of cosmetic and household products, microencapsulation technology has proved itself to be powerful in providing the possibilities of achieving cost-reduction targets by protecting fragrances and other expensive actives, for improved performance created *via* controlled release, and stabilising the sensitive ingredient from the environment.[8] Microcapsules have been extensively used as a perfume carrier, odour mask and enzyme container.[97] **Figure 6** shows cotton fabric after washing with a laundry product containing perfume microcapsules.[98] The melamine formaldehyde microcapsules containing perfume oils were made by *in situ* polymerization method, and have attached to the fabric during the washing cycle. Therefore, sustained release can be achieved when the microcapsules are ruptured.

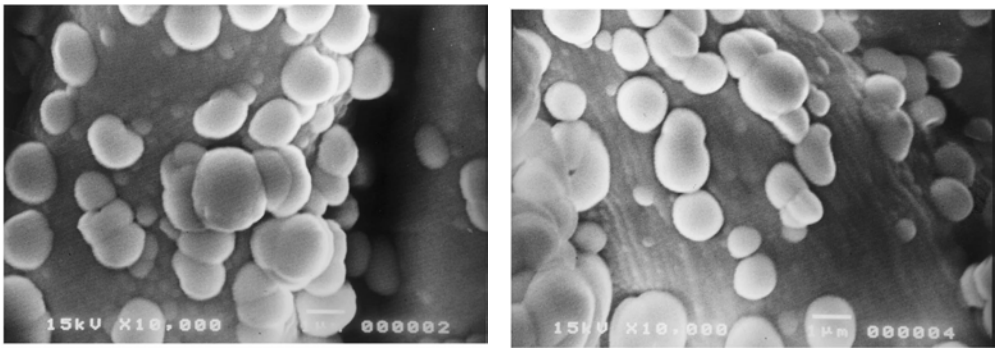


Figure 6. SEM photographs of fragrant cotton fabric treated with the microcapsules after laundry.[98]

Despite the benefits, there are still some technical challenges that are faced and waiting to be resolved:

- there is a need to develop multicomponent delivery systems to achieve the controlled release of substances with incompatible properties, *via* sequential ruptures of microcapsules.[97]
- laundry products face a problem of weak adhesion between the microcapsules and the fibres due to the presence of surfactant that is used for cleaning purposes.[97]
- leaking of the core content during the storage stage is problematic, which leads to a reduction in the quality of the product and increases the manufacturing cost.[97]

Therefore, the need to find new wall materials to enhance the adhesion of the microcapsules and reduce the permeability of the wall is significant. Moreover, gelatine (an animal protein) has been banned in the European skin care markets due to the possibility of developing the Bovine Spongiform Encephalophthy.[97] Hence, it is essential to find alternative water soluble, amphoteric polymers to replace it. Development of microcapsules that not only can survive the harsh environments of heavy-duty liquid/fabric-softener/detergents systems, but are also capable of releasing fragrance in a controlled fashion is required.

1.4.2 Microcapsules in Food

Microencapsulation has been used in the food industry to enhance or alter the appearance, improve nutrition or prolong food shelf-life.[17] Reducing permitted levels of food additives and replacing chemically derived substances with alternatives perceived to be of natural origin becomes increasingly desirable. One of the commonly encapsulated ingredients are flavours, as they are volatile and sensitive to air and light which means microencapsulation

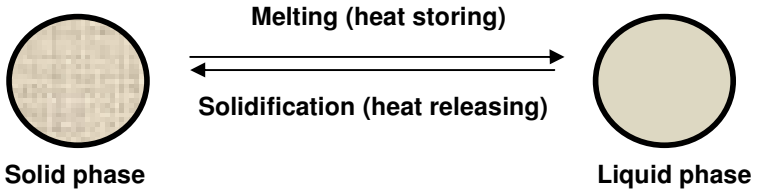
offers an option of converting liquid flavours to a solid form, and protects the ingredient from air, light and evaporation. Examples are lemon oils,[99] peppermint oils,[100] onion and garlic oils,[101] spice oleoresins and whole spices.[102, 103]

1.4.3 Cell Microencapsulation

Cell encapsulation is a strategy to entrap live cells within a semi-permeable membrane.[104] The membranes are expected to be permeable for transporting nutrients essential for cell survival, but do not allow the transport of molecules larger than a desired critical size.[105] Cell encapsulation has been carried out since 1964 when T. M. S. Chang first used ultrathin polymer membrane microcapsules for the immune protection of transplanted cells and introduced the term "artificial cells" to define the concept of bioencapsulation.[18]

1.4.4 Microencapsulation of Phase Change Materials (PCM)

A phase change material is a substance with a high heat of fusion which enables it to store and release a large amount of energy upon phase changing between solid and liquid (**Scheme 12**); thus, PCMs are classified as latent heat storage (LHS) units.



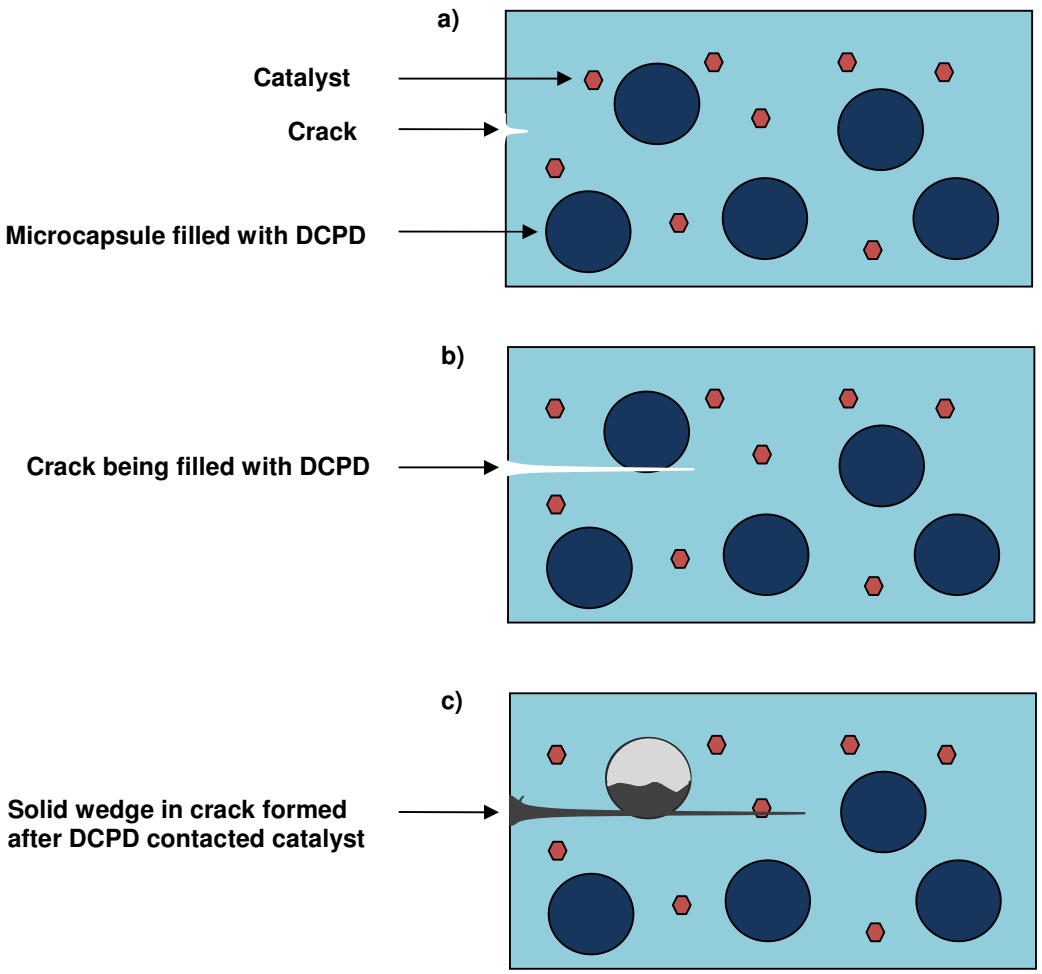
Scheme 12. Schematic representation of phase changing process.

Microencapsulated PCMs have been most commonly used in textile industry; in so doing, the fibre and textile can possess automatic acclimatising properties,[106] and the textiles which

have these properties are often referred as a "smart textile". Microencapsulated PCMs has also been used in solar energy systems,[107, 108] buildings,[109] greenhouses,[110] and to protect heat-sensitive parts of missiles and spacecrafts.[111]

1.4.5 Microencapsulation of Self-healing Materials

Recently, there has been growing interest in encapsulation of self-healing materials.[110] Such materials have the built-in ability to partially repair damage, thereby prolonging their useful service life.[112, 113] In 2001, the first encapsulated self-healing material was reported by White *et al.* in Nature,[114] where a monomer contained in the microcapsules was released when a microcrack occurs in the material, and polymerization of the monomer is triggered by contact with the embedded catalyst to fill the crack. A schematic diagram is shown in **Scheme 13** where a typical self-healing process is illustrated. Microcapsules are ruptured by the propagating crack fronts resulting in release of the healing agent into the cracks by capillary action. In the process below, dicyclopentadiene (DCPD) is the healing agent, and catalyst is bis(tricyclohexylphosphine) benzylidine ruthenium (IV) dichloride (Grubbs' catalyst).



Scheme 13. Schematic representation of the self-healing process by microencapsulated material, a) crack occurs, b) microcapsules containing healing agent ruptured, c) healing agent releases and filled the crack.[115]

1.5 Release Mechanism of Microcapsules

The microencapsulation technique enables, in principle, the core material to be released at the right time and at a controlled rate. The release rate of core content of microcapsules is determined by many factors:[97]

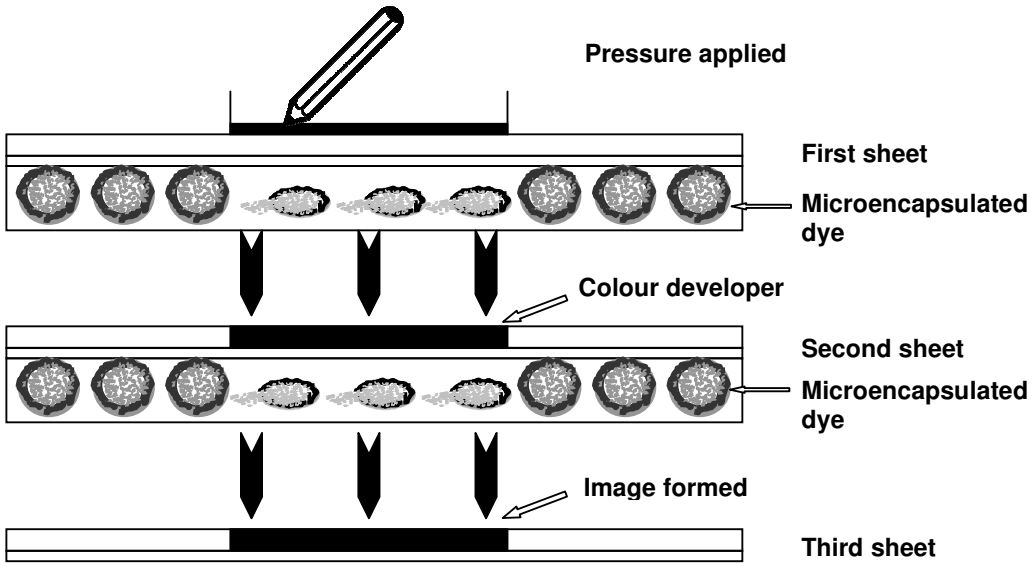
- Density of the microcapsules wall,
- crystallinity and cross-linking of the wall material,
- size of the microcapsules,
- wall thickness of the microcapsules,
- mechanical properties of the microcapsules,
- structure of the microcapsules,
- temperature of the storage environment,
- pH of the storage media,
- moisture of the environment,
- solvent system used during the particle formulation.

Previous studies[97] have shown that the release mechanisms are primarily governed by the type of the polymer wall used and the core materials. In the paragraphs below some of the important mechanisms are discussed in details.

1.5.1 Rupture

The direct exertion of pressure or shear force during application of the product causes rupture of the wall and release of active materials. Based on the mechanical strength test,[41, 116] the rupture strength of microcapsules is inversely proportional to the size of the microcapsules,[116] and it can be controlled and modified during the formulation phase of capsules preparation. Key parameters include the degree of cross-linking and the core/wall ratio.[97] Carbonless copying paper was one of the first commercial microencapsulation products, where rupture is used as the release mechanism to deliver the core content of the microcapsules. As shown in **Scheme 14** the back of the first sheet is coated with micro-encapsulated dye. The top of the middle sheet is coated with a colour developer that quickly

reacts with the dye to form a permanent mark and the back of the middle sheet is also coated with the encapsulated dye. The bottom sheet is coated on the surface with the colour developer with no coating applied to the back side.



Scheme 14. Schematic representation of the microencapsulated dye in carbonless copy paper.

Other products that deliver the encapsulated product *via* rupture are fragrance capsules coated to a magazine insert.[97] Research has been carried out on microcapsules containing tooth whitening ingredients embedded in the tooth pastes that are ruptured by an applied shearing force when brushing.[117]

1.5.2 Diffusion

Diffusion is a net transport of molecules from a region of high concentration to one of low concentration by random molecular motion.[118] Diffusion occurs in microcapsules since the microcapsules walls may function as a semi-permeable membrane which allows the

molecules of the core material to move through the membrane. Due to the very large surface area per unit volume of microcapsules, controlled release is frequently accomplished through diffusion processes.[119]

The diffusion process is driven by a concentration gradient, hence the core material must dissolve at the high concentration side of the membrane, and diffuse through the film driven by a concentration gradient.[118] Diffusion processes can be described using Fick's law[120] of diffusion.

The diffusion rate of the core material through the microcapsules wall is determined by several factors.

- Size of the microcapsules,
- Shape of the microcapsules,
- polarity of the core material,
- solubility of the core material in the environment,
- cross-linking and the crystallinity of the microcapsule wall.[100, 121-124]

Other factors include the weight ratio of the wall material to the core material, and temperature of the environment.[100] Studies have also shown that the thickness of the membrane controls the release rate of the core material.[125]

1.5.3 Dissolution

Controlled release can be achieved by destroying the wall through dissolution.[126] The solubility of the wall is of particular concern in both food and pharmaceutical applications

where the capsules need to be digested. Varying the pH in the system can trigger the transition from insoluble to soluble forms of the wall and lead to subsequent release of core material. Changes in the surrounding environment, such as increasing humidity level can dissolve water soluble wall materials.[126]

1.6 Characterization of Microcapsules

Formulation and process parameters of the described preparation techniques will strongly affect the performance of the microcapsules. A precise characterization of the physicochemical parameters is important in order to develop a product of high quality. The properties of the microcapsules that have been usually characterized include the mechanical properties, average particle size and size distribution, morphology, wall thickness, and release rate. The methods are discussed in detail as follows.

1.6.1 Mechanical Properties

Sufficient mechanical strength was found to be one of the primary factors that need to be taken into consideration for production, handling and application of microcapsules. Thus, precise evaluation of the rupture force, or rupture stress, of the microcapsules is essential for delivery of the core content.

1.6.1.1 Mechanical Properties of Ensembles of Microcapsules

Numerous techniques are available for characterizing the mechanical properties of the microcapsules.

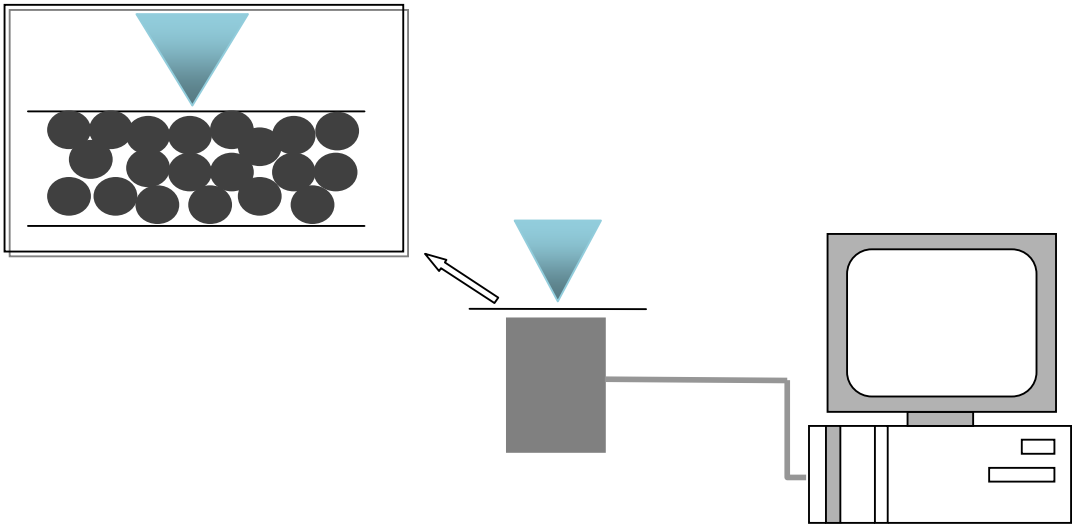
1.6.1.1.1 Compressing between Two Plates

Compressing multiple microcapsules is achieved by placing the microcapsules on one plate and bringing a plate down with increasing force until the microcapsules break (**Scheme 15**).[48, 127] The average rupture force can be calculated subsequently.

1.6.1.1.2 Osmotic Pressure

For semi-permeable microcapsules, an osmotic pressure test has proven to be a simple and quantitative method of rapidly assessing the strength of a large number of microcapsules.[128]

However, due to the inhomogeneity of the microcapsules which attributes to different mechanical strengths, the inability of providing information of individual microcapsules becomes the significant drawback of these techniques.[129]



Scheme 15. Schematic representation for characterizing the mechanical properties of microcapsules by compression.[48]

1.6.1.2 Mechanical Properties of Single Microcapsules

1.6.1.2.1 Micropipette Aspiration

Micropipette aspiration is used to evaluate the mechanical properties of a single microcapsule. [130] The deformation of the particles can be obtained by measuring the pressure difference between inside and outside the pipette when a single microcapsule is aspirated by the pipette. However, it is difficult to measure the rupture strength of the microcapsules since the technique can not generate large deformation of single microcapsules.

1.6.1.2.2 Atomic Force Microscope (AFM)

The deformation of a microcapsule under applied load can be characterized by using atomic force microscopy (AFM).[131] However, to accurately control the force probe with a sharp tip on one single microcapsule is very difficult and time consuming.

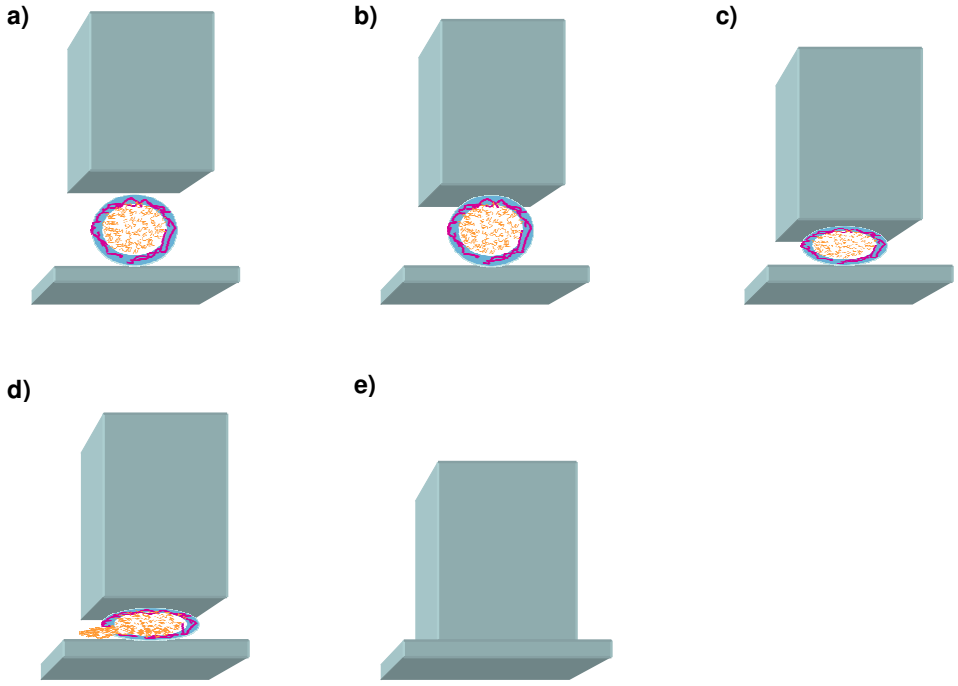
1.6.1.2.3 Texture Analyser

A texture analyser which, consists of a stress gauge, has also been utilised for assessing the mechanical properties of single large particles (> 500 μm).[132] The uniaxial compression of single particles provides an accurate measure of a particle's resistance to compressive force. However, the technique is not sensitive enough to characterise smaller microcapsules.

1.6.1.2.4 Micromanipulation

Recently, a novel micromanipulation technique has been developed by Zhang *et al*.[133, 134] It offers the ability to determine the rupture force, rupture stress, and deformation at rupture of single microcapsules (1 μm-1 mm). The basic concept for micromanipulation is to compress a single microcapsule by a glass probe which is connected to a force transducer that is

programmed to travel downwards to compress the microcapsule. The force transducer is connected to a data acquisition card where the voltage generated from the transducer due to compression of the microcapsule will then be converted to force. **Scheme 16** shows a glass probe which is attached to a force transducer (not shown), and travels down to compress one single microcapsule. The micromanipulation technique has been demonstrated to be very powerful to characterize the mechanical properties of a wide range of biological and non-biological materials, including cells,[135] yeast,[136] micro-crystals,[137] microspheres,[138] and microcapsules.[134]



Scheme 16. Schematic representation of the side view of compressing one single microcapsule using micromanipulation, a) probe moving in the air before it has made contact with the microcapsule, b) probe touches the microcapsule, c) probe compresses the microcapsule, d) the microcapsule ruptured, e) the microcapsule has been completely squashed and the probe touches the glass slide.

1.6.2 Particle Size and Size Distribution

There are many ways to evaluate the particle size and size distribution of microcapsules. One of the most direct means is to use an optical microscope in conjunction with image analysing software.[139, 140] However, it is time consuming and the accuracy of the result is limited by the number of microcapsules measured. A more accurate and quicker way to evaluate the size of the microcapsules is laser diffraction technique on a dispersion of microcapsules.[141] Information about particle size distribution is obtained through measurements of scattering intensity as a function of the scattering angle.[141] The laser diffraction technique can also be used to study the stability[142] (aggregation behaviour) of the microcapsules.

1.6.3 Morphology

The morphology of microcapsules depends on the deposition process of the shell.[26] Scanning electron microscope (SEM)[143] has been used to evaluate the surface morphology of microcapsules. This technique can analyse samples ranging in size from nanometre to centimetre scale. It can produce very high-resolution images of a microcapsule wall surface, revealing details which are down to nm in size.[143] Information is obtained by scanning a specimen with a high-energy beam of electrons in a raster scan pattern. Signals containing information about the surface morphology and composition are received from the electron interacting with the sample atoms. However, for SEM, sample scanning must be performed under high vacuum condition, which may cause deformation and even destruction of the microcapsule wall or loss of volatile core material. Also, the morphology of the microcapsules might be disturbed by sample preparation, *i.e.* coating with gold to avoid specimen charging. To overcome those limitations, environmental scanning electron microscope (ESEM)[144] was introduced. It is a new innovation in SEM specifically designed to study wet, oil bearing, or insulating materials. Its primary advantages lie in permitting

microcapsules to be examined through a range of different pressures, temperatures and humidity. ESEM has been demonstrated to be very powerful technique.[145-148]

1.6.4 Wall Structure and Thickness

TEM uses a beam of electrons to transmit through an ultra thin specimen, interacting with the specimen as they pass through and forming an image. The specimen must be extremely thin (approximately 100 nm) for the electrons to pass through it. Hence, the microcapsules are normally sampled by fixing them into resins, and this section is then cut by ultra microtome.[149]

1.6.5 Release Rate

Release rate of the microcapsules can be evaluated by different techniques depending on their release mechanisms. Thermal gravitational analysis (TGA) is one of the techniques used to evaluate the release behaviour of microcapsules, which is triggered by heat.[150, 151] UV/Vis spectrophotometers is another technique that monitors the release rate by measuring the concentration of the core material or one representative component of the core material, which is released from the shell.[152, 153] However, this technique is restricted to substances that absorb UV/Vis light. This limitation can be overcome by using gas chromatography.[154, 155]

1.7 Conclusion

The literature review reflects the benefits of using the encapsulated perfume oil in consumer products. It is not only able to protect the active ingredients from the environment, preventing potential reactions with the products, and reduce evaporation of the volatile components. In addition, it can deliver the perfume oil in a controlled manner. Since a perfume oil is a mixture of different components, some of which are very volatile, it is likely that those ingredients are lost through the pores of microcapsule wall during the encapsulation process and storage stage. Hence, encapsulation of perfume oil with a very compact and less permeable microcapsule wall is essential in order to maintain the quality of the products.

In situ polymerization is one of the most widely used methods for microencapsulation. It is simple, and can be tailor made accordingly by changing the process variables to encapsulate the material of interest. Moreover, the polymer wall needs to be highly cross-linked and compact. With careful selection of encapsulation conditions and materials, high encapsulation efficiency can be achieved. Melamine formaldehyde polymer is one of the most commonly used wall materials formed by *in situ* polymerization. Its high acid and alkaline and thermal resistance, highly cross-linked wall structure, appropriate mechanical strength, and low cost have lead its use in diverse applications. The properties of melamine formaldehyde microcapsules made from *in situ* polymerisation are affected by many factors. It was found that the F/M molar has a direct control of the wall thickness, mechanical properties, and leakage of the microcapsules. The particle diameter can be affected by the stirring rate and the viscosity of the dispersed phase. In addition, the morphology and wall thickness can be altered by using different emulsifiers and wall formation times, respectively.

In order to achieve controlled and accurate delivery of perfume oils, understanding the release mechanism is essential. The release mechanism is primarily governed by the wall material and the core material. The delivery is very dependent on the mechanical properties of the microcapsules in particular the rupture.

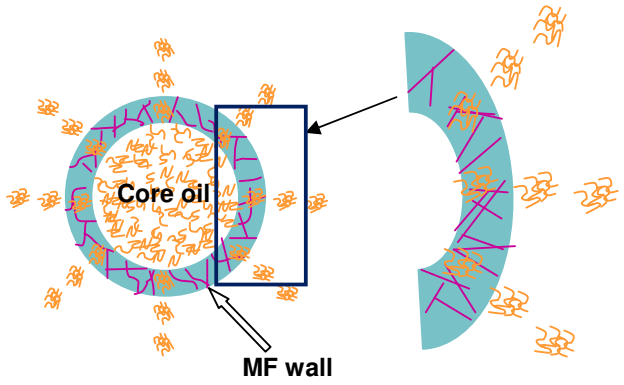
Understanding the mechanical properties of microcapsules is very important for processing, handling and end-use applications. A series of current available techniques to evaluate the mechanical properties of microcapsules has been reviewed, and it was suggested that single particle compression technique provides the most reliable and useful results. Other techniques to evaluate the particle size and size distribution, morphology, wall structure and thickness, and leakage were also reviewed.

To summarise, the research scope of the current work is to characterize and reduce the leakiness of the melamine formaldehyde microcapsules. The formulations and processes conditions chosen should be cost effective, simple and easy to scale up. The properties of the resulted perfume microcapsules should be suitable for a series of processes from manufacturing to end application.

1.8 Objectives

1.8.1 The Challenge

Microcapsules formed from an *in situ* polymerization of melamine and formaldehyde have a size in the range 10 – 80 µm. The microcapsules contain a core oil of short chain hydroxylated organics with molecular weight ~ 250. The problem that occurs with these microcapsules is that the hydroxylated oil leaks out from the microcapsules. Schematic representation is shown is **Scheme 17**.



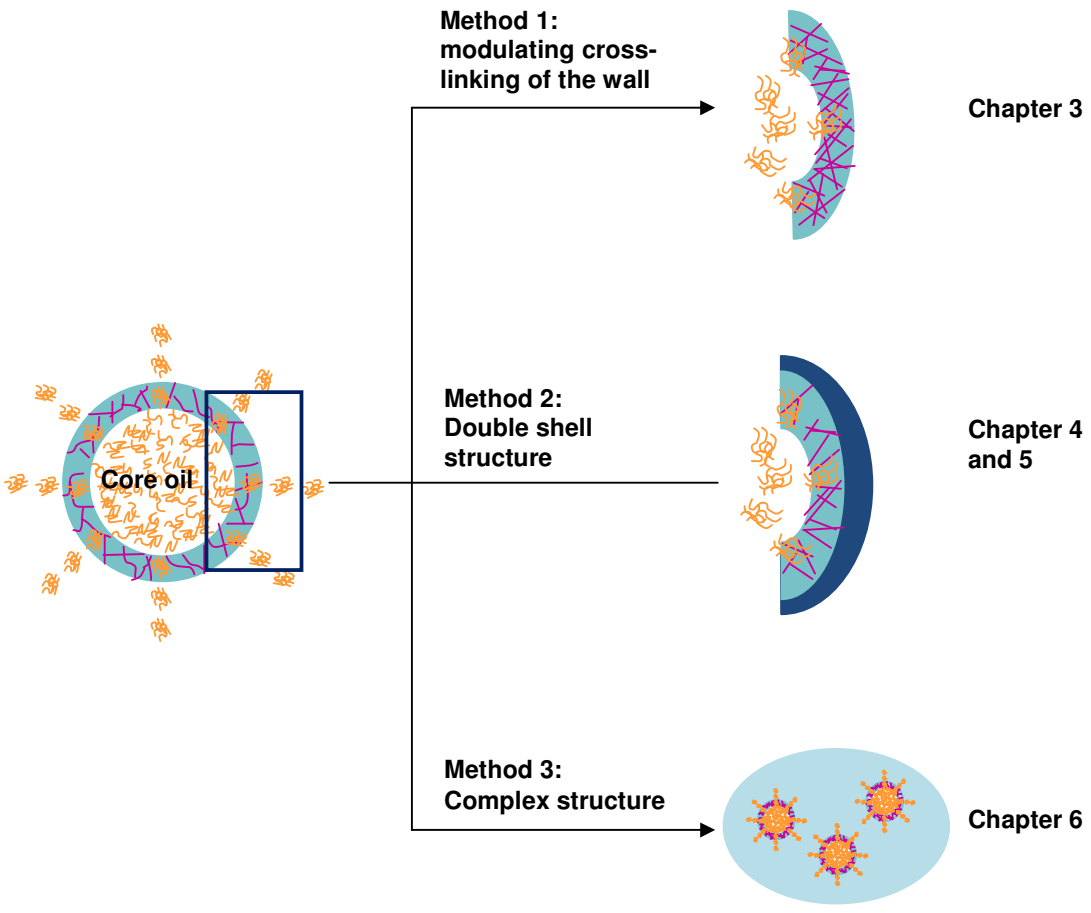
Scheme 17. Schematic representation of core oil leaking through the microcapsules wall.

1.8.2 Proposed Solution

The objective of the research described in this thesis is to reduce/eliminate the leakage of the perfume oil of the melamine formaldehyde microcapsules and produce microcapsules with desirable mechanical properties, *i.e.* is to ensure the microcapsules are robust enough to survive the handling and shipping process, whilst are easily ruptured when the product is being used. We are interested in reducing the leakage from several approaches:

1. Due to the toxicity of the formaldehyde, to minimise the amount used in the formulation is required. In addition, to investigate the effect of formaldehyde on the properties of the MF microcapsules (**Chapter 3**).
2. Reducing the permeability of the microcapsules by producing a double shell structured wall (**Chapter 4** and **5**).
3. Reducing the leakage of the microcapsules through the production of complex-structured microcapsules i.e. embedding the MF microcapsules into a larger microcapsule (**Chapter 6**).

A schematic presentation of these difference approaches is given in **Scheme 18**.



Scheme 18. Schematic representation of the difference approaches for reducing the leaking of the oil from the microcapsules.

1.9 Overview of Thesis

An overview of this thesis is summarised:

Chapter 2 An overview of the characterisation techniques is described in detail. The main characterisation technique used in this study including gas chromatography, micromanipulation, static light scattering, scanning electron microscopy (SEM), focused ion beam (FIB) and transmission electron microscopy (TEM).

The results presented in this thesis are divided into four chapters which concerns three different approaches of reducing and characterizing the leakiness of the microcapsules. **Chapters 3-6** are the results chapters of this thesis.

Chapter 3 This chapter detailed the chemical modification of the melamine formaldehyde (MF) microcapsules (**Figure 7**) and reducing the content of formaldehyde used in the conventional formulation. The properties of the microcapsules such as average diameter, morphology, wall thickness, mechanical properties and leakage produced by using F/M molar ratio between 0.2-0.49 were compared with those formed at F/M molar ratio 2.3 (conventional formulation).

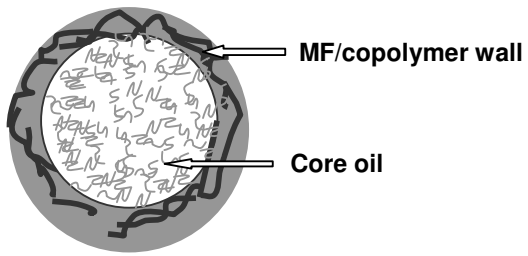


Figure 7. Schematic representation of MF microcapsule.

Chapter 4 This chapter presents a new dual strategy for controlling the leakage of the microcapsules by producing organic/inorganic double shell composite microcapsules with ripened $CaCO_3$ nanoparticulate wall as the outer shell and MF/copolymer as the inner shell (**Figure 8**). The double shell structure was examined using the EDX analysis on ultra-microtome section of the microcapsules. The properties of these double shell composite microcapsules were also characterised, and compared to the non-composite material microcapsules: inorganic ripened $CaCO_3$ nanoparticulate microcapsules and organic MF/copolymer microcapsules. The effects of the $CaCO_3$ nanoparticles ripening process on the properties of the microcapsules was also examined.

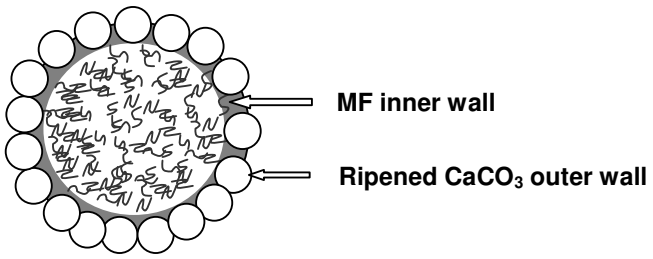


Figure 8. Schematic representation of double shell composite microcapsule.

Chapter 5 This chapter is about engineering the mechanical and physical properties of the double shell composite microcapsules. The effect of the parameters *i.e.* MF polymerization reaction time and concentration of the aqueous $CaCl_2$ and Na_2CO_3 used for the $CaCO_3$ nanoparticle ripening process were studied by varying the MF reaction time (4, 8 and 24 hours) and the concentrations of the aqueous $CaCl_2$ and Na_2CO_3 concentration (1.0,

1.5 and 2.0 M). The properties of these double shell composite microcapsules were characterized and compared.

Chapter 6 This chapter describes a different approach to reduce the leakage of the microcapsules through the production of calcium shellac matrix containing MF microcapsules or unripened nanoparticulate $CaCO_3$ microcapsules (complex microcapsules) (**Figure 9**). The inner structure of these microcapsules was studies by FIB and SEM. Other physical properties like morphology, mechanical properties and leakage were also illustrated.

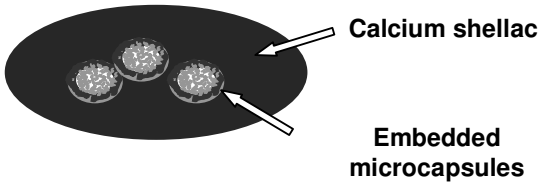


Figure 9. Schematic representation of calcium shellac matrix containing MF microcapsules or unripened nanoparticulate $CaCO_3$ microcapsules.

Chapter 7 An overall summary of the experiments completed and the results obtained, followed by the future work.

Chapter 2

Introduction of the Experimental Techniques

Abstract

This chapter describes the techniques used for evaluating the properties of the microcapsules. The experimental technique used to characterize the leakage and encapsulation efficiency of the microcapsules was gas chromatography (GC). A novel micromanipulation technique for compression of single particles to rupture was used to evaluate the mechanical properties of the microcapsules. The physical properties such as the average diameter and size distribution, morphology and wall thickness of the microcapsules were analysed by using static light scattering (SLS), scanning electron microscope (SEM) and transmission electron microscope (TEM), respectively. Details of these techniques are discussed in this chapter. The techniques for preparing microcapsules are presented in later chapters.

2.1 Gas Chromatography (GC)

Gas chromatography is a chemical analysis technique for separating mixtures of volatile chemicals. A GC set-up is shown in **Figure 1.**[156] A gas chromatograph uses a flow-through narrow tube, known as the column, through which the different chemical constituents of the sample pass in a gas stream (carrier gas or mobile phase). Depending upon their chemical and physical interactions with the column, called a stationary phase, the volatiles pass at different rates. Mixtures are separated in the column and exit the column at different times (retention time).[157] A detector is used to monitor the outlet stream from the column. If known constituents are analysed, then the retention time of complex mixture can be used to identify

what is in the mixture and the area under each peak can be used to estimate mixture composition.[158]

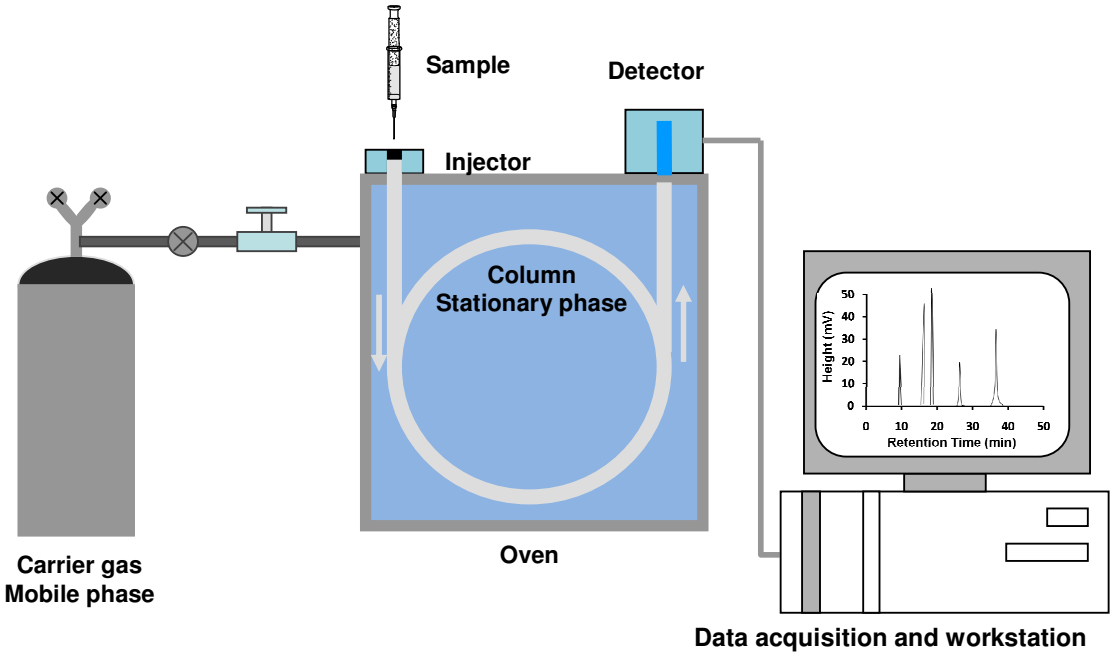


Figure 1. Schematic representation of gas chromatography.

2.1.1 Carrier Gas

In gas chromatography, the mobile phase is an inert carrier gas. Commonly used gases include nitrogen, helium, argon, and carbon dioxide. The choice of carrier gas is often dependent upon the type of detector which is used. The carrier gas system also contains a molecular sieve to remove water and other impurities.[159] The carrier gas used in the experimental work presented in this thesis is helium.

2.1.2 Columns

The column used in the GC studies used in this thesis is a capillary column. A capillary column possesses a very small internal diameter, on the order of a few tenths of a millimetre,

and lengths are normally between 20-100 meters.[160] They can be one of two types; wall coated open tubular (WCOT) or support-coated open tubular (SCOT).[161] Most capillary columns are made of fused-silica with polyimide outer coating. These columns are mechanically flexible, so a column can be wound into a coil.

2.1.3 Sample Injection Port

The injection port provides the means to introduce a sample into a continuous flow of carrier gas. It is a piece of hardware attached to the column head. The injector can be used in one of two modes; split or splitless (as shown in **Figure 2**).[162] The injector contains a heated chamber containing a glass liner into which the sample is injected through the septum. The carrier gas enters the chamber and can leave by three routes (when the injector is in split mode). The sample vapourises to form a mixture of carrier gas, vapourised solvent and vapourised solutes. A proportion of this mixture passes onto the column, but most exits through the split outlet.[163]

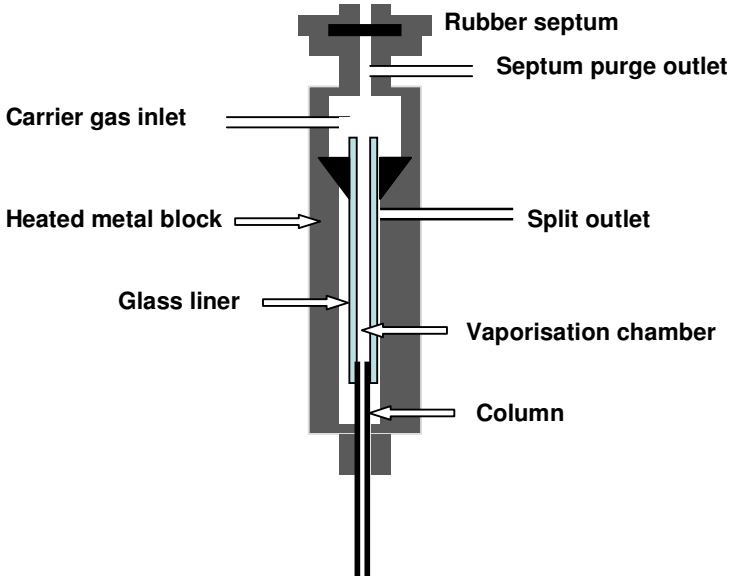


Figure 2. Schematic representation of sample injection port.

2.1.4 Flame Ionization Detector (FID)

Support gases for flame the ionization detector are hydrogen and air. The effluent from the column is mixed with the support gases, and ignited. Organic compounds burning in the flame, produce ions and electrons which facilitate a current through the flame when a electrical potential is applied at the burner tip, and a collector electrode is located above the flame. FIDs are mass sensitive rather than concentration sensitive, giving the advantage that changes in mobile phase flow rate do not affect the detector's response.[164] A schematic representation is shown in **Figure 3**.

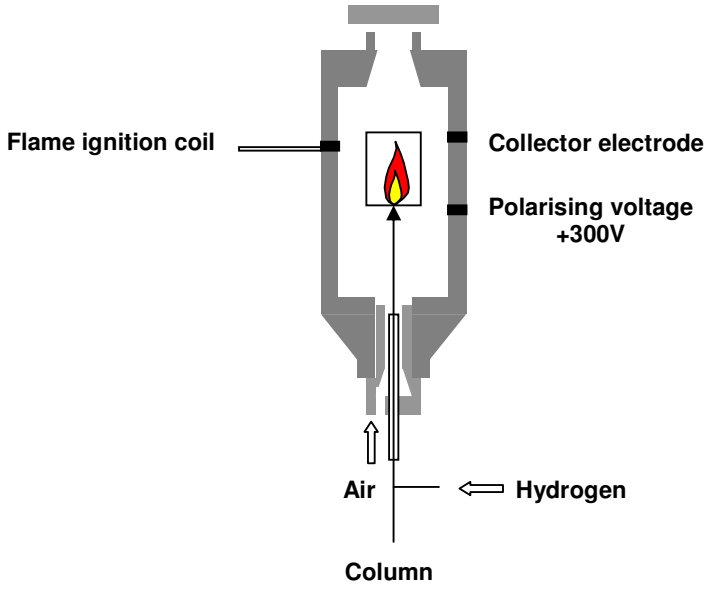


Figure 3. Schematic representation of a flame ionization detector.

2.1.5 Output

A typical GC trace is presented in **Figure 4**, where the y axis is the peak height (mV), and x axis is the retention time (min).

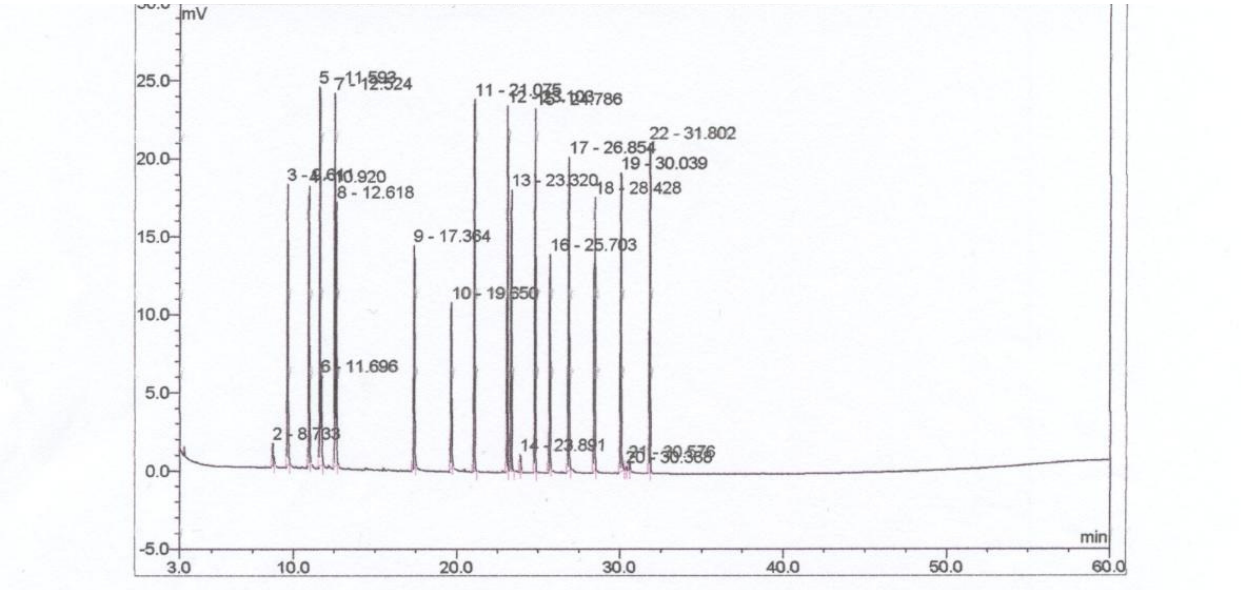


Figure 4. A typical GC trace and data of a mixture of 22 components (perfume oil).

2.2 Micromanipulation

2.2.1 Compressing a Single Microcapsule

The micromanipulation technique has been demonstrated to be very powerful tool for the characterization of the mechanical properties of a wide range of biological and non-biological materials, including yeast,[136] bacteria,[165] animal cells,[166] and microcapsules.[116, 134]

A glass probe mounted on a force transducer (Model 405A, Aurora Scientific Inc., Canada) was positioned perpendicular to the glass slide as shown in **Figure 5a**. The microcapsules in an aqueous dispersion are dried on the glass slide, and observed through side and bottom-view cameras. A single microcapsule is compressed by the glass probe travelling at 2 μm s^{-1}. The voltage output generated by the transducer due to compression of the microcapsules is recorded through a data acquisition card in a personal computer. From the sensitivity of the

transducer, the voltage is converted to force, hence the rupture force of the microcapsules is determined.

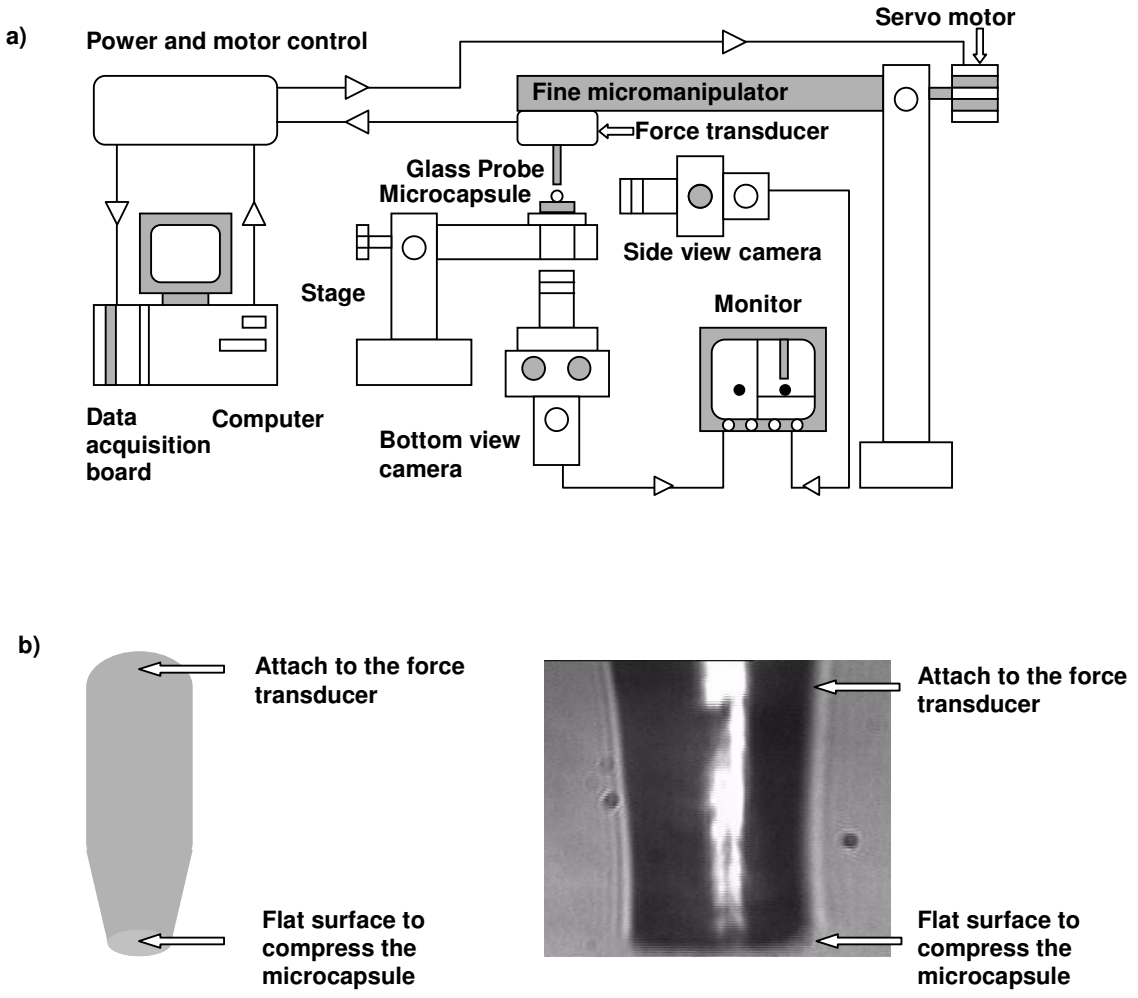


Figure 5. a) Schematic diagram of the micromanipulation rig, b) Glass probe for compression of single microcapsules.

2.2.2 Preparation of Transducer Probes

A borosilicate glass capillary with 1.0 mm O.D. and 0.58 mm I. D. is placed on a glass puller (Micro Forge, MF-900 Narishige, Japan) and heated and pulled to produce a glass probe with a taper shape as shown in **Figure 5b**. The resulting glass probe is further ground on the contact surface using a grinding machine (EG-40, Narishige, Japan) for 24 hours. After grinding, the glass probe with a flat end surface was ready for attaching to the force transducer using superglue. The diameter of the glass probe is required to be at least 3 times the microcapsule diameter to ensure the microcapsule can be trapped between two parallel surfaces. The diameter of the glass probe used in this work is between 50 to 100 μm.

2.2.3 Output

A typical relationship of the force imposed on a single microcapsule as a function of the probe moving distance is plotted and shown in **Figure 6**. The distance between 0 and **I** corresponds to the transducer probe moving in the air before it has made contact with the microcapsule. After point **I** the probe touches the microcapsule, and the force imposed on the microcapsule increases until point **II** at which point the microcapsule ruptures. As a result, the force drops to point **III**. The probe continues to compress the debris of the microcapsule (**III**-**IV**) until it touches the slide at point **IV**, afterwards the force increases rapidly as the probe pushes onto the slide.

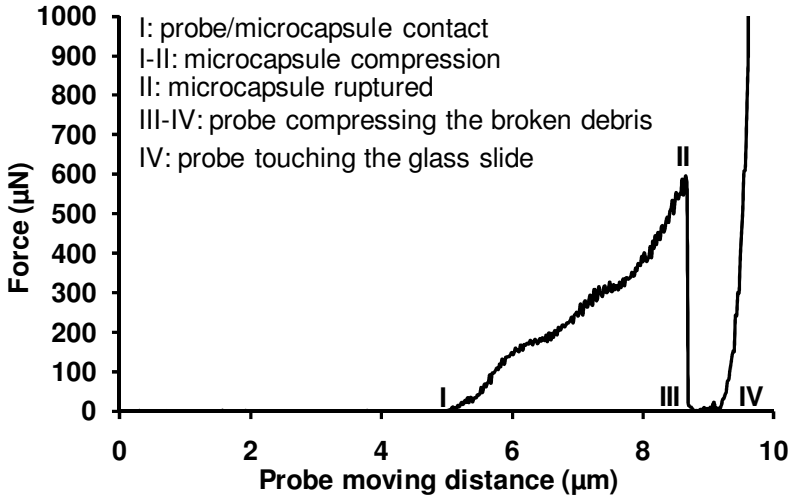


Figure 6. Force vs. probe moving distance for compressing single microcapsules to rupture.

2.3 Static Light Scattering (SLS)

Static light scattering technique[141] is also called laser diffraction. It is used to determine the size distribution of small particles. During the interaction of the laser light with particles, diffraction, refraction, reflection and absorption result in light scattering patterns characteristic for the particle size (as shown in **Figure 7**). If the particle size is considerably bigger than the wavelength of the incident light (for particle sizes from several micrometers upwards), this preferentially results in light scattering patterns caused by diffraction.[142]

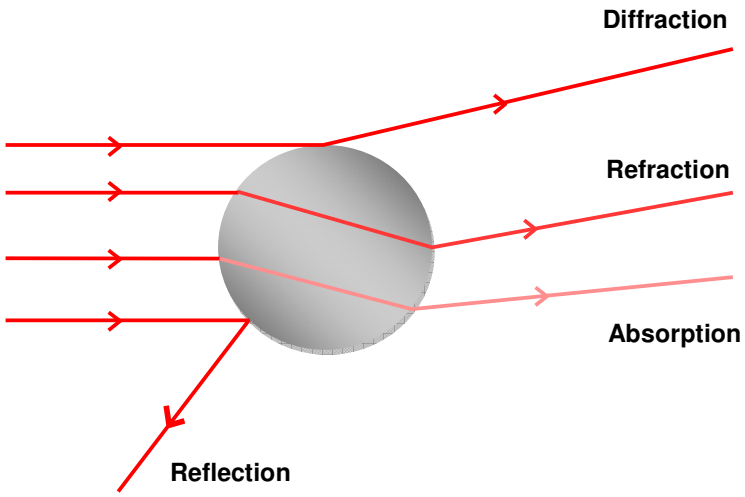


Figure 7. Light scattered by particles.

Information about particle size distribution is obtained through measurements of scattering intensity as a function of the scattering angle.[141] When particles passing through a laser beam, light is scattered at an angle that is directly related to their size.[141] As the particle size decreases, the observed scattering angle increases logarithmically. The scattering intensity is also dependent on the particle sizes. Large particles scatter light at narrow angles with high intensity, whereas small ones scatter at wider angles but with low intensity.[167]

A typical system consists of a laser (**Figure 8**), to provide a source of coherent, intense light with fixed wavelength. A particle dispersion unit, to ensure the sample passes through the laser beam as a homogeneous stream of particles. A large angle detector, to measure the scattered light in a wide range of angles. Some instruments also include back scatter detectors, to facilitate the measurement of small particles.

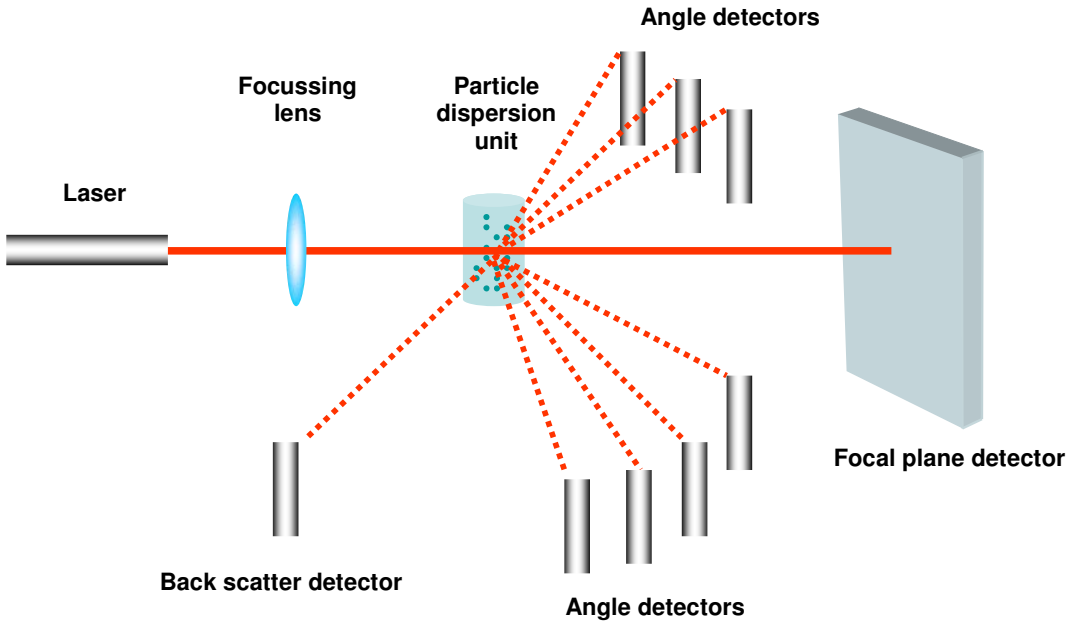


Figure 8. Schematic representation of dynamic light scattering.

2.3.1 Output

A typical size distribution curve of microcapsules in aqueous dispersion is shown in **Figure 9**.

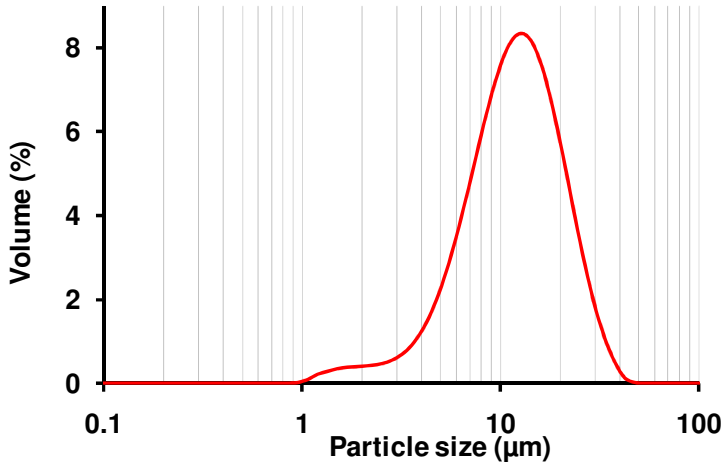


Figure 9. A typical size distribution curve obtained from SLS measurement.

2.4 Scanning Electron Microscopy (SEM)

A beam of electrons is produced at the top of the microscope by an electron gun (**Figure 10**). The beam is condensed by the first condenser lens, and is then constricted by the condenser aperture to eliminating some high-angle electrons. The second condenser lens forms the electrons into a thin, tight, coherent beam and the objective aperture further eliminates high-angle electrons from this beam. A set of coils then scan the beam in a grid fashion, and the final objective lens focuses the scanning beam onto the part of the specimen desired.

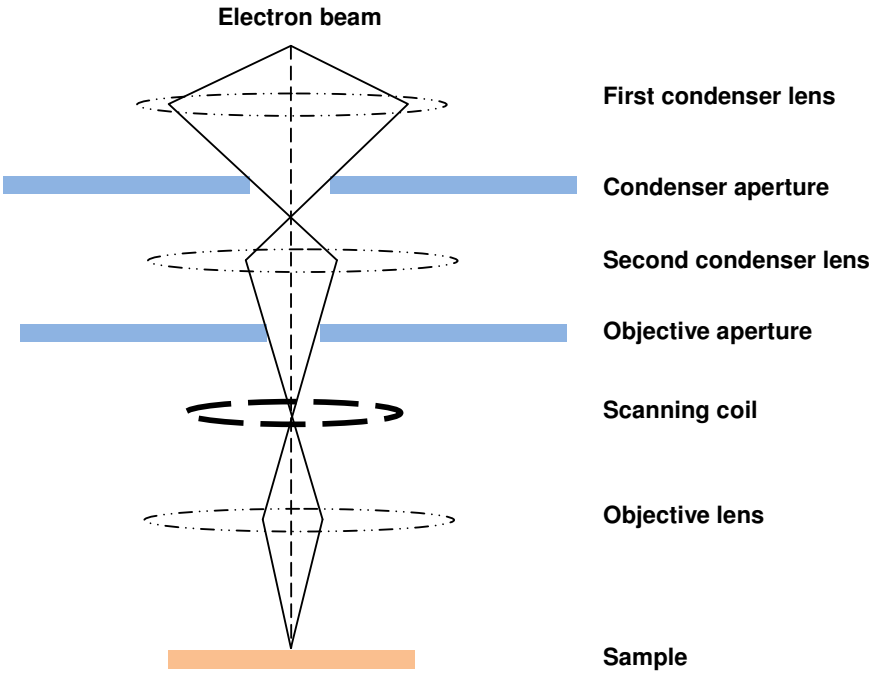


Figure 10. Schematic representation of scanning electron microscope.

Once the beam hits the sample, electrons and X-rays are ejected from the sample (**Figure 11**). The electrons are detected by an Everhart Thornley detector. Secondary electrons are low energy electrons, only those close to the surface exit the sample. Hence secondary electrons are used for topographic imaging. Backscattered electrons have a much higher energy. Production of backscattered electrons varies with atomic number. Higher atomic number elements appear brighter than lower atomic number element, such resulting images shows elemental contrast.[143]

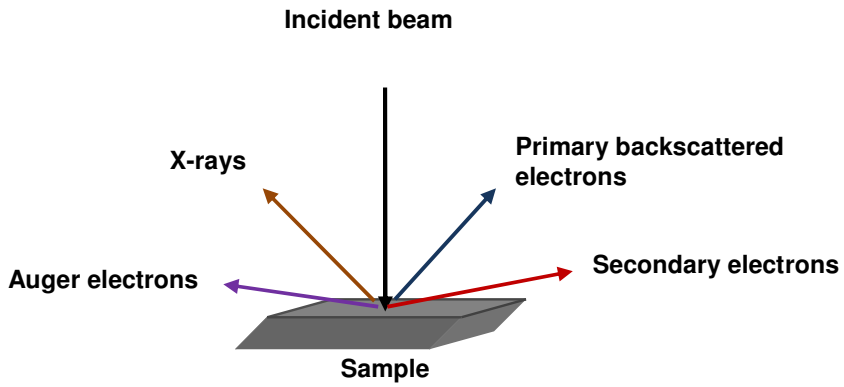


Figure 11. Schematic representation of the interaction between the electron beam and the sample.

2.5 Environmental Scanning Electron Microscope (ESEM)

Conventional SEM requires assessing the samples in high vacuum conditions, which limits its applications in samples such as emulsions, paints and biological tissues. Moreover, the coating can obscure the fine surface detail on some insulators. These problems can now be overcome by using Environmental SEM (ESEM), which permits the imaging of wet systems with no prior specimen preparation.[144]

Not like the Everhart Thornley detector used in SEM, the Environmental Secondary detector used in ESEM can function in non-vacuum environment. The Environmental Secondary detector uses the principle of gas ionization (shown in **Figure 12**).[168] By applying a positive potential to the detector, the secondary electrons emitted from the sample are attracted to the detector. As the electrons accelerate in the detector field, they collide with gas molecules. The resulting ionizations create additional electrons, amplifying original secondary electron

signal, and positive ions. The detector collects the secondary electron signal and passes it directly to an electron amplifier. In nonconductive samples, positive ions are attached to the sample surface as charge accumulates from the beam.[169]

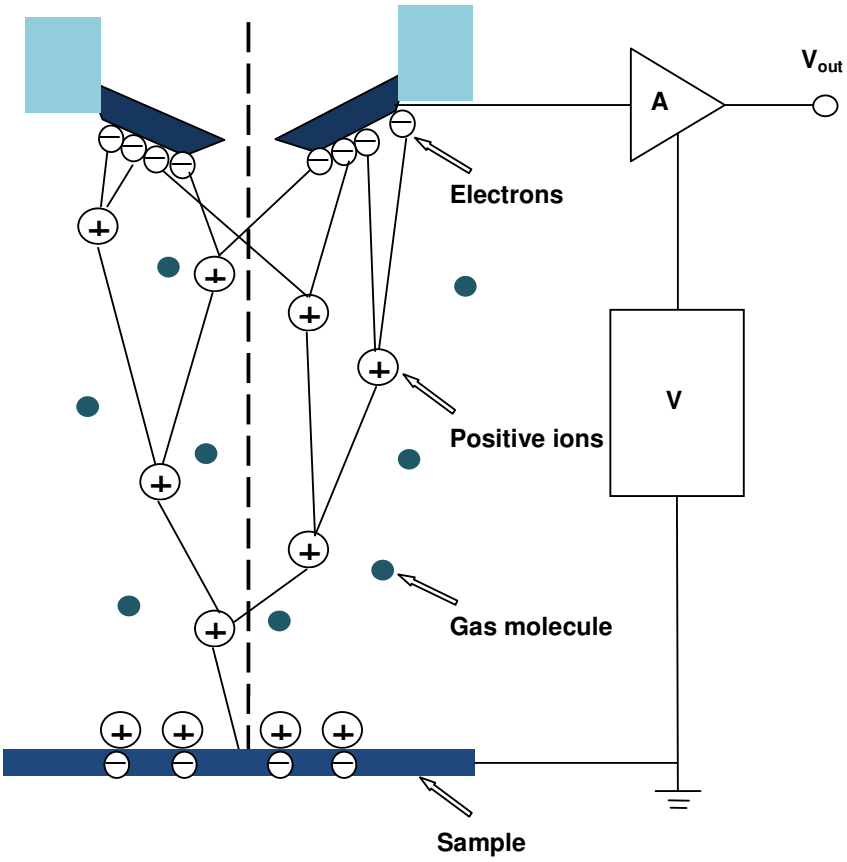


Figure 12. Schematic representation of the Environmental Secondary Detector.

2.5.1 Output

A typical ESEM image of microcapsules is shown in **Figure 13**.

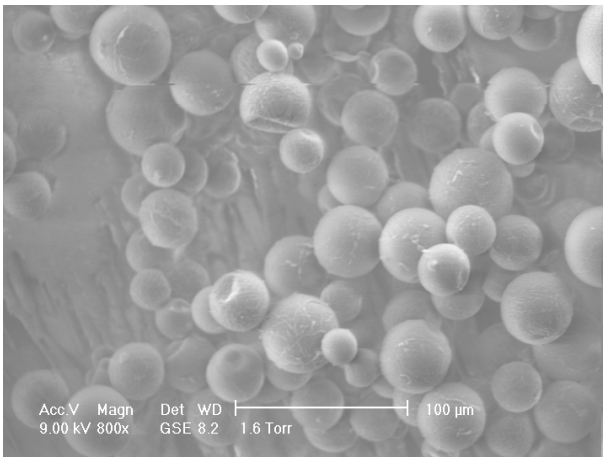


Figure 13. A typical ESEM image of microcapsules.

2.6 Transmission Electron Microscopy (TEM)

An electron gun (**Figure 14**) produces a stream of monochromatic electrons, which is focused to a coherent beam by the use of condenser lenses. The beam is restricted by the condenser aperture, knocking out high angle electrons. The beam strikes the specimen and some of the electrons are transmitted through the sample. These are focused by the objective lens into an image. The objective aperture enhances the contrast by blocking out high-angle diffracted electrons. The image is passed down through the intermediate and projector lenses to magnify the image. The image strikes the phosphor image screen and light is generated, allowing the user to see the image. The darker areas of the image represent those areas of the sample that fewer electrons were transmitted through (they are thicker or denser). The lighter areas of the image represent those areas of the sample that more electrons were transmitted through (they are thinner or less dense).[170] Materials for TEM must be specially prepared to thicknesses which allow electrons to transmit through the sample. The wavelength of electrons is much

smaller than that of light, the optimal resolution attainable for TEM images is much higher than that obtained from a light microscope.[171]

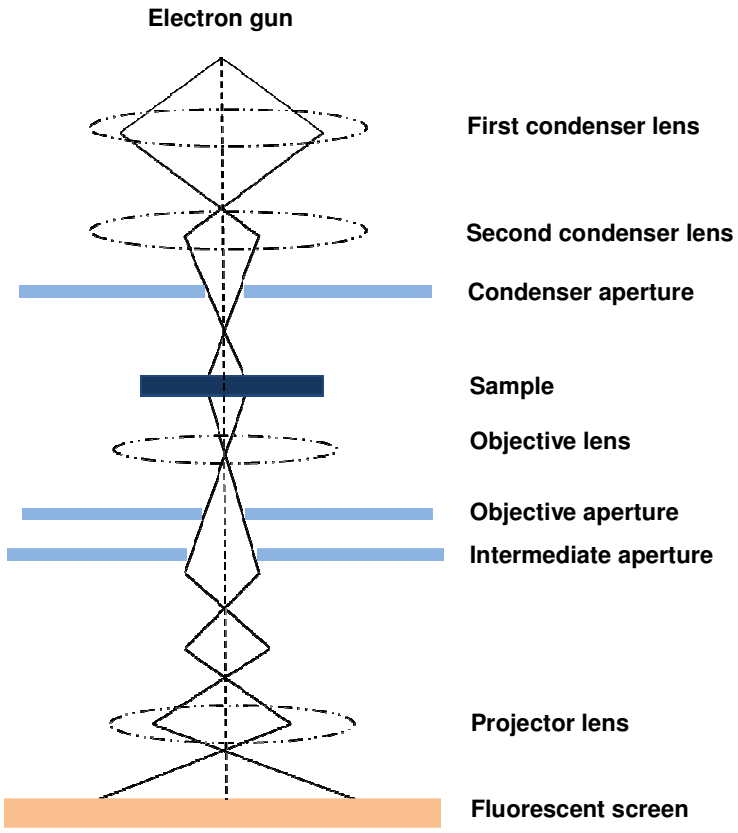


Figure 14. Schematic representation of transmission electron microscope.

Materials examined by TEM require pre-processing to produce a suitable sample. Embedding is one of the common techniques for biological samples. After dehydration, the sample is passed through a "transition solvent" such as ethanol and then infiltrated with a resin. After the resin has been polymerized the sample is thin sectioned (ultrathin sections) and it is then ready for viewing. The sectioning process is carried out using an ultramicrotome with a diamond knife to produce ultrathin slices about 60-90 nm thick.[170]

2.6.1 Output

A typical TEM image of the ultra-microtome section of the microcapsules is shown in **Figure 15**, where the microcapsules have been embedded in a resin, and ultramicrotome sectioned.

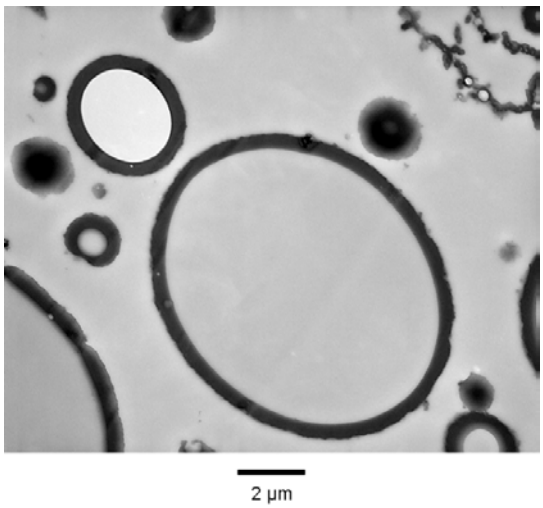


Figure 15. A TEM image of the ultra-microtome section of the microcapsules.

2.7 Focused Ion Beam (FIB)

FIB systems operate in a similar fashion to SEM except, in that rather than a beam of electrons, a beam of ions is focussed that can be operated at high beam currents for site specific milling. Most of the FIB instruments use gallium ion sources, but ion sources based on elemental gold and iridium are also available.[172] The ion beam allows the milling of the sample at localized sites. Material removal occurs by sputtering (as shown in **Figure 16**), which is an atomic scale process. High energy ions from the source impact the sample and eject surface atoms from the sample surface. The ion beam is scanned over a predefined pattern to create desired shape and the machining time scales with increasing surface area of the scan pattern.[173] Nowadays most instruments combine a SEM and FIB column. Generally

the ion beam will be used for milling and the electron beam for imaging. It allows non-destructive imaging at higher magnifications and with better image resolution, and also more accurate control of the progress of the milling.[174]

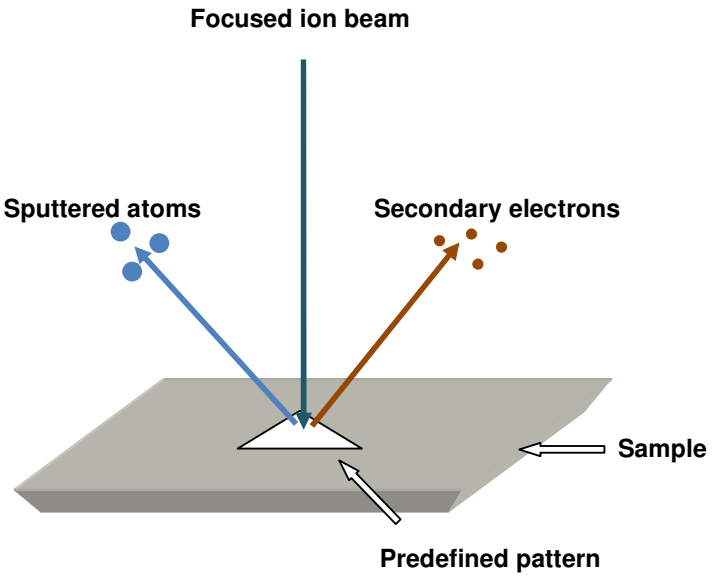


Figure 16. Schematic representation of FIB.

2.7.1 Output

A typical SEM image of a microcapsule being cut by FIB is shown in **Figure 17** (a combination of SEM and FIB techniques).

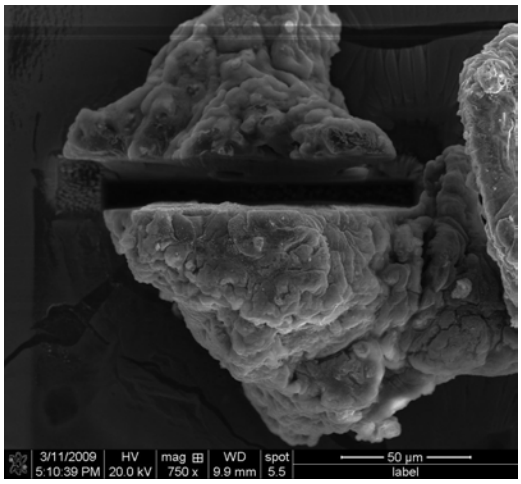


Figure 17. A single microcapsule is cut by FIB over a predefined area.

Chapter 3

Microcapsules with Low Content of Formaldehyde : Preparation and Characterization

This work presented in **Chapter 3** has been published in the following journal paper: Y. Long, D. York, Z. B. Zhang, J. A. Preece, *J. Mater. Chem.* **2009**, *19*, 6882.[175]

Abstract

In this work, an *in situ* polymerization process has been used to produce melamine formaldehyde microcapsules containing an oil-based industrial precursor. Here the microcapsules were produced with a low formaldehyde to melamine molar ratio (0.20-0.49) compared to previous literature reports (2.30–5.50). The properties of the microcapsules such as morphology, particle diameter and distribution, wall thickness, mechanical strength, encapsulation efficiency, and leakiness were characterized, and it was found that the wall thickness and mechanical properties of microcapsules were modulated as a function of formaldehyde to melamine (F/M) molar ratio. The wall thickness of the microcapsules measured by Transmission Electron Microscopy (TEM) increased from 80 ± 1.9 to 308 ± 1.7 nm (285 ± 2.4 % increase) when the F/M molar ratio was increased from 0.20 to 0.49 (145 % increase), the nominal rupture stress of the microcapsules measured by a micromanipulation technique increased from 1.3 ± 0.1 to 4.2 ± 0.4 MPa (223 ± 11.5 % increase), and the percentage leakage evaluated by gas chromatography decreased from 6.7 ± 0.35 % to 2.1 ± 0.19 % (219 % decrease). In contrast, when the F/M molar ratio increased from 0.49 to 2.30 (369 %), the wall thickness of microcapsules only increased by 14 ± 0.8 %, the nominal rupture stress of the microcapsules increased by 66 ± 12.8 % and the leakiness of the microcapsules decreased by 63 %. Thus, it has been shown that significant reduction in the levels of formaldehyde content is possible from previous literature reports, whilst only marginally reducing

the mechanical properties and slightly increasing the leakiness. The encapsulation efficiency is still maintained of ~75%.

3.1 Introduction

Microencapsulation is used, or is been explored to be used, in a diverse number of applications for making functional products, including carbonless copying paper,[176] cosmetics,[177] foods,[178] insecticides,[179] adhesives,[180] and pharmaceuticals.[181] The widespread interest in microencapsulation is due to the functionality it can bestow, such as protection of the active component in a single mixture, mixing of immiscible and incompatible materials, increased environmental stability, conversion of liquids or tacky solids to free flowing powders, and targeting of active ingredients to specific sites.[23] Encapsulation of oil-based materials by amino resin polymers such as melamine formaldehyde (MF) or urea formaldehyde (UF) for consumer products has recently gained much attention due to the possibility of increasing oil shelf-life and targeted delivery.[59, 182]

Typical molar ratios of formaldehyde to melamine in the MF precondensate for microcapsules production reported in the literature are in the range of 2.3 to 5.5.[59, 183, 184] Lee *et al.*[185] has previouly studied the effect of F/M molar ratio range from 2.3 to 5.5 on the properties of the microcapsules, and it was reported that as the F/M molar ratio increased, content of the residual formaldehyde increased, and the reaction reached an equilibrium state earlier. In addition, it was found that the encapsulation efficiency increased with a higher F/M molar ratio and a smoother surface morphology resulted. Whilst the vast majority of the formaldehyde is consumed in the process, the relative

toxicity of this material provides an interest in seeking to reduce the amount that is used. Thus, the aim of this study is to prepare microcapsules with low formaldehyde to melamine molar ratios (**A** = 0.20, **B** = 0.39, **C** = 0.44, **D** = 0.49) and evaluate the morphology, mean particle diameter, particle size distribution, wall thickness, mechanical properties, leakiness, and encapsulation efficiency as compared to microcapsules formed at F/M ratio of 2.30 (Microcapsule **E**). The hypothesis being that when we reduce the F/M molar ratio, the degree of crosslinking in the melamine formaldehyde polymer wall is reduced, and hence the mechanical properties of the microcapsules are altered. It is intended to investigate how the mechanical properties modulate with a reduction in formaldehyde in order to prepare desirable microcapsules using as little free formaldyhyde as possible.

3.2 Experimental

3.2.1 Materials

The core oil is a typical perfume blend of various components, which has a relatively low solubility in water and is used in consumer products. MF precondensate (70 % (aq) w/w, formaldehyde to melamine molar ratio 0.20), and was supplied by British Industrial Plastics Ltd, Birmingham, UK. Formaldehyde (37 % (aq) w/w) was supplied by Sigma-Aldrich, UK and poly (acrylamide-acrylic acid, sodium salt) was supplied by Polymersciences, Inc., US, which were used without further purification.

3.2.2 Preparation of Microcapsules

3.2.2.1 Microcapsule A

An aqueous solution of MF precondensate (2.50 g) and copolymer (0.58 g, poly (acrylamide-acrylic acid, sodium salt) in water (70 ml) was stirred (400 rpm) with a Rushton turbine (Φ 31 mm, in a vessel with standard configuration) for 105 min at pH 4 (adjusted by acetic acid (1 M), monitored by a pH meter) at room temperature. Core oil (9.33 g) was added to the resulting mixture and stirred using a homogenizer (Model L4RT, Silverson Machines Ltd, UK) at a speed of 2500 rpm for 30 min at 15 °C to form an oil in water (o/w) emulsion. The resulting emulsion was stirred at 400 rpm in a vessel (Φ 65mm × 65mm) with a standard Rushton turbine impeller (Φ 31mm) for 30 min at 15 °C, then the temperature was raised to 65 °C, at which the stirring was maintained for 6 hours. The resulting microcapsules dispersion was cooled to 25 °C, and the pH was raised to 10 with the addition of aqueous NaOH (1 M, monitored by a pH meter) to terminate the polymerization reaction. This dispersion was used for all the following analyses except the encapsulation efficiency measurements.

3.2.2.2 Microcapsule B, C, D and E

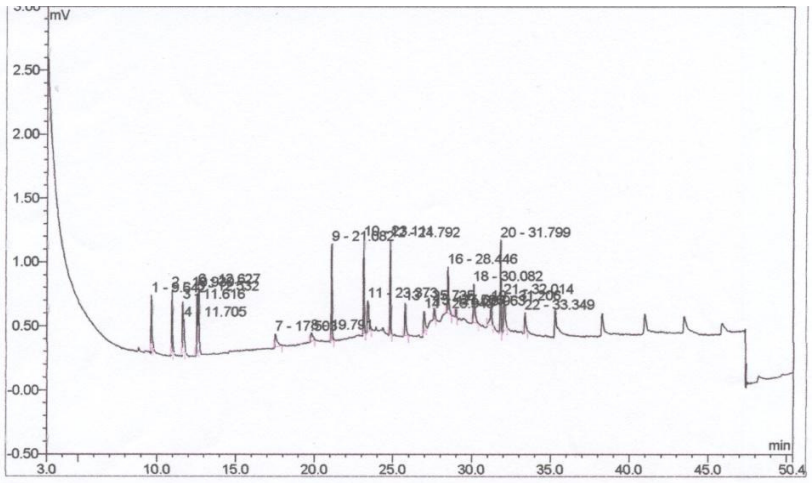
Microcapsule samples **B**, **C**, **D** and **E** were made following the same procedure as microcapsule **A**, with the exception that in the first step an additional quantity of formaldehyde (0.20 g, 0.25 g, 0.30 g, and 2.30 g, respectively) was added to the MF precondensate aqueous solution. The molar ratio of the total formaldehyde content to the melamine content for samples **A**, **B**, **C**, **D** and **E** are 0.20, 0.39, 0.44, 0.49 and 2.30, respectively.

3.2.3 Gas Chromatography

A Trace 2000 series gas chromatogram with a flame ionization detector and 30 m × 0.32 mm ZB5 inferno column was used for data acquisition for the encapsulation efficiency and leakage experiment. Analysis was performed using a Dionex Chromeleon Workstation. The volume of injected samples each was 1µl. The injection port temperature was 250 °C. The temperature ramp for the column was increased by 10 °C/s from 50-300 °C, and held at 300 °C for 35 min. The detection temperature was 300 °C. Helium was used as the carrier gas.

3.2.3.1 Calibration

Perfume oil with concentrations 0.6 mg/ml, 1.0 mg/ml, 2.0 mg/ml, 6.0 mg/ml and 9.0 mg/ml was dissolved in hexane, and analysed by GC. The GC trace for 0.6 mg/ml is shown in **Figure 1**. The GC traces for 1.0, 2.0, 6.0 and 9.0 ml/mg are shown in **appendix A**



No.	Ret.Time min	Peak Name	Height mV	Area mV*min	Rel.Area %	Amount	Type
1	9.64	n.a.	0.430	0.025	4.32	n.a.	BMB*
2	10.94	n.a.	0.504	0.029	5.04	n.a.	BMB*
3	11.62	n.a.	0.407	0.026	4.41	n.a.	BM *
4	11.71	n.a.	0.262	0.018	3.03	n.a.	MB*
5	12.53	n.a.	0.470	0.030	5.11	n.a.	BM *
6	12.63	n.a.	0.510	0.030	5.21	n.a.	MB*
7	17.50	n.a.	0.111	0.019	3.31	n.a.	BMB*
8	19.79	n.a.	0.076	0.012	2.14	n.a.	BMB*
9	21.08	n.a.	0.763	0.046	7.83	n.a.	BMB*
10	23.11	n.a.	0.747	0.044	7.54	n.a.	BMB*
11	23.37	n.a.	0.249	0.027	4.68	n.a.	BMB*
12	24.79	n.a.	0.739	0.041	7.06	n.a.	BMB*
13	25.74	n.a.	0.255	0.023	4.00	n.a.	BMB*
14	26.94	n.a.	0.171	0.019	3.30	n.a.	BMB*
15	27.59	n.a.	0.096	0.008	1.42	n.a.	BMB*
16	28.45	n.a.	0.361	0.031	5.34	n.a.	BMB*
17	28.96	n.a.	0.071	0.004	0.75	n.a.	BMB*
18	30.08	n.a.	0.303	0.033	5.58	n.a.	BMB*
19	31.21	n.a.	0.174	0.021	3.66	n.a.	BMB*
20	31.80	n.a.	0.726	0.044	7.49	n.a.	BMB*
21	32.01	n.a.	0.272	0.034	5.87	n.a.	BMB*
22	33.35	n.a.	0.163	0.017	2.93	n.a.	BMB*
Total:			7.859	0.584	100.00	0.000	

Figure 1. GC trace for perfume oil in hexane at a concentration of 0.6 mg/ml.

10 retention times with the largest area were selected to be plotted as a function of perfume concentration in the hexane. These retention times were 9.03, 10.31, 10.92, 11.84, 11.99, 20.50, 22.57, 22.76, 24.27 and 25.16 min. The plot of area vs. oil concentration for retention time 9.03 is shown in **Figure 2**. In **appendix A2**, plots of the other retention times are recorded.

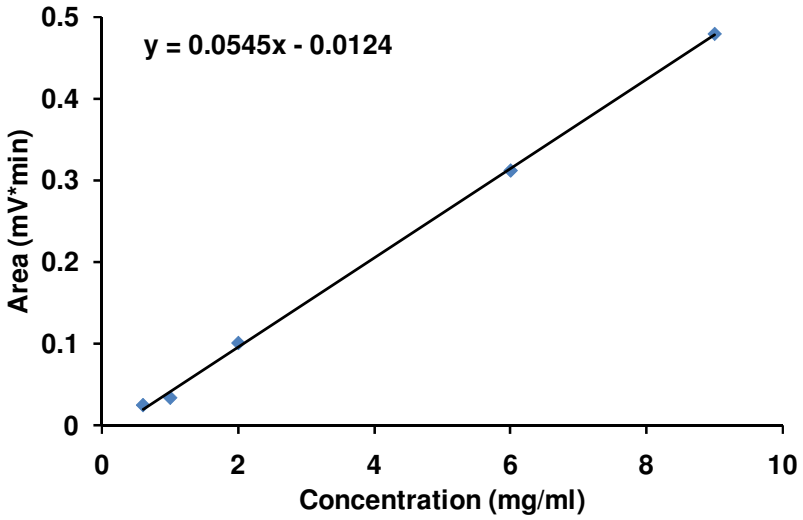


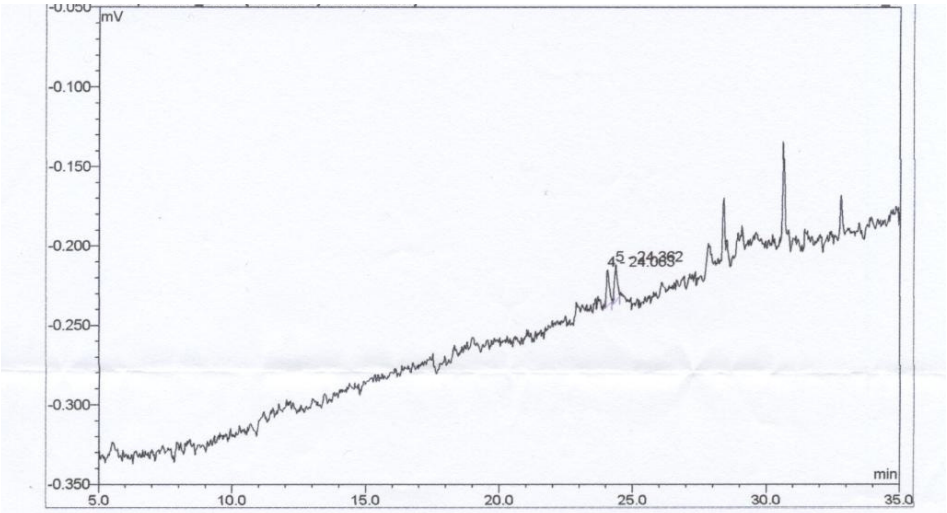
Figure 2. Calibration curves for GC analysis with a retention time of 9.03 min.

The oil concentrations for encapsulation effeciency and leakage measurements of the "unknown" sample is calculated by using the average value obtained from the 10 calibration curves, obtained from the 10 retention times.

3.2.4 Encapsulation Efficiency Measurement

The microcapsules were filtered from the original aqueous dispersion and resuspended in deionized water (120 ml). Glass beads (35 g, 3 mm in diameter) were added to the aqueous microcapsule dispersion (10 ml) and stirred at 100 rpm for 4 hours, after which the microcapsules were fully ruptured (observed with the optical microscope). Hexane (30 ml) was added to the top of the resulting aqua-oil mixture containing the broken microcapsules while stirring was maintained to extract the oil. After 10 minutes stirring, the hexane layer was separated, and 1 µl was taken to measure the concentration of the oil by GC, and from the concentration the mass of the oil was calculated. This procedure was repeated until no oil was found dissolved in the hexane (3×). A sample (1 µl) was also

taken from the aqueous layer and a GC ran on it (data is shown in **Figure 3**). As shown, only several peaks appear. Two peaks with retention times 24.06 and 24.36 min were detected and the area of both peaks are 0.0003 mV*min. Hence it can be concluded that the oil has very little solubility in water (retention times 3.02, 3.09 and 3.18 are due to water). The total amount of oil encapsulated was the sum of the oil extracted into the hexane. The encapsulation efficiency was calculated using the ratio of the weight of encapsulated oil to the weight of the initial amount of oil used.



No.	Ret.Time min	Peak Name	Height mV	Area mV*min	Rel.Area %	Amount	Type
1	3.02	n.a.	1240.336	152.021	68.89	n.a.	BM
2	3.09	n.a.	1240.385	66.447	30.11	n.a.	M
3	3.18	n.a.	72.852	2.212	1.00	n.a.	MB
4	24.06	n.a.	0.023	0.003	0.00	n.a.	BMB*
5	24.36	n.a.	0.023	0.003	0.00	n.a.	BMB*
Total:			2553.618	220.685	100.00	0.000	

Figure 3. GC data of sample taken from the aqueous layer in the encapsulation efficiency test.

3.2.5 Leakage Measurement

Microcapsules (**A**, **B**, **C**, **D** and **E**) were filtered from the original aqueous dispersion, and re-dispersed in water (50 ml). To the resulting aqueous dispersion, hexane was added (30 ml), which was stirred for 10 min. A hexane aliquot (1 µl) was then removed and analysed by GC to determine the amount of oil. Further aliquots (1 µl each) were removed at various time intervals between 1 to 24 hours prior to which the dispersion was stirred for 10 minutes, to ensure oil transfer to the hexane layer.

3.2.6 Size Analysis

Mean particle size and size distribution of the microcapsules in aqueous dispersions were evaluated by static light-scattering (Mastersizer 2000, Malvern Instruments Ltd., UK). The measurements were carried out using a Helium-Neon laser with a measurement range of 0.05 – 900 µm, connected to a sample dispersion unit. Experiments were performed at 25 °C. The mean diameter and size distribution of microcapsules were the average value of five measurements. The refractive index (RI) of the solid melamine-formaldehyde polymer is 1.65 (obtained from the supplier).

3.2.7 Transmission Electron Microscopy (TEM)

Transmission Electron Microscopy (JEOL 1200EX, Jeol Ltd, UK) operating at 80 eV was used to examine the structure and thickness of the microcapsule wall. Microcapsules were embedded in the LR white hard grade acrylic resin, and the ultra thin sections (90-150 nm) were obtained by using ultracut microtome (Reichert-Jung), see **Chapter 2** (experimental techniques **2.4.1**) for more details.

3.2.7.1 Sampling by Ultra-microtome

The microcapsule dispersions (2 ml) were centrifuged at a speed of 500 rpm for 3 min, and the supernatant liquid was separated. Gluteraldehyde (2 ml) was added and the microcapsules were re-dispersed by gently shaking the vial manually. The resulting microcapsule dispersions were stored for 1 hour to harden the outer shell of the microcapsules, and then centrifuged for 3 min at 500 rpm. The supernatant liquid (excess gluteraldehyde) was separated, and a solution of ethanol and water (1:1 v/v, 2 ml) was added, and shaken by hand. The resulting mixture was centrifuged again at 500 rpm for 15 min, and the supernatant ethanol/water mixture was separated. The ethanol/water process was repeated four times, but with ethanol/water 70 %, 90 %, 96 % (v/v), and finally the microcapsules were suspended in absolute ethanol. The resulting microcapsules dispersion was centrifuged again at 500 rpm for 15 min, and the supernatant liquid (excess absolute ethanol) was decanted. To the microcapsule slurry was added absolute ethanol and LR white resin (1:1, 2 ml), and the microcapsules were re-dispersed by gently shaking the vial manually. The resulting mixture was put on a rotator at a speed of 4 rpm. After ~3 min the microcapsules were displaced to the bottom of the vial, and rotating continued for a total of 3 hours. The supernatant ethanol/resin solution was separated. 100 % of LR white resin (2 ml) was added to the resulting microcapsule slurry, before they were rotated again at 4 rpm for 12 hours, and the microcapsules were separated from the supernatant. Two beam capsules (15 × 5 mm) were filled to the top with the air free LR white resin (2 ml). The separated microcapsules were added to each resin filled beam capsule. The microcapsules settled on the bottom of the beam capsules. The mixture was heated (60 °C) under vacuum for 30 min, then left to cure for 48 hours at 60 °C, affording a polymerized resin-microcapsule block. The resulting block was secured into a REICHERT-JUNG ultramicrotome apparatus and the

microcapsule end was trimmed to sections of thickness 90-150 nm. The gold coloured sections were placed on carbon coated grids (G2500C, 2 mm × 1 mm slot, copper, 3.05 mm) ready to be examined by TEM. The wall thicknesses of microcapsules were measured from their TEM images of the ultra microtome sections using an image analysis system (Image J, National Institute of Health).

3.2.8 Environmental Scanning Electron Microscopy (ESEM)

Environmental-SEM (FEI/Philips XL30 ESEM-FEG, Philips, UK) with operating voltage shown in images was used to study the morphology of the microcapsules. Samples were operated in the wet mode with a pressure of 1.5 torr and humidity of 55%.

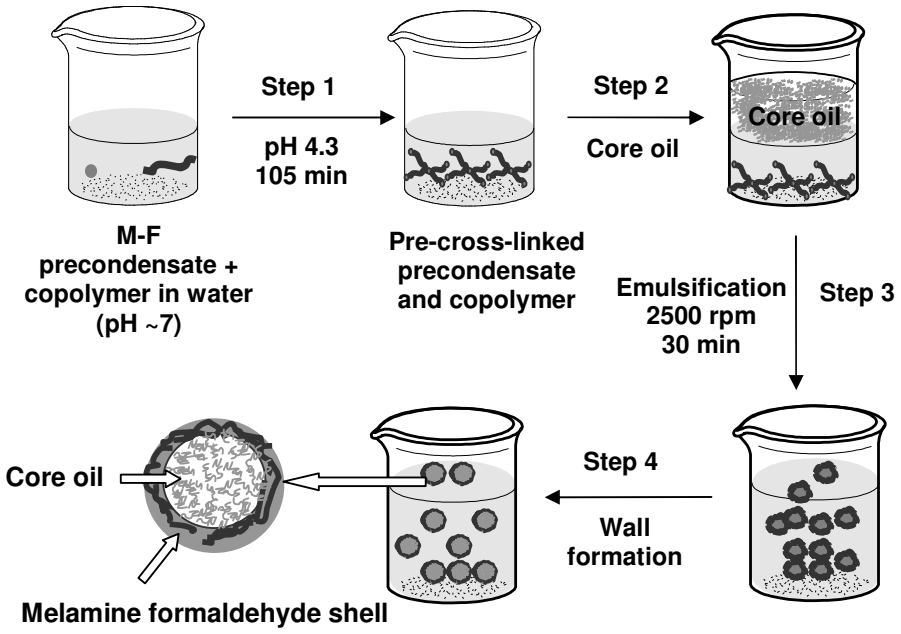
3.2.9 Micromanipulation

The mechanical properties of the microcapsules were determined by micromanipulation. A glass probe with a diameter of 50 μm mounted on a force transducer (Model 405A, Aurora Scientific Inc., Canada) was positioned perpendicular to the glass slide (schematic diagram of the micromanipulation rig is shown in **Chapter 2**, **Figure 4**). The microcapsules in aqueous dispersion were dried on the glass slide, and observed through side and bottom-view cameras. A single microcapsule was compressed by the glass probe travelling at 2 μm s^{-1}. The voltage output generated by the transducer due to compression of the microcapsules was recorded through a data acquisition card in a personal computer. From the sensitivity of the transducer, the voltage was converted to force, hence the rupture force of the microcapsules was determined. Details of this technique are described elsewhere.[186]

3.3 Results and Discussion

3.3.1 Synthesis

MF microcapsules were made using an *in situ* polymerization process (**Scheme 1**), the MF precondensate and copolymer are firstly pre-crosslinked in water (w) (**step 1**), oil (o) is added (**step 2**) to form an o/w emulsion by agitation (**step 3**), the temperature of the emulsion is raised leading to polymerization of the pre-crosslinked monomer and the copolymer to form a wall on the dispersed oil surface (**step 4**).



Scheme 1. Schematic presentation of microcapsule formation by *in situ* polymerization.

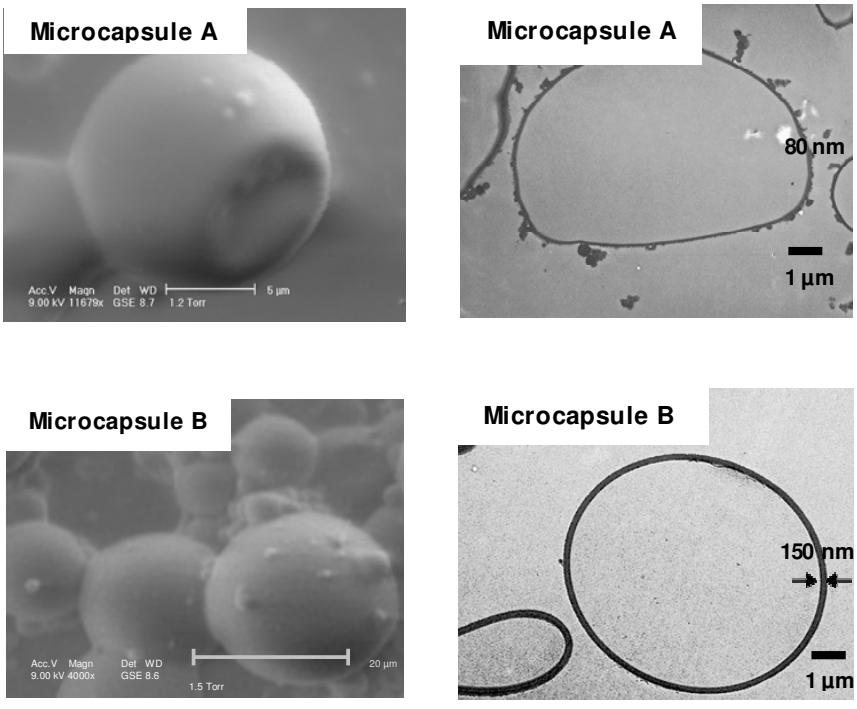
3.3.2 Encapsulation Efficiency

Results showed that the encapsulation efficiencies of the 5 microcapsules did not vary with the F/M molar ratio and were around 75 % (**A**: 75.2 ± 0.8, **B**: 75.3 ± 0.4, **C**: 75.6 ±

0.5, **D**: 75.8 ± 0.7 and **E**: 74.3 ± 0.5). Presumably, the loss of the core material was due to evaporation during the polymerisation at elevated temperature (65 °C) for 6 hours, since there was no significant solubility of the core oil in water by GC analysis (experimental methods section, encapsulation efficiency measurement).

3.3.3 Morphology

The ESEM (LHS) and TEM (RHS) images of microcapsules **A**-**E** are presented in **Figure 4**. The ESEM images show that the microcapsules in all the samples had a smooth morphology on the surface, but microcapsules **A** were slightly deformed whilst microcapsules **B**-**E** kept their spherical shape. This observation suggests that microcapsules **A** were weaker, and indeed they tended to rupture after air drying. Also, for all the samples, some smaller particles (~1-2 µm) can be seen in the ESEM images, and are also observed in the dynamic light scattering measurement (2 % volume fraction, **Figure 6b**).



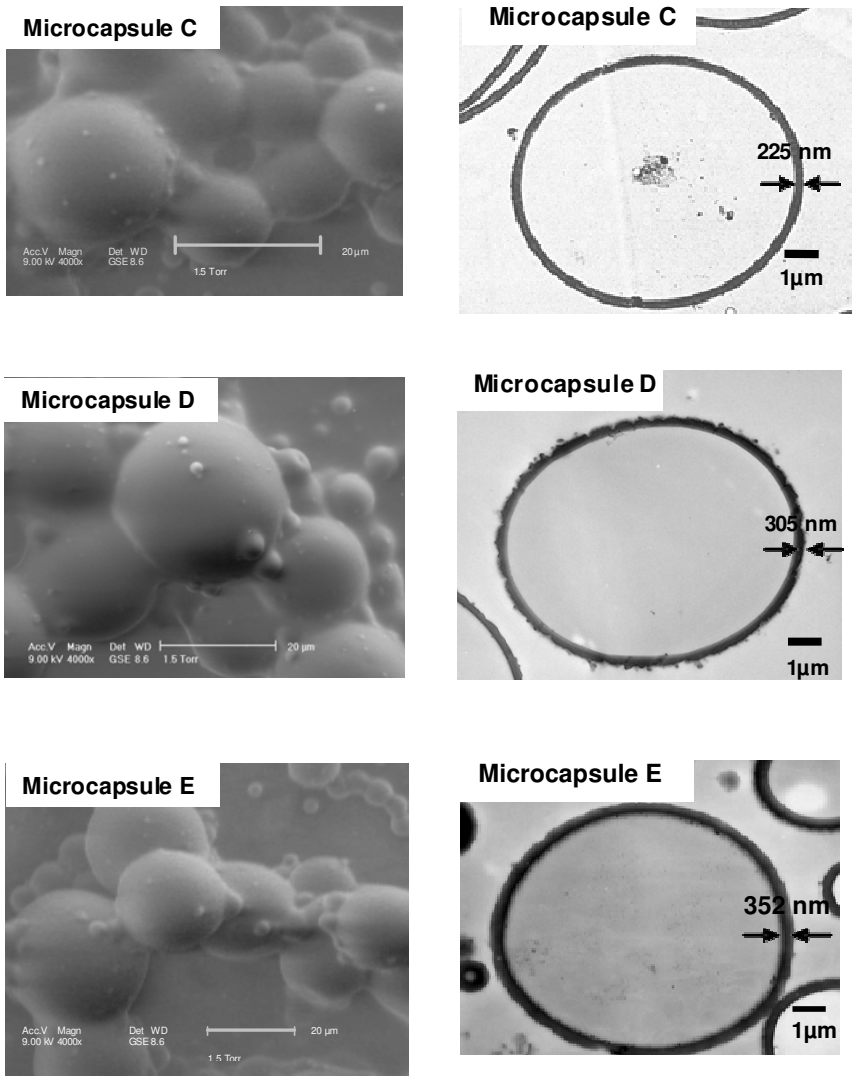


Figure 4. ESEM images of microcapsules **A**-**E** (LHS), and TEM images of ultra thin sections for microcapule **A**-**E** (RHS).

Moreover, agglomeration of the microcapsules was observed from the ESEM images, which is due to the drying process since no agglomerate was seen in the emulsion through the optical microscope shown in **Figure 5**.

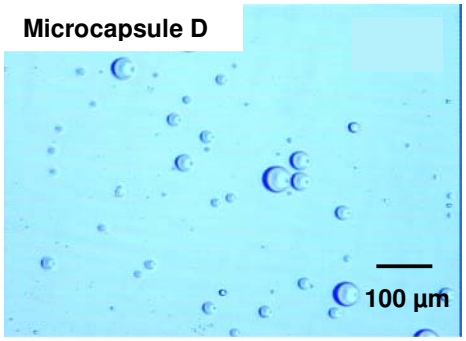
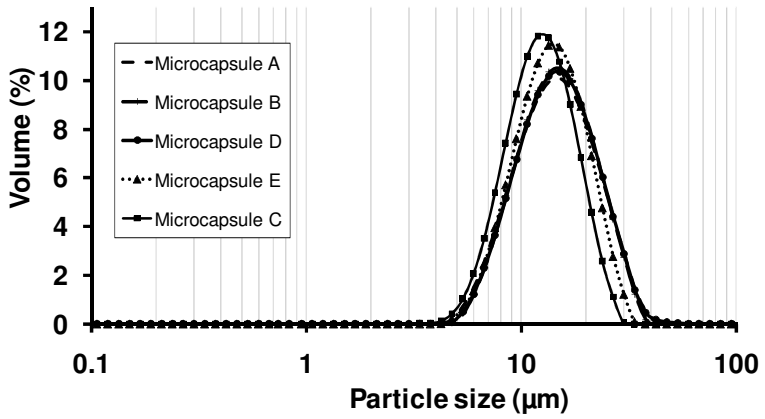


Figure 5. A microscopic image of microcapsules **D** dispersed in water (microcapsules **A**, **B**, **C** and **E** all look similar to **D** (not aggregated) when dispersed in aqueous).

3.3.4 Particle Diameter and Distribution

The size distribution curves of oil droplets in the o/w emulsion (**Scheme 1**, **step 3**) for preparing microcapsules **A**-**E** are shown in **Figure 6a**, and the size distribution curves of the corresponding microcapsules in aqueous dispersion (**Scheme 1**, **step 4**) are shown in **Figure 6b**. The oil droplets in of all 5 samples show monomodal distributions centered on ~14-15 µm. In contrast, the microcapsules in the 5 samples show bimodal distributions centered on 1-2 µm and 14-15 µm, and the volume fraction of the first peak is ~2 %. This bimodal distribution is consistent with the ESEM images, where some smaller (~1-2 µm) particles can be observed. Hence, it can be deduced that the wall formation process induces the 2 % of small particluates to be formed. A plot of average particle diameter as a function of F/M molar ratio is shown in **Figure 7**. It can be seen that the mean particle diameters of all 5 samples do not change significantly with the changing of F/M molar ratios.

a)



b)

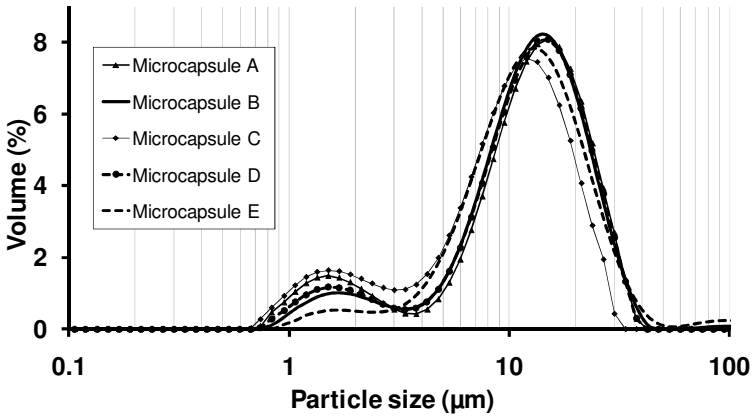


Figure 6. (a) Size distribution chart for oil droplets in the o/w emulsions for preparing microcapsules **A-E** (DLS), b) Size distribution chart for microcapsules **A**-**E** in aqueous dispersion (DLS).

3.3.5 Wall Thickness

Typical TEM images of the microcapsules are presented in **Figure 4** (RHS). The average wall thickness of each type of microcapsule was calculated from 60 microcapsules, and the wall thickness for each individual microcapsule is the average value taken from 10 different parts of the microcapsule wall. It can be observed from **Figure 7** that unlike the diameter, the wall thickness of microcapsules increases from 80±1.9 to 308±1.7 nm

(285±4.6 % increase) when the F/M molar ratios increases from 0.20 to 0.49 (145 % increase). Also, **Figure 7** clearly shows that there are two stages in terms of the increase in wall thickness that is controlled by the F/M ratio. Below 0.49 F/M ratio the wall thickness increases relatively rapidly, whilst above 0.49 the rate of increase is much lower. However, with the increase of 369 % in F/M molar ratio from 0.49 to 2.30, there is only 14±0.8 % increase in wall thickness. Thus, there is a relatively small window of F/M ratio between 0.22 and 0.49 in which the wall thickness can be modulated.

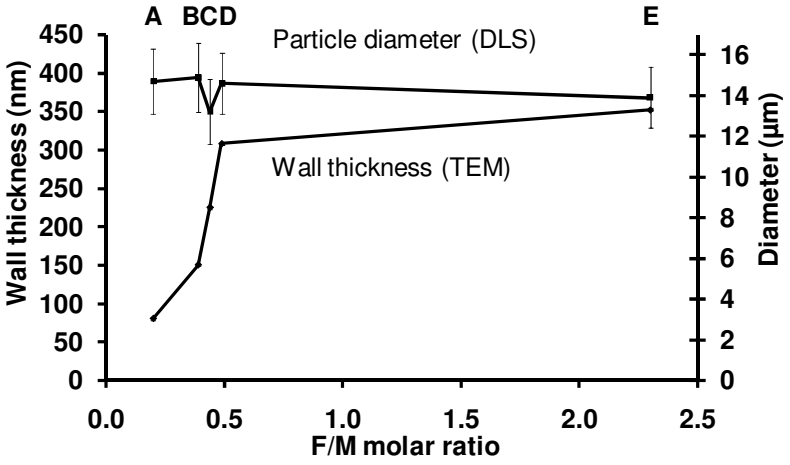
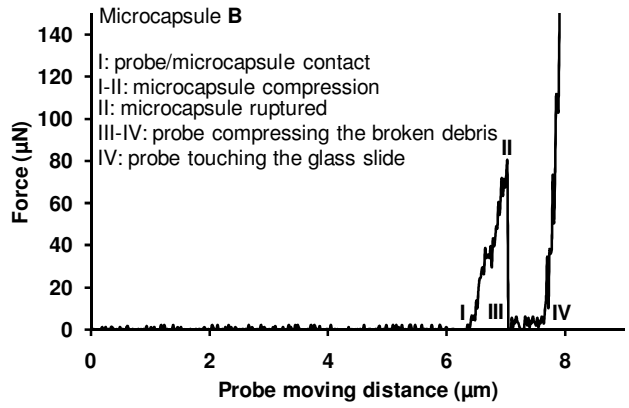


Figure 7. A plot of microcapsule diameter and wall thickness vs. F/M molar ratio.

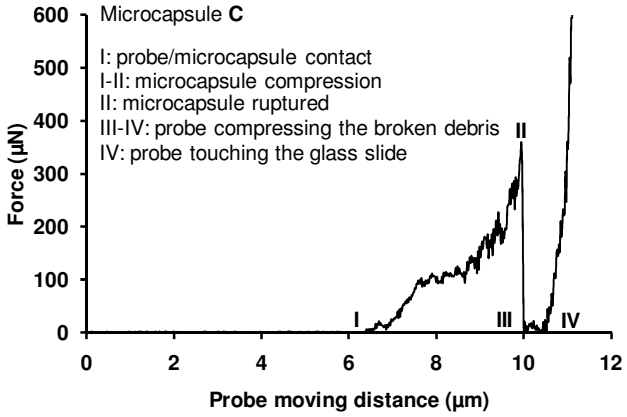
3.3.6 Mechanical Properties

It was observed that microcapsules **A** ruptured during air drying and hence were too weak for their mechanical properties to be measured. **Figure 8a-d** shows typical relationship of the force imposed on a single microcapsule (**B**-**E**) as a function of the probe moving distance.

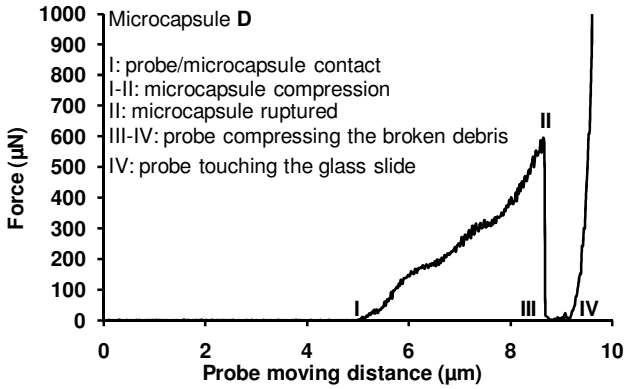
a)


Microcapsule B
I: probe/microcapsule contact
I-II: microcapsule compression
II: microcapsule ruptured
III-IV: probe compressing the broken debris
IV: probe touching the glass slide
Force (μN)
Probe moving distance (μm)
I
II
III
IV

b)


Microcapsule C
I: probe/microcapsule contact
I-II: microcapsule compression
II: microcapsule ruptured
III-IV: probe compressing the broken debris
IV: probe touching the glass slide
Force (μN)
Probe moving distance (μm)
I
II
III
IV

c)


Microcapsule D
I: probe/microcapsule contact
I-II: microcapsule compression
II: microcapsule ruptured
III-IV: probe compressing the broken debris
IV: probe touching the glass slide
Force (μN)
Probe moving distance (μm)
I
II
III
IV

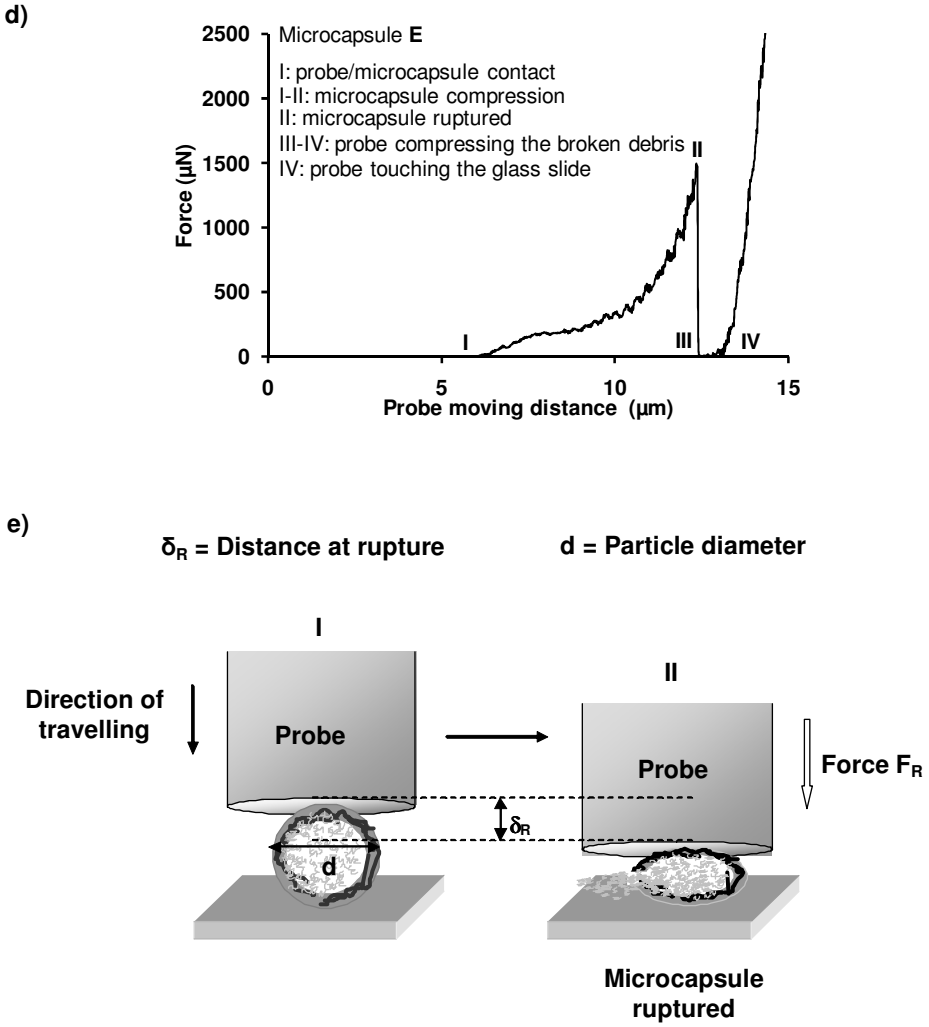


Figure 8. (a-d) Force vs. probe moving distance for compressing single microcapsules to rupture for microcapsules **B**-**E**, (e) schematic diagram of the probe compressing a single microcapsule to rupture.

The distance between 0 and **I** (**Figure 8a-d)** corresponds to the transducer probe moving in the air before it has made contact with the microcapsule. After point **I** the probe touches the microcapsule, and the force imposed on the microcapsule increases until point **II** at which point the microcapsule ruptures. As a result, the force drops to point **III**. The probe continues to compress the debris of the microcapsule (**III**-**IV**) until it touches the slide at point **IV**, afterwards the force increases rapidly as the probe pushes onto the slide.

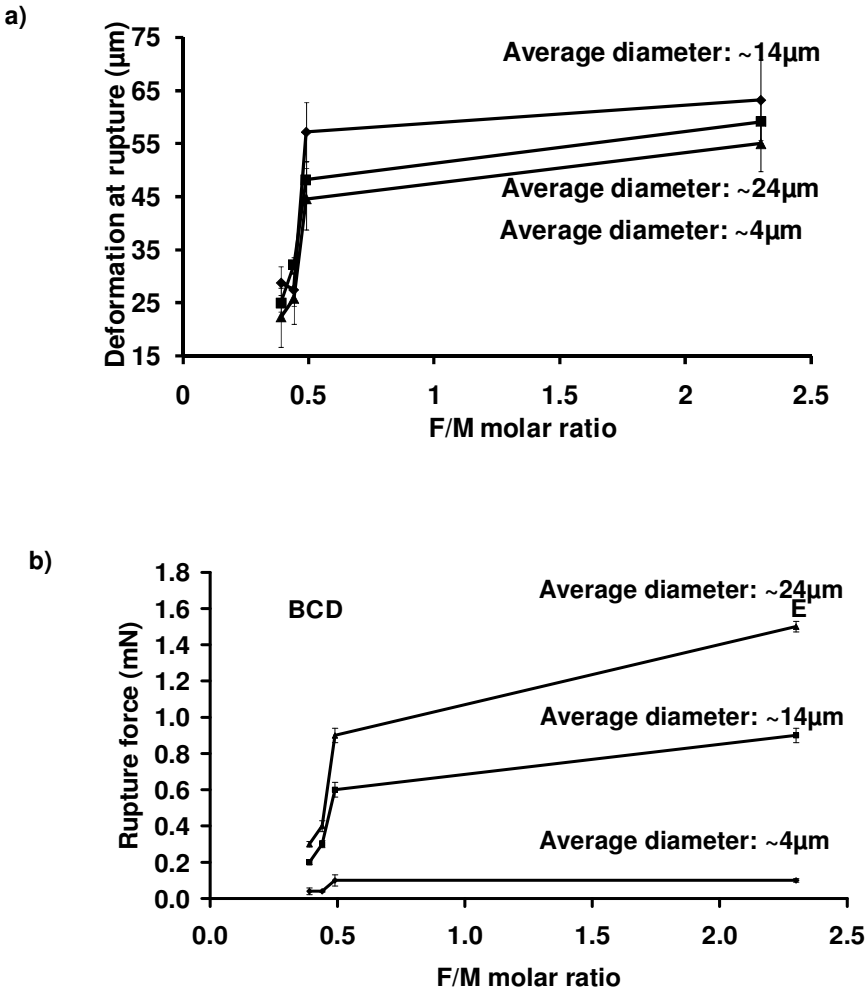
From this curve, the rupture force of the microcapsule can be determined (point **II**). The displacement at rupture (δ_R) is denoted as the distance that the probe travels from contact with particle until rupture (**Figure 8e**). The deformation at rupture is calculated using equation (**1**) (d = initial particle diameter), and the nominal rupture stress is calculated using equation (**2**) (F_R = rupture force).

$$\text{Deformation at rupture } (\%) = \frac{\delta_R}{d} \times 100 \qquad (1)$$

$$\text{Nominal rupture stress} = \frac{F_R}{\pi\left(\frac{d}{2}\right)^2} \qquad (2)$$

Figure 9a, **9b** and **9c** presents the deformation at rupture, rupture force, and nominal rupture stress of microcapsules **B**-**E** as a function of F/M molar ratio. It was found that the deformations at rupture for MF microcapsules were very similar over the size range 4-24 μm (**Figure 9a**). This similar deformation at rupture for MF microcapsules regardless of the size is also reported by Sun and Zhang.[41] Among microcapsules **B**-**D, D** shows the largest nominal rupture stress of 4.2±0.4 MPa (for size ~14 μm) and those in **B** give the smallest nominal rupture stress of 1.3±0.1 MPa (for size ~ 14 μm). Microcapsule **E** shows a nominal rupture stress of 7.0±0.6 MPa (for size ~ 14 μm). It can be seen that an increase by 145 % of F/M molar ratio from 0.20 to 0.49 has resulted in 223±11.5 % increase in the nominal rupture stress. However, there is only an increase in rupture stress by 66±12.8 % upon increasing the F/M molar ratio by 369 % from 0.49 to 2.30. This result shows that there is a relatively small window of F/M ratio, between 0.20 and 0.49, in which the nominal rupture stress can be modulated significantly. Using a F/M molar ratio greater than 0.49 only increases the mechanical properties of M-F microcapsules by a marginal amount. By comparing **Figure 7** with **9a**, **9b** and **9c**, a clear relation between the wall thickness and the mechanical properties

of the microcapsules can be seen. Moreover, **Figure 9a** shows that microcapsules **E** show the largest deformation at rupture (58.4±3.1 %) in comparison to **B** which gives the smallest value (24.8±1.5 %). This result suggests that higher F/M ratio makes the microcapsules more deformable. Thus, this explains why microcapsules **A**, with the lowest F/M ratio are too brittle even to survive in air.



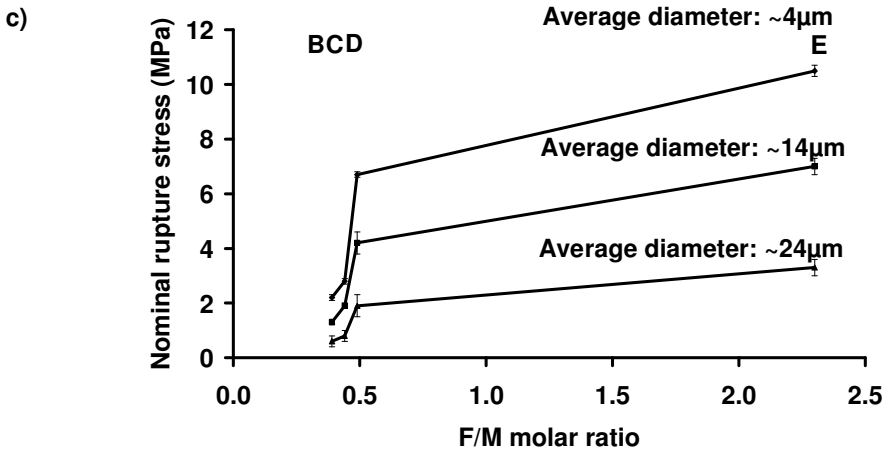


Figure 9. Mechanical property parameters vs. F/M molar ratio (average value of 3 size ranges) for microcapsules **B**-**E**. (a) Deformation at rupture, (b) Rupture force, (c) Nominal rupture stress.

In addition, the detailed relationship of how the displacement at rupture, rupture force, and nominal rupture stress varied with diameter at constant F/M molar ratio is shown in **Figure 10a**, **10b**, and **10c**, respectively. The graph shows that within the same F/M molar ratio, the displacement at rupture (**Figure 10a**) and rupture force (**Figure 10b**) increase as the diameter of the microcapsules increases. In contrast, a general trend of the nominal stress at rupture (**Figure 10c**) decreases as the diameter of the microcapsules increases. This trend is observed in all microcapsules **B**-**E**. The stress at rupture of microcapsules may be directly related to their rupture behavior since larger microcapsules were found to rupture more easily than smaller ones.[127]

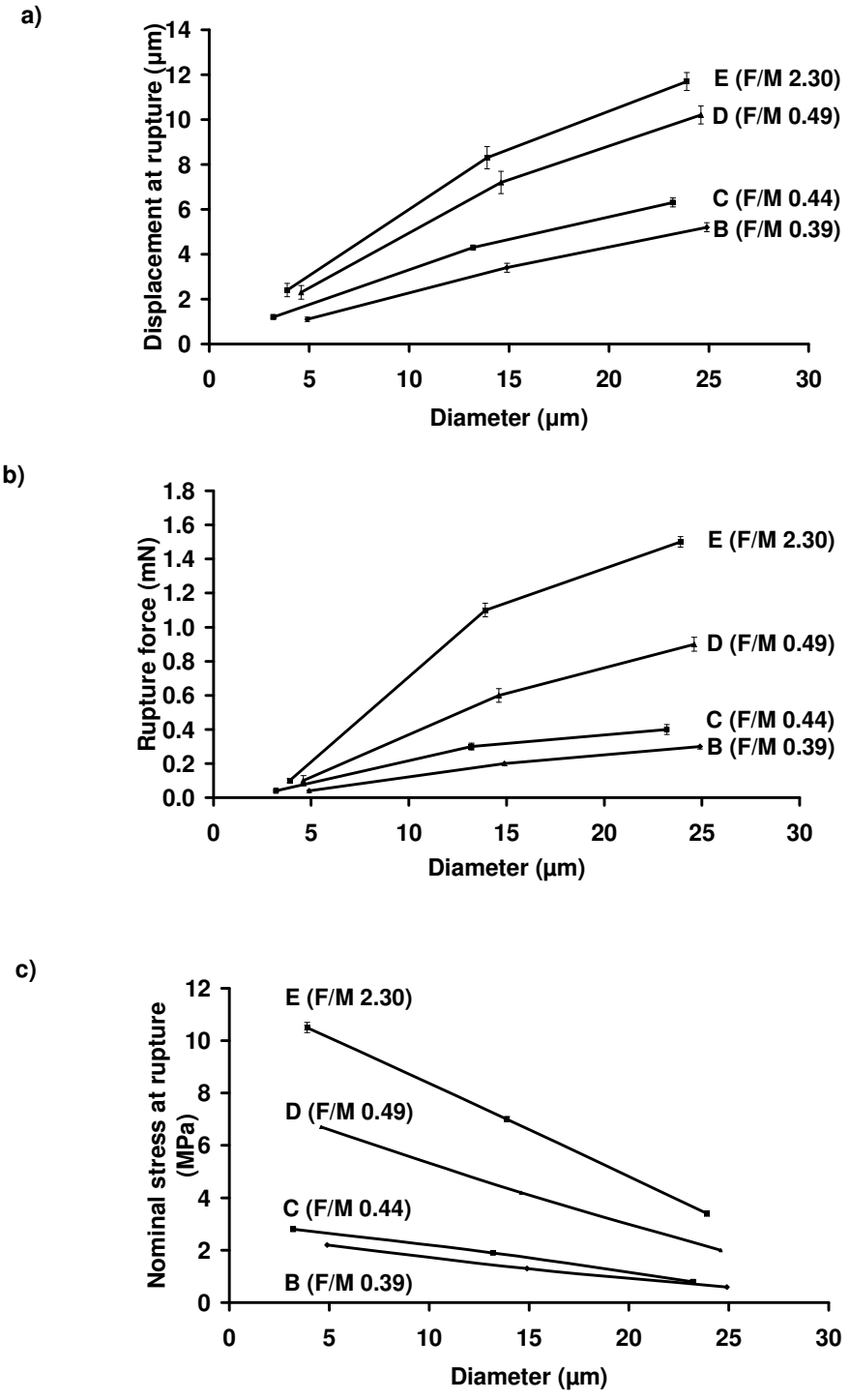


Figure 10. Mechanical property parameters vs. diameter for microcapsules **B-E**. (a) Displacement at rupture, (b) Rupture force, (c) Nominal rupture stress.

3.3.7 Oil Leakage and Kinetics

The leakiness of microcapsules **A**-**E** as a function of time is illustrated in **Figure 11**. Microcapsules **A** show the highest leakage 6.7 ± 0.35 % at the end of storage for 20 days, and microcapsules **B**, **C**, **D**, and **E** are 5.1 ± 0.21 %, 3.7 ± 0.20 %, 2.1 ± 0.18 %, and 1.3 ± 0.17 %, respectively.

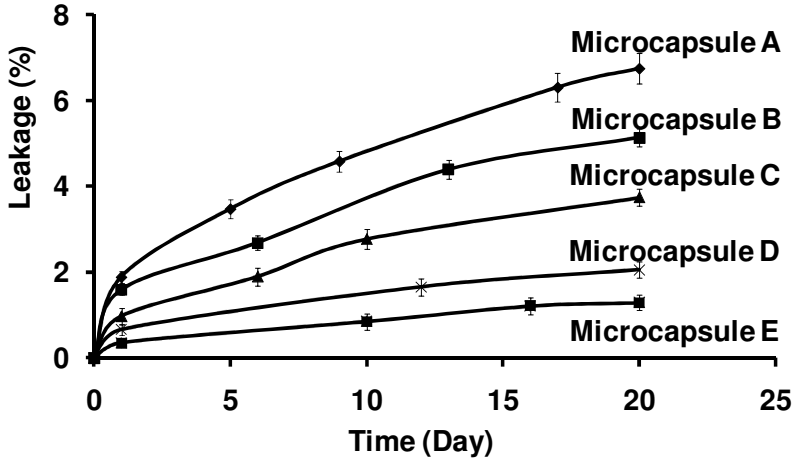


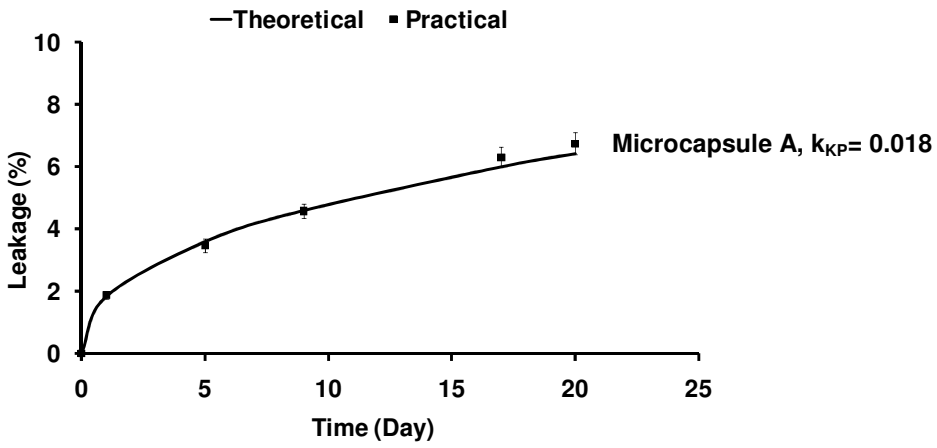
Figure 11. Leakiness vs. time of microcapsules **A**-**E** over 20 days.

In order to characterize the kinetics of the oil leakage from the microcapsules, Korsmeyer-Peppas model[187] is used here:

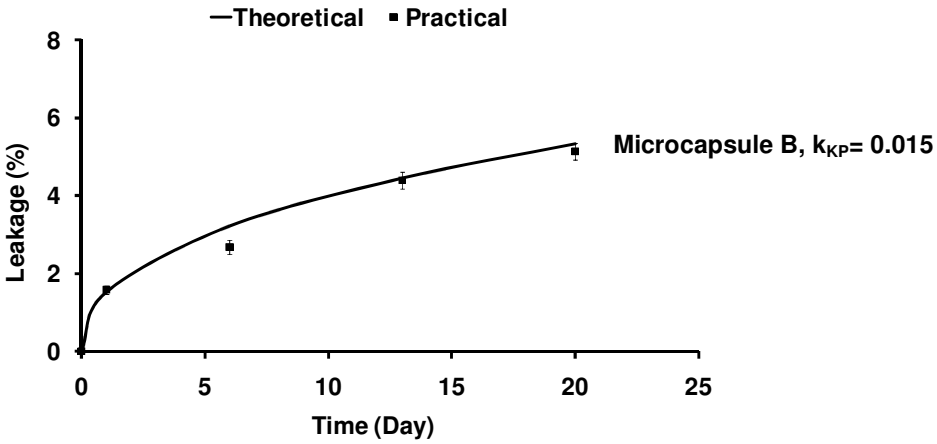
$$\frac{M_t}{M_\infty} = k_{KP}\, t^n \qquad (3)$$

Where M_t is the amount of oil leaked at time t, M_∞ is the amount of the oil leaked at infinite time, k_{KP} is the rate constant for Korsmeyer-Peppas model and n is the Power Law constant, an indication of release mechanism. The average value of n for microcapsules **A**-**E** is 0.42 ± 0.01. To apply Korsmeyer-Peppas model to the leakage profile (n = 0.42, equation (**3**)), the leakage curves fitted with the model for microcapsules **A**-**E** are shown in **Figure 12a-e**.

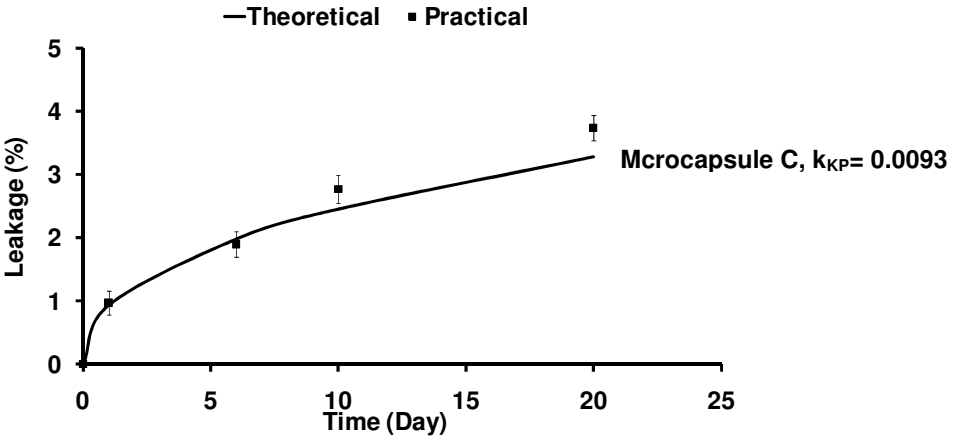
a)


—Theoretical ▪ Practical
Leakage (%)
Time (Day)
Microcapsule A, k_{KP}= 0.018

b)


—Theoretical ▪ Practical
Leakage (%)
Time (Day)
Microcapsule B, k_{KP}= 0.015

c)


—Theoretical ▪ Practical
Leakage (%)
Time (Day)
Mcrocapsule C, k_{KP}= 0.0093

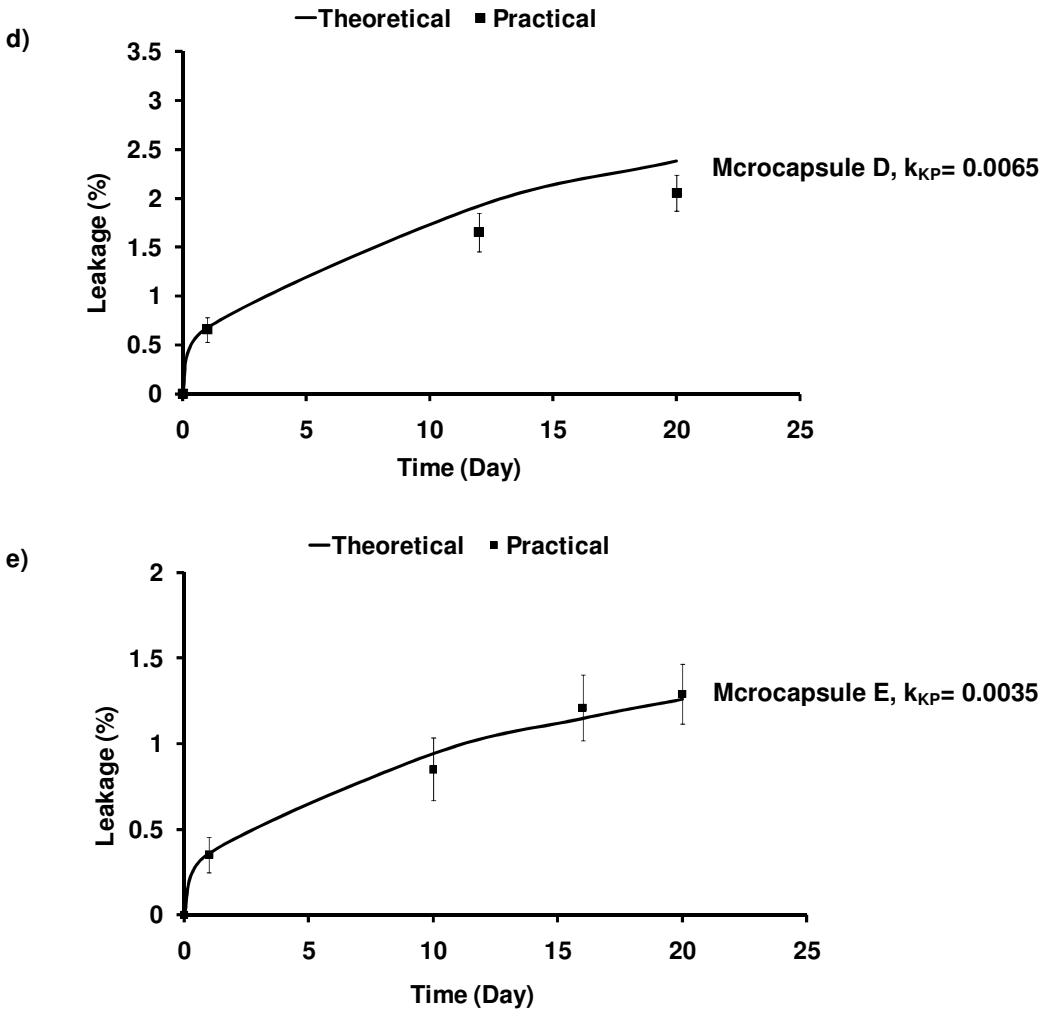


Figure 12. The experimental leakage curve and the Korsmeyer-Peppas model for microcapsules **A**-**E**.

It can be seen that the leakage for microcapsules **A**-**E** fit to all the curves reasonably well (n = 0.42). When n approximates to 0.5 a Fickian/diffusion (Higuchi's model) release is implied.[188] The result suggests that the leakage mechanism for microcapsules **A**-**E** is primarily governed by diffusion. However, there might be other leakage mechanisms involved. Moreover, the result shows that the leakage rate of the MF microcapsules **A**-**E** decreases with the increase of F/M molar ratio (from 0.018 to 0.0035 day^2), which suggests that the core oil leaked more slowly when the F/M molar ratio is increased. This slower

leakage is probably due to the more cross-linked MF polymer wall when more formaldehyde is used.

3.4 Conclusions

MF microcapsules containing an oil-based core material were prepared by *in situ* polymerization. No significant differences were found in mean particle diameter (~14 μm), size distribution, particle morphology, and encapsulation efficiency (~75 %) of the microcapsules when the F/M molar ratio was increased from 0.20 to 2.30. However, the wall thickness of the microcapsules increased from 80±1.9 to 308±1.7 nm (285±4.6 %), the nominal rupture stress increased from 1.3±0.1 to 4.2±0.4 MPa (223±11.5 % increase), and the amount of oil leakage at the end of storage of 20 days decreased from 6.7 ± 0.35 % to 2.1 ± 0.19 % (219 % decrease) when the F/M molar ratio was increased from 0.20 to 0.49 (145%). In contrast, when the F/M molar ratio increased from 0.49 to 2.30 (369 %), the wall thickness and nominal rupture stress of the microcapsules only increased by 14±0.8 % and 66±12.8 %, respectively, and the amount of oil leakage of the microcapsules only decreased by 63 %. This difference suggests that a relatively small window of F/M molar ratio between 0.20 and 0.49 exists in which the wall thickness and nominal rupture stress of the microcapsules can be modulated significantly. Above 0.49 increases in F/M molar ratio only increases these properties marginally. Thus, microcapsules with desirable mechanical properties have been created, with a much lower molar ratio of formaldehyde (≤ 0.49) *via* this work, a key criterion for applications.

CHAPTER 4

A New Dual Strategy for Controlling the Leakage of Microcapsules: Organic/inorganic Composite Microcapsules from MF/$CaCO_3$ Nanoparticles

Part of this work presented in **Chapter 4** has been accepted as a communication in the journal Chemical Communications.

Abstract

In this chapter ripened double shell composite microcapsules (ripened $CaCO_3$ nanoparticles outer shell and melamine formaldehyde (MF) polymer inner shell) were produced. These were prepared using a method based on an *in situ* polymerization method to form a MF polymer shell inside the ripened $CaCO_3$ nanoparticles microcapsules wall by migrating the MF precondensate and copolymer between the gaps of the ripened $CaCO_3$ nanoparticles and reacting at the oil-water interface. The properties of these ripened double shell composite microcapsules (encapsulation efficiency, size distribution, morphology, wall structure and thickness, nominal rupture stress and leakage) were characterized, and contrasted with the MF/copolymer, ripened nanoparticulate $CaCO_3$ and unripened double shell (unripened $CaCO_3$ nanoparticles as the outer shell) microcapsules. The ripened double shell composite microcapsules were shown to have reduced core oil leakage over the non-composite materials (20 fold reduction in leakage lower than the MF microcapsules, and 25 fold reduction than the ripened nanoparticulate $CaCO_3$ microcapsules). The $CaCO_3$ nanoparticle ripening process gave the microcapsules wall a more compact and smooth structure, and the inner MF polymer shell increased the completeness of the wall. It was also found that the mechanical properties of the double shell composite microcapsules are dominated by the outer ripened $CaCO_3$ shell in terms of both deformation at rupture and the nominal rupture

stress. In addition, the effect of pH (4.5, 5.0, 5.5, 6.0 and 7.0) on the formation and properties of the microcapsules were investigated. When the pH is lower than 6.0 (4.5, 5.0 and 5.5), the microcapsules were leaked more with lower encapsulation efficiency and lower degree of $CaCO_3$ wall formation were produced.

4.1 Introduction

Inorganic materials, such as silica, can form strong and impervious microcapsule walls.[189, 190] However, such materials and processes are typically complex, slow and costly to make. Recently, simpler processes utilising calcium carbonate or phosphate have been shown to form microcapsule walls, which are cheap, relatively unreactive toward the active ingredient, are environmentally friendly and allow release of the core material by a change in pH.[190-192] In addition, the inorganic nanoparticles have demonstrated very beneficial impacts on improving the stiffness and resistance to deformation when embedded in organic polymer microcapsule shells, preventing heat-shrinking during the encapsulation process, and provide the possiblity of producing multifunctional microcapsules.[89, 90, 93, 193] However, in comparison with organic materials, making walls out of such inorganic materials can result in greater porosity, which is a major drawback and limits their applications for the encapsulation of small molecules.[194, 195]

In this study, a novel methodology of reducing the porosity is to use double shell composite microcapsules of ripened $CaCO_3$ nanoparticules as an outer shell, and MF polymer/composite as an inner shell. Organic-inorganic hybrid microspheres and microcapsules have been reported previously, using different methods and different shell materials. Bon *et al.*[33] utilised the Pickering emulsion polymerization method to form hollow microspheres with TiO_2 nanoparticles as the outer shell, and an organic polymer

as the inner shell. Layer-by-layer deposition method has also been used to produce hybrid microcapsules.[145, 196, 197] In our study, the double shell composites were prepared using a method based on an *in situ* polymerization method to form a MF polymer shell inside the ripened $CaCO_3$ nanoparticles microcapsules wall by migrating the MF precondensate and copolymer between the gaps of the ripened $CaCO_3$ nanoparticles and polymerization at the oil-water interface.

4.2 Experimental

4.2.1 Materials

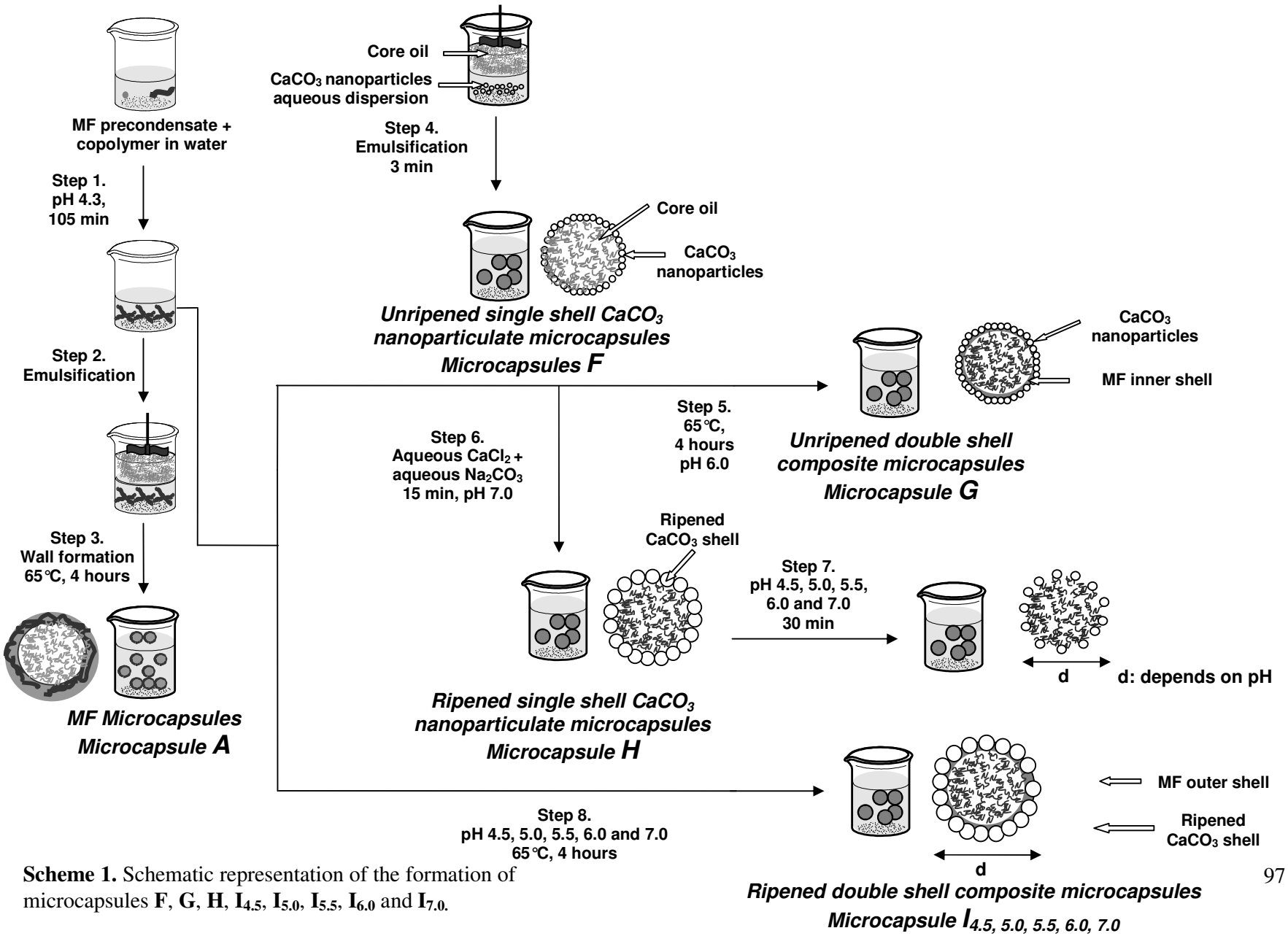
The core oil is a typical organic blend of various fragrant components which has a relatively low solubility in water and is used in consumer products. MF precondensate (70 % (aq) w/w, formaldehyde to melamine molar ratio 0.20) was supplied by British Industrial Plastics Ltd, Birmingham, UK. Formaldehyde (37 % (aq) w/w) was supplied by Sigma-Aldrich, UK. Poly(acrylamide-acrylic acid, sodium salt) was supplied by Polymersciences, Inc., US and calcium carbonate nanoparticles were supplied by Omya, UK. All chemicals were used without further purification.

4.2.2 Preparation of Microcapsules

4.2.2.1 Preparation of MF Microcapsules (Microcapsule A, Scheme 1, Step 1, 2, 3)

An aqueous solution of MF precondensate (2.50 g) and copolymer (0.58 g, poly (acrylamide-acrylic acid, sodium salt) in water (35 ml) was stirred (400 rpm) in a vessel (Φ 65 mm × 65 mm) with a Rushton turbine (Φ 31 mm, in a vessel with standard configuration) for 105 min at pH 4 (adjusted by acetic acid (1M), monitored by a pH

meter) at room temperature (**step 1**). The core oil (9.33 g) was added to the resulting mixture and stirred using a homogenizer (Model L4RT, Silverson Machines Ltd, UK) at a speed of 2500 rpm for 30 min at 15 °C, to form an oil in water (o/w) emulsion (**step 2**). The resulting emulsion was stirred at 400 rpm in a vessel (Φ 65 mm × 65 mm) with a standard Rushton turbine impeller (Φ 31 mm) for 30 min at 15 °C, then the temperature was raised to 65 °C, at which the stirring was maintained for 4 hours. The resulting microcapsules dispersion was cooled to room temperature, and the pH raised to 10 with the addition of aqueous NaOH (1 M, monitored by a pH meter) to terminate the polymerization reaction (**step 3**).



Scheme 1. Schematic representation of the formation of microcapsules **F**, **G**, **H**, $\mathbf{I_{4.5}}$, $\mathbf{I_{5.0}}$, $\mathbf{I_{5.5}}$, $\mathbf{I_{6.0}}$ and $\mathbf{I_{7.0}}$.

4.2.2.2 Preparation of Ripened Double Shell Composite Microcapsules (Microcapsule F, Scheme 1, Step 4)

The oil (9.3 g) was added to an aqueous $CaCO_3$ nanoparticle dispersion (40 ml, 10 % wt) and stirred using a homogenizer (Model L4RT, Silverson Machines Ltd, UK) at a speed of 2500 rpm for 3 min to form the o/w emulsion stabilized by $CaCO_3$ nanoparticles.

4.2.2.3 Preparation of Unripened Double Shell Composite Microcapsules (Microcapsule G, Scheme 1, Step 5)

To the o/w emulsion stabilized by $CaCO_3$ nanoparticles (**step 4**), the aqueous pre-crosslinked MF solution (**step 1**) was added, and the pH was adjusted to 6.0 (unless specified otherwise) with the addition of aqueous NaOH (1 M, monitored by a pH meter). The resulting dispersion was stirred at 400 rpm at 65 °C for 4 hours, and allowed to cool to room temperature.

4.2.2.4 Preparation of Ripened Single Shell Nanoparticulate $CaCO_3$ Microcapsules (Microcapsule H, Scheme 1, Step 6 and 7)

To the o/w emulsion (50 ml) stabilized by $CaCO_3$ nanoparticles (pH 6.0) was added dropwise aqueous $CaCl_2$ (1.5 M, 10 ml) and aqueous Na_2CO_3 (1.5 M, 10 ml), *via* a pump system (Model 101U, Water Marlow, UK) over 15 min, whilst being stirred at 400 rpm. Stirring was continued for a further 10 min at the same speed to form the ripened nanoparticulate $CaCO_3$ single shell microcapsules (**H**) (**step 6**). To the resulting aqueous dispersion of microcapsules **H**, acetic acid was added to adjust the pH to 4.5, 5.0, 5.5, 6.0 and 7.0 (monitored by a pH meter) and stirred for another 30 min (**step 7**) before their size were measured.

4.2.2.5 Preparation of Ripened Double Shell Composite Microcapsules (Microcapsule I, Scheme 1, Step 8)

To the aqueous dispersion (70 ml) of microcapsules **H** (pH 7.0) was added the aqueous pre-crosslinked MF solution (35 ml) (from **step 1**), and the pH was adjusted to either 4.5, 5.0, 5.5, 6.0 or 7.0 with the addition of aqueous acetic acid (1 M) or NaOH (1 M) (monitored by a pH meter). The temperature of the resulting dispersion was raised to 65 °C, which was stirred at a speed of 400 rpm for 4 hours, and was allowed to cool to room temperature to afford microcapsules $\mathbf{I_{4.5}}$, $\mathbf{I_{5.0}}$, $\mathbf{I_{5.5}}$, $\mathbf{I_{6.0}}$ and $\mathbf{I_{7.0}}$.

4.2.3 Gas Chromatography (GC)

A Trace 2000 series gas chromatogram with a flame ionization detector and 30 m × 0.32 mm ZB5 inferno column was used to determine the encapsulation efficiency and leakage of the oil from the microcapsules. Analysis was performed using a Dionex Chromeleon Workstation. Samples injection volumes were 1μl. The injection port temperature was 250 °C. The temperature ramp for the column was increased by 10 °C/s from 50-300 °C, and held at 300 °C for 35 min. The detection temperature was 300 °C. Helium was used as the carrier gas. Details of calibration of the GC are illustrated in **Chapter 3 (3.2.3)**.

4.2.4 Encapsulation Efficiency Measurement

The microcapsules were filtered from the original aqueous dispersions for microcapsules **A**, **G**, **H**, $\mathbf{I_{4.5}}$, $\mathbf{I_{5.0}}$, $\mathbf{I_{5.5}}$, $\mathbf{I_{6.0}}$ and $\mathbf{I_{7.0}}$ and resuspended in deionized water (120 ml). Glass beads (35 g, 3 mm in diameter) were added to the aqueous microcapsule dispersion (10 ml) and stirred at 100 rpm for 4 hours, after which the microcapsules were fully ruptured (observed with the optical microscope). Hexane (30 ml) was added to the top of the resulting aqua-oil mixture containing the broken

microcapsules while stirring was used to extract the oil. After 10 min stirring, the hexane layer was separated, and an aliquot (1 µl) was analysed by GC to obtain the mass of the oil from calibration data (see appendix **A1** and **A2**). This addition of hexane was repeated until no oil was found in the hexane (typically 3×). The total amount of oil encapsulated was the sum of the oil extracted into the hexane. The encapsulation efficiency was calculated using the ratio of the weight of encapsulated oil to the weight of the initial amount of oil used. An aliquot (1 µl) was also taken from the aqueous layer and a GC ran. No oil was detected, thus confirming the low solubility of the oil in water.

4.2.5 Leakage Measurement

Microcapsules (**A**, **G**, **H**, $\mathbf{I_{4.5}}$, $\mathbf{I_{5.0}}$, $\mathbf{I_{5.5}}$, $\mathbf{I_{6.0}}$ and $\mathbf{I_{7.0}}$) were filtered from the original aqueous dispersion, and re-dispersed in water (50 ml). To the resulting aqueous dispersion, hexane was added (30 ml) which was stirred for 10 min and the stirring was stopped. A hexane aliquot (1 µl) was removed and analysed by GC to determine the amount of oil. Further aliquots (1 µl) were removed at various time intervals between 1 to 24 hours prior to which the dispersion was stirred for 10 minutes, to ensure oil transfer to the hexane layer.

4.2.6 Size Analysis

Mean particle size and size distribution of the microcapsules in aqueous dispersions were evaluated by laser diffraction technique (Mastersizer 2000, Malvern Instruments Ltd, UK). The measurements were carried out using a Helium-Neon laser with a measurement range of 0.05 – 900 µm connected to a sample dispersion unit. Experiments were performed at 25°C. The mean diameter and size distribution of microcapsules were the average value of five measurements.

4.2.7 Transmission Electron Microscopy (TEM)

Transmission Electron Microscopy (JEOL 1200EX, Jeol Ltd, UK) was used to examine the structure and thickness of the microcapsule wall. Microcapsules were embedded in the LR white hard grade acrylic resin, and the ultra thin sections were obtained by using ultracut microtome apparatus (Reichert-Jung), details of the ultracut microtome sampling is illustrated in **Chapter 3** (**3.2.7**). Operating voltage was 80 eV.

4.2.8 Environmental Scanning Electron Microscopy (ESEM)

An environmental-SEM (FEI/Philips XL30 ESEM-FEG, Philips, UK) was used to study the morphology of the microcapsules. Samples were operated in high vacuum mode, and operating voltage as shown on the images.

4.2.9 Calculation of the Degree of the Wall Formation Formed by the Unripened or Ripened Nanoparticulate $CaCO_3$ Nanoparticles from TEM Images

The degree of completeness of the unripened or ripened $CaCO_3$ nanoparticle wall was calculated using image analysis software (Image J, National Institute of Health) from the ultra microtome TEM images, by measuring the sum of the smallest perpendicular distance between each disconnected piece of the wall, subtracting this value from the total wall perimeter, and dividing by the total wall perimeter.

4.2.10 Micromanipulation

The mechanical properties of the microcapsules were determined by micromanipulation. A glass probe with a diameter of 50 μm mounted on a force transducer (Model 405A, Aurora Scientific Inc., Canada) was positioned

perpendicular to the glass slide. The microcapsules in the aqueous dispersion were dried on the glass slide (15 min), and observed through side and bottom-view cameras. A single microcapsule was compressed by the glass probe travelling at 2 μm s^{-1}. The voltage output generated by the transducer due to compression of the microcapsules was recorded through a data acquisition card. From the sensitivity of the transducer, the voltage was converted to force, hence the rupture force of the microcapsules was determined. Details of this technique are described elsewhere.[134] 30 microcapsules were tested for each sample.

4.2.11 Solubility Test for $CaCO_3$ Nanoparticles

Solid $CaCO_3$ nanoparticles (0.5 g) were added to water (10 ml) while stirring was maintained. To the resulting dispersion, acetic acid (1 M) was added to adjust the pH (monitored using a pH meter). Such aqueous dispersions of $CaCO_3$ nanoparticles were prepared at pH 4.5, 5.0, 5.5, 6.0 and 7.0, and the average diameters of the particles were evaluated by laser diffraction technique.

4.3 Results and Discussion

4.3.1 Synthesis

A series of microcapsules (non-composite (**A** and **H**) and composite (**G** and **I**)) were synthesized as shown in **Scheme 1**. Microcapsules **A**[175] were formed using an *in situ* polymerization process, the MF precondensate and copolymer (poly (acrylamide-acrylic acid, sodium salt)) are firstly pre-crosslinked in water (**step 1**), oil is added to form an o/w emulsion by agitation (**step 2**), the temperature of the emulsion is raised leading to polymerization of the pre-crosslinked MF precondensate and the copolymer to form a

wall at the oil-water interface (**step 3**). Microcapsules **F** were prepared by mixing the core oil with aqueous $CaCO_3$ nanoparticles dispersion for 3 min (**step 4**). Microcapsules **G** were formed by mixing (**step 5**) the pre-crosslinked MF/copolymer (from **step 1**) with the emulsion stabilized by $CaCO_3$ nanoparticles (from **step 4**). Microcapsules **H** were formed by adding equivalent amounts of $CaCl_2$ and Na_2CO_3 to the o/w emulsion to ripen the $CaCO_3$ nanoparticles wall (**step 6**). The pH of the resulting microcapsules **H** dispersion was adjusted (4.5, 5.0, 5.5, 6.0 and 7.0) (**step 7**). Finally, microcapsules $\mathbf{I_{4.5\text{-}7.0}}$ were formed by adding the pre-crosslinked MF precondensate and copolymer (from **step 1**) to the $CaCO_3$ microcapsules **H** (pH 7.0), and adjusting the pH (4.5, 5.0, 5.5, 6.0 and 7.0), and heating at 65 ºC for 4 hours (**step 8**).

4.3.2 Encapsulation Efficiency

The encapsulation efficiency of microcapsules **A**, **G**, **H**, $\mathbf{I_{4.5}}$, $\mathbf{I_{5.0}}$, $\mathbf{I_{5.5}}$, $\mathbf{I_{6.0}}$ and $\mathbf{I_{7.0}}$ are plotted in **Figure 1**. Microcapsules **A**, **G**, **H**, $\mathbf{I_{6.0}}$ and $\mathbf{I_{7.0}}$ have very similar encapsulation efficiencies of ~75 %, whereas, microcapsules $\mathbf{I_{4.5}}$, $\mathbf{I_{5.0}}$ and $\mathbf{I_{5.5}}$ have lower encapsulation efficiencies (~15 %, 25 % and 35 %, respectively). In order to investigate this encapsulation efficiency decrease upon lowering the pH, the average particle size of the $CaCO_3$ nanoparticles was monitored as a function of pH and time (see solubility test for $CaCO_3$ nanoparticles in the experimental section). The size reduction of the $CaCO_3$ nanoparticles was proportional to pH over the range 4.5-5.5. After 4 hours immersion (pH 4.5) the $CaCO_3$ nanoparticles size had decreased significantly, whilst they were stable at pH 6.0 and 7.0 over 4 hours (data not shown). Hence one might expect that microcapsules $\mathbf{I_{4.5\text{-}5.5}}$ to have a wall comprising of smaller $CaCO_3$ nanoparticles relative to microcapsules $\mathbf{I_{6.0}}$ and $\mathbf{I_{7.0}}$, which is indeed the case (see wall thickness section).

Consequently, there were lower encapsulation efficiencies as the pH of formation was lowered.

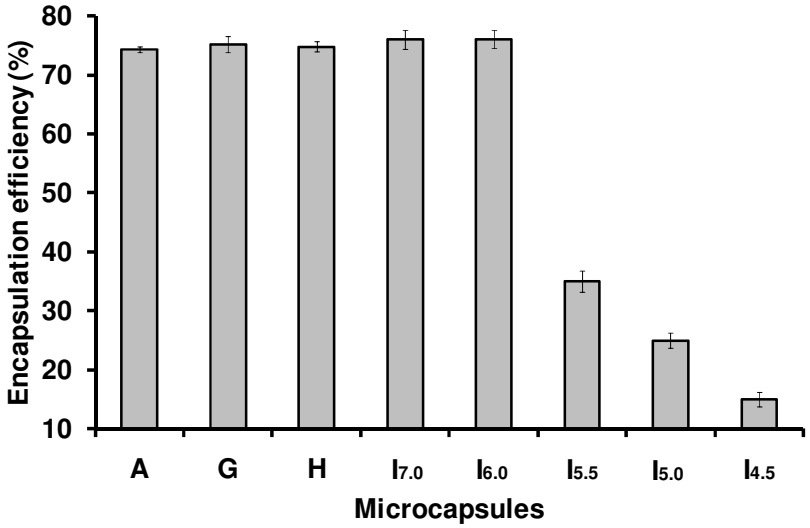
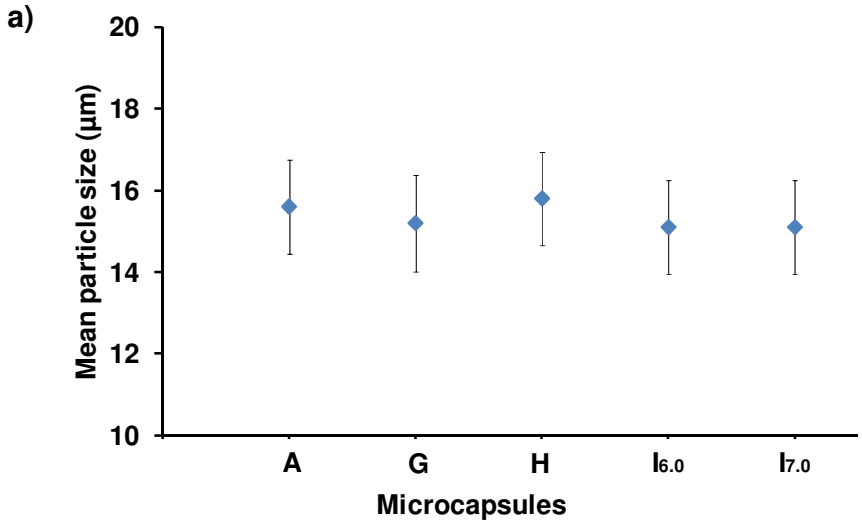


Figure 1. Encapsulation efficiencies of microcapsules **A**, **G**, **H**, $\mathbf{I_{4.5}}$, $\mathbf{I_{5.0}}$, $\mathbf{I_{5.5}}$, $\mathbf{I_{6.0}}$ and $\mathbf{I_{7.0}}$.

4.3.3 Particle Diameter and Distribution

The average particle size for microcapsules **A**, **G**, **H**, $\mathbf{I_{6.0}}$ and $\mathbf{I_{7.0}}$ are plotted in **Figure 2a**, and those for $\mathbf{I_{7.0}}$, $\mathbf{I_{6.0}}$, $\mathbf{I_{5.5}}$, $\mathbf{I_{5.0}}$ and $\mathbf{I_{4.5}}$ are presented in **Figure 2b** in order to illustrate the size of **I** microcapsules as a function of pH. As shown the average diameters for **A**, **G**, **H**, $\mathbf{I_{7.0}}$ and $\mathbf{I_{6.0}}$ are all ~15 μm, whilst for $\mathbf{I_{5.5}}$, $\mathbf{I_{5.0}}$ and $\mathbf{I_{4.5}}$ are significantly larger (26.5 ± 1.8 μm, 35.5 ± 1.2 μm and 66.3 ± 2.0 μm, respectively). In order to investigate the cause of the increased particle size as a function of pH for **I** microcapsules, the average particle diameters for microcapsules **H** after adjusting the pH to 7.0, 6.0, 5.5, 5.0 and 4.5 were measured (**step 7**), and the results are also plotted in **Figure 2b (▲)**. It can be seen that the average particle diameter of microcapsule **H** at pH 7.0 and 6.0 are ~15 μm (same as $\mathbf{I_{7.0}}$ and $\mathbf{I_{6.0}}$). However, the average particle diameter of **H** at pH 5.5, 5.0 and 4.5 are 16.5 ± 0.8, 25.7 ± 1.1 and 56.8 ± 1.3 μm, respectively. Thus, the average particle size increased

as the pH decreased for both microcapsules **H** and **I**. As reported in the encapsulation efficiency section the $CaCO_3$ nanoparticles are increasingly soluble at pH 5.5 and below. Thus, we propose when the $CaCO_3$ nanoparticle wall starts dissolving in the acidic aqueous media, the size of the $CaCO_3$ nanoparticles reduce, and subsequently the stability of the microcapsules are decreased. Eventually, the $CaCO_3$ nanoparticles are too small to stabilize the oil droplet. These unstable oil droplets then coalesce to form a larger microcapsule (as shown in **Scheme 2**). Moreover, between **H** and **I** microcapsules, at the same pH in the range of 4.5-5.5, **I** microcapsules on average were larger.



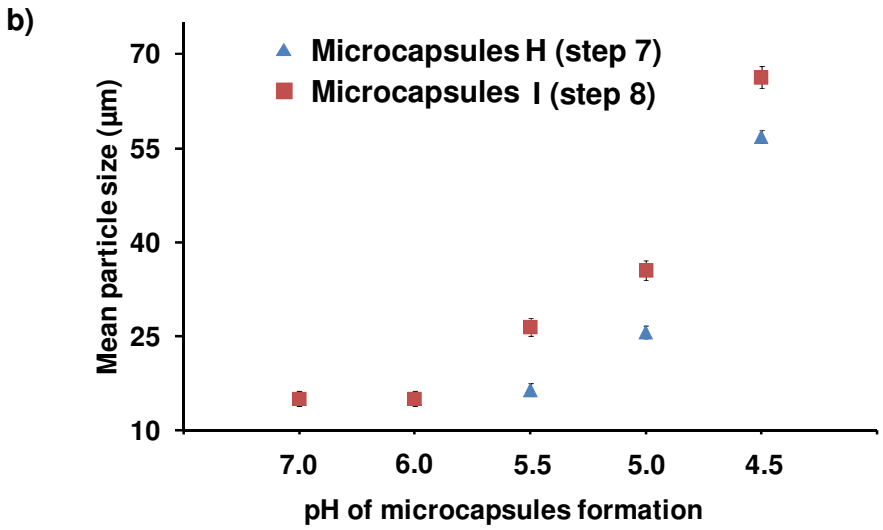
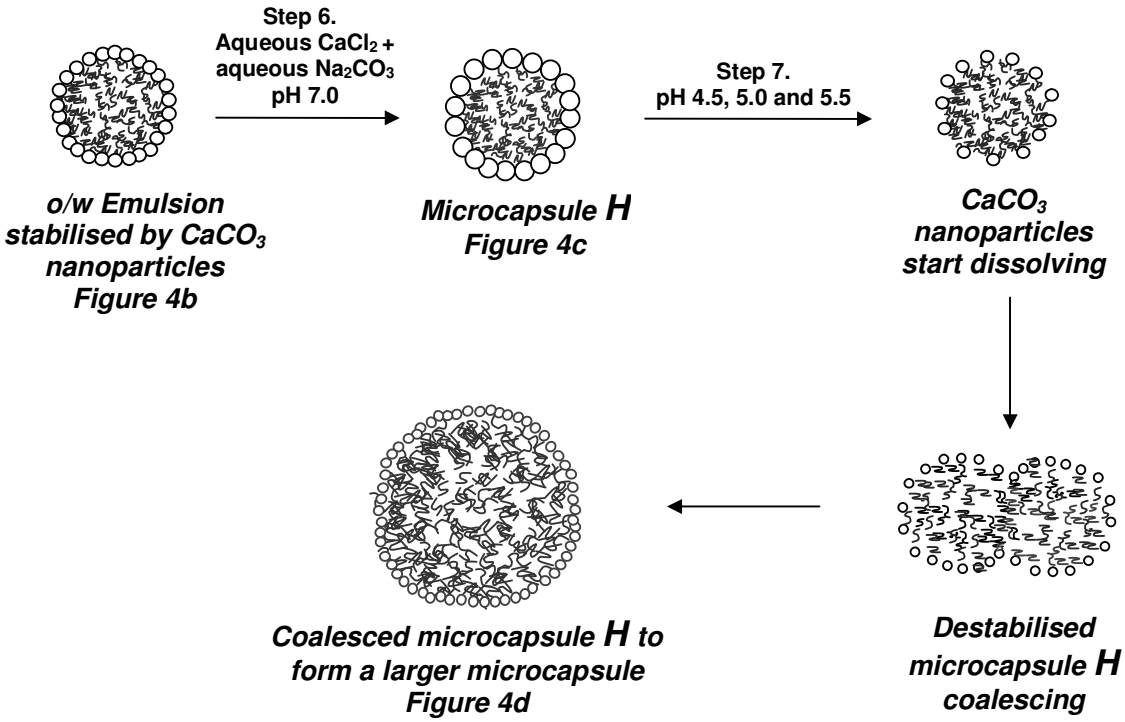


Figure 2. a) Average particle size for microcapsules **A**, **G**, **H**, $\mathbf{I_{7.0}}$ and $\mathbf{I_{6.0}}$, b) Average particles size for microcapsules **H** and **I** at pH 4.5, 5.0, 5.5, 6.0 and 7.0.

As previously discussed, the size reduction rate of the $CaCO_3$ nanoparticles was proportional to both pH and time. Hence, the diameter of microcapsules **I** at pH 5.5, 5.0 and 4.5 were then able to grow in a similar manner to that shown in **Scheme 2**, leading to a larger particle size for microcapsules **I** at the lower pH (**Figure 2b**). Furthermore, when two microcapsules coalesce, core oil might escape from the original microcapsules ($\mathbf{I_{4.5}}$, $\mathbf{I_{5.0}}$ and $\mathbf{I_{5.5}}$), which accounts for the lower encapsulation efficiency of microcapsules $\mathbf{I_{4.5}}$, $\mathbf{I_{5.0}}$ and $\mathbf{I_{5.5}}$.



Scheme 2. A schematic representation of the pH effect on the particle size of the microcapsules **H** at pH 4.5, 5.0 and 5.5.

4.3.4 Morphology

The morphology of microcapsules **A**, **G**, **H** and $\mathbf{I_{6.0}}$ were evaluated using ESEM. Images are shown in **Figure 3**. It can be seen that all of the microcapsules are spherical. Microcapsules **A** reveals a smooth surface (**Figure 3a**). In contrast, the surface of microcapsules **G** is coarse (**Figure 3b**). This rougher morphology might be caused by the aggregation of the $CaCO_3$ nanoparticles as seen from the enlarged TEM images in **Figure 4b**. Significant reduction in the coarseness of the morphology of the microcapsules **H** was observed (**Figure 3c)**, which is probably due to the $CaCO_3$ nanoparticles ripening process leading to a smoothing of the original microcapsule wall. A further reduction in the coarseness (**Figure 3d**) of the microcapsule wall was observed in the double shell

composite microcapsules ($\mathbf{I_{6.0}}$), which is probably due to the smoothing effect of the cross-linked MF polymer filling the gaps in the ripened nanoparticulate $CaCO_3$ wall (see wall structure and thickness section **4.3.5**).

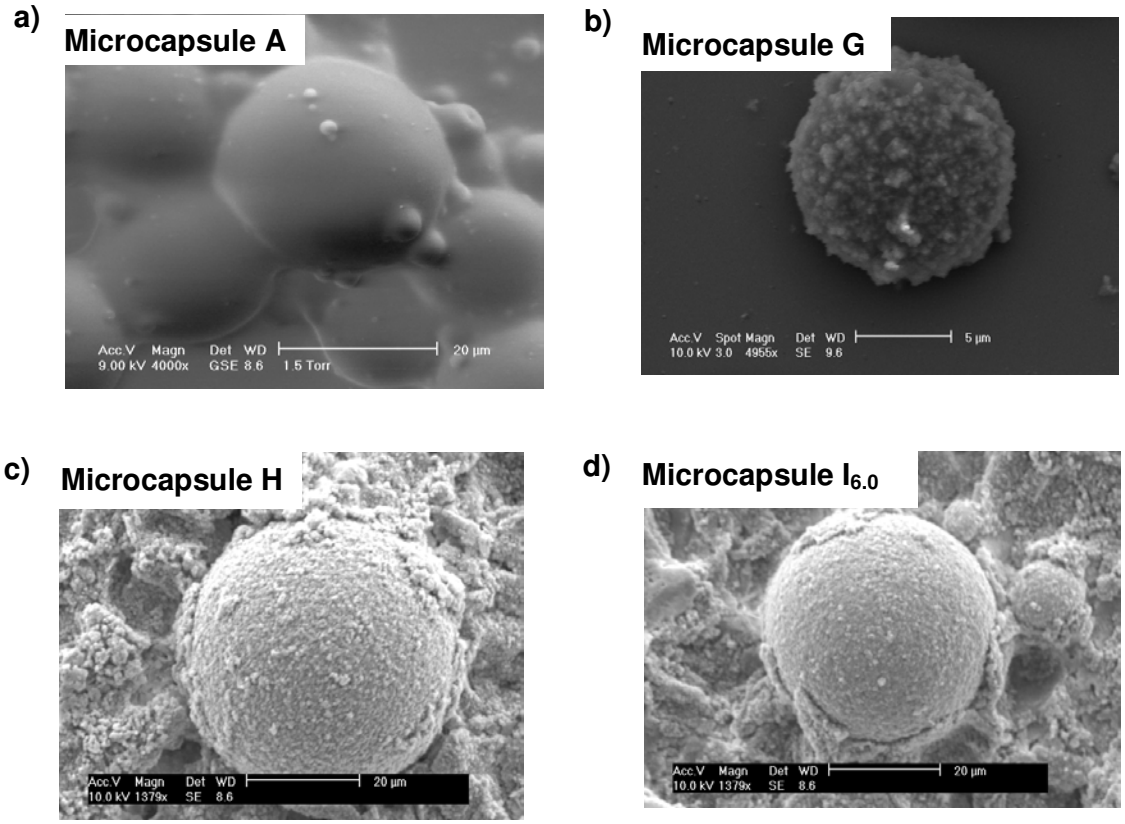


Figure 3. ESEM images of morphology of microcapsules **A**, **G**, **H** and $\mathbf{I_{6.0}}$.

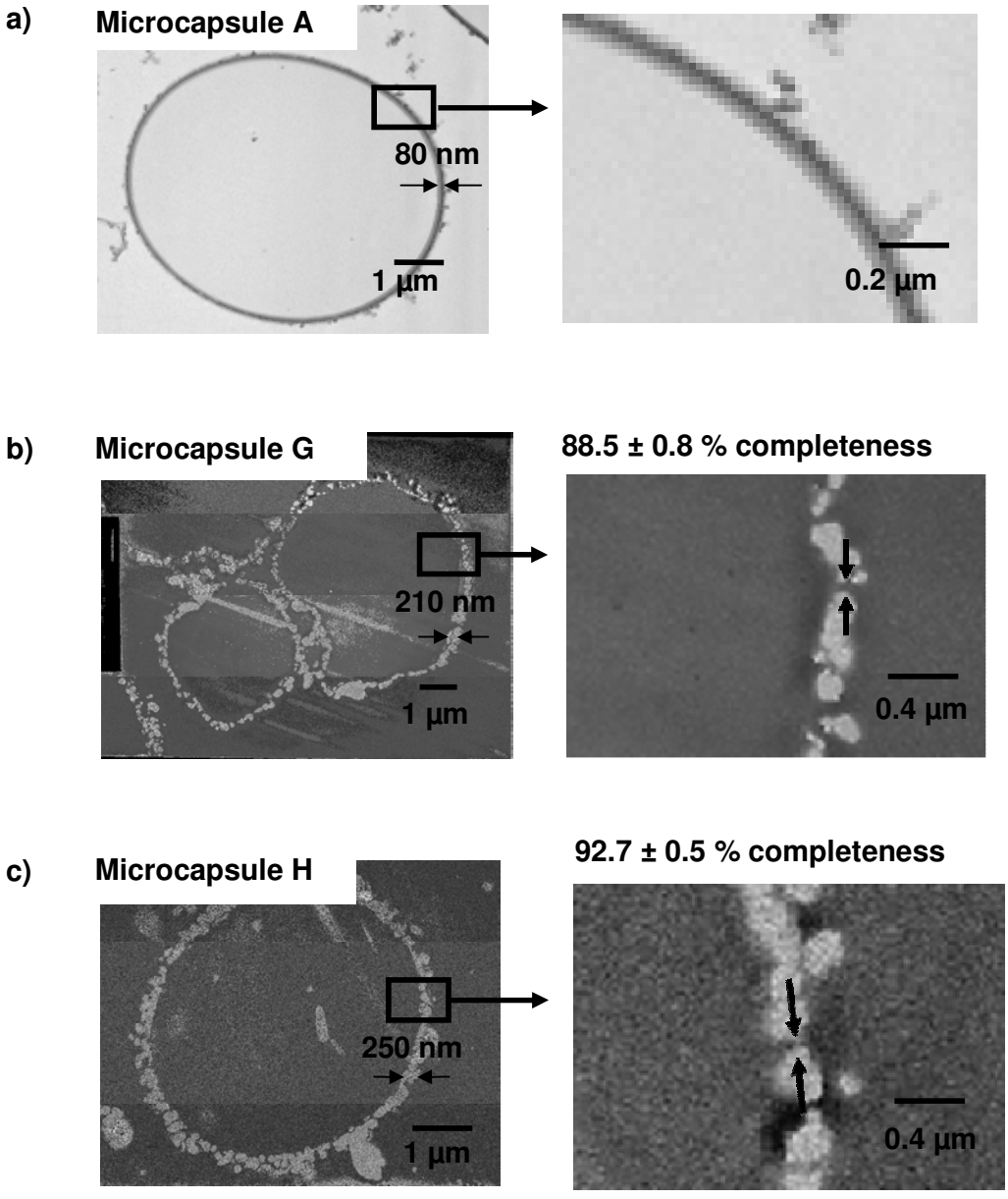
4.3.5 Wall Structure and Thickness

The wall thicknesses of the microcapsules were evaluated from the ultra-microtome sections of the microcapsules using TEM. **Figure 4** (LHS) shows the typical TEM images of an ultra-microtome section of microcapsules **A**, **G**, **H**, $\mathbf{I_{5.5}}$ and $\mathbf{I_{6.0}}$. The average wall thickness of the $CaCO_3$ outer shell for each type of microcapsule was calculated

from 40 microcapsules: **A =** 80 ± 3.2 nm, **G** = 210 ± 8.2 nm, **H =** 250 ± 8.2 nm $\mathbf{I_{5.5}}$ = 72 ± 3.5 nm and $\mathbf{I_{6.0}}$ = 402 ± 6.8 nm. It can be seen that $\mathbf{I_{5.5}}$ has a much thinner $CaCO_3$ wall than that of $\mathbf{I_{6.0}}$, and large sections of the $CaCO_3$ wall are incomplete. This thinner $CaCO_3$ nanoparticulate wall of $\mathbf{I_{5.5}}$ agrees with the hypothesis in **Scheme 2**, where the $CaCO_3$ nanoparticles dissolve at pH 5.5 and below, causing the $CaCO_3$ nanoparticle wall of microcapsules $\mathbf{I_{5.5}}$ to be comprised of much smaller $CaCO_3$ nanoparticles. Indeed, microcapsule $\mathbf{I_{5.5}}$ reveals that the ultra microtome process appears to rupture the microcapsules. Indeed, it was not possible to obtain (i) intact ultra microtome microcapsule walls for $\mathbf{I_{4.5}}$ and $\mathbf{I_{5.0}}$ and (ii) micromanipulation force data on $\mathbf{I_{4.5}}$, $\mathbf{I_{5.0}}$ and $\mathbf{I_{5.5}}$ (see the mechanical properties section), presumably because these microcapsules are very weak.

Microcapsules **A** have a smooth interior and exterior wall. This smooth interior and exterior wall is in contrast with microcapsules **G**, **H**, $\mathbf{I_{5.5}}$ and $\mathbf{I_{6.0}}$ where their exterior wall appears less regular (**Figure 4b-e** (LHS)) than the interior wall. This dissimilarity between outside and inside is probably a result of the assembly of the $CaCO_3$ nanoparticles at the o/w interface: the hydrophilic nature of the $CaCO_3$ nanoparticles minimising the contact area with the inner oil, giving the smoother interior surface, and conversely maximising surface area, in contact with the outer aqueous medium, affording the rougher exterior surface. Also, it can be seen from the cross sections that the wall of microcapsule **G** is distorted. The distortion of the wall is probably due to the sample preparation by ultra-microtome (details are described in the experimental section), which suggests that the wall is not as robust as the ripened microcapsule walls formed in **H** and $\mathbf{I_{6.0}}$. In addition, the microcapsule $CaCO_3$ walls for **G**, **H**, $\mathbf{I_{5.5}}$ and $\mathbf{I_{6.0}}$ appear

discontinuous. This discontinuity in the wall structure also accounts for the rougher morphology observed from the ESEM images.



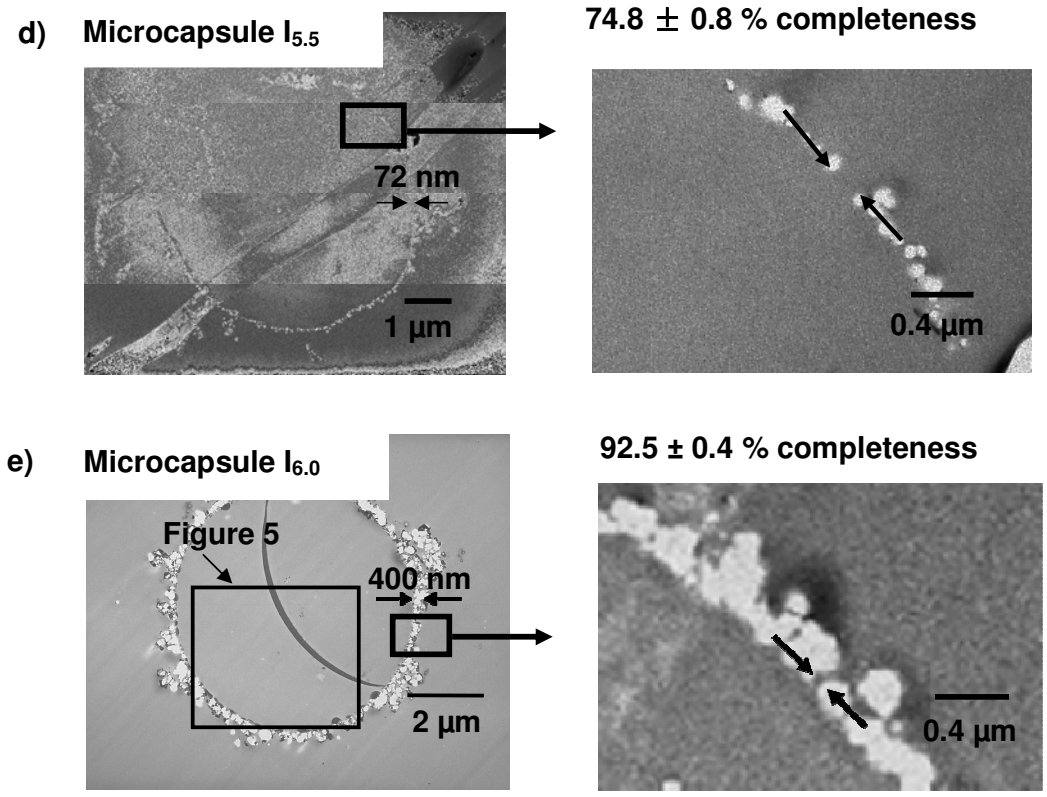
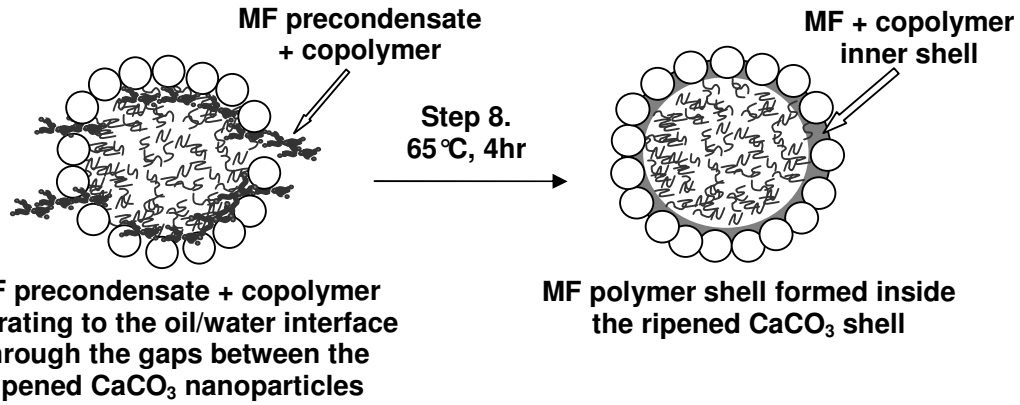


Figure 4. TEM images of microcapsule walls; a) microcapsules **A**, b) microcapsules **G**, c) microcapsules **H**, d) microcapsules $\mathbf{I_{5.5}}$, e) microcapsule $\mathbf{I_{6.0}}$.

In addition, the TEM image of microcapsule $\mathbf{I_{6.0}}$ (**Figure 4e**) reveals a double shell structure of a MF polymer inner shell and a ripened NP $CaCO_3$ outer shell. This double shell structure matches our hypothesis that the MF precondensate and copolymer migrates between the gaps of the ripened $CaCO_3$ nanoparticles and reacts at the oil-water interface to form the MF polymer inner shell, as shown in **Scheme 3**.



Scheme 3. Schematic representation of the MF inner wall formation of the double shell composite microcapsules.

To confirm the structure, EDX analysis was carried out on the ultramicrotome section (**Figure 5a** enlarged image of **Figure 4e**) of the double shell microcapsules, and the results are shown in **Figure 5b-d**. The EDX analysis confirms that the inner shell is MF polymer (**Figure 5b**) and the outer shell consists of the ripened NP $CaCO_3$ (**Figure 5c**). The line in the middle of the double shell microcapsules is MF polymer (**Figure 5d**), which has detached from the outer shell due to the ultramicrotome section process.

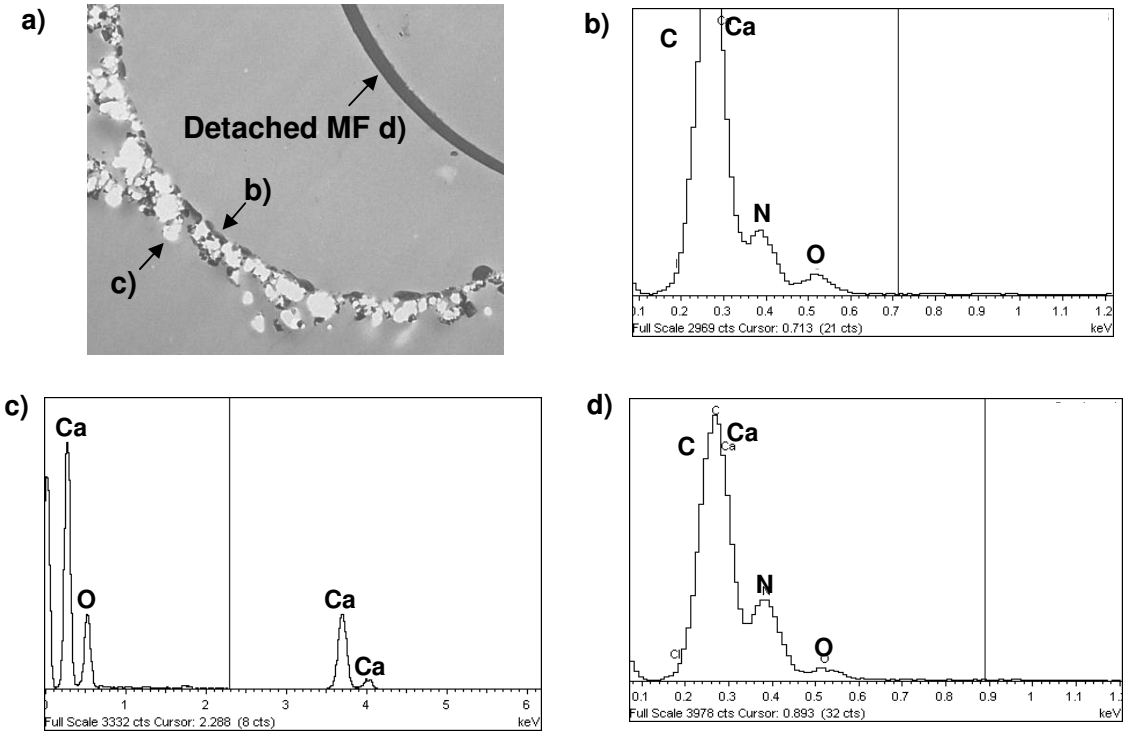


Figure 5. a) Enlarged TEM image of the double shell composite microcapsules. b-d) EDX analysis of the ultramicrotome section of the double shell composite microcapsules.

4.3.6 Degree of Wall Formation of the Unripened or Ripened $CaCO_3$ Nanoparticles

TEM images of ultra microtome sections of microcapsules **A**, **G**, **H**, $\mathbf{I_{5.5}}$ and $\mathbf{I_{6.0}}$ are illustrated in **Figure 4a-e** (RHS). The discontinuous nature of the $CaCO_3$ component of the walls formed from the unripened (**G**) or ripened (**H**, $\mathbf{I_{5.5}}$ and $\mathbf{I_{6.0}}$) $CaCO_3$ nanoparticles shows the degree of wall formation are 88.5 %, 92.7 %, 74.8 % and 92.5 %, respectively. The increase from **G** to **H** is as expected due to the $CaCO_3$ ripening process. Interestingly, by modulating the pH in **step 7** (**Scheme 1**) we are able to control the degree of $CaCO_3$ wall formation such that at pH 5.5 it is ~75 %, and at pH 6.0 it is ~92 %.

4.3.7 Mechanical Properties

The mechanical properties of the microcapsules **A**, **G**, **H**, $\mathbf{I_{6.0}}$ and $\mathbf{I_{7.0}}$ were evaluated using the micromanipulation technique. A typical relationship of the force imposed on a single microcapsule as a function of the probe moving distance is shown **Figure 6a** for microcapsule $\mathbf{I_{6.0}}$. The distance between **0** and **I** corresponds to the transducer probe moving in the air, before it has made contact with the microcapsule, and the force imposed on the microcapsule is zero. After point **I** the probe touches the microcapsule, and the force imposed on the microcapsule increases until point **II**, at which the microcapsule ruptures. As a result, the force drops to point **III**. The probe continues to compress the debris of the microcapsule (**III**-**IV**) until it touches the slide at point **IV**, after which the force increases as the probe pushes onto the slide. From this curve, the rupture force of the microcapsule can be determined (point **II**). The displacement at rupture (δ_R) is denoted as the distance that the probe travels from contact with microcapsule until rupture. The deformation at rupture is calculated using equation 1 (d = initial microcapsule diameter) (see **Chapter 3**, equation 1), and the nominal rupture stress is calculated using equation 2 (see **Chapter 3**, equation 2) as shown below, where F_R is the rupture force (point **II**). Microcapsules $\mathbf{I_{4.5}}$, $\mathbf{I_{5.0}}$ and $\mathbf{I_{5.5}}$ were too weak to be tested using the micromanipulation technique.

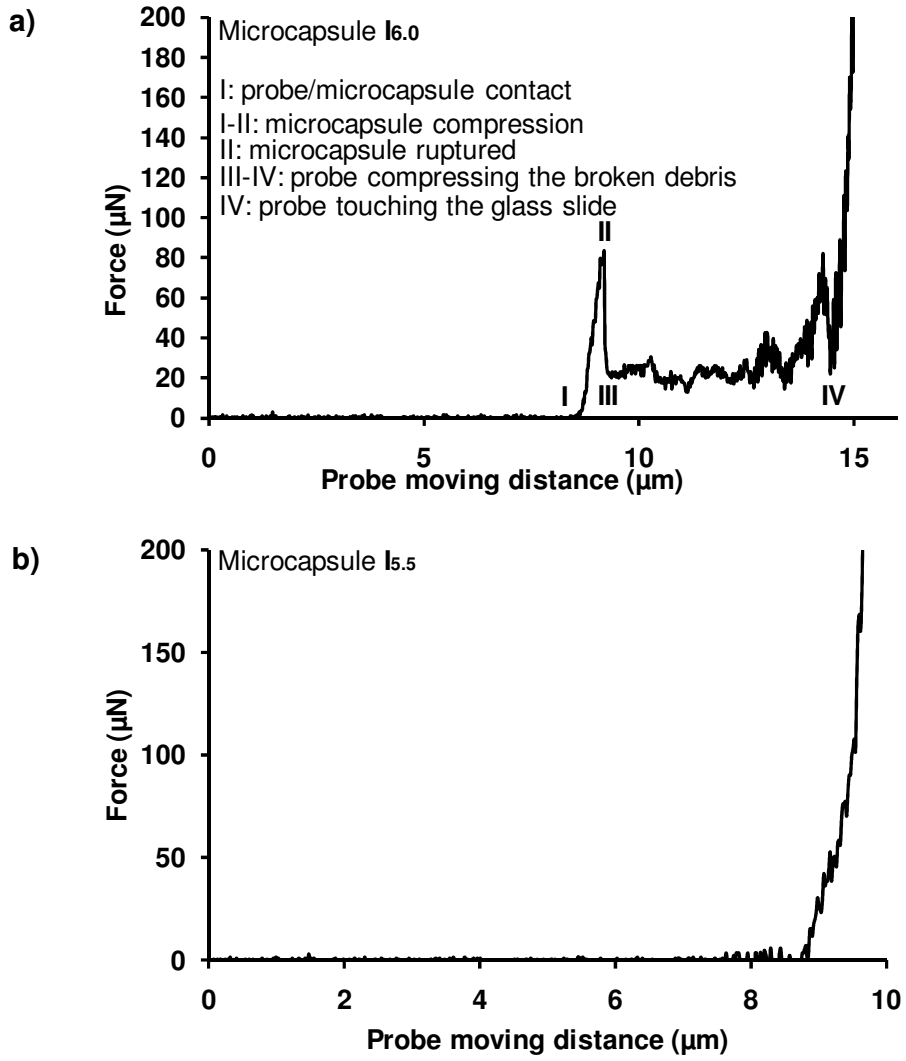


Figure 6. a) Force vs. probe moving distance for compressing single microcapsules $\mathbf{I_{6.0}}$ to rupture, b) force vs. probe moving distance for compressing single microcapsules $\mathbf{I_{5.5}}$.

It can be seen from the optical microscopic images, microcapsules $\mathbf{I_{4.5}}$ and $\mathbf{I_{5.5}}$ (**Figure 7a** and **7b)** still maintain a spherical shape in the aqueous media, but some of the $\mathbf{I_{4.5}}$ microcapsules are ruptured. However, the side view optical microscopic images show that after air dried, $\mathbf{I_{4.5}}$ microcapsules (**Figure 7c**) were ruptured on the glass substrate, whereas $\mathbf{I_{5.5}}$ microcapsule (**Figure 7c**) still maintained a spherical shape. Nevertheless, no

rupture force was observed for microcapsule $\mathbf{I_{5.5}}$, as shown in the force vs. probe moving distance graph (**Figure 6b**).

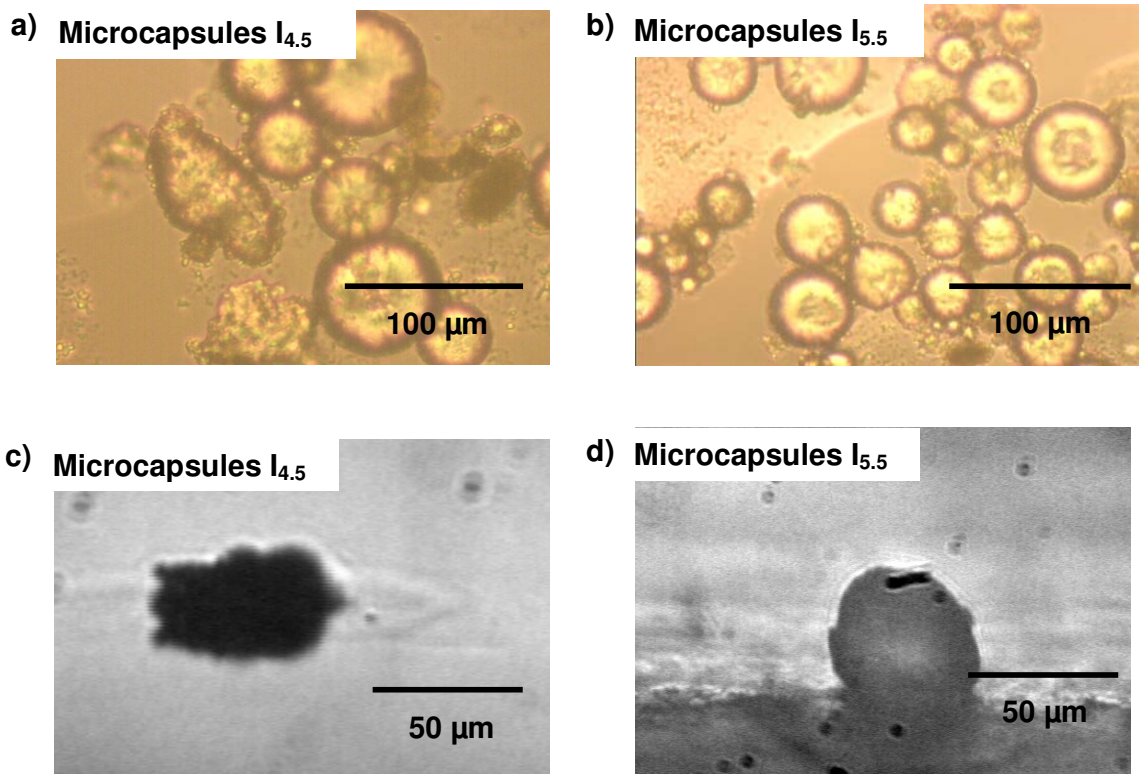


Figure 7. a) and b) Optical microscopic images of microcapsules $\mathbf{I_{4.5}}$ and $\mathbf{I_{5.5}}$ in aqueous, c) and d) side view optical microscopic images of microcapsules $\mathbf{I_{4.5}}$ and $\mathbf{I_{5.5}}$ on a glass substrate for the macromanipulation measurement.

The nominal rupture stress and deformation at rupture for microcapsules **A**, **G**, **H**, $\mathbf{I_{6.0}}$ and $\mathbf{I_{7.0}}$ are plotted in **Figure 8**. The nominal rupture stresses obtained are 1.3 ± 0.1 0.20 ± 0.03, 0.47 ± 0.04, 0.55 ± 0.07 and 0.50 ± 0.05 MPa for microcapsules **A**, **G**, **H**, $\mathbf{I_{6.0}}$ and $\mathbf{I_{7.0}}$, respectively. Clearly the organic non-composite microcapsules **A** can endure a greater stress than the other particles. The relatively low value of the nominal rupture stress of microcapsules **G** correlates well with the distortion of the wall shown in the

TEM images in **Figure 4b**, where the ultra microtome process led to wall deformation. This result is in contrast to microcapsules **H**, $\mathbf{I_{6.0}}$, and $\mathbf{I_{7.0}}$ which maintained their shape and have higher rupture stress than **G**.

The deformation at rupture for microcapsule **A** is 24.9 ± 1.5 %, whereas the $CaCO_3$ containing microcapsules **G**, **H**, $\mathbf{I_{6.0}}$, and $\mathbf{I_{7.0}}$ have values of 7.4 ± 0.3 %, 8.1 ± 0.6 %, 7.3 ± 0.5 % and 7.1 ± 0.4, respectively. These results reveal that all the microcapsules that contain the ripened $CaCO_3$ nanoparticulate inorganic wall possess similar deformation. Moreover, their smaller deformation at rupture reveals that they are more brittle than the MF microcapsules (**A**). It can be seen that the mechanical properties of the double shell microcapsules are dominated by the ripened $CaCO_3$ nanoparticulate outer shell, and the microcapsules have a higher rupture stress after ripening.

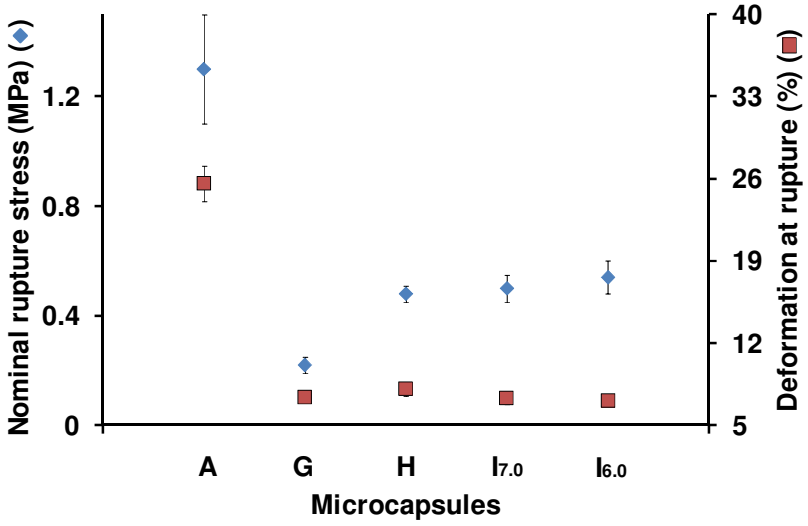
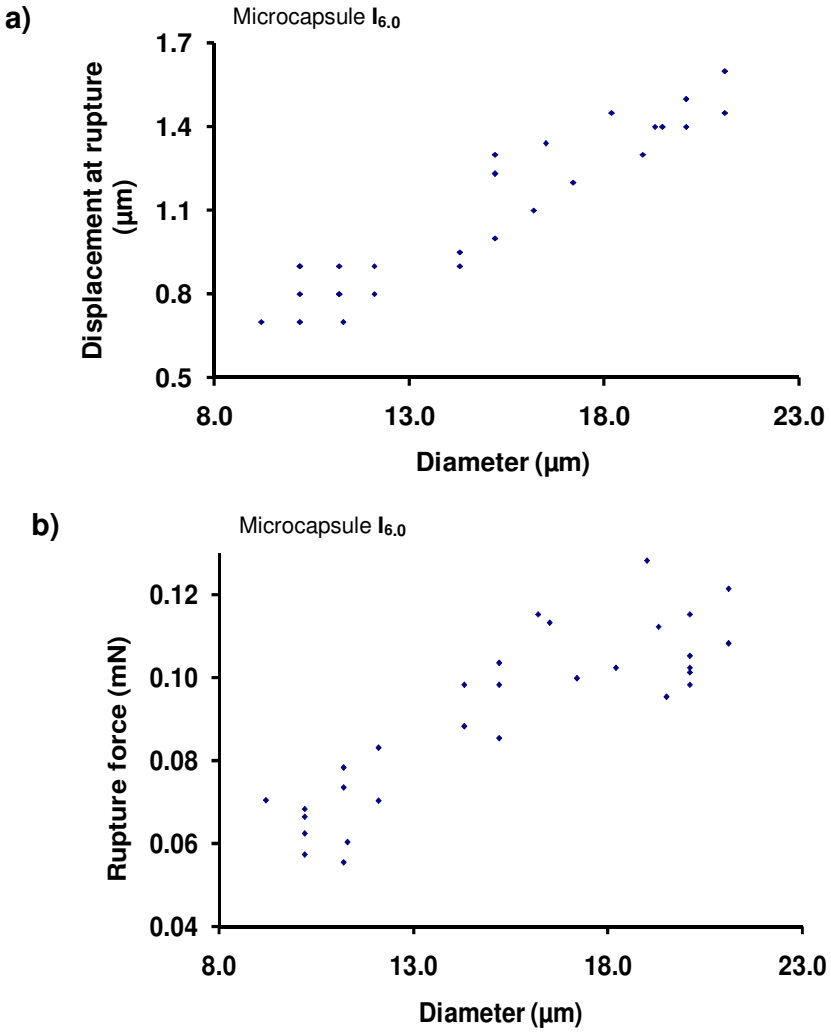


Figure 8. Nominal rupture stress and deformation at rupture of microcapsules **A**, **G**, **H**, $\mathbf{I_{7.0}}$ and $\mathbf{I_{6.0}}$.

The displacement at rupture, rupture force and nominal stress at rupture are plotted as a function of particle diameter for microcapsules $\mathbf{I_{6.0}}$, and are shown in **Figure 9a**, **9b** and **9c**, respectively. The graph shows that for the same type of microcapsules, the displacement at rupture (**Figure 9a**) and rupture force (**Figure 9b**) increase as the diameter of the microcapsules increase. In contrast, a downward trend of the nominal stress at rupture (**Figure 9c**) was observed when the particle diameter increases. It is suggesting that larger microcapsules were found to rupture more easily than smaller ones, this is also found in the previous studies.[41]



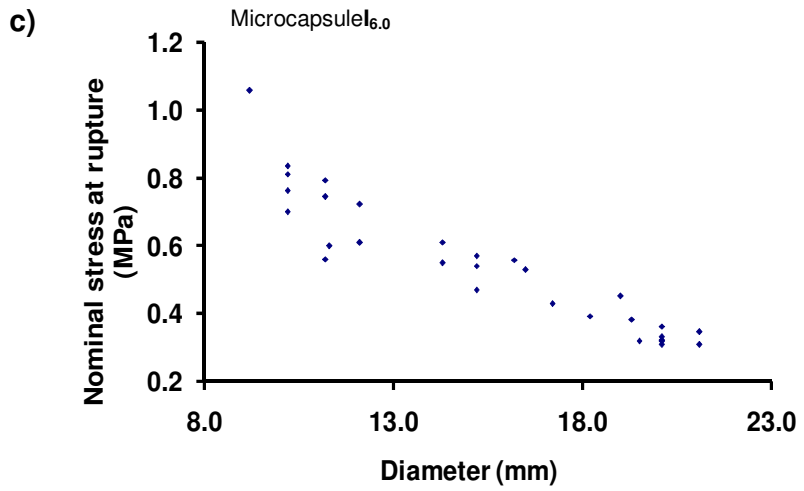


Figure 9. Displacement at rupture, rupture force and nominal stress at rupture for microcapsule $\mathbf{I_{6.0}}$ as a function of diameter.

4.3.8 Oil Leakage and Kinetics

The oil leakage in weight percentage for microcapsules **A**, **G**, **H**, $\mathbf{I_{4.5}}$, $\mathbf{I_{5.0}}$, $\mathbf{I_{5.5}}$, $\mathbf{I_{6.0}}$ and $\mathbf{I_{7.0}}$ is illustrated in **Figure 10**. The leakage for non-composite microcapsules **H** (inorganic) and **A** (organic) at the end of 24 hours are 2.25 ± 0.02 % and 1.78 ± 0.01 %, respectively. An order of magnitude drop was observed from the unripened composite microcapsules **G** (0.15 ± 0.011 %). The ripened composite microcapsules $\mathbf{I_{7.0}}$ and $\mathbf{I_{6.0}}$ show the least leakage 0.095 ± 0.012 % and 0.094 ± 0.024 %, respectively. Thus, the composite microcapsules **G**, $\mathbf{I_{7.0}}$ and $\mathbf{I_{6.0}}$ leak less than microcapsules **H** and **A**. In addition, microcapsules **A** leak less than **H**, suggesting the MF/copolymer wall is more effective in reducing the leakage than the ripening process of the $CaCO_3$ nanoparticles. Microcapsules $\mathbf{I_{7.0}}$ and $\mathbf{I_{6.0}}$ leak less than **G**, suggesting the ripening process does induce another barrier to leakage. However, when one considers the degree of wall formation of the $CaCO_3$ nanoparticles and the rupture stress, there is no correlation between them and the leakiness of the microcapsules. In contrast, the degree of the wall formation and

rupture stress are correlated since the ripened microcapsules $\mathbf{I_{6.0}}$, and $\mathbf{I_{7.0}}$ have high rupture stress (0.54 MPa and 0.50 MPa) and a more complete wall structure (~92.5 %). This indicates that the degree of wall formation of the $CaCO_3$ nanoparticles and the rupture stress may be dominated by the macrostructure of microcapsules whilst leakiness is determined by the fine structure of the wall. When comparing the leakage of microcapsules $\mathbf{I_{4.5}}$, $\mathbf{I_{5.0}}$, $\mathbf{I_{5.5}}$, $\mathbf{I_{6.0}}$, and $\mathbf{I_{7.0}}$ as shown in **Figure 10**, it was found that the leakage increased when the pH was decreased from 6.0 to 4.5 (79.21 ± 1.52 % for $\mathbf{I_{4.5}}$). The higher leakage for microcapsules $\mathbf{I_{4.5}}$, $\mathbf{I_{5.0}}$ and $\mathbf{I_{5.5}}$ and their lower encapsulation efficiency than $\mathbf{I_{6.0}}$ and $\mathbf{I_{7.0}}$ are all attributed to their incomplete wall structures (shown in the TEM images in **Figure 4d**), which are probably due to the dissolution of the ripened outer $CaCO_3$ nanoparticulate wall at low pHs (**Scheme 2**).

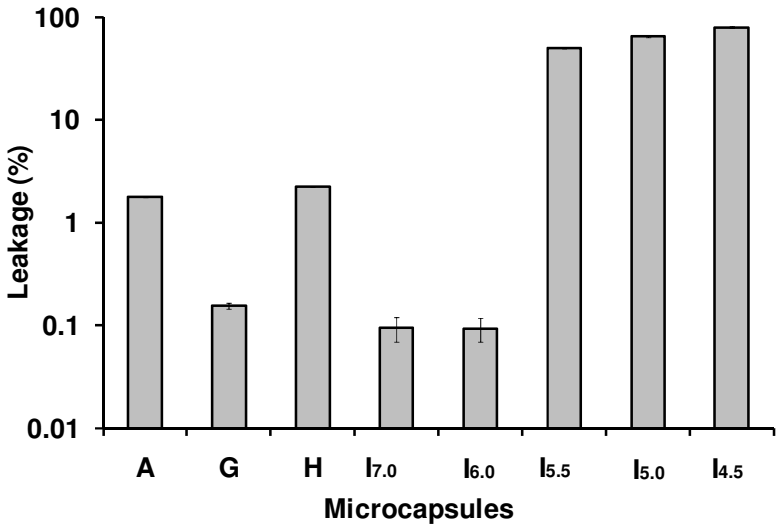
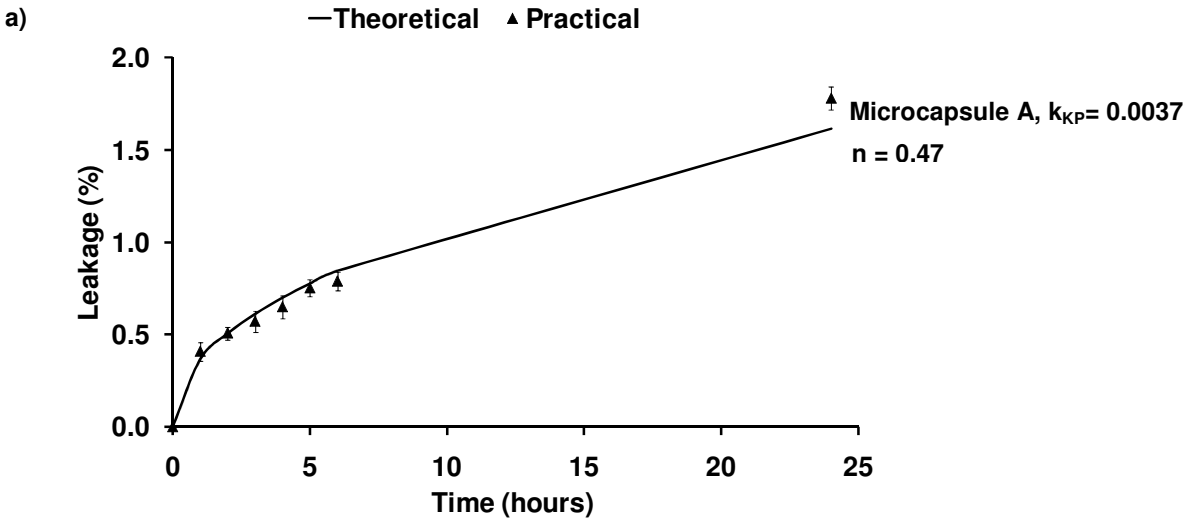


Figure 10. Leakage for microcapsules **A**, **G**, **H**, $\mathbf{I_{4.5}}$, $\mathbf{I_{5.0}}$, $\mathbf{I_{5.5}}$, $\mathbf{I_{6.0}}$ and $\mathbf{I_{7.0}}$.

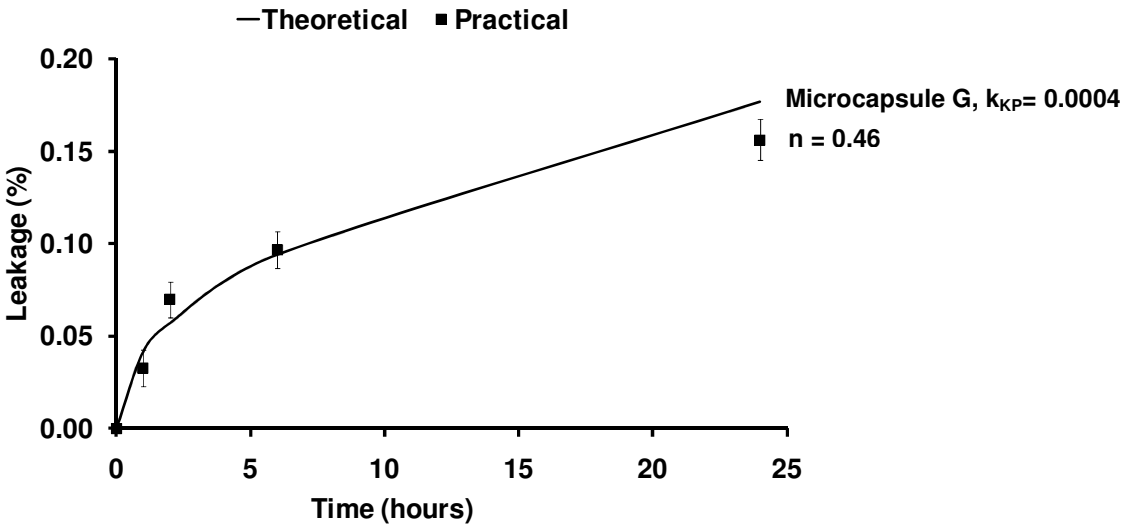
To characterize the kinetics of the oil leakage from the microcapsules, Korsmeyer-Peppas model is used is used:

$$\frac{M_t}{M_\infty} = k_{KP}\, t^n \qquad (3)$$

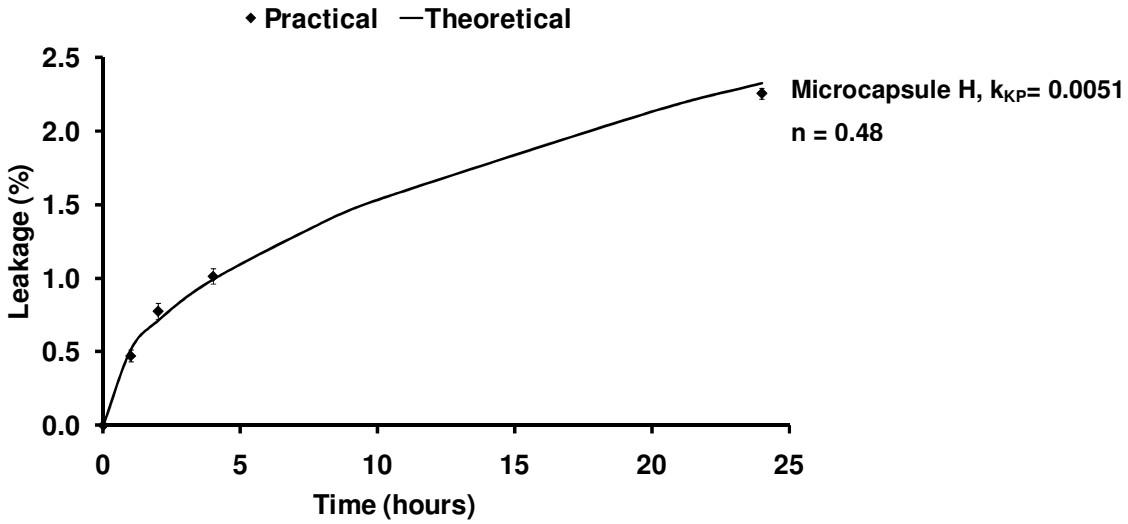
where M_t is the amount of oil leaked at time t, M_∞ is the amount of the oil leaked at infinite time, k_{KP} is the rate constant for Korsmeyer-Peppas model and n is the Power Law constant, an indication of release mechanism. The leakage profiles for microcapsules **A**, **G**, **H**, $\mathbf{I}_{6.0}$ and $\mathbf{I}_{7.0}$ were fitted by Korsmeyer-Peppas model (equation (**3**)) using the least square method, and the results are shown in **Figure 11a-e**.



b)


—Theoretical ■ Practical
0.20
0.15
0.10
0.05
0.00
Leakage (%)
0
5
10
15
20
25
Time (hours)
Microcapsule G, k_{KP}= 0.0004
n = 0.46

c)


◆ Practical —Theoretical
2.5
2.0
1.5
1.0
0.5
0.0
Leakage (%)
0
5
10
15
20
25
Time (hours)
Microcapsule H, k_{KP}= 0.0051
n = 0.48

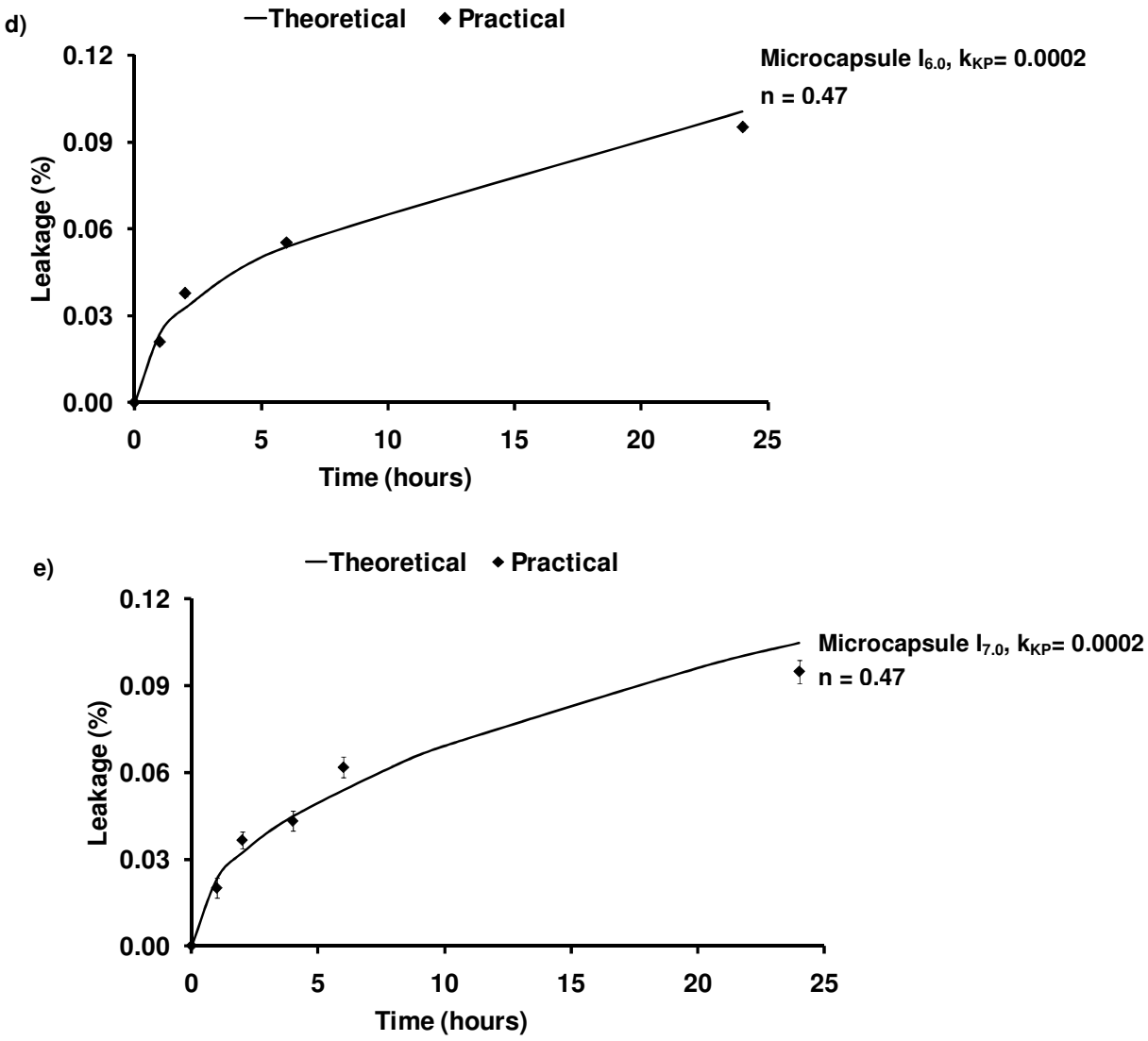


Figure 11. Leakage kinetics of microcapsules **A**, **G**, **H**, $\mathbf{I_{6.0}}$ and $\mathbf{I_{7.0}}$.

It can be seen that all the leakage profiles for microcapsules **A**, **G**, **H**, $\mathbf{I}_{6.0}$ and $\mathbf{I}_{7.0}$ fit the model reasonably well. The release mechanism is diffusion when n equals 0.5 (Higuchi's model).[188] The result suggests that the leakage mechanism for microcapsules **A**, **G**, **H**, $\mathbf{I}_{6.0}$ and $\mathbf{I}_{7.0}$ is primarily governed by diffusion. However, there might be other leakage mechanisms involved. Moreover, the leakage rate for non-composite microcapsules **A** and **H** (indicated by k_{kp} 0.0037 and 0.0051, respectively) are higher than that of the composite microcapsules **G** and $\mathbf{I_{6.0}}$ (k_{kp} 0.0004 and 0.0002, respectively). However, the

value of n for microcapsules $\mathbf{I_{5.5}}$, $\mathbf{I_{5.0}}$ and $\mathbf{I_{4.5}}$ are 0.32, 0.36 and 0.35 (fitting not shown), respectively, indicating that the release mechanism for these microcapsules is not dominated by diffusion. Moreover, the leakage rate (k_{kp}) for microcapsules $\mathbf{I_{5.5}}$, $\mathbf{I_{5.0}}$ and $\mathbf{I_{4.5}}$ are 0.10, 0.20 and 0.23, respectively. It can be seen that when pH is decreased, the leakage rate of the microcapsules increases.

4.4 Conclusions

The double shell composite microcapsules with ripened $CaCO_3$ outer shell and MF polymer/composite inner shell were shown to have reduced core oil leakage over the non-composite materials (20 fold reductions of leakage from the MF microcapsules (**A**), and 25 fold reductions from the ripened $CaCO_3$ nanoparticulate microcapsules (**H**)). The leakage mechanism for microcapsules **A**, **G**, **H** and $\mathbf{I_{6.0}}$ are all primarily governed by diffusion. It was also found that by ripening the $CaCO_3$ nanoparticles outer wall with the aqueous $CaCl_2$ and Na_2CO_3, the completeness of the microcapsules wall was increased from ~88 % to ~92 %, and consequently the leakage of the microcapsules was reduced. The mechanical properties of the ripened double shell composite microcapsules (**I**) are dominated by the outer ripened $CaCO_3$ nanoparticulate shell in terms of both the deformation at rupture and the nominal rupture stress. From the pH dependent study it was found that the stability and properties of the ripened double shell microcapsules ($\mathbf{I_{4.5}}$, $\mathbf{I_{5.0}}$, $\mathbf{I_{5.5}}$, $\mathbf{I_{6.0}}$, and $\mathbf{I_{7.0}}$) are influenced by pH. As the pH increases from 4.5 to 6.0, the encapsulation efficiency of the microcapsules increased from ~15 % to ~75 %, the average diameter of the microcapsules decreased from ~66 μm to ~15 μm, and the leakage of the microcapsules decreased from 79.2 ± 1.5 % to 0.095 ± 0.002 %. The wall thickness of the microcapsules increased from 72 ± 3.5 nm to 402 ± 5.6 nm when pH

increases from 5.5 to 6.0, and the degree of wall formation formed by the ripened $CaCO_3$ nanoparticles increased from 74.8 ± 0.8 % to 92.5 ± 0.4 %. However, the above properties of the microcapsules remain unchanged when the pH increased from 6.0 to 7.0. Therefore, we have presented a new methodology of reducing the porosity of the inorganic $CaCO_3$ nanoparticulate microcapsules by ripening with another layer of $CaCO_3$, before adding the MF precondensate and forming the inner shell. This composite material is low cost and the release of core material could be triggered by mechanical fracture, enabling stabilization and controlled delivery of small molecules in various environments.

CHAPTER 5

Engineering the Mechanical and Physical Properties of Organic/inorganic Composite Microcapsules

Abstract

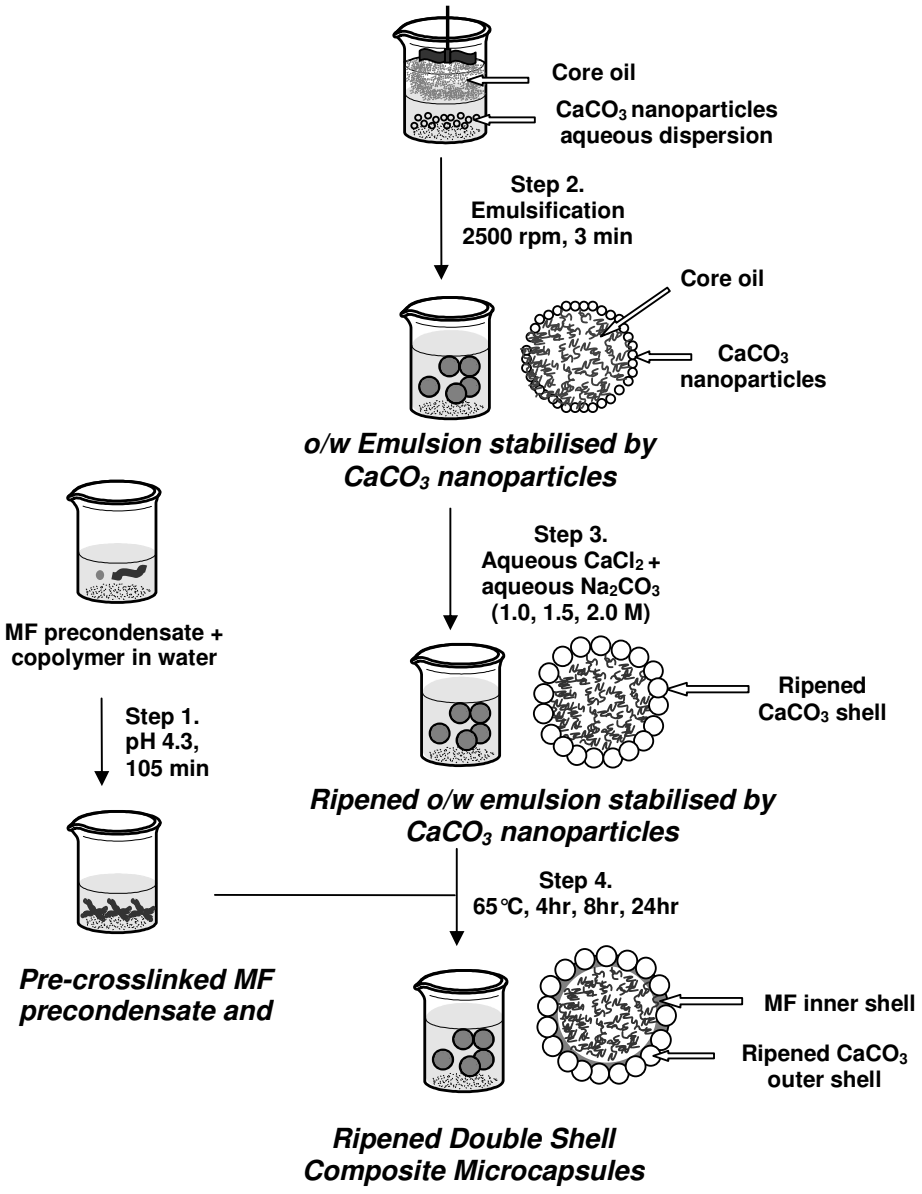
In the work reported in the previous chapter (**4**) ripened double shell composite microcapsules with a ripened $CaCO_3$ nanoparticle outer shell and melamine formaldehyde (MF)/copolymer inner shell were produced. The method was based on *in situ* polymerization to form a MF/copolymer shell inside the ripened $CaCO_3$ nanoparticles shell. The MF precondensate and copolymer migrated through the interstice of the ripened $CaCO_3$ nanoparticles leading to polymerization at the oil-water interface. In this study, the effects of certain formulation parameters on the properties of the double shell composite microcapsules were investigated, *i.e.* the MF cross-linking time and the concentration of the aqueous $CaCl_2$ and Na_2CO_3 used for the ripening process of $CaCO_3$ nanoparticles were varied. The properties of the microcapsules such as encapsulation efficiency, wall thickness, degree of wall formation formed by the ripened $CaCO_3$ nanoparticles, diameter, nominal rupture stress and leakiness were characterized. It was found that as the reaction time for the MF polymerization increased from 4 to 24 hours during the formulation process, the thickness of the inner MF/copolymer shell increased from 129 ± 2.5 nm to 160 ± 3.1 nm, the leakage of the microcapsules decreased from 0.095 ± 0.002 % to 0.047 ± 0.001 %. As the concentration of aqueous $CaCl_2$ and Na_2CO_3 was increased in the $CaCO_3$ nanoparticulate ripening process from 1.0 M to 2.0 M, the thickness of the $CaCO_3$ nanoparticulate outer shell increased from 360 ± 5.7 nm to 580 ± 5.2 nm, and the nominal rupture stress of the microcapsules increased from 0.39 ± 0.07 MPa to 0.91 ± 0.09 MPa, as might be expected. However, a much smaller reduction in leakage was observed (from 0.052 ± 0.001 % to 0.045 ± 0.001 %).

5.1 Introduction

Calcium carbonate is a natural core-shell material.[198] It is non-toxic, stable, biocompatible and strong.[198] Therefore, in nature it is able to act as a physical barrier in shells to protect organisms from the environment, while allowing the gas and nutrient exchange through the shell. Biomimetic core-shell structured microcapsules have been developed to encapsulate active ingredients to protect them from an external environment.[192, 199, 200] Recently, calcium carbonate has attracted considerable attention for making walls of microcapsules due to its biocompatibility.[190, 192, 201] Thomas *et al.*[202] has utilised an emulsion liquid membrane technique to prepare $CaCO_3$ microcapsules, creating a pseudo water-in-oil-in-water emulsion system to precipitate calcium carbonate at the oil-water interface. The preparation of hollow $CaCO_3$ microspheres for biological applications is also an active field.[203-205] Such $CaCO_3$ microcapsules and microspheres have been used in a variety of industrial products, especially in biological applications.[206-208] However, the calcium carbonate wall possesses greater porosity when compared to organic wall materials,[209, 210] which limits its applications in encapsulation of small molecules.

It was previously reported in **Chapter 4** a methodology of reducing the permeability of the $CaCO_3$ wall by forming a MF polymer wall inside the ripened $CaCO_3$ wall. These resulting double shell composites were prepared using a method based on *in situ* polymerization of melamine formaldehyde with a copolymer migrating through the interstice of a ripened $CaCO_3$ shell, and polymerized at the oil-water interface inside the ripened $CaCO_3$ nanoparticulate shell. The synthesis is illustrated in **Scheme 1**. It was found in our previous study that by ripening the outer $CaCO_3$ nanoparticulate wall of the

composite microcapsules (**Scheme 1**, **step 3**), the wall thickness, degree of wall formation, and nominal rupture stress of the microcapsules were increased, as well as observing a 1.7 fold decrease in the leakage. It was also found that the leakage of ripened nanoparticulate $CaCO_3$ microcapsules is reduced by 25 fold when coated with MF. In that work the melamine formaldehyde copolymer cross-linking reaction time was 4 hours (**Scheme 1**, **step 4**). In this chapter, we are modulating **step 3** and **4** to examine the effect of $CaCO_3$ nanoparticulate ripening process and MF cross-linking reaction time on the following physical properties of the microcapsules: encapsulation efficiency, wall thickness, particle size, nominal rupture stress and leakage of core oil, in order to see how the changes affect the leakage.



Scheme 1. Schematic diagram of the formation of the double shell composite microcapsules.

5.2 Experimental

5.2.1 Materials

The core oil is a typical organic blend of various fragrant components which has a

relatively low solubility in water and is used in consumer products. MF precondensate (70 % (aq) w/w, formaldehyde to melamine molar ratio 0.20) was supplied by British Industrial Plastics Ltd, Birmingham, UK, formaldehyde (37 % (aq) w/w) was supplied by Sigma-Aldrich, UK. Poly(acrylamide-acrylic acid, sodium salt) was supplied by Polymersciences, Inc., US and calcium carbonate nanoparticles were supplied by Omya, UK. All chemicals were used without further purification.

5.2.2 Preparation of Ripened Double Shell Composite Microcapsules (Microcapsules $\mathbf{I_{6.0}}$, **J**, **K**, **L** and **M**)

An aqueous solution of MF precondensate (2.50 g) and copolymer (0.58 g, poly(acrylamide-acrylic acid, sodium salt) in water (70 ml) was stirred (400 rpm) with a Rushton turbine (Φ31 mm, in a vessel with standard configuration) for 105 min at pH 4 (adjusted by acetic acid (1M), monitored by a pH meter) to form pre-crosslinked MF precondensate and copolymer (**step 1**). The core oil (9.3 g) was added to an aqueous $CaCO_3$ nanoparticle dispersion (40 ml, 10 % wt) and stirred using a homogenizer (Silverson Machines Ltd) at a speed of 2500 rpm for 3 min to form an o/w emulsion (**step 2**). To the resulting emulsion, aqueous $CaCl_2$ (10 ml) and Na_2CO_3 (10 ml) (1.0, 1.5 and 2.0 M for microcapsules **K**, **L** and **M** (**Table 1**), respectively) was added *via* a pump system (Model 101U, Water Marlow, UK) over 15 min, and stirred for another 10 min at a speed of 400 rpm (**step 3**). To the resulting aqueous dispersion, the pre-crosslinked MF precondensate and copolymer solution (formed in **step 1**) was then added *via* a pump sysmtem (Model 101U, Water Marlow, UK) over 10 minutes, and the pH was raised to 6.0 with the addition of aqueous NaOH (1 M, monitored by a pH meter). The resulting dispersion was stirred at a speed of 400 rpm at 65 °C for 4, 8, and 24 hours for microcapsules $\mathbf{I_{6.0}}$, **J**, and **L**, respectively, and was allowed to cool to room temperature

(**step 4**). The exact conditions for producing the double shell composite microcapsules **$I_{6.0}$**, **J**, **K**, **L** and **M** are listed in **Table 1**.

Table 1. Encapsulation efficiency of microcapsules **$I_{6.0}$**, **J**, **K**, **L** and **M**.

Microcapsules	Reaction time (**step 4**) (hours)	Concentration of $CaCl_2$ (aq) & Na_2CO_3 (aq) (**step 3**) (M)	Encapsulation efficiency (%)
$I_{6.0}$	4	1.5	76.0 ± 1.5
J	8	1.5	75.3 ± 1.1
K	24	1.0	74.8 ± 1.4
L	24	1.5	74.2 ± 1.5
M	24	2.0	75.1 ± 1.6

5.2.3 Gas Chromatography (GC)

The leakage and encapsulation efficiency of the microcapsules were evaluated by GC. A Trace 2000 series gas chromatogram with a flame ionization detector and 30 m × 0.32 mm ZB5 inferno column was used to determine the encapsulation efficiency and leakage rate of the oil from the microcapsules. Analysis was performed using a Dionex Chromeleon Workstation. Samples injection volumes were 1µl. The injection port temperature was 250 °C. The temperature ramp for the column was increased by 10 °C/s from 50-300 °C, and held at 300 °C for 35 min. The detection temperature was 300 °C. Helium was used as the carrier gas. Details of calibration of the GC are illustrated in **Chapter 3 (3.2.3)**.

5.2.4 Encapsulation Efficiency Measurement

The microcapsules were filtered from the original aqueous dispersion and resuspended in deionized water (120 ml). Glass beads (35 g, 3 mm in diameter) were

added to the aqueous microcapsule dispersion (10 ml) and stirred at 100 rpm for 4 hours, after which the microcapsules were fully ruptured (observed with the optical microscope). Hexane (30 ml) was added to the top of the resulting aqua-oil mixture containing the broken microcapsules while stirring to extract the oil. After 10 minutes stirring, the hexane layer was seperated, and 1 µl was taken to measure the concentration of the oil by GC, and from the concentration the mass of the oil was calculated from calibration data (see supporting information). This procedure was repeated until no oil was found dissolved in the hexane (typically 3×). A sample (1 µl) was also taken from the aqueous layer and a GC ran on it, and no oil was detected. The encapsulation efficiency was calculated using the ratio of the weight of encapsulated oil to the weight of the initial amount of oil used.

5.2.5 Leakage Measurement

The microcapsules were filtered from the original aqueous dispersion, and re-dispersed in deionised water (50 ml). To the resulting aqueous dispersion (microcapsules $\mathbf{I_{6.0}}$, **J**, **K**, **L** and **M**), hexane (30 ml) was added and stirred for 10 minutes and then stopped. A hexane aliquot (1 µl) was removed and analysed by GC. Further aliquots (1 µl) were removed at various time intervals between 1 to 24 hours, prior to which the dispersion was stirred for 10 minutes.

5.2.6 Size Analysis

Mean particle size and size distribution of the microcapsules in aqueous dispersions were evaluated by laser diffraction technique (Mastersizer 2000, Malvern Instruments Ltd, UK). The measurements were carried out using a Helium-Neon laser with a measurement range of 0.05 – 900 µm connected to a sample dispersion unit. Experiments were

performed at 25°C. The mean diameter and size distribution of microcapsules were the average value of five measurements.

5.2.7 Transmission Electron Microscopy (TEM)

Transmission Electron Microscopy (JEOL 1200EX, Jeol Ltd, UK) was used to examine the structure and thickness of the microcapsule wall. Microcapsules were embedded in the LR white hard grade acrylic resin, and the ultra thin sections were obtained by using ultracut microtome apparatus (Reichert-Jung), details of the ultracut microtome sampling is illustrated in **Chapter 3** (**3.2.7**). Operating voltage was 80 eV.

5.2.8 Environmental Scanning Electron Microscopy (ESEM)

An environmental-SEM (FEI/Philips XL30 ESEM-FEG, Philips, UK) was used to study the morphology of the microcapsules. Samples were operated in high vacuum mode, and operating voltage as shown on the images.

5.2.9 Calculation of the Degree of the Wall Formation Formed by the Ripened Nanoparticulate $CaCO_3$ Nanoparticles from TEM Images

The degree of completeness of the unripened or ripened $CaCO_3$ nanoparticle wall was calculated from image analysis software (Image J, National Institute of Health) on the ultra microtome TEM images, by measuring the sum of the smallest perpendicular distance between each disconnected piece of the wall, subtracting this value from the total wall perimeter, and dividing by the total wall perimeter.

5.2.10 Micromanipulation

The mechanical properties of the microcapsules were determined by micromanipulation. A glass probe with a diameter of 50 µm mounted on a force

transducer (Model 405A, Aurora Scientific Inc., Canada) was positioned perpendicular to the glass slide. The microcapsules in the aqueous dispersion were dried on the glass slide (15 min), and observed through side and bottom-view cameras. A single microcapsule was compressed by the glass probe travelling at 2 μm s^{-1}. The voltage output generated by the transducer due to compression of the microcapsules was recorded through a data acquisition card. From the sensitivity of the transducer, the voltage was converted to force, hence the rupture force of the microcapsules was determined. Details of this technique are described elsewhere.[134] 30 microcapsules were tested for each sample.

5.3 Results and Discussion

5.3.1 Synthesis

The double shell composite microcapsules **$I_{6.0}$**, **J**, **K**, **L** and **M** were synthesized as shown in **Scheme 1**. The MF precondensate and copolymer (poly (acrylamide-acrylic acid, sodium salt)) are firstly pre-crosslinked in water (**step 1**). Core oil was mixed with the aqueous $CaCO_3$ nanoparticulate dispersion to form the o/w emulsion (**step 2**) followed by the addition of equivalent amount of aqueous $CaCl_2$ and Na_2CO_3 (1.0, 1.5 and 2.0 M) to ripen the $CaCO_3$ nanoparticles (**step 3**). Finally, the pre-crosslinked MF precondensate and copolymer formed from **step 1** was added to the resulting ripened $CaCO_3$ nanoparticulate aqueous dispersion and heating at 65 ºC at 4, 8 and 24 hours, respectively (**step 4**). The exact conditions for producing the double shell composite microcapsules **$I_{6.0}$**, **J**, **K**, **L** and **M** are listed in **Table 1**.

5.3.2 Encapsulation Efficiency

The encapsulation efficiency of microcapsules $\mathbf{I_{6.0}}$, **J**, **K**, **L** and **M** are all ~75 % (shown in **Table 1**) suggesting that neither increasing the reaction time of the MF coating from 4 to 24 hours in **step 4** (**Scheme 1**) or the concentrations of aqueous $CaCl_2$ and Na_2CO_3 used in the $CaCO_3$ nanoparticulate ripening process in **step 3** (**Scheme 1**), has any effect on the stability of the initial o/w emulsion formed in **step 2** (**Scheme 1**).

5.3.3 Wall Thickness and Degree of Wall Completeness

The wall thickness and degree of wall completeness formed by the ripened $CaCO_3$ nanoparticles for microcapsules $\mathbf{I_{6.0}}$, **J**, **K**, **L** and **M** were evaluated and studied from the TEM images of the ultra-microtome sections, as shown in **Figure 1**. As one might expect neither the outer $CaCO_3$ wall thickness of the ripened double shell composite microcapsules (402 ± 4.6, 406 ± 3.5 and 410 ± 3.8 nm for microcapsules $\mathbf{I_{6.0}}$, **J**, and **L**, respectively (**Figure 2**)) or the degree of wall formation formed by the ripened $CaCO_3$ nanoparticles (92.9 ± 0.5 %, 93.0 ± 0.5 % and 93.3 ± 0.4 % for microcapsules $\mathbf{I_{6.0}}$, **J**, and **L**, respectively) is significantly affected by the MF cross-linking reaction time (**step 4**). However, during the ultra-microtome sampling, some parts of the MF polymer inner wall were detached from the outer $CaCO_3$ nanoparticluate wall. The detachment allowed us to measure the MF wall thickness as a function of reaction time (**step 4**). The wall thickness of the MF polymer increased from 129 ± 2.5 nm (microcapsules $\mathbf{I_{6.0}}$, 4 hours) to 160 ± 3.1 nm (microcapsules **L**, 24 hours).

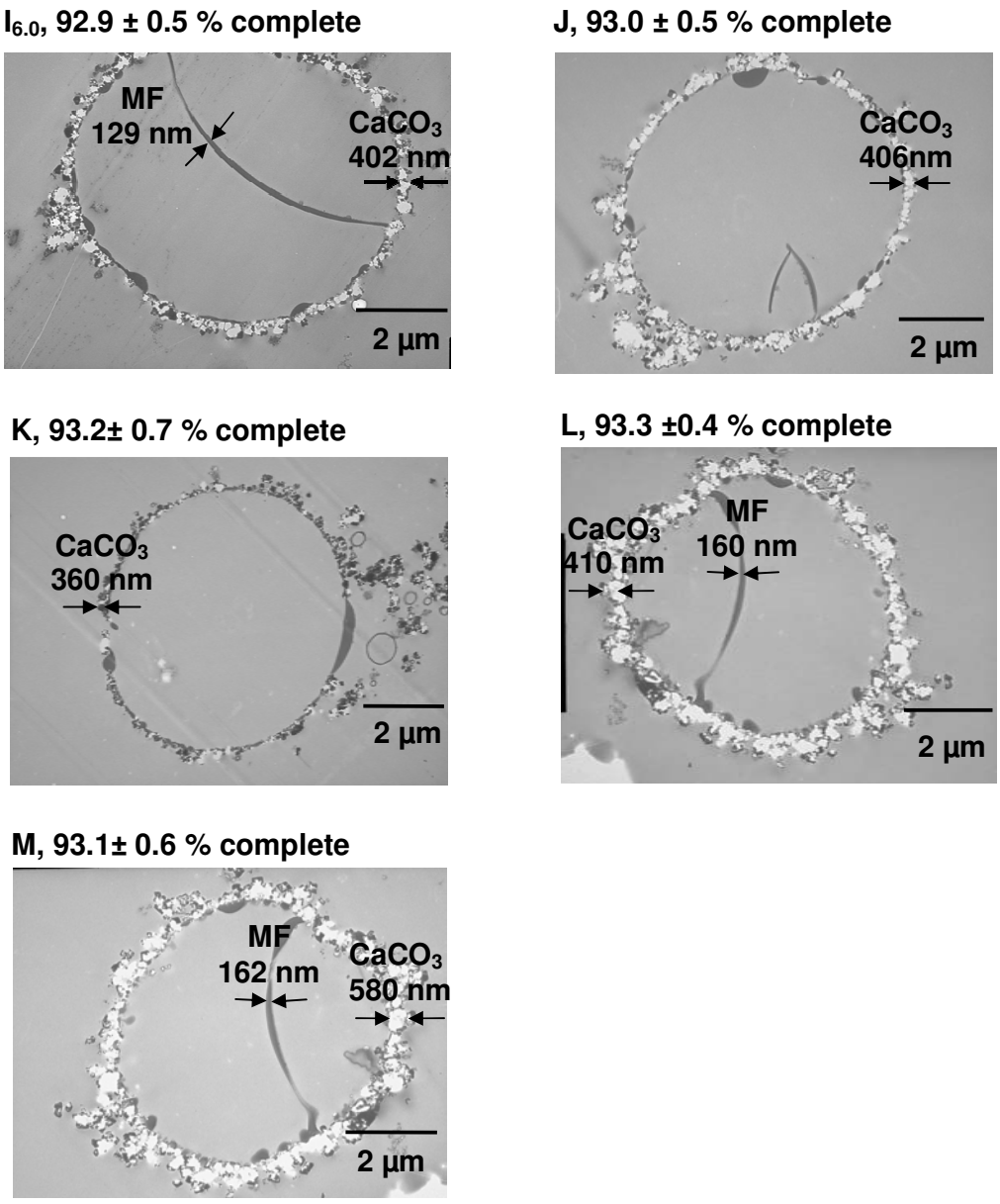
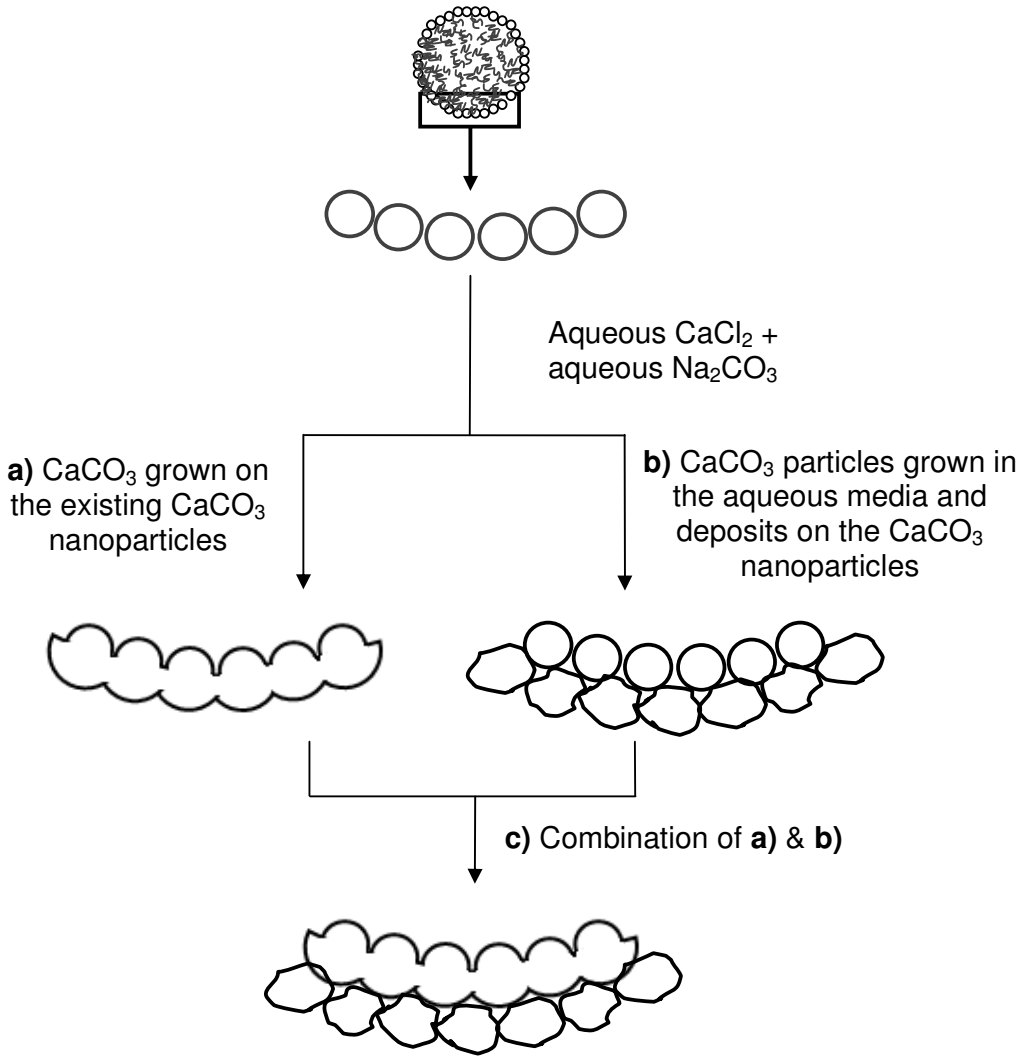


Figure 1. Wall thicknesses and the degree of wall completeness of the ripened double shell composite microcapsules $\mathbf{I_{6.0}}$, **J**, **K**, **L** and **M**.

A significant increase in the $CaCO_3$ wall thickness (360 ± 5.7 nm to 580 ± 5.2 nm) was observed when the concentration of aqueous $CaCl_2$ and Na_2CO_3 (**step 3**) was increased from 1.0 M (microcapsules **K**) to 2.0 M (microcapsules **M**, **Figure 2**). However, the degree of wall formation formed by the ripened $CaCO_3$ nanoparticles remained unchanged (~93 %), so does the inner MF/copolymer wall thickness (~160 nm). Analysis

of **Figure 1** microcapsules **K**, **L** and **M** in which increasing concentration of $CaCl_2$ and Na_2CO_3 were added during the ripening process, leads to the growth mechanism of the nanoparticulate $CaCO_3$ wall. In principle, there are two limiting ways in which the wall could ripen as illustrated in **Scheme 2**. In **Scheme 2a** we can imagine the $CaCl_2$ and Na_2CO_3 solution nucleate growth on the surface of the $CaCO_3$ nanoparticles, whereas in **Scheme 2b** we can imagine the $CaCl_2$ and Na_2CO_3 forming particulates in the solution and depositing on the nanoparticulate $CaCO_3$ wall. An analysis of microcapsules **K** (**Figure 1**, the lowest concentration of $CaCl_2$ and Na_2CO_3) reveals that the **Scheme 2a** mechanism predominates. As the concentration of $CaCl_2$ and Na_2CO_3 increases (microcapsules **L** and **M**), then a combination of $CaCO_3$ nanoparticulate growth (**Scheme 2a**) and $CaCO_3$ particles deposition occurs (**Scheme 2b**) leading to **Scheme 2c** type structure.



Scheme 2. Schematic diagram of the possible wall structure of the microcapsules wall from increase the volume of aqueous $CaCl_2$ and Na_2CO_3 (**step 3**).

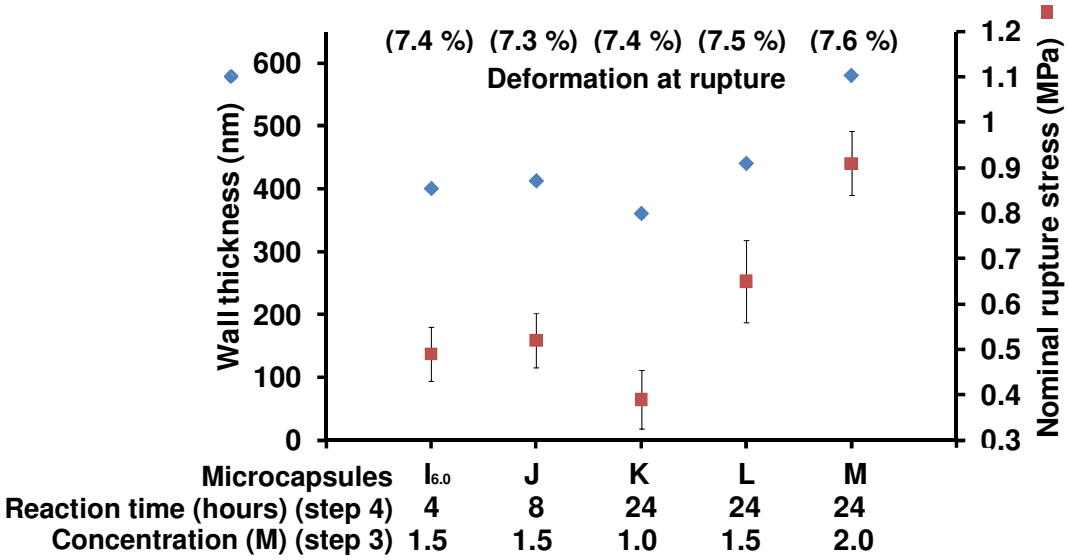


Figure 2. Average diameter and size distribution of the ripened double shell composite microcapsules (microcapsules **$I_{6.0}$**, **J**, **K**, **L** and **M**).

5.3.4 Average Particle Diameter and Distribution

The average particle diameter and distribution of microcapsules **$I_{6.0}$**, **J**, **K**, **L** and **M** are measured by laser diffraction and graphically presented in **Figure 3**. It shows that the average diameters for microcapsules **$I_{6.0}$**, **J**, **K**, **L** and **M** are ~14 µm. All 5 microcapsules show bimodal distributions centered on 1-2 µm and 13-15 µm. The first peak (centered on 1-2 µm) is probably due to small melamine formaldehyde particulates formed at elevated temperature during the MF cross-linking process (**Scheme 1**, **step 4**)[52, 175] combined with the solid $CaCO_3$ nanoparticles that were not contributing to the wall formation process (**Scheme 1**, **step 2** & **3**).

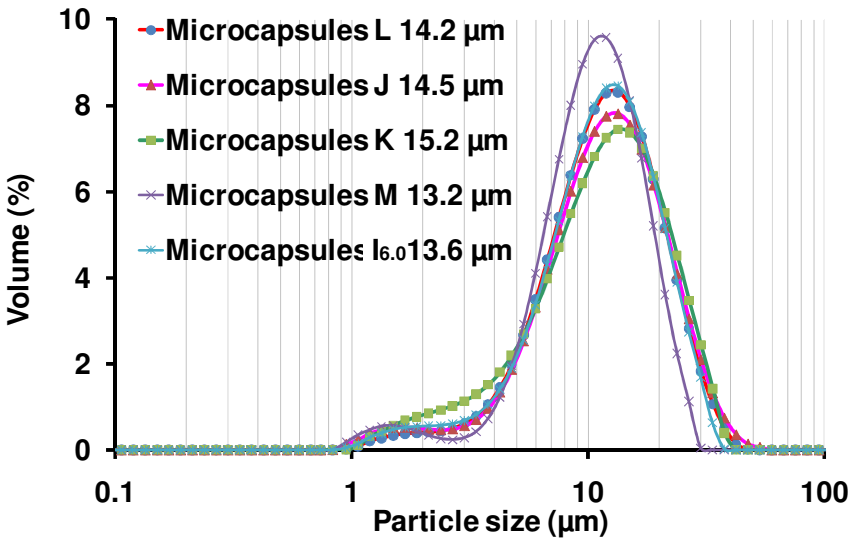


Figure 3. Average diameter and size distribution of the ripened double shell composite microcapsules (microcapsules $\mathbf{I_{6.0}}$, **J**, **K**, **L** and **M**).

5.3.5 Mechanical Properties

The mechanical properties of microcapsules $\mathbf{I_{6.0}}$, **J**, **K**, **L** and **M** are evaluated using the micromanipulation technique. A typical relationship of the force imposed on a single microcapsule as a function of the probe moving distance is shown in **Figure 4** for a microcapsules $\mathbf{I_{6.0}}$. The distance between 0 and **I** corresponds to the transducer probe moving before contact with the microcapsule, and the force imposed on the microcapsule is zero. After point **I** the probe touches the microcapsule, and the force imposed on the microcapsule increases until point **II** at which the microcapsule ruptures. As a result, the force drops to point **III**. The probe continues to compress the debris of the microcapsule (**III**-**IV**) until it touches the slide at point **IV**, after which the force increases as the probe pushes onto the slide. From this curve, the rupture force of the microcapsule can be determined (point **II**).

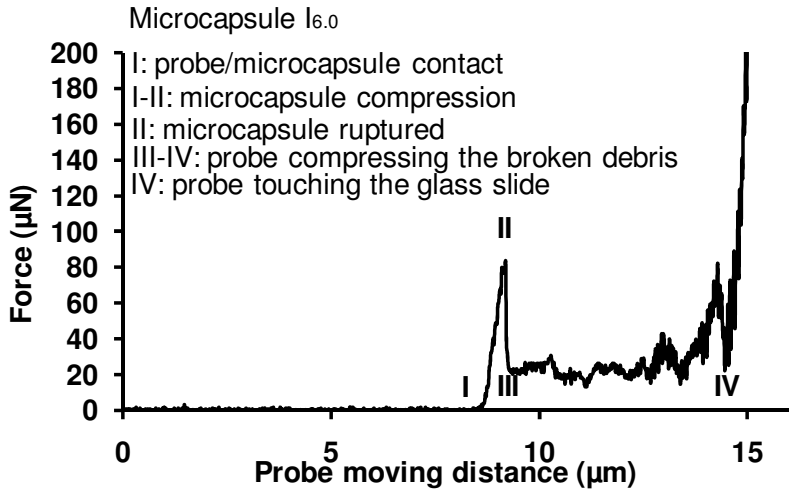
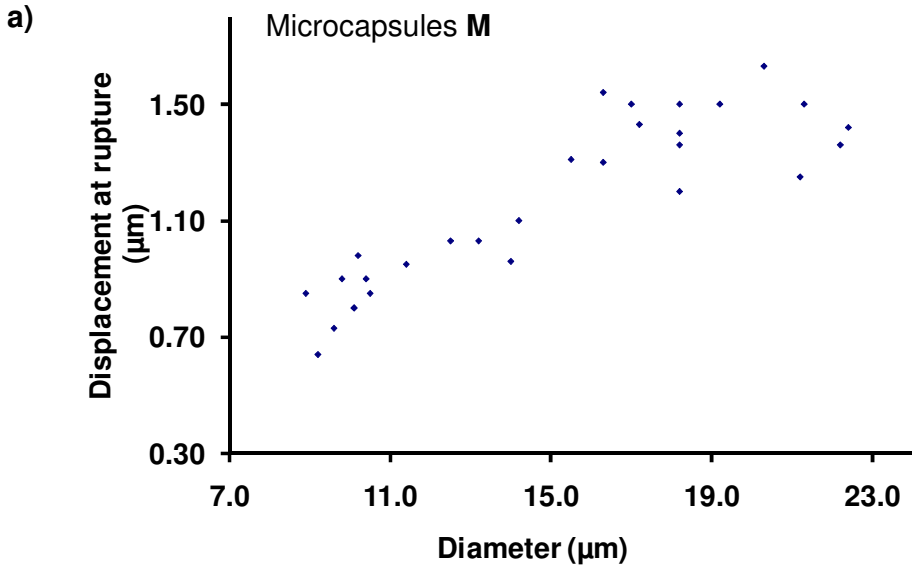


Figure 4. Typical force vs. probe moving distance curve obtained by compressing one of the microcapsules in $\mathbf{I_{6.0}}$.

The displacement at rupture (δ_R) is denoted as the distance that the probe travels from contact with microcapsule until rupture. The deformation at rupture is calculated using equation 1 (d = initial microcapsule diameter) (see **Chapter 3**, euqation 1), and the nominal rupture stress is calculated using equation 2 (see **Chapter 3**, euqation 2) as shown below, where F_R is the rupture force (point **II**).

The deformation at rupture, nominal rupture stress and wall thickness for all the 5 batches are presented in **Figure 2**. The deformation at rupture for all 5 batches are indeterminate of altering the $CaCO_3$ nanoparticulate ripening process (**step 3**) or the MF cross-linking reaction time (**step 4**), as all microcapsules deformed by ~7.5 %. However, the nominal rupture stress was only indeterminate of the cross-linking time (0.49 ± 0.06, 0.52 ± 0.06 and 0.65 ± 0.09 for microcapsules $\mathbf{I_{6.0}}$, **J** and **L**, respectively), whilst the $CaCO_3$ nanoparticulate ripening process increased the nominal rupture stress from 0.39 ± 0.07 to 0.91 ± 0.07 MPa (**Figure 2**). Also, we can see that the increase in nominal rupture stress

follows closely the increase in wall thickness of the $CaCO_3$ inner wall. Hence, we conclude the nominal rupture stress is dominated by the inorganic $CaCO_3$ outer shell and not the organic polymer inner shell. The displacement at rupture, rupture force and nominal stress at rupture as a function of diameter for microcapsules $\mathbf{I_{6.0}}$, **J**, **K**, **L** and **M** are plotted, and are shown in **Figure 5a**, **5b** and **5c**, respectively. It was observed that for the same type of microcapsules, the displacement at rupture (**Figure 5a**) and rupture force (**Figure 5b**) increase as the diameter of the microcapsules increase. In contrast, the nominal stress at rupture (**Figure 5c**) decreases as the particle diameter increases. The stress at rupture of the microcapsules may be directly related to their rupture behavior. Larger microcapsules were found to rupture more easily than smaller ones in the previous studies.[41]



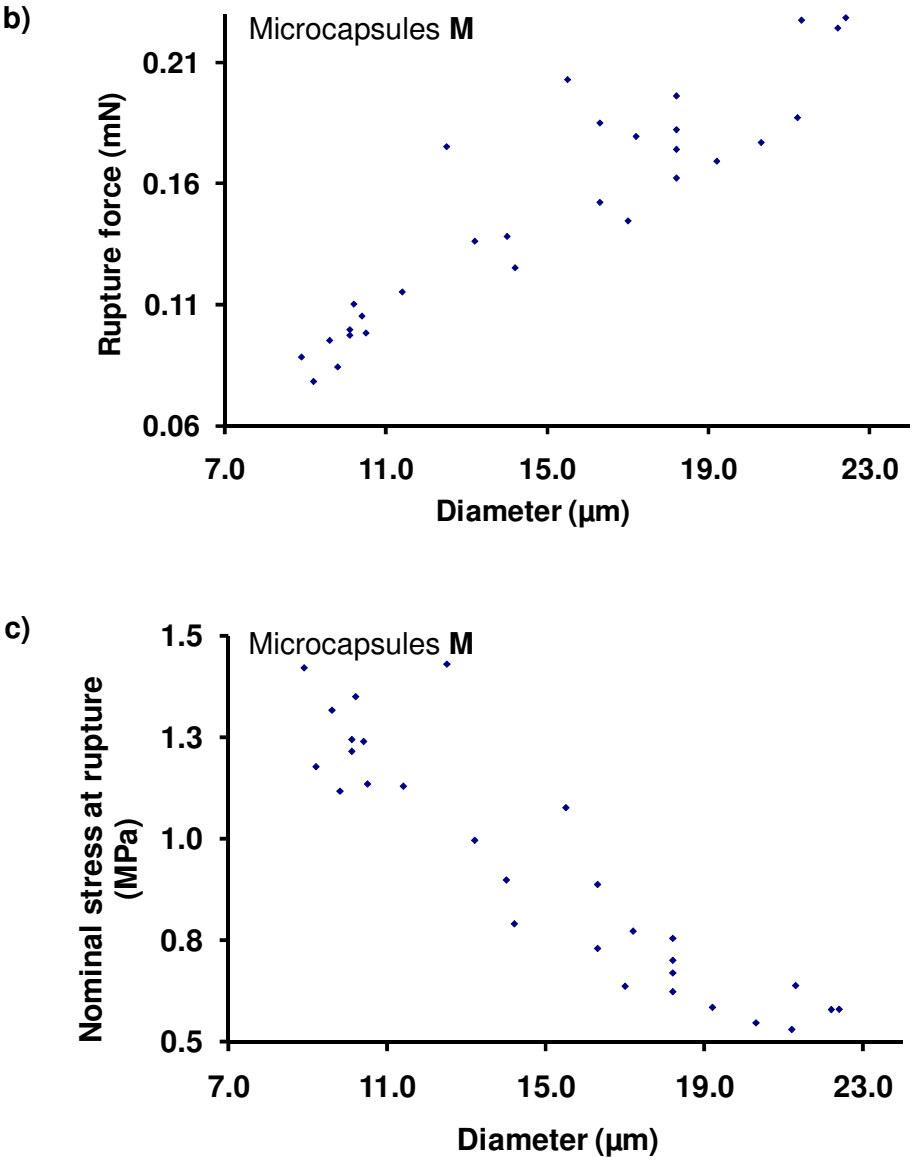


Figure 5. Displacement at rupture vs. diameter, rupture force vs. diameter, and nominal stress at rupture vs. diameter for the ripened double shell composite microcapsules **M**.

5.3.6 Oil Leakage

It can be seen in **Figure 6** that when the MF cross-linking reaction time (**step 4**) is increased, the leakage of the ripened double shell composite microcapsules decreased

(from 0.095 ± 0.002 % to 0.047 ± 0.001 %). This decrease in leakage is probably due to the formation of a thicker MF polymer wall (**Figure 1**, microcapsules $\mathbf{I_{6.0}}$ and **L**) resulting from the longer cross-linking reaction time. However, a much smaller reduction in leakage was observed when the concentration of the aqueous $CaCl_2$ and Na_2CO_3 was increased (**step 3**) in the ripening process 0.052 ± 0.001 % (batch **3**) to 0.045 ± 0.001 % (batch **5**). The leakage behavior indicates that the organic MF/copolymer inner shell is more effective for preventing the oil leakage than the inorganic $CaCO_3$ nanoparticulate outer shell.

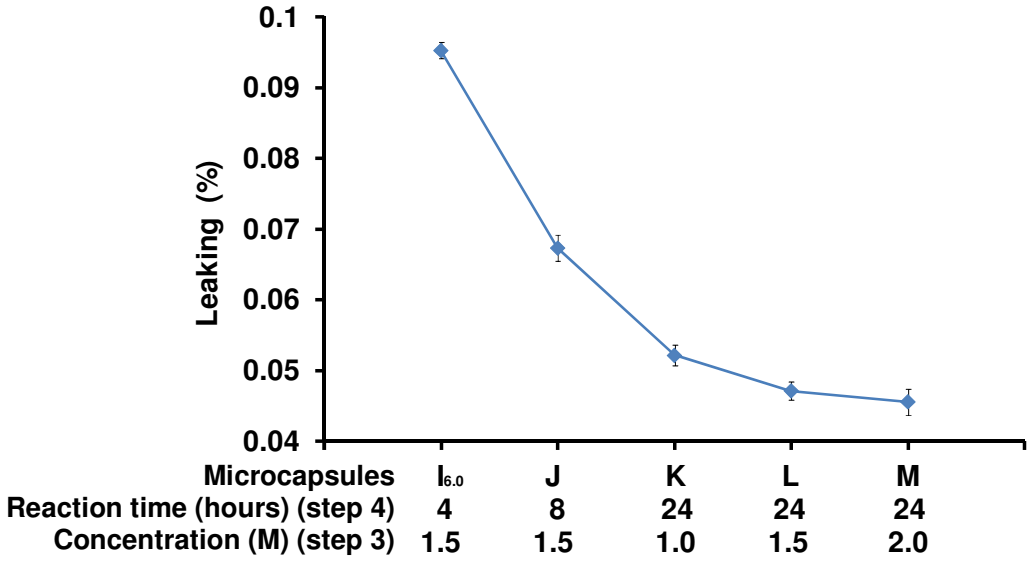


Figure 6. Leakiness of the ripened double shell composite microcapsules $\mathbf{I_{6.0}}$, **J**, **K**, **L** and **M**.

5.4 Conclusions

The ripened double shell composite microcapsules with organic MF/copolymer inner shell and inorganic ripened $CaCO_3$ nanoparticulate outer shell were successfully prepared. It was found that when the MF polymerization time increased from 4 to 24 hours (**step 4**),

the MF/copolymer inner wall thickness increased from 129 nm to 160 nm, and the leakage of the microcapsules decreased from 0.095 ± 0.002 % to 0.047 ± 0.001 %. However, the outer $CaCO_3$ nanoparticulate wall thickness remained constant (~400 nm), so did the degree of the wall formation formed by the ripened $CaCO_3$ nanoparticles (~93 %). As the concentration of the aqueous $CaCl_2$ and Na_2CO_3 was increased leading to the $CaCO_3$ nanoparticulate ripening process (**step 3**), the ripened $CaCO_3$ wall thickness of the microcapsules increased from 360 ± 5.7 nm to 580 ± 5.2 nm, the nominal rupture stress of the microcapsules increased from 0.39 ± 0.07 MPa to 0.91 ± 0.09 MPa, and the leakage of the microcapsules was reduced from 0.052 ± 0.001 % to 0.045 ± 0.001 %. However, the MF/copolymer inner wall thickness remained unchanged (~160 nm). Therefore, we conclude that the mechanical properties of the double shell composite microcapsules were dominated by the $CaCO_3$ outer shell, whereas the leakage of the microcapsules was primarily governed by the MF inner shell. Thus, a process whereby the strength of the microcapsules can be engineered independently of the leakiness is prepared.

CHAPTER 6

Preparation and Characterization of Calcium Shellac Matrix with Microcapsules Embedded (Complex Microcapsules)

Abstract

This chapter reports use of calcium shellac encapsulating melamine formaldehyde (MF) microcapsules (**A**) and unripened $CaCO_3$ nanoparticles stabilised microcapsules (**F**) respectively, where both types of microcapsules contained an oil based active ingredient, in order to reduce its leakage from the primary microcapsules. The encapsulation efficiency of primary microcapsules, average diameter, surface morphology, inner structure, nominal rupture stress and leakage of the calcium shellac matrix containing microcapsules **A** and **F** were characterized, and compared with microcapsules **A** and **F** and calcium shellac microparticles except the leakage. The results show that calcium shellac matrix containing microcapsules **A** and **F** possessed larger nominal rupture stress than microcapsules **A** and **F**, and the mechanical properties do not appear to be affected by the type of microcapsules embedded. In addition, a 37 fold reduction in oil leakage was observed between microcapsules **A** alone and those embedded in the calcium shellac matrix, and a 14 fold reduction was observed between microcapsules **F** alone and those embedded in the calcium shellac matrix.

6.1 Introduction

Microencapsulated materials have been shown to have advantages such as protection of an active ingredient in mixture, allowing mixing of immiscible and incompatible materials, and affording prolonged and controlled release of the active ingredient.[23]

However, leakage of the core material through the microcapsule wall is problematic, as it reduces the shelf-life of the product and increases the cost.

Shellac is a natural polyester with free hydroxyl, carboxylic acid and ester functional groups. Due to its very low water and acid permeability, shellac has been commonly used as a coating material in pharmaceutical[211, 212] and food products.[213, 214] However, shellac was found to be unstable in its acid form, due to the polyesterification among the functional groups. Studies were carried out to improve the stability of shellac, and it was found that preparation of shellac in ammonium or 2-amino-2-methyl-1-propanol (AMP) salt form,[215, 216] or the combination of the two[217] could enhance its stability by reducing the polymerization. Recently, shellac has been further developed to be a encapsulating agent for producing microcapsules[218] and tablets.[219]

Calcium shellac microcapsules with encapsulated carbamide peroxide (CP) were prepared by Xue and Zhang.[117, 218] A water in oil (w/o) emulsion was generated by dissolving CP in the shellac ammonium aqueous salt solution and dispersed in sunflower oil, followed by the addition of powdered calcium chloride leading to gelation between shellac and the calcium ions.

In this work, complex capsules were prepared based on the above method and use of calcium shellac matrix to encapsulate (i) melamine formaldehyde (MF) microcapsules (**A**) and (ii) unripened $CaCO_3$ nanoparticles stabilised microcapsules (**F**), both of which contained an oil based active ingredient. The aim was to reduce the leakage of the microcapsules. Calcium shellac microparticles were also prepared, as were microcapsules **A** and **F** which were not embedded in calcium shellac matrix. The encapsulation

efficiency of primary microcapsules (**A** and **F**), average diameter, surface morphology, inner structure, nominal rupture stress and leakage of these five types of microcapsules or microparticles except leakage were characterized and compared.

6.2 Experimental

6.2.1 Material

Shellac ammonium salt aqueous solution (25±0.4 % w/w, pH 7.3 ± 0.3, density 1.04±0.03 kg/L, Syntapharm, Emerson Resouces Inc., USA), calcium chloride (Sigma Aldrich, UK), and tween 80 (Sigma Aldrich, UK) were used without any further purification. The core oil is a typical perfume blend of various components, with a low water solubility and is used in consumer products. MF precondensate (70 % (aq) w/w, formaldehyde to melamine molar ratio 0.20), was supplied by British Industrial Plastics Ltd, Birmingham, UK. Formaldehyde (37 % (aq) w/w) was supplied by Sigma-Aldrich, UK, poly(acrylamide-acrylic acid, sodium salt) was supplied by Polymersciences, Inc., US, and calcium carbonate nanoparticles (average diameter 80 nm) were supplied by Omya, UK and were used without further purification.

6.2.2 Formation of Microcapsules

6.2.2.1 Formation of MF Microcapsules (A)[175]

These have been described in **Chapter 3** (3.2.2). An aqueous solution of MF precondensate (2.50 g) and copolymer (0.58 g, poly(acrylamide-acrylic acid, sodium salt) in water (70 ml) was stirred (400 rpm) with a Rushton turbine (Φ31 mm, in a vessel with standard configuration) for 105 min at pH 4 (adjusted by acetic acid (1M), monitored by a pH meter) at room temperature. The core oil (9.33 g) was added to the

resulting mixture and stirred using a homogenizer (Model L4RT, Silverson Machines Ltd, UK) at a speed of 2500 rpm for 30 min at 15°C to form an oil in water (o/w) emulsion. The resulting emulsion was stirred at 400 rpm in a vessel (Φ 65mm × 65mm) with a standard Rushton turbine impeller (Φ31mm) for 30 min at 15°C before the temperature was raised to 65°C , at which stirring was maintained for 6 hours. The resulting dispersion of MF microcapsules was cooled to 25 °C, and the pH was raised to 10 with the addition of aqueous NaOH (1 M, monitored by a pH meter) to terminate the polymerization reaction. This dispersion was used for all the further analyses except the encapsulation efficiency measurements.

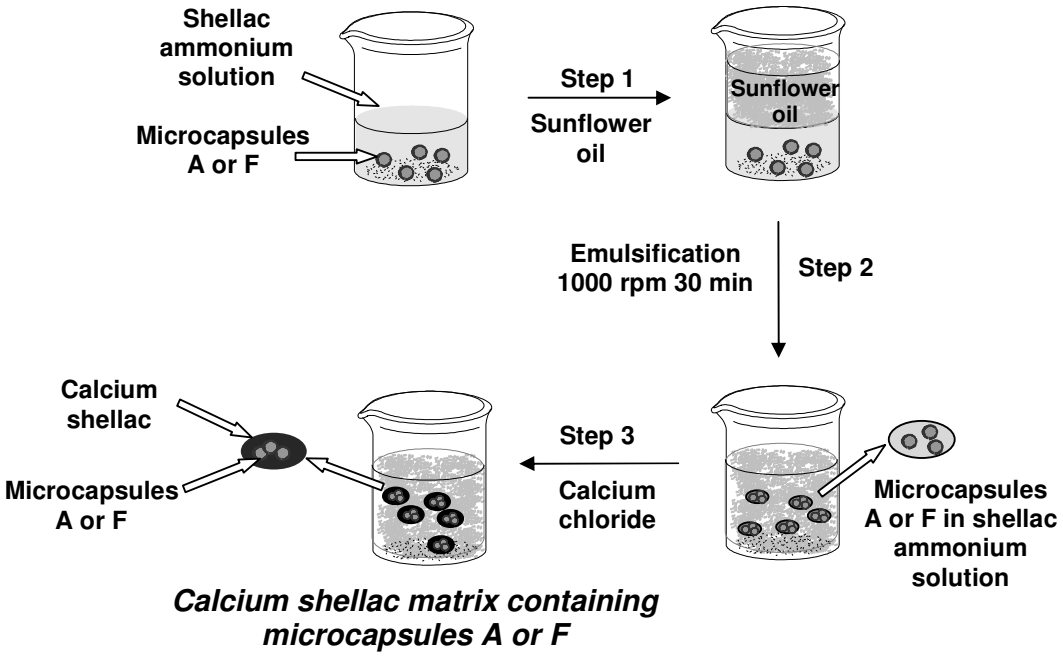
6.2.2.2 Formation of Unripened $CaCO_3$ Nanoparticles Stabilised Microcapsules (F)

Thses have been described in **Chapter 4** (4.2.2). The core oil (9.3 g) was added to an aqueous $CaCO_3$ nanoparticle dispersion (40 ml, 10 % wt) and stirred using a homogenizer (Model L4RT, Silverson Machines Ltd, UK) at a speed of 2500 rpm for 3 min to form an o/w emulsion stabilized by $CaCO_3$ nanoparticles.

6.2.2.3 Formation of Calcium Shellac [117, 218] Matrix Containing MF Microcapsules (A) or Unripened $CaCO_3$ Nanoparticles Microcapsules stabilised (F) (Complex Capsules)

MF microcapsules (powder, 1 g) were dispersed in shellac ammonium salt aqueous solution (5 ml). Sunflower oil (200 ml) was added to the resulting dispersion (**step 1**), and stirred using a homogenizer (Model L4RT, Silverson Machines Ltd, UK) at a speed of 1000 rpm for 30 min (**step 2**). Calcium chloride (hand ground for 10 min to a fine powder) (0.1 g) was added every minute over 10 minutes (1 g in total) to the resulting emulsion, and the stirring was maintained for another 2 hours, after which no $CaCl_2$

powder remained (**step 3**). The resulting capsules were filtered from the sunflower oil and freeze dried for further characterization except for the encapsulation efficiency and leakage test.



Scheme 1. Schematic representation of the formation of calcium shellac matrix containing microcapsules **A** and **F**.

6.2.2.4 Formation of Calcium Shellac Microparticles

To the aqueous shellac ammonium salt solution (5 ml), sunflower oil (200 ml) was added, and the resulting mixture was emulsified using a homogenizer (Model L4RT, Silverson Machines Ltd, UK) at a speed of 1000 rpm for 30 min. Calcium chloride (0.1 g) was added every minute over 10 minutes (1 g in total) to the resulting emulsion, and the stirring was maintained for another 2 hours, after which no $CaCl_2$ powder remained. The

resulting microparticles were filtered from the sunflower oil and freeze dried for further characterization.

6.2.3 Freeze Drying

A freeze dryer (Edwards High Vacuum Freeze Drier, EF03, UK) was used to dry the microcapsules or microparticles. The drying temperature was 40-45 °C. The microcapsules or microparticles were left drying for 24 hours pressure was 4-5 mbar at the end of the drying process.

6.2.4 Encapsulation Efficiency of Primary Microcapsules

An aqueous dispersion of calcium shellac matrix containing microcapsules **A** was centrifuged at 3000 rpm for 15 min. The un-encapsulated microcapsules **A** were collected from the surface of the liquid *via* a pipette, and the calcium shellac matrix containing microcapsules **A** were collected from the bottom of the centrifugation tube by decanting the supernatant liquid. The supernatant liquid was re-centrifuged for another 15 min at 3000 rpm, and the non-embedded microcapsules **A** and calcium shellac matrix containing **A** in it was separated as above. The collected microcapsules **A** which had not been encapsulated were combined and freeze dried for 24 hours (temperature - (40 – 45) °C, pressure 4-5 mbar). The encapsulation efficiency was calculated from the total weight of microcapsules **A** used minus the recovered weight of microcapsules **A** (*i.e.* the weight of encapsulated microcapsules **A**), which was then divided by the total weight of microcapsules **A** used. The encapsulation efficiency of the calcium shellac matrix containing **F** was not evaluated using this method due to the fact that calcium shellac matrix containing **F** did not separate from the microcapsules **F** which had not been encapsulated upon centrifugation. Hence, the encapsulation efficiency of calcium shellac

matrix containing **F** was evaluated by using the volume ratio of encapsulated microcapsules **F** (obtained from the microscope images) to the total volume of the calcium shellac matrix.

6.2.5 Environmental Scanning Electron Microscopy (ESEM)

Environmental-SEM (FEI/Philips XL30 ESEM-FEG, Philips, UK) with operating voltage shown on images was used to study the morphology of the microcapsules and microparticles. Samples were operated in the high vacuum mode.

6.2.6 Focused Ion Beam (FIB) and SEM

FIB/SEM (Quanta 3D FEG, FEI, US) with the operating voltage shown on images was used to examine the inner structure of complex microcapsules and calcium shellac microparticles. Samples were operated in high vacuum mode.

6.2.7 Optical Microscope

An optical microscope (Leica, 3CCD colour vision camera, Donpisha) was used to study the shape and structure of the microcapsules and calcium shellac microparticles. An image analysis system (Quantiment Q570 image analyzer, Leica Ltd, UK) was used to evaluate the size of the microcapsules from the images.

6.2.8 Size Analysis (SLS)

Mean particle size and size distribution of the microcapsules and calcium shellac microparticles in the aqueous dispersions were evaluated by static light-scattering (Mastersizer 2000, Malvern Instruments Ltd, UK). The measurements were carried out using a Helium-Neon laser, connected to a sample dispersion unit. The size range which

can be measured is 0.05–900 μm. Experiments were performed at 25°C. The mean diameter and size distribution of microcapsules and calcium shellac microparticles were the average value of five measurements.

6.2.9 Micromanipulation

The mechanical properties of the microcapsules were determined by micromanipulation. A glass probe with a diameter of 300 μm mounted on a force transducer (Model 405A, Aurora Scientific Inc., Canada) was positioned perpendicular to the glass slide. The dried microcapsules or calcium shellac microparticles were placed on the glass slide, and observed through side and bottom-view cameras. A single microcapsule or calcium shellac microparticles was compressed by the glass probe travelling at 2 μm s^{-1}. The voltage output generated by the force transducer due to compression of the microcapsules or calcium shellac microparticles was recorded through a data acquisition card in a personal computer. From the sensitivity of the transducer, the voltage was converted to force, hence the rupture force of the microcapsules or calcium shellac microparticles was determined.

6.2.10 Leakage Measurement

Calcium shellac matrix containing **A** and **F** were filtered from the original oil dispersion, and re-dispersed in water (50 ml). To the resulting aqueous dispersion, hexane was added (30 ml), which was stirred for 10 minutes and then stopped. A hexane aliquot (1 μl) was removed and analysed by gas chromatography (GC) to determine the amount of oil in it. Further aliquots (1 μl) were removed at various time intervals between 1 to 20 hours, prior to which the dispersion was stirred for 10 minutes, to ensure oil transfer to the hexane layer.

6.2.11 Gas Chromatography (GC)

A Trace 2000 series gas chromatogram with a flame ionization detector and 30 m × 0.32 mm ZB5 inferno column was used for data acquisition for the encapsulation efficiency and leakage experiments. Analysis was performed using Dionex Chromeleon Workstation. Samples injection volumes were 1µl. The injection port temperature was 250 °C. The temperature ramp for the column was increased by 10 °C/s from 50-300 °C, and held at 300 °C for 35 min. The detection temperature was 300 °C. Helium was used as the carrier gas.

6.3 Results and Discussion

6.3.1 Synthesis

A series of microcapsules were synthesized. Microcapsules **A** were formed using an *in situ* polymerization process, the MF precondensate and copolymer (poly(acrylamide-acrylic acid, sodium salt)) were firstly pre-crosslinked in water, oil was added to form an o/w emulsion by agitation, and the temperature of the emulsion was raised leading to polymerization of the pre-crosslinked MF precondensate and the copolymer to form a wall on the dispersed oil surface. Microcapsules **F** were formed by emulsifying the mixture of aqueous $CaCO_3$ nanoparticles and core oil. Complex capsules, *i.e.* calcium shellac matrix containing **A** or **F** (**Scheme 1**) were formed by emulsifying the shellac ammonium aqueous solution containing microcapsules **A** or **F** in oil (**step 1** and **2**), and followed by the addition of powdered calcium chloride leading to gelation between shellac and the calcium ions (**step 3**). Finally, calcium shellac microparticles were formed

following the same process above, with the exception that there was no microcapsule dispersed in the shellac ammonium aqueous solution in the emulsification step.

6.3.2 Encapsulation Efficiency of Primary Microcapsules

The encapsulation efficiency of the calcium shellac matrix containing microcapsules **A** is as described in the experimental section (**6.2.4**) based on equation (**1**). Result shows that the encapsulation efficiency of microcapsules **A** in calcium shellac matrix is 85 ± 1 %. The encapsulation efficiency of the calcium shellac matrix containing microcapsules **F** was not evaluated by using the same method (equation (**1**)), as centrifugation did not separate the calcium shellac matrix containing microcapsules **F** from the microcapsules **F** which had not been encapsulated (as described in the experimental section). The average number of microcapsules **A** encapsulated in each calcium shellac matrix is 6.32, and for **F** is 5.89 (obtained from the optical microscope images for 40 complex microcapsules, images are not shown), with 10.5 % and 11.8%, respectively, of the calcium shellac being empty. Hence, the encapsulation efficiency of calcium shellac matrix containing **F** was evaluated by using the volume ratio of the encapsulated microcapsules **F** to the total volume of calcium shellac matrix based on the value obtained from the microscope images (equation (**2**)), and the encapsulation efficiency is 92 %.

$$\text{Encapsulation efficiency of } \mathbf{A} = \frac{\text{Amount of encapsulated microcapsule } \mathbf{A}}{\text{Amount of total microcapsule } \mathbf{A} \text{ input}} \quad (1)$$

$$\text{Encapsulation efficiency of } \mathbf{F} = \frac{\text{Volume of encapsulated microcapsules } \mathbf{F}}{\text{Volume of total calcium shellac matrix}} \quad (2)$$

where,

$$\text{Volume of encapsulated microcapsules } \mathbf{F} = \text{Number of encapsulated microcapsules } \mathbf{F} \times \text{average particle diameter}^3 \times (\pi / 6)$$

$$\text{Volume of total calcium shellac matrix} = \text{Number of calcium shellac matrix} \times \text{average particle diameter}^3 \times (\pi / 6)$$

6.3.3 Microcapsules Structure

Optical images of microcapsules **A** and **F**, calcium shellac microparticles, and calcium shellac matrix containing microcapsules **A** and **F** are shown in **Figure 1a-e**, respectively. Microcapsules **A** and **F** and calcium shellac microparticles are all spherical (**Figure 1a-c**). In contrast, the calcium shellac matrix containing microcapsules **A** or **F** (**Figure 1d-e**) show less regular shapes, suggesting microcapsules **A** and **F** are distorting the calcium shellac matrix's structure.

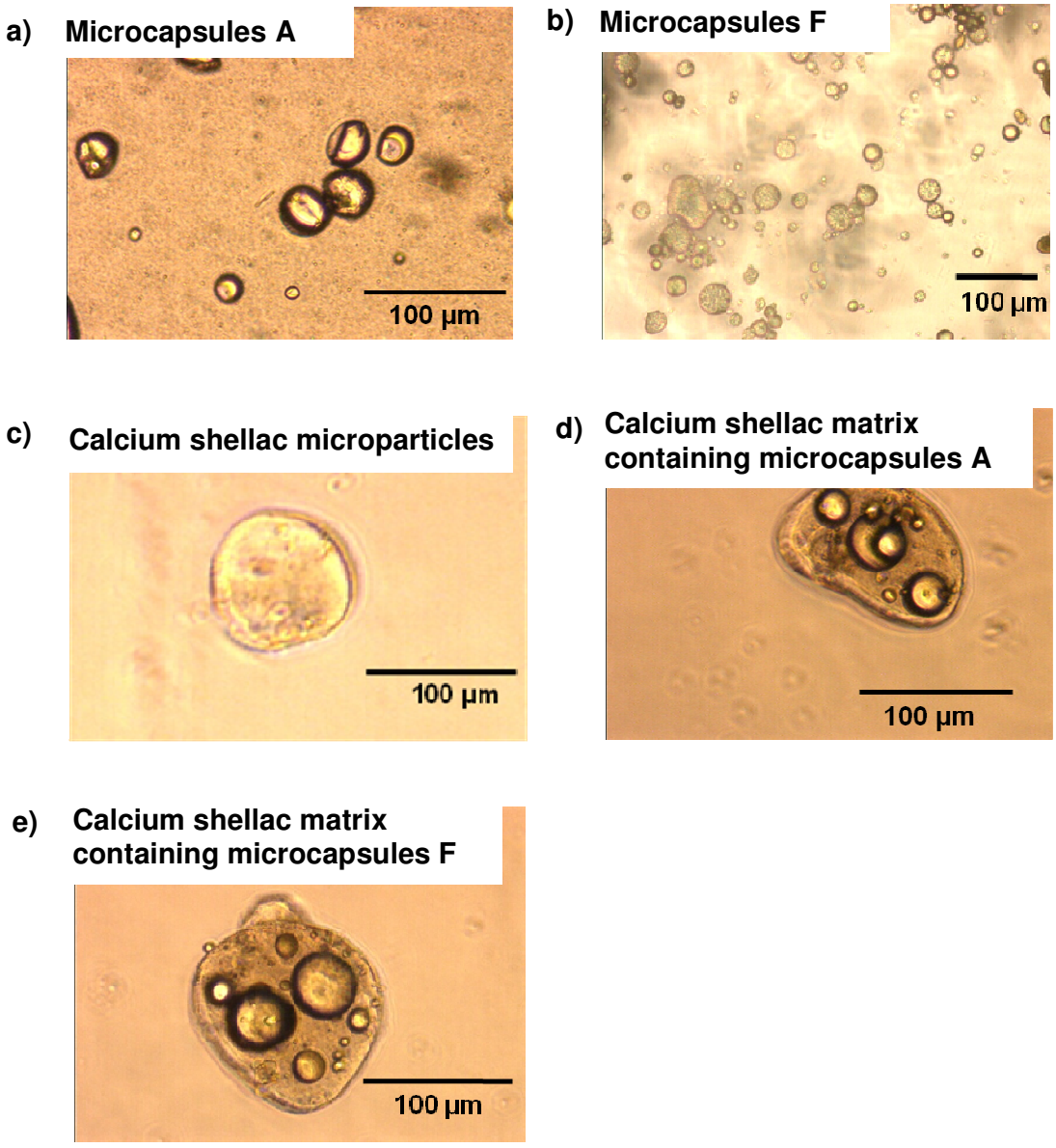


Figure 1. Optical microscope images of a) microcapsules **A**, b) microcapsules **F**, c) calcium shellac microparticles, d) calcium shellac matrix containing microcapsules **A**, e) calcium shellac matrix containing microcapsules **F**.

6.3.4 Average Particle Size and Distribution

The size distribution curve of calcium shellac microparticles, microcapsules **A** and **F**, and calcium shellac matrix containing microcapsules **A** and **F** are presented in **Figure 2a-c**. As shown in **Figure 2a**, calcium shellac microparticles gave a bimodal distribution curve centred on 6.7 μm and 42.6 μm. The two peaks on the curve could be caused by the emulsification step. It has been reported previously that under 30 min emulsification, a bimodal distribution curve would be resulted.[21] In **Figure 2b**, the size distribution curve for microcapsules **A** shows a bimodal distribution centred at 1.3 μm and 13.1 μm. The first peak is probably due to the solid MF particles formed in the aqueous solution at the elevated temperatures as observed previously, and the second peak is due to microcapsules **A** (details are shown in **Chapter 3**, **3.3.4**, **Figure 6**).[175] The calcium shellac matrix containing microcapsules **A** also show a bimodal distribution centred at 10.6 μm and 83.0 μm. From **Figure 2c**, microcapsules **F** gave a monomodal distribution curve and the average particle diameter is 13.8 μm. Similar to the calcium shellac matrix containing microcapsules **A**, the calcium shellac matrix containing microcapsules **F** also has a bimodal distribution centred at 8.7 μm and 84.0 μm. It can be seen that the average particle size and size distribution of calcium shellac matrixes are not affected by the type of embedded microcapsules. The larger particle size obtained from the calcium shellac matrix containing microcapsules **A** and **F** in comparison with calcium shellac microparticles is probably due to change of the apparent viscosity of the whole dispersed aqueous phase when microcapsules **A** and **F** are embedded. Previous literature reported that the average particle size of microcapsules increases with increasing viscosity of the dispersed phase.[59] When microcapsules **A** or **F** mixed with the aqueous shellac ammonium solution, the apparent viscosity of the dispersed aqueous phase is increased, so does the final microcapsule size.

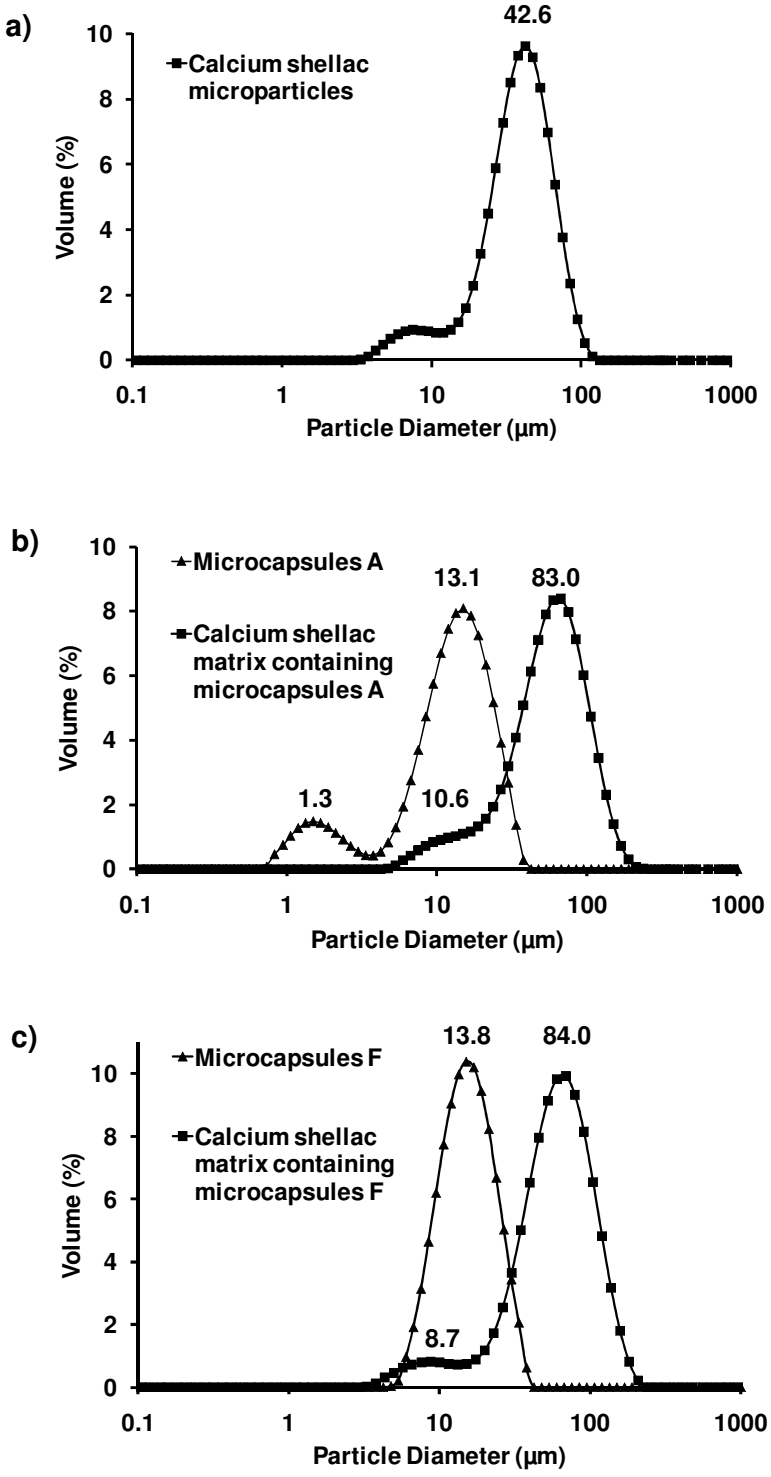
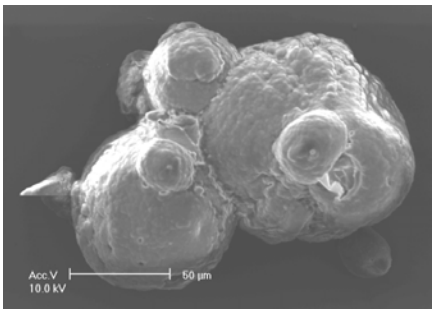


Figure 2. Static light scattering measurement of a) size distribution for calcium shellac microparticles, b) size distribution for microcapsules **A** and calcium shellac matrix containing microcapsules **A**, c) size distribution for microcapsules **F** and calcium shellac matrix containing microcapsules **F**.

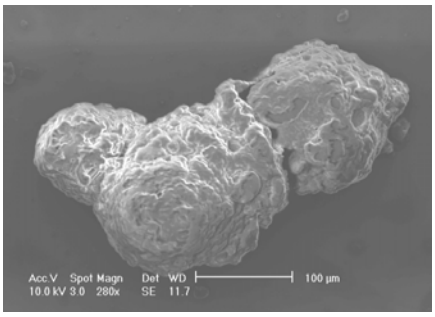
6.3.5 Surface Morphology and Storage Stability

Calcium shellac matrix containing microcapsules **A** or **F** and calcium shellac microparticles were examined by ESEM after 1 day and 25 days (**Figure 3a-f**). The ESEM images show that the surface of the calcium shellac matrix containing **A** or **F** (**Figure 3a** and **c**), and the calcium shellac microparticles (**Figure 3e**) are quite rough and have less regular shapes similar to the optical microscope images. After 25 days of storage, the calcium shellac matrix containing **A** or **F** (**Figure 3b** and **d**), and the calcium shellac microparticles (**Figure 3f**) show no significant change in shape or morphology, which suggests that the calcium shellac matrix possessed good stability during storage.

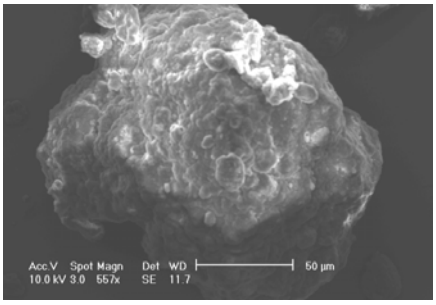
a) **Calcium shellac matrix containing microcapsules A (1 day)**



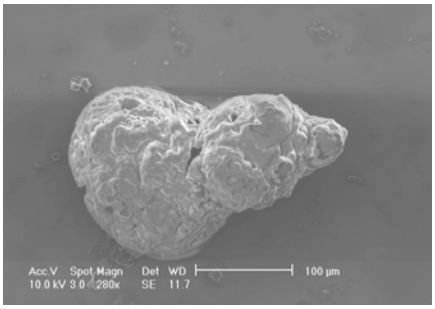
b) **Calcium shellac matrix containing microcapsules A (25 days)**



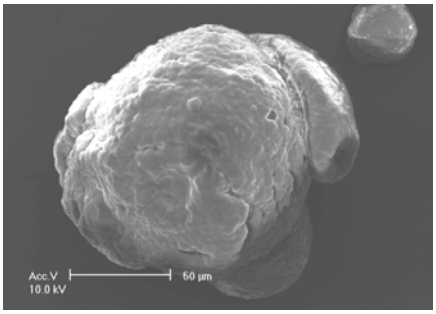
c) **Calcium shellac matrix containing microcapsules F (1 day)**



d) **Calcium shellac matrix containing microcapsules F (25 days)**



e) **Calcium shellac microparticles (1 day)**



f) **Calcium shellac microparticles (25 days)**

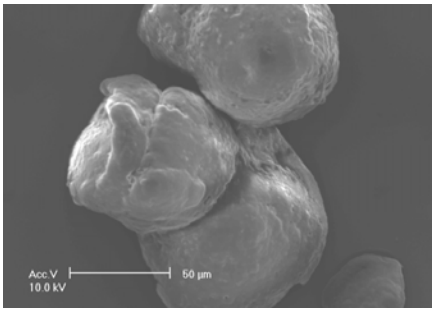


Figure 3. SEM images of a) calcium shellac matrix containing microcapsules **A** (1 day), b) calcium shellac matrix containing microcapsules **A** (25 days), c) calcium shellac matrix containing microcapsules **F** (1 day), d) calcium shellac matrix containing microcapsules **F** (25 days), e) calcium shellac microparticles (1 day), f) calcium shellac microparticles (25 days).

6.3.6 Inner Structure

From the optical microscope image (**Figure 1**), it can be seen that the inner structure of calcium shellac matrix containing microcapsules **A** is very similar to the one containing microcapsules **F**. Here, only the inner structure of calcium shellac microparticles and calcium shellac matrix containing microcapsules **F** examined using FIB combined with SEM are presented (**Figure 4a-b**). A calcium shellac microparticle was cut open using the FIB, and the inner structure of the particle was examined by SEM, which revealed it to be solid (**Figure 4a**), similar to what has been reported previously.[117] In contrast, **Figure 4b** shows a SEM image of a calcium shellac matrix containing microcapsules **F**, which has been cut by FIB. The image reveals that the inside of the calcium shellac matrix containing **F** has a hollow from which core oil is seeping from the bottom edge of the hollow. The hollow in the image (**Figure 4b**) has a diameter of 30 µm corresponding to the diameter of single microcapsules **F**, which ranged from 3 µm to 37 µm.

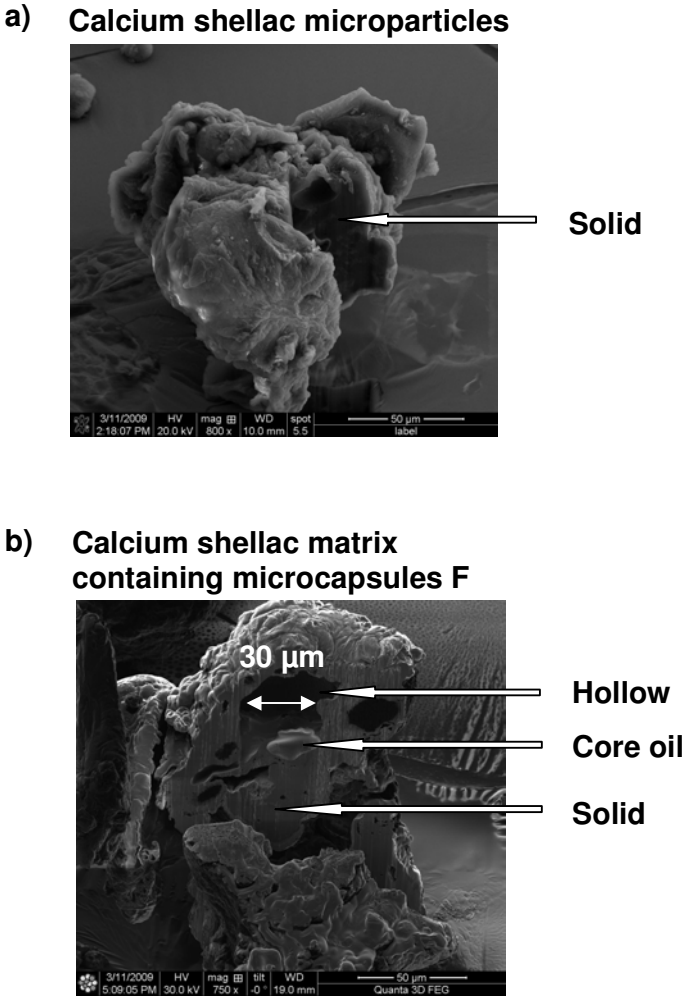


Figure 4. SEM images of microcapsules cut by a FIB; a) cross sectional image of calcium shellac microparticles, b) cross sectional image of calcium shellac matrix containing microcapsules **F**.

6.3.7 Mechanical Strength

The mechanical properties of the microcapsules **A** and **F**, calcium shellac matrix containing microcapsules **A** and **F**, and calcium shellac microparticles were evaluated by the micromanipulation technique.[134] A typical relationship of the force imposed as a

function of the probe moving distance is shown in **Figure 5** for the compression of a calcium shellac matrix containing microcapsules **A**.

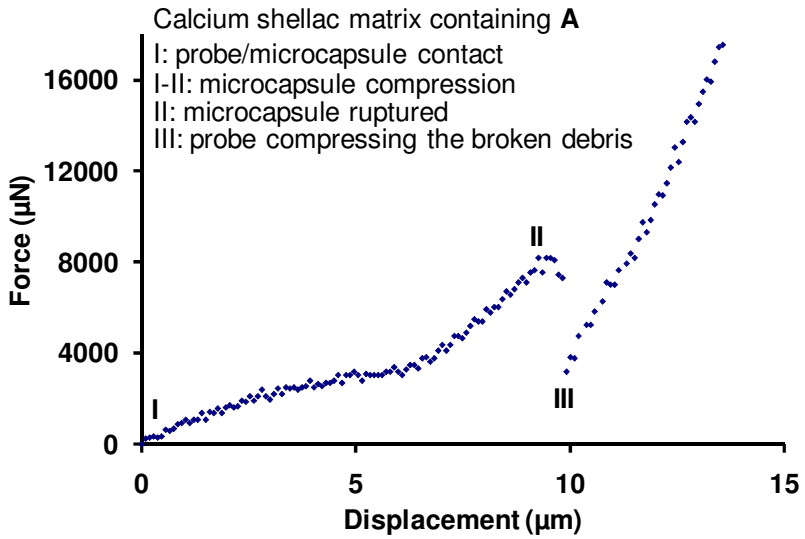


Figure 5. Force vs. probe moving distance for compressing single microcapsules (calcium shellac matrix containing microcapsules **A**) to rupture.

The displacement at rupture (δ_R) denotes as the distance that the probe travels from contact with particle until rupture. The deformation at rupture is calculated using the equation **1** in **Chapter 3** (equation 1) (d = initial particle diameter), and the nominal rupture stress is calculated using the equation **2** in **Chapter 3** (equation 2) (F_R = rupture force).

The deformation at rupture and nominal rupture stress for different types of microcapsules and calcium shellac microparticles are plotted in **Figure 6a-b**. Analysis of **Figure 6a** reveals a significant difference in the deformation at rupture for microcapsules **A** (24.9±1.5 %) and **F** (7.2±0.4 %). However, the deformation at rupture for calcium

shellac matrix containing microcapsules **A** is 25.7±1.0 %, and with **F** is 26.7±1.9 %, which is even greater than that of calcium shellac microparticles (20.9±1.8%). Analysis of the nominal rupture stress in **Figure 6b** gives a similar picture. The average nominal rupture stress of microcapsules **A** and **F** are 1.30±0.10 MPa and 0.20±0.03 MPa, respectively. However, the average nominal rupture stress of the corresponding complex capsules are 21.0±2.4 and 21.8±1.4, respectively, which are significantly greater even than that of calcium shellac microparticles (14.1±0.6 MPa). Previous literature reports that the relative cross-sectional solid area of the calcium shellac microparticles produced by the same method is 92 %,[117] suggesting that there are pores in the calcium shellac microparticles. We propose that the reason for the strength enhancement is that when microcapsules **A** and **F** were embedded, the original pores inside the calcium shellac matrix were filled, which led to the greater nominal rupture stress of the complex capsules than that of calcium shellac microparticles.

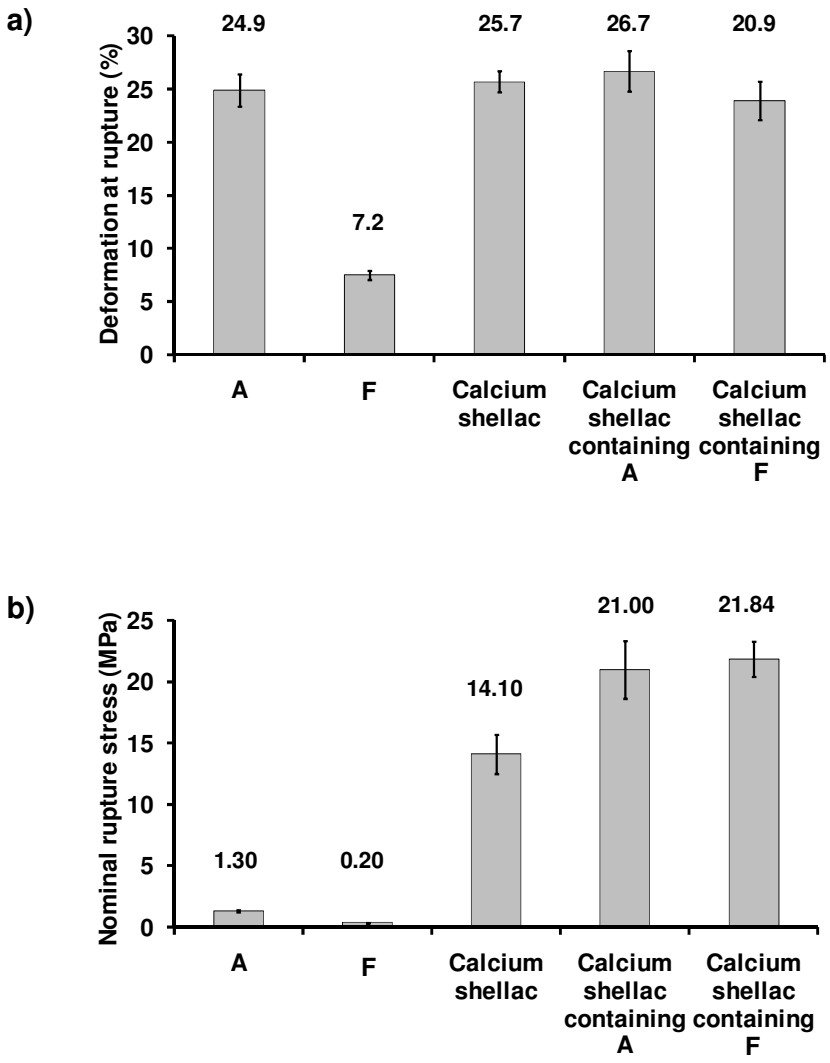


Figure 6. Mechanical properties of a) deformation at rupture of microcapsules **A** and **F**, calcium shellac matrix containing microcapsules **A** and **F** and calcium shellac microparticles, b) nominal rupture stress of microcapsules **A** and **F**, calcium shellac matrix containing microcapsules **A** and **F** and calcium shellac microparticles.

6.3.8 Leakage

The leakage of the microcapsules **A** and **F**, calcium shellac matrix containing **A** and **F** was monitored over a period of 20 days and the result are plotted in **Figure 7a**. Microcapsules **F** shows the highest leakage by the end of 20 days (10.3±0.42 %),

followed by the microcapsules **A** (6.8±0.3 %). Calcium shellac matrix containing microcapsules **F** shows a significant reduction of leakage (0.76±0.02 %), and the smallest leakage was observed on the calcium shellac matrix containing microcapsules **A** (0.18±0.02 %). However, due to the size difference between microcapsules **A** (13.1 μm) and **F** (13.8 μm), and the calcium shellac matrix containing **A** and **F** (83.0 and 84.0 μm, respectively), the effect of surface area/volume on the leakage of the microcapsules should be considered when the leakage is assessed. An equation (equation (**3**)) which is adapted from Lapidus and Lordi[220] is applied to evaluate the effect of surface area/volume on the leakage of the capsules, where the leakage mechanism is assumed to be dominated by diffusion.

$$\frac{M_t}{M_o} = 2\left(\frac{S}{V}\right)\left(\frac{D_{eff}\, t}{\pi}\right)^{1/2} \qquad (3)$$

Where M_t is the amount of oil released at time t, M_o is the total oil input, S is the capsule's surface area, V is the capsule's volume, and D_{eff} is the effective oil diffusion coefficient of the microcapsule.

Re-arranging equation (**3**) gives

$$\pi \left(\frac{M_t/M_o}{2S/V}\right)^2 = D_{eff}\, t \qquad \text{or}$$

$$y = D_{eff}\, t \qquad (\mathbf{4})$$

Where $y = \pi \left(\frac{M_t/M_o}{2S/V}\right)^2$

The average diameter of each sample, d_{32} was used to determine the ratio of S and V in equation (**4**), from which D_{eff} for microcapsules **A** and **F**, calcium shellac matrix containing microcapsules **A** and **F** were obtained by plotting y vs. t, as shown in Figure **7b**. The leakage data of all four types of capsules were found to fit the straight lines reasonably well (with the R^2 value all greater than 0.95). Moreover, after taking the surface area/volume into consideration, calcium shellac matrix containing microcapsules **A** still gives the smallest D_{eff} (1.77×10^2 m^2s^{-1}), followed by the calcium shellac matrix containing microcapsules **F** (4.27×10^3 $m^2s^{-1)}$, suggesting that calcium shellac matrix did induce an effective additional barrier for preventing the core oil leaking from the microcapsules.

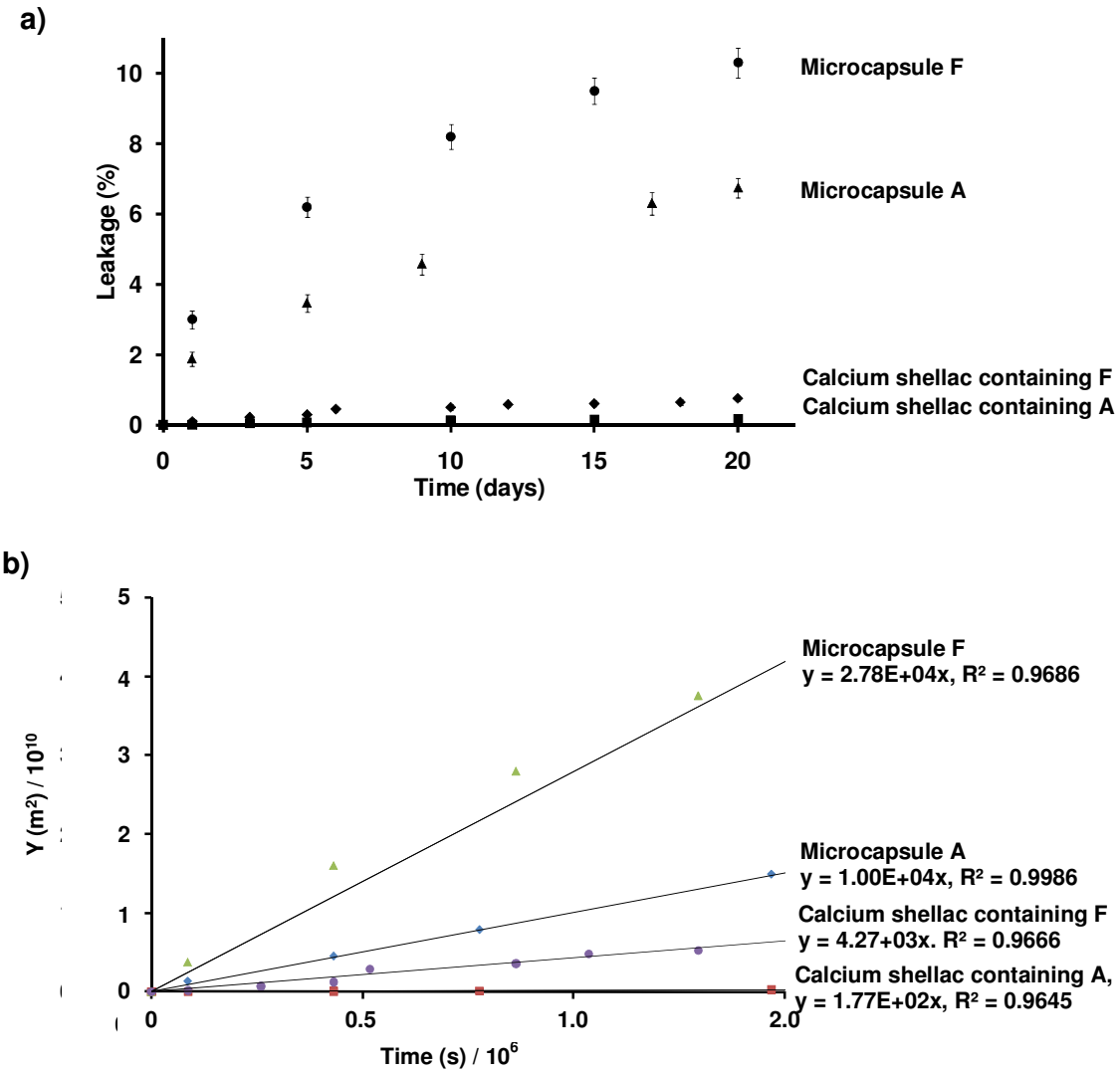


Figure 7. Leakage profile of a) microcapsules **A** and **F**, and calcium shellac matrix containing microcapsules **A** and **F** over 20 days, b) linear plots for calculation of D_{eff} for microcapsules **A** and **F**, and calcium shellac matrix containing microcapsules **A** and **F**.

6.4 Conclusions

Calcium shellac matrix containing MF microcapsules (**A**) and unripened $CaCO_3$ nanoparticles stabilised microcapsules (**F**) (complex capsules) were successfully prepared.

The properties of these calcium shellac matrix containing microcapsules **A** and **F** were compared with those of the microcapsules **A** and **F**, and calcium shellac microparticles. It was found that calcium shellac matrix containing **A** and **F** possessed a less regular shape with an average diameter of 83.0 and 84.0 μm, respectively, compared to calcium shellac microparticles which were spherical and had an average diameter of 46.2 μm. Moreover, the calcium shellac matrix containing microcapsules **A** and **F** showed average nominal rupture stress of 21.00 and 21.84 MPa, respectively, which is approximately 20 fold greater than microcapsules **A** (1.30 MPa) and 95 fold larger than microcapsules **F** (0.20 MPa). The similar nominal rupture stress of the calcium shellac matrix containing **A** and **F** implies that the mechanical properties of these capsules was not significantly affected by the type of the microcapsules that were embedded. However, the calcium shellac microparticles had a smaller average nominal rupture stress (14.10 MPa) than those containing microcapsules **A** and **F**, suggesting that calcium shellac matrix was more difficult to rupture when the microcapsules were inside, which is probably because the embedded microcapsules filled the pores of the calcium shellac matrix, and subsequently enhanced the rupture stress. It was also found from the leakage test that there is a ~14 fold reduction of leakage between calcium shellac matrix containing microcapsules **F** (0.76 %) and microcapsule **F** (10.3 %), and a ~37 fold reduction between calcium shellac matrix containing microcapsules **A** (0.18 %) and microcapsule **A** (6.75 %). After taking the size into consideration, calcium shellac matrix containing microcapsules **A** or **F** still show smaller D_{eff} value (1.77×10^{2} m^2s^{-1} and 4.27×10^{3} m^2s^{-1}, respectively) than that of microcapsules **A** and **F** alone (1.00×10^{4} m^2s^{-1} and 2.78×10^{4} m^2s^{-1}, respectively). This reduction in leakage proves that calcium shellac wall has induced another barrier for the core oil, which provides effective protection of the core oil from leakage.

CHAPTER 7

Overall Conclusions and Future Work

7.1 Overall Conclusions

Melamine formaldehyde microcapsules were formed from an *in situ* polymerization method containing a perfume oil. There are several technical challenges associated with this type of microcapsules.

Firstly, formaldehyde used in making MF microcapsules is not an environmentally friendly chemical, thus, the quantity used should be minimised.

Secondly, the core oil leaks from the melamine formaldehyde wall.

Thirdly, the microcapsules should have optimum mechanical strength for the application.

The main objective of this research was to reduce the leakage of the oil from the MF microcapsules, and to optimise their mechanical properties, and to use the minimum amount of formaldehyde without compromising their desirable properties. Therefore, three approaches were undertaken:

1. A low F/M molar ratio (0.20-0.49) compared to the conventional literature formulations (2.30-5.50) was used to produce the MF microcapsules in order to reduce the formaldehyde content in the microcapsules.

2. Organic/inorganic double shell composite microcapsules with MF/copolymer as the inner shell, and ripened $CaCO_3$ nanoparticles as the outer shell were produced to reduce the leakage of the microcapsules.
3. Calcium shellac matrix containing MF microcapsules or unripened $CaCO_3$ nanoparticulate microcapsules were also produced to reduce the leakage of the microcapsules.

Their effects on the leakage and mechanical properties of the microcapsules were characterized. The encapsulation efficiency, physical, mechanical properties and leakage data of all the microcapsules made in this project are summarized and shown in **Table 1**.

Table 1. Summary of encapsulation efficiency, physical and mechanical properties and leakage data of microcapsules.

Microcapsules (Chapters)	Type	Single shell (S) / double shell (D)	Encapsulation efficiency (%)	Average diameter (μm)	MF wall thickness (nm)	$CaCO_3$ wall thickness (nm)	Nominal rupture stress (MPa)	Deformation at rupture (%)	Leakage (24 hours) (%)	Leakage (20 days) (%)
A (3)	MF	S	75.2 ± 0.8	14.7 ± 1.6	80 ± 1.9	–[a]	–[b]	–[b]	–[c]	6.7 ± 0.35
B (3)	MF	S	75.3 ± 0.4	14.9 ± 1.7	150 ± 1.5	–[a]	1.3 ± 0.1	24.8 ± 1.5	–[c]	5.1 ± 0.21
C (3)	MF	S	75.6 ± 0.5	13.6 ± 1.6	225 ± 2.1	–[a]	1.9 ± 0.1	34.3 ± 1.7	–[c]	3.7 ± 0.20
D (3)	MF	S	75.8 ± 0.7	14.6 ± 1.5	308 ± 1.7	–[a]	4.2 ± 0.4	56.2 ± 1.0	–[c]	2.1 ± 0.18
E (3)	MF	S	74.3 ± 0.5	13.9 ± 1.5	352 ± 1.8	–[a]	7.0 ± 0.6	58.4 ± 3.1	–[c]	1.3 ± 0.17
F (4 and 6)	Unripened $CaCO_3$ single shell	S	76.0 ± 0.5	13.8 ± 1.2	–[d]	–[e]	0.20 ± 0.03	7.2 ± 0.3	–[c]	10.3 ±0.42
G (4)	Unripened composite double shell	D	75.2 ± 0.5	15.8 ± 1.3	–[e]	210 ± 8.2	0.22 ± 0.03	7.4 ± 0.3	0.16 ± 0.01	–[g]
H (4)	Ripened $CaCO_3$ single shell	S	74.8 ± 0.4	15.7 ± 1.2	–[d]	250 ± 8.2	0.47 ± 0.04	8.1 ± 0.6	2.25 ± 0.02	–[g]
$I_{4.5}$ (4)	Ripened composite double shell	D	15.1 ± 1.2	66.3 ± 1.8	–[e]	–[e]	–[b]	–[b]	79.20 ± 1.15	–[g]
$I_{5.0}$ (4)	Ripened composite double shell	D	25.1 ± 1.3	35.5 ± 1.5	–[e]	–[e]	–[b]	–[b]	65.20 ± 1.28	–[g]
$I_{5.5}$ (4)	Ripened composite double shell	D	34.9 ± 1.8	26.5 ± 1.5	–[e]	72 ± 3.5	–[b]	–[b]	50.21 ± 0.53	–[g]
$I_{6.0}$ (4 and 5)	Ripened composite double shell	D	76.0 ± 1.5	15.1 ± 1.1	129 ± 2.5	402 ± 5.8	0.55 ± 0.07	7.3 ± 0.5	0.094 ± 0.025	–[g]
$I_{7.0}$ (4)	Ripened composite double shell	D	76.0 ± 1.6	15.1 ± 1.3	–[f]	–[f]	0.50 ± 0.05	7.1 ± 0.4	0.095 ± 0.024	–[g]
J (5)	Ripened composite double shell	D	75.3 ± 1.1	14.5 ± 1.1	–[f]	406 ± 3.5	0.51 ± 0.06	7.3 ± 0.2	0.067 ± 0.0019	–[g]
K (5)	Ripened composite double shell	D	74.8 ± 1.4	15.2 ± 2.0	–[f]	360 ± 5.7	0.39 ± 0.08	7.4 ± 0.3	0.052 ± 0.0015	–[g]
L (5)	Ripened composite double shell	D	74.2 ± 1.5	14.2 ± 1.5	160 ± 3.1	410 ± 3.8	0.65 ± 0.10	7.5 ± 0.6	0.047 ± 0.0013	–[g]
M (5)	Ripened composite	D	75.1 ± 1.6	13.2 ± 1.6	162 ± 3.3	580 ± 5.2	0.91 ± 0.09	7.6 ± 0.5	0.046 ± 0.0018	–[g]
Calcium shellac microparticles (6)	Microparticles	–[i]	–[h]	42.6 ± 1.8	–[d]	–[a]	14.1 ± 1.6	20.9 ± 1.8	–[h]	–[h]
Calcium shellac matrix containing A (6)	Complex	–[i]	85.0 ± 1.1	83.0 ± 1.2	–[d]	–[a]	21.0 ± 2.4	25.7 ± 1.0	–[c]	0.76 ± 0.02
Calcium shellac matrix containing F (6)	Complex	–[i]	92	84.0 ± 1.5	–[d]	–[a]	21.8 ± 1.4	26.7 ± 1.9	–[c]	0.18 ± 0.02

[a] MF microcapsules do not possess $CaCO_3$ wall
[b] Microcapsules are too weak to be tested by micromanipulation
[c] Leakage of the microcapsules are monitored for 20 days
[d] Microcapsules do not possess MF wall
[e] Microcapsules are too weak to be processed by ultra microtome sampling, hence their wall thickness can not be evaluated by using TEM
[f] Wall thickness of the microcapsules are not evaluated
[g] Leakage of the microcapsules are monitored for 24 hours
[h] Calcium shellac microparticles do not have any core material
[i] Calcium shellac microparticles/matrix are not single or double shell microcapsules

7.1.1 Microcapsules with low content of formaldehyde (Chapter 3, microcapsules A-E)

A low F/M molar ratio (0.20-0.49) compared to the conventional formulation (2.30-5.50) was used to produce the MF microcapsules in this study. The leakage and mechanical properties of these microcapsules made by a lower formaldehyde content were compared with the conventional microcapsules (F/M molar ratio 2.30), as were the other physical properties such as average particle size, wall thickness, and morphology (**Table 1**). The release kinetics of these MF microcapsules was also characterized. It was found that the amount of formaldehyde in the formulation has a strong influence on the properties of the microcapsules. When the F/M molar ratio was increased from 0.20 to 2.30 (microcapsules **A**-**E**, **Table 1**), the wall thickness and the average nominal rupture stress increased, and the amount of oil leakage decreased. However, it was found that a relatively small window of F/M molar ratio between 0.20 and 0.49 exists in which the wall thickness and nominal rupture stress of the microcapsules can be modulated significantly. Above 0.49 increases in F/M molar ratios only increase these properties marginally.

7.1.2 Organic/inorganic composite double shell microcapsules (Chapter 4 and 5, microcapsules F, G, H, $I_{4.5}$, $I_{5.5}$, $I_{6.0}$, $I_{7.0}$, J, K, L and M)

In order to reduce the leakage of the MF microcapsules, organic/inorganic double shell composite microcapsules were produced with MF/copolymer as the inner shell, and ripened $CaCO_3$ nanoparticulate as the outer shell (microcapsules **I**). These double shell composite microcapsules were made based on the *in situ* polymerization method to form a MF/copolymer shell inside the ripened $CaCO_3$ nanoparticulate microcapsules wall, resulting from the migration of a MF precondensate and copolymer through the interstices of the ripened $CaCO_3$ nanoparticles and their reaction at the oil-water interface.

The double shell structure was confirmed using EDX analysis on the ultra-microtome section of the microcapsules. These double shell composite microcapsules were found to have reduced leakage over the MF microcapsules (microcapsules **A**) by 20 fold and the ripened $CaCO_3$ nanoparticulate microcapsules (microcapsules **H**) by 25 fold based on the leakage data over 24 hours. It was also found that the $CaCO_3$ nanoparticle ripening process gave the microcapsules wall a more compact and smooth structure, and consequently reduced the oil leakage (microcapsules **G**). The mechanical properties of the double shell composite microcapsules were dominated by the inorganic outer shell in terms of both deformation at rupture and nominal rupture stress. In addition, the effect of pH (4.5, 5.0, 5.5, 6.0, and 7.0) on the formation and properties of the microcapsules was investigated (microcapsules $\mathbf{I_{4.5}}$, $\mathbf{I_{5.0}}$, $\mathbf{I_{5.5}}$, $\mathbf{I_{6.0}}$, and $\mathbf{I_{7.0}}$). The microcapsules became much leakier when the pH is lower than 6.0 (4.5, 5.0 and 5.5), and lower encapsulation efficiency and lower degree of wall formation also resulted.

Moreover, the effects of certain formulation parameters on the properties of the double shell composite microcapsules were investigated, *i.e.* the MF cross-linking time and the concentration of the aqueous $CaCl_2$ and Na_2CO_3 used for the ripening process of $CaCO_3$ nanoparticles was varied. It was found that when the MF polymerization time increased from 4 to 24 hours (microcapsules **I**, **J** and **L**), the MF/copolymer inner wall thickness increased from 129 nm to 160 nm, and the leakage of the microcapsules decreased from 0.095 ± 0.002 % to 0.047 ± 0.001 % after 24 hours. However, the outer $CaCO_3$ nanoparticulate wall thickness remained constant (~400 nm), so did the degree of the wall formation formed by the ripened $CaCO_3$ nanoparticles (~93 %). As the concentration of the aqueous $CaCl_2$ and Na_2CO_3 was increased leading to the $CaCO_3$ nanoparticulate ripening process (microcapsules **K**, **L** and **M**), the ripened $CaCO_3$ wall thickness of the

microcapsules increased from 360 ± 5.7 nm to 580 ± 5.2 nm, the nominal rupture stress of the microcapsules increased from 0.39 ± 0.07 MPa to 0.91 ± 0.09 MPa, and the leakage of the microcapsules was reduced from 0.052 ± 0.001 % to 0.045 ± 0.001 % after 24 hours. However, the MF/copolymer inner wall thickness remained unchanged (~160 nm).

7.1.3 Calcium shellac matrix with microcapsules embedded (complex microcapsules) (Chapter 6, calcium shellac microparticles, calcium shellac matrix containing A, and calcium shellac matrix containing F)

Another approach to reduce the leakage of the microcapsules is to prepare calcium shellac matrix containing MF microcapsules (microcapsules **A**) and unripened single shell $CaCO_3$ nanoparticulate microcapsules (microcapsules **F**) (complex microcapsules). It was found that the calcium shellac matrix containing microcapsules **A** and **F** showed average nominal rupture stress of 21.00 and 21.84 MPa, respectively, which is approximately 20 fold greater than microcapsules **A** (1.30 MPa) and 95 fold larger than microcapsules **F** (0.20 MPa). The similar nominal rupture stress of the calcium shellac matrix containing **A** and **F** implies that the mechanical properties of these capsules was not significantly affected by the type of the microcapsules that were embedded. However, the calcium shellac microparticles had a smaller average nominal rupture stress (14.10 MPa) than those containing microcapsules **A** and **F**, which is probably because the embedded microcapsules filled the pores of the calcium shellac matrix, and subsequently enhanced the rupture stress. It was also found from the leakage data that there is a ~14 fold reduction of leakage between microcapsule **F** (10.3 %) and calcium shellac matrix containing microcapsules **F** (0.76 %), and a ~37 fold reduction between microcapsule **A** (6.75 %) and calcium shellac matrix containing microcapsules **A** (0.18 %).

7.1.4 Overall comparison of the mechanical properties of the microcapsules

The nominal rupture stress and deformation at rupture of all the microcapsules studied in this project are listed in **Table 1**, from which it can be seen that the nominal rupture stress of MF microcapsules ranges from 1.3 to 7.0 MPa (microcapsules **B**-**E**, F/M molar ratio 0.39-2.30), and the deformation at rupture ranges from 24.8 % to 58.4 % (**Chapter 3**, **3.3.6**). In comparison, inorganic microcapsules: unripened $CaCO_3$ nanoparticles stabilised microcapsules (**F**) and ripened $CaCO_3$ nanoparticles microcapsules (**H**) possess much lower nominal rupture stress (0.20 MPa and 0.47 MPa, respectively) and deformation at rupture (7.2 % and 8.1 %, respectively) than those of the organic MF microcapsules (**Chapter 4**, **4.3.6**). However, it can be seen that the $CaCO_3$ nanoparticles ripening process enhanced the stress of the microcapsules, but the deformation at rupture remained the same. Similar effects could be seen on the unripened double shell composite microcapsules (**G**) and ripened double shell composite microcapsules ($\mathbf{I_{6.0}}$ and $\mathbf{I_{7.0}}$) where the nominal rupture stress increased from 0.22 MPa (**G**) to 0.55 MPa ($\mathbf{I_{6.0}}$ and $\mathbf{I_{7.0}}$) after ripening, with the deformation at rupture remaining the same (7.4±0.3 % and 7.3±0.2 %, respectively). It was also found that the mechanical properties of the double shell composite microcapsules are primarily governed by the inorganic $CaCO_3$ nanoparticles outer shell. When increasing the MF cross-linking reaction time from 4 to 24 hours (microcapsules $\mathbf{I_{6.0}}$, **J** and **L**), both of the nominal rupture stress and deformation at rupture remained the same (**Chapter 5**, **5.3.5**). However, when the concentration of the $CaCl_2$ and Na_2CO_3 used in the ripening process increased from 1.0 M to 2.0 M (microcapsules **K**, **L** and **M**), the nominal rupture stress increased from 0.39 MPa to 0.91 MPa, while the deformation at rupture remained unchanged. The complex microcapsules (calcium shellac containing MF microcapsules (**A**) and unripened $CaCO_3$ nanoparticles

stabilised microcapsules (**F**)) possess much larger nominal rupture stress (21.0 MPa and 21.8 MPa, respectively) and deformation at rupture (25.7 % and 26.7 %, respectively) (**Chapter 6**, **6.3.6**) than the calcium shellac microparticles (14.1 MPa and 20.9 %, respectively), which is probably because the embedded microcapsules filled the pores of the calcium shellac matrix, and subsequently enhanced the rupture stress. It was also found that the mechanical properties of the complex microcapsules were not affected by the type of microcapsules embedded.

7.1.5 Overall comparison of the leakage of the microcapsules

The leakage of the MF microcapsules was found to be reduced when the F/M molar ratio increased from 0.20 to 2.30 (microcapsules **A**-**E**, 6.7 % to 1.3 % at the end of 20 days). In comparison, inorganic microcapsules ripened $CaCO_3$ nanoparticles microcapsules (**H**) showed a higher leakage (2.25 %) than the MF microcapsules (1.78 %) at the end of 24 hours (**Chapter 4**, **4.3.8**). A significant reduction in leakage was observed for the double shell composite microcapsules **G** (unripened) and $\mathbf{I_{6.0}}$ (ripened) (0.16 % and 0.094 %, respectively at the end of 24 hours). Moreover, it was found that the leakage of the double shell composite microcapsules increased when the pH was decreased from 6.0 to 4.5 (79.21 % to 0.09 % for $\mathbf{I_{4.5}}$ and $\mathbf{I_{6.0}}$, respectively) at the end of 24 hours. In addition, when the MF polymerization time increased from 4 to 24 hours (microcapsules, $\mathbf{I_{6.0}}$, **J** and **L**), the leakage of the microcapsules was reduced from 0.095 ± 0.001 % to 0.047 ± 0.001 % (**Chapter 5**, **5.3.6**). However, varying the concentration of the aqueous $CaCl_2$ and Na_2CO_3 on the ripening process does not have an impact on the leakage of the microcapsules. Furthermore, by embedding the MF microcapsules (**A**) into the calcium shellac matrix, a ~37 fold reduction of leakage was observed between microcapsule **A** alone (6.75 %) and calcium shellac matrix containing MF microcapsules (0.18 %)

(**Chapter 6**, **6.3.7**), and a ~14 fold reduction of leakage was found between microcapsule **F** (10.3 %) alone and calcium shellac matrix containing unripened $CaCO_3$ nanoparticles stabilised microcapsules (**F**) (0.76 %). Therefore, it can be concluded that the approaches to make the double shell composite microcapsules and the complex microcapsules have a positive impact on the reduction of the leakage of the MF microcapsules.

7.1.6 Overall discussion of the relation between leakage and mechanical stress

For the MF microcapsules **A**-**E**, as the wall thickness increases, the nominal rupture stresses of the microcapsules increased and the leakage of the microcapsules decreased. It can be seen that the rupture stress of the microcapsules increase with wall thickness, whereas the leakage of the microcapsules is inversely proportional to the rupture stress and wall thickness. Hence, it can be seen that thicker microcapsule walls result in stronger microcapsules and are less leaky. However, when comparing the double shell composite microcapsules with the MF microcapsules. MF microcapsules have a thinner wall, but higher nominal rupture stress. In this case, the wall thickness and the nominal ruptures are not related. Nevertheless, among the double shell composite microcapsules, as the $CaCO_3$ wall thickness increases (microcapsules **K**, **L** and **M**), the nominal rupture stress increased, and the leakage of the microcapsules decreased. From the study of the double shell composite microcapsules, their mechanical properties are dominated by the $CaCO_3$ outer shell. Therefore, it can be concluded that the wall thickness, nominal rupture stress and leakage are only related within the same type of the microcapsules. A different relation between the nominal rupture stress and leakage was observed for the complex microcapsules. The calcium shellac matrix containing microcapsules **A** and **F** have very similar nominal rupture stress (21.0 ± 2.4 MPa and 21.8 ± 1.4 MPa, respectively). However, the leakage for calcium shellac matrix containing **A** (0.18 ±

0.02 %) is lower than that of calcium shellac matrix containing **F** (0.76 ± 0.02 %). The reason for this different leakage behaviour is probably due to the embedded microcapsules. Microcapsules **A** having a lower leakage (6.7 ± 0.35 %) than that of the microcapsules **F** (10.3 ± 0.42 %).

7.2 Future work

In **Chapter 3** the amount of formaldehyde used in the formulation was significantly reduced in comparison with the conventional literature formulations for producing MF microcapsules. However, it has been found in other work[56] that free formaldehyde is released during the application. Hence, to find wall materials which possess similar properties to MF, but are environmentally benign is required.

Calcium shellac matrix containing MF microcapsules or unripened $CaCO_3$ nanoparticulate microcapsules (complex microcapsules) were produced (**Chapter 6**). These complex microcapsules showed a significant reduction in leakage than the MF microcapsules, and a much greater nominal rupture stress. However, this large rupture stress could cause difficulties when delivering the core material by rupture during application. Therefore, it is necessary to find a system in which the outer matrix material is less permeable, has lower rupture stress or can release the embedded microcapsules in a more facile route *e.g.* acid or base dissolution.

To enhance the adhesion between microcapsules and fibres is important for applications in order to improve the performance of the end product. One possible way is to coat the microcapsules with polyelectrolyte that electrostatically bind with fibres. Alternatively,

the attachment of microcapsules to fibres could be achieved by covalently bonding. In addition, attachment of the microcapsules to non-spheroid shapes could assist the entrapment of the microcapsules to fibres.

Finally, in order to gain a deeper understanding of the relation between leakage and mechanical properties of the microcapsules, the microstructure of the microcapsules wall which might control the leakage and mechanical properties of the microcapsules need to be further characterized and studied.

References

[1] N. Tro, *Chemistry in Focus: A Molecular View of Our World*, Brooks/Cole, Cengage Learning, Belmont, **2007**.

[2] C. S. Sell, *The Chemistry of Fragrances*, The Royal Society of Chemistry, Dorchester, **2006**.

[3] E. Breitamaier, *Terpenes-Flavors, Fragrances, Pharmaca, Pheromones*, Wiley-VCH, Weinheim, **2006**.

[4] H. Surburg, J. Panten, *Common Fragrance and Flavor Materials: Preparation, Properties and Uses*, Wiley-VCH Verlag GmbH & Co. KGaA, Weinheim, **2006**.

[5] E. W. Flick, *Cosmetic and Toiletry Formulations*, Noyes Publications, New Jersey, **1995**.

[6] H. Panda, *Herbal Soups and Detergents Hand Book*, National Institute of Industrial Research, Shahzada Bagh, **2000**.

[7] P. M. Muller, *Persumes: Art, Science and Technology*, Blackie Academic and Professional, Glasgow, **1991**.

[8] J. S. Jellinek, *The Use of Fragrance in Consumer Products*, John Wiley & Sons, Inc., New York/London/Sydney/Toronto, **1975**.

[9] C. Sell, *A Fragrant Introduction to Terpenoid Chemistry*, The Royal Society of Chemistry, Cambridge, **2003**.

[10] D. F. Williams, W. H. Schmitt, *Chemistry and Technology of the Cosmetics and Toiletries Industry*, Blackie Academic & Professional, New York, **1992**.

[11] C. H. Bamford, C. F. H. Tipper, *Ester Formation and Hydrolysis and Related Reactions*, Elsevier Publishing Company, New York, **1972**.

[12] A. Hermann, *Angew. Chem. Int. Ed.* 2007, *46*, 5836.

[13] C. Knipe, *Organic Reaction Mechanisms*, John Wiley & Sons Ltd, Chichester, **2008**.

[14] A. Salvador, A. Chisvert, *Analysis of Cosmetic Products*, Elsevier, Amsterdam, **2007**.

[15] R. R. Calkin, J. S. Jellinek, *Perfumery: Practice and Principles*, John Wiley & Sons, Inc., New Jersey, **1994**.

[16] P. Parker, *Encapsulating: Webster's Questions, Facts and Phrases*, ICON Group International, Inc., California, **2008**.

[17] M. S. Rahman, *Handbook of Food Preservation*, Taylor & Francis Group, Florida, **2007**.

[18] T. M. S. Chang, *Science* **1964**, *146*, 524.

[19] M. Re, *Drying Technol.* **1998**, *16*, 1195.

[20] R. J. Flores, M. D. Wall, D. W. Carnahan, T. A. Orofina, *J. Microencapsulation* **1992**, *9*, 287.

[21] J. S. Hwang, J. H. Kim, Y. J. Wee, H. G. Jang, S. H. Kim, H. W. Ryu, *Biotechnol. Bioprocess Eng.* **2006**, *11*, 391.

[22] K. Hong, S. Park, *React. Funct. Polym.* **1999**, *42*, 193.

[23] R. Arshady, *Microspheres, Microcapsules & Liposomes, Volume 1: Preparation & Chemical Applications*, Citrus Books, London, **1999**.

[24] S. Benita, *Microencapsulation: Method and Industrial Applications*, Marcel Dekker, Inc., New York, **1996**.

[25] T. L. Whateley, *Microencapsulation of Drugs*, Harwood Academic Publishers, Chur, **1992**.

[26] S. K. Ghosh, *Functional Coatings: by Polymer Microencapsulation*, Wiley-VCH, Weinheim, **2006**.
[27] J. L. Arias, *Molecules* **2008**, *13*, 2340.
[28] W. J. Tong, C. Y. Gao, *J. Mater. Chem.* **2008**, *18*, 3799.
[29] V. L. Lagrnha, G. Baldo, T. G. de Carvalho, *Metabolic Brain Dis.* **2008**, *23*, 469.
[30] H. Y. Lee, I. W. Cheong, J. H. Kim, *J. Microencapsulation* **2002**, *19*, 559.
[31] M. J. Jiang, X. Q. Song, G. D. Ye, *Compos. Sci. Technol.* **2008**, *68*, 2231.
[32] P. Monllor, M. A. Bonet, F. Cases, *Eur. Polym. J.* **2007**, *43*, 2481.
[33] H. Liu, B. Chen, Z. W. Mao, C. Y. Gao, *J. Appl. Polym. Sci.* **2007**, *106*, 4248.
[34] Y. S. Han, D. Radziuk, D. Shchukin, *J. Mater. Chem.* **2008**, *18*, 5162.
[35] J. Weiss, E. A. Decker, D. J. MeClements, K. Kristbergsson, T. Helgason, T. Awad, *Food Biophys.* **2008**, *3*, 146.
[36] G. O. Fanger, *Chem. Tech.* **1974**, *4*, 397.
[37] P. Somasundaran, *Encyclopedia of Surface and Colloid Science*, CRC Press Inc., London, **2006**.
[38] S. Magdassi, E. Touitou, *Novel Cosmetic Delivery Systems*, CRC Press, **1998**.
[39] P.Sinclair, in *UK patent, Vol. GB: 2073132A* (Ed.: U. patent), UK, **1981**.
[40] M. Okano, Y. Ogata, *J. Am. Chem. Soc.* **1951**, *74*, 5728.
[41] G. Sun, Z. Zhang, *J. Microencapsulation* **2001**, *18*, 593.
[42] A. Berge, T. Mejdell, *Polymer* **2006**, *47*, 3249.
[43] K. Sato, *Bull. Chem. Soc. Jpn.* **1966**, *41*, 7.
[44] A. Kumar, V. Katiyar, *Macromolecules* **1990**, *23*, 3729.
[45] M. Dawbarn, J. R. Ebdon, S. J. Hewitt, *Polymer* **1978**, *19*, 1309.
[46] C. S. L. Ong, Thesis thesis, University of Birmingham (Birmingham), **1984**.
[47] J. Su, Z. Huang, L. Ren, *Colloid. Polym. Sci.* **2007**, *285*, 437.
[48] J. Su, L. Wang, L. Ren, *J. Appl. Polym. Sci.* **2007**, *103*, 1295.
[49] S. Jahromi, *Macromol. Chem. Phys.* **1999**, *200*, 2230.
[50] W. J. Luo, W. C. Yang, S. Jiang, J. M. Feng, M. B. Yang, *Polym. Degrad. Stab.* **2007**, *92*, 1359.
[51] X. Zhang, X. Tao, K. Yick, X. Wang, *Colloid. Polym. Sci.* **2004**, *282*, 330.
[52] S. Jahromi, *Macromol. Chem. Phys.* **1999**, *200*, 2230.
[53] L. Wei, J. P. Wang, X. C. Wang, S. Z. Wu, X. X. Zhang, *Colloid. Polym. Sci.* **2007**, *285*, 1691.
[54] Y. Hoshi, T. Hayashu, in *U.S. Patent Vol. 4409156*, US, **1983**.
[55] W. Li, X. Zhang, W. Wang, J. Niu, *Mater. Chem. Phys.* **2007**, *106*, 437.
[56] X. X. Zhang, Y. F. Fan, X. M. Tao, K. L. Yick, *Mater. Chem. Phys.* **2004**, *88*, 300.
[57] Y. H. Lee, C. A. Kim, W. H. Jang, H. J. Cio, M. S. John, *Polymer* **2001**, *42*, 8277.
[58] W. J. Luo, S. Jiang, J. M. Feng, M. B. Yang, *Polym. Degrad. Stab.* **2007**, *92*, 1359.
[59] S. Park, Y. S. Shin, J. R. Lee, *J. Colloid Interface Sci.* **2001**, *241*, 502.
[60] K. Dietrich, H. Herma, R. Nastke, E. Bonatz, W. Teige, *Acta Polym.* **1989**, *40*, 243.
[61] M. Sgraja, J. Blomer, J. Bertling, P. Jansens, *J. Appl. Polym. Sci.* **2008**, *110*, 2366.
[62] J. K. Song, H. J. Chio, I. Chin, *J. Microencapsulation* **2007**, *24*, 11.
[63] S. O. Sohn, S. M. Lee, Y. M. Kim, J. H. Yeum, J. H. Choi, H. Do Ghim, *Fiber. Polym.* **2007**, *8*, 163.
[64] H. T. Wang, X. F. Meng, W. Wen, X. W. Gao, S. M. Zhang, M. S. Yang, *Mater. Lett.* **2008**, *62*, 3745.
[65] Y. C. Yuan, M. Z. Rong, M. Q. Zhang, *Acta Seismol. Sin.* **2008**, *5*, 472.
[66] J. F. Su, Z. Huang, L. Ren, *Colloid. Polym. Sci.* **2007**, *285*, 1581.
[67] Y. Shin, D. I. Yoo, K. Son, *J. Appl. Polym. Sci.* **2005**, *96*, 2005.

[68] H. Ichiura, M. Morikawa, J. Ninomiya, *J. Mater. Sci.* **2006**, *41*, 7019.
[69] M. Z. Zhang, P. H. Ni, N. X. Yan, *J. Microencapsulation* **1995**, *12*, 425.
[70] I. Montasser, S. Briancon, H. Fessi, *Int. J. Pharm.* **2007**, *335*, 176.
[71] M. L. Soto-Portas, J. F. Argillier, F. Mechin, N. Zydowicz, *Polym. Int.* **2003**, *52*, 522.
[72] J. J. Ramsden, Y. M. Lvov, G. Decher, *Thin Solid Films* **1995**, *254*, 246.
[73] G. Sukhorukov, E. Donath, S. Davis, H. Lichtenfeld, *Polym. Adv. Technol.* **1998**, *9*, 759.
[74] G. Ladam, P. Schaad, J. C. Voegel, P. Schaaf, G. Decher, F. Cuisinier, *Langmuir* **2000**, 16, 1249.
[75] L. Richert, P. Lavalle, E. Payan, X. Z. Shu, G. D. Prestwich, J. Stoltz, P. Schaaf, J. Voegel, C. Picart, *Langmuir* **2004**, *20*, 448.
[76] F. Caruso, K. Niikura, D. N. Furlong, Y. Okahata, *Langmuir* **1997**, *13*, 3422.
[77] C. Picart, G. Ladam, B. Senger, J. C. Voegel, P. Schaaf, F. J. G. Cuisinier, C. Gergely, *J. Chem. Phys.* **2001**, *115*, 1086.
[78] D. L. Elbert, C. B. Herbert, J. A. Hubbell, *Langmuir* **1999**, *15*, 5355.
[79] C. Picart, P. Lavalle, P. Hubert, F. J. G. Cuisinier, G. Decher, P. Schaaf, J. C. Voegel, *Langmuir* **2001**, *17*, 7414.
[80] C. Picart, J. Mutterer, L. Richert, Y. Luo, G. D. Prestwich, P. Schaaf, J. C. Voegel, P. Lavalle, *Proc. Natl. Acad. Sci. U.S.A.* **2002**, *99*, 12531.
[81] E. J. Pollauf, D. W. Pack, *Biomaterials* **2006**, *27*, 2898.
[82] S. N. Qiao, L. H. Li, M. Wang, L. X. Mo, *J. Beijing Institute Graphic Commun.* **2007**, *15*, 826.
[83] J. Su, L. Ren, L. Wang, *Colloid. Polym. Sci.* **2005**, *284*, 224.
[84] H. C. Shum, J. W. Kim, D. Weitz, *J. Am. Chem. Soc.* **2008**, *130*, 9543.
[85] J. Su, Z. Huang, L. Ren, *Colloid. Polym. Sci.* **2007**, *285*, 1581.
[86] Y. Luo, S. Chen, *Color. Technol.* **2003**, *119*, 37.
[87] H. Chen, Y. Zhao, Y. Song, *J. Am. Chem. Soc.* **2008**, *130*, 7800.
[88] X. Song, L. Gao, *J. Phys. Chem.* **2007**, *111*, 8180.
[89] M. F. Bedard, A. Munoz-Javier, R. Mueller, *Soft Matter* **2009**, *5*, 148.
[90] P. R. Gil, L. L. Mercato, P. Pino, A. Munoz-Javier, W. J. Parak, *Nanotoday* **2008**, *3*, 12.
[91] F. Salaun, E. Devaux, S. Bourbigot, P. Urmeau, P. Chapuis, S. K. Saha, S. Volz, *Thermochim. Acta.* **2008**, *477*, 25.
[92] A. Tan, S. Simovic, A. K. Davey, T. Rades, C. A. Prestidge, *J. Controlled Release* **2009**, *134*, 62.
[93] A. G. Skirtach, A. A. Antipov, D. G. Shchukin, G. B. Sukhorukov, *Langmuir* **2004**, *17*, 6988.
[94] A. G. Skirtach, C. Dejugnat, D. Braun, A. Susha, A. Rogach, W. J. Parak, H. Mohwald, G. Sukhorukov, *Nano Lett.* **2005**, *5*, 1371.
[95] N. Gaponik, I. L. Radtchenko, G. Sukhorukov, A. Rogach, *Langmuir* **2004**, *20*, 1449.
[96] F. Caruso, M. Spasova, A. Susha, M. Giersig, R. A. Caruso, *Chem. Mater.* **2001**, *13*, 109.
[97] M. Rosen, *Delivery System Handbook for Personal Care and Cosmetic Products: Technology, Application, and Formulations*, William Andrew, Inc., Norwich, **2005**.
[98] K. Hong, S. Park, *Mater. Chem. Phys.* **1999**, *58*, 128.
[99] F. Weinbreck, M. Minor, C. G. De Kruif, *J. Microencapsulation* **2004**, *21*, 667.
[100] J. Hwang, J. Kim, Y. Wee, J. Yun, *Biotechnol. Bioeng.* **2006**, *11*, 332.

[101] Y. Yeo, E. Bellas, W. Firstone, R. Langer, D. S. Kohane, *J. Agric. Food. Chem.* **2005**, *53*, 7518.
[102] S. Krishnan, R. Bhosale, R. S. Singhal, *Carbohydr. Polym.* **2005**, *61*, 95.
[103] S. Krishnan, A. C. Ckshirsagar, R. S. Singhal, *Carbohydr. Polym.* **2005**, *62*, 309.
[104] M. L. Torre, M. Faustini, K. M. E. Attilio, D. Vigo, *Recent Pat. Drug Deliv. Formul.* **2007**, *1*, 81.
[105] H. Uludag, P. De Vos, *Adv. Drug Delivery Rev.* **2000**, *42*, 29.
[106] M. M. Farid, A. M. Khudhair, S. A. K. Razack, *Energ. Convers. Manage.* **2004**, *45*, 1597.
[107] D. J. Morrison, S. I. Abdul, *Solar Energy* **1978**, *20*, 57.
[108] R. Marshall, C. Dietsche, *Solar Energy* **1982**, *29*, 503.
[109] V. V. Tyagi, D. Buddhi, *Renewable Sustainable Energy Rev.* **2007**, *11*, 1146.
[110] A. Kurklu, *Technical Note* **1998**, *13*, 89.
[111] R. Prudhoe, *Australian J. Refr., Air Cond., and Heating* April **1991**, 33.
[112] M. R. Kessler, S. R. White, *Composites Part A* **2001**, *32*, 683.
[113] M. R. Kessler, S. R. White, N. R. Sottos, in *Tenth European Conference on Composite Materials (ECCM-10), Vol. 1*, Brugge, Belgium, **2002**.
[114] S. R. White, N. R. Sottos, J. S. Geubelle, M. R. Kessler, S. R. Sriram, E. N. Brown, S. Viswanathan, *Nature* **2001**, *409*, 794.
[115] D. Y. Wu, S. Meure, D. Solomon, *Prog. Polym. Sci.* **2008**, *33*, 479.
[116] G. Sun, Z. Zhang, *Int. J. Pharm.* **2002**, *242*, 307.
[117] J. Xue, Z. Zhang, *J. Appl. Polym. Sci.* **2009**, *113*, 1619.
[118] E. L. Cussler, *Diffusion: Mass Transfer in Fluid Systems*, Cambridge University Press, Cambridge, **1997**.
[119] M. F. A. Goosen, *Fundamentals of Animal Cell Encapsulation and Immobilization*, CRC Press, Inc., **1992**.
[120] W. Kays, *Convective Heat and Mass Transfer*, The McGraw-Hill Companies, Inc., New York, **2005**.
[121] K. P. R. Chowdary, M. S. Rao, *Asian J. Chem.* **2008**, *20*, 5901.
[122] K. Chowdary, M. Rao, *Asian J. Chem.* **2008**, *20*, 5383.
[123] K. P. R. Chowdary, S. Panguluri, V. Enturi, *Asian J. Chem.* **2008**, *20*, 5461.
[124] I. T. Degim, N. Celebi, *Curr. Pharm. Des* **2007**, *13*, 99.
[125] W. Qi, J. Ma, Y. Liu, X. Liu, *J. Membr. Sci.* **2006**, *269*, 126.
[126] J. I. Wells, M. H. Rubinstein, *Pharmaceutical Technology: Controlled Drug Release*, Ellis Horwood Limited, Norton, **1991**.
[127] T. Ohtsubo, S. Tsuda, K. Tsuji, *Polymer* **1991**, *32*, 2395.
[128] J. M. Van Raamsdonk, P. L. Chang, *J. Biomater. Sci. Polym. Ed.* **2001**, *54*, 264.
[129] U. Schuldt, D. Hunkeler, *Minerva Biotechnol.* **2000**, *12*, 223.
[130] A. W. L. Jay, M. A. Edwards, *Can. J. Physiol. Pharmacol.* **1968**, *46*, 731.
[131] V. V. Lulevich, L. L. Radtchenko, G. B. Sukhorukov, O. L. Vinogradova, *Macromolecules* **2003**, *36*, 2832.
[132] F. Edwards-Levy, M. Levy, *Biomaterials* **1999**, *20*, 2069.
[133] Z. Zhang, M. A. Ferenczi, A. C. Lush, C. R. Thomas, *Appl. Microbiol. Biotechnol.* **1991**, *36*, 208.
[134] Z. Zhang, R. Saunders, C. R. Thomas, *J. Microencapsulation* **1999**, *16*, 117.
[135] Z. Zhang, M. A. Ferenczi, C. R. Thomas, *Chem. Eng. Sci.* **1992**, *47*, 1347.
[136] M. Mashmoushy, Z. Zhang, C. R. Thomas, *Biotechnol. Tech.* **1998**, *12*, 925.
[137] R. J. H. Stenekes, W. E. Hennink, *Polymer* **2000**, *41*, 5563.
[138] L. Zhao, Z. Zhang, *Artif. Cells, Blood Substitutes, Immobilization Biotechnol.* **2004**, *32*, 25.

[139] C. P. Chang, T. Leung, S. Lin, C. Hsu, *Colloids Surf. B* **2006**, *50*, 136.
[140] N. B. Shankar, N. U. Kumar, P. K. Balakrishna, R. P. Kumar, *Research J. Pharm. and Tech.* **2008**, *1*, 433.
[141] R. Xu, *Particle Characterization: Light Scattering Methods*, Kluwer Academic Publishers, Norwell, **2000**.
[142] M. Elimelech, J. Gregory, X. Jia, R. A. Williams, *Particle Deposition and Aggregation: Measurement, Modelling and Simulation*, Butterworth-Heinemann, Woburn, **1995**.
[143] J. Goldstein, D. New bury, D. Joy, C. Lyman, *Scanning Electron Microscopy and X-ray Microanalysis*, Kluwer Academic/Plenum Publishers, New York, **2002**.
[144] P. W. Hawkes, *Advances in Electrons and Electron Physics*, Academic Press, Inc., London, **1990**.
[145] Y. Jiang, D. Yang, L. Zhang, Q. Sun, *Adv. Funct. Mater.* **2009**, *19*, 150.
[146] L. Yuan, A. Gu, G. Z. Liang, *Mater. Chem. Phys.* **2008**, *110*, 417.
[147] Y. L. Ren, A. M. Donald, Z. Zhang, *Mater. Sci. Technol.* **2007**, *23*, 857.
[148] H. Qi, P. Hu, J. Xu, A. Wang, *Biomacromolecules* **2006**, *7*, 2327.
[149] B. Xie, H. Shi, G. Liu, Y. Zhou, Y. J. Wang, Y. Zhao, D. Wang, **2008**, *20*.
[150] C. Alkan, S. Ahment, A. Karaipekli, O. Uzun, *Sol. Energy Mater. Sol. Cells* **2009**, *93*, 143.
[151] Y. B. Jiang, D. J. Wang, T. Zhao, *J. Appl. Polym. Sci.* **2007**, *104*, 2799.
[152] J. P. Wang, Z. Wang, J. Chen, J. Yun, *Mater. Res. Bull.* **2008**, *12*, 3374.
[153] Z. Lu, C. M. Li, Q. Zhou, Q. Bao, X. Cui, *J. Colloid Interface Sci.* **2007**, *314*, 80.
[154] H. Frafati, S. N. Ebrahimi, H. Rezadoost, *Iran. Polym. J.* **2008**, *17*, 273.
[155] R. A. F. Rodrigues, C. R. F. Grosso, *J. Microencapsulation* **2008**, *25*, 13.
[156] J. Kenkel, *Analytical Chemistry for Technicians*, CRC press LLC, Florida, **2002**.
[157] V. G. Berezkin, V. R. Alishoyev, I. B. Nemirovskaya, *Journal of Chromatography*, Elsevier Scientific Publishing Company, New York, **1997**.
[158] F. Burner, *Gas Chromatographic Environmental Analysis*, VCH Publishers, Inc., New York, **1993**.
[159] T. Cserhati, E. Forgaces, *Chromatography in Food Science and Technology*, Technomic Publishing Company, Inc., Lancaster, **1999**.
[160] V. G. Berezkin, V. R. Alishoyev, I. B. Nemirovskaya, *Journal of Chromatography*, Elsevier Scientific Publishing Company, New York, **1977**.
[161] R. P. W. Scott, *Introduction to Analytical Gas Chromatography*, Marcel Dekker, Inc., New York, **1998**.
[162] R. L. Grob, E. F. Barry, *Modern Practice of Gas Chromatography*, John Wiley & Sons. Inc., New Jersey, **2004**.
[163] F. Burner, *Gas Chromatographic Environmental Analysis*, VCH Publishers, New York, **1993**.
[164] M. Dressler, *Selective Gas Chromatographic Detectors*, Elsevier Science Publishers B. V., New York, **1985**.
[165] C. Shiu, Z. Zhang, C. R. Thomas, *Biotechnol. Tech.* **1999**, *13*, 707.
[166] C. R. Thomas, Z. Zhang, C. Cowen, *Biotechnol. Lett.* **2000**, *22*, 531.
[167] E. Kissa, *Dispersions, Characterization, Testing and measurement*, Marcel Dekker, Inc., New York, **1999**.
[168] B. D. Fahlman, *Materials Chemistry*, Springer Science and Business Media B. V., Dordrecht, **2008**.
[169] D. J. Stokes, *Principles and Practice of Variable Pressure/Environmental Scanning Electron Microscopy*, John Wiley & Sons Ltd, Chichester, **2008**.

[170] L. Reimer, H. Kohl, *Transmission Electron Microscopy Physics of Image Formation*, Springer Science and Business Media, LLC, New York, **2008**.
[171] D. B. Williams, C. B. Cater, *Transmission Electron Microscopy: A Textbook for Materials Science*, Kluwer Academic Publishers Group, **1996**.
[172] J. Orloff, M. Utlaut, L. Swanson, *High Resolution Focused Ion Beams*, Kluwer Academic and Plenum Publishers, New York, **2003**.
[173] J. D. Irwin, *The Industrial Electronics Handbook*, CRC press LLC, New York, **1997**.
[174] L. A. Giannuzzi, F. A. Stevie, *Introduction to Focused Ion Beams*, Springer Science and Business Media, Inc., New York, **2005**.
[175] Y. Long, D. York, Z. Zhang, J. A. Preece, *J. Mater. Chem.* **2009**, *19*, 6882.
[176] Y. T. Wang, X. P. Zhao, D. W. Wang, *J. Microencapsulation* **2006**, *23*, 762.
[177] J. Kapusniak, P. Tomasik, *J. Microencapsulation* **2006**, *23*, 341.
[178] R. Wegmuller, M. B. Zimmermann, V. G. Buhr, E. J. Windhab, R. E. Hurrell, *J. Food Sci.* **2006**, *71*, S181.
[179] B. Boh, A. Kornhauser, *Crit. Rev. Anal. Chem.* **2003**, *33*, 281.
[180] F. Giroud, J. M. Pernot, H. Brun, B. Pouyet, *J. Microencapsulation* **1995**, *12*, 389.
[181] S. Stolnik, *Adv. Drug. Deliv. Rev.* **1995**, *16*, 195.
[182] K. Hong, S. Park, *Mater. Chem. Phys.* **1999**, *58*, 128.
[183] J. S. Hwang, J. N. Kim, Y. J. Wee, J. S. Yun, H. G. Jang, S. H. Kim, H. W. Ryu, *Biotechnol. Bioprocess. Eng.* **2006**, *11*, 332.
[184] J. Hwang, J. Kim, Y. Wee, H. Jang, S. Kim, H. Ryu, *Biotechnol. Bioprocess. Eng.* **2006**, *11*, 391.
[185] H. Y. Lee, S. J. Lee, I. W. Cheong, J. H. Kim, *J. Microencapsulation* **2002**, *19*, 559.
[186] Z. Zhang, R. Saunders, C. R. Thomas, *J. Microencapsulation* **1999**, *16*, 117.
[187] J. Siepmann, N. A. Peppas, *Adv. Drug Delivery Rev.* **2001**, *48`*, 139.
[188] N. M. Ranjha, I. U. Khan, *J. Sol-Gel Sci. Technol.* **2009**, *50*, 281.
[189] J. Wang, Z. Wang, J. Chen, J. Yun, *Mater. Res. Bull.* **2008**, *43*, 3374.
[190] M. Fujiwara, K. Shiokawa, K. Morigaki, Y. Zhu, Y. Nakahara, *Chem. Eng. J.* **2008**, *137*, 14.
[191] A. Petrov, A. Gavryushkin, G. Sukhorukov, *J. Phys. Chem.* **2003**, *107*, 868.
[192] R. F. Fakhrullin, R. T. Minullina, *Langmuir* **2009**, *25*, 6617.
[193] I. W. Hamley, M. J. Krysmann, V. Castelletto, L. Noirez, *Adv. Mater.* **2008**, *20*, 4394.
[194] C. Y. Wang, C. Y. He, Z. Tong, X. X. Liu, B. Y. Ren, F. Zeng, *Int. J. Pharm.* **2006**, *308*, 160.
[195] G. B. Sukhorukov, D. V. Volodkin, A. M. Gunther, A. Petrov, D. B. Shenoy, H. Mohwald, *J. Mater. Chem.* **2004**, *14*, 2073.
[196] X. D. Li, Q. L. Hu, L. H. Yue, J. C. Shen, *Chem. Eur. J.* **2006**, *12*, 5770.
[197] K. Ariga, A. Vinu, M. Miyahara, *Curr. Nanosci.* **2006**, *2*, 197.
[198] G. J. Vermeij, *A Natural History of Shells*, Princeton University Press, New Jersey, **1993**.
[199] D. V. Andreeva, D. A. Gorin, H. Mohwald, G. B. Sukhorukov, *Langmuir* **2007**, *23*, 9031.
[200] G. M. Luz, J. F. Mano, *Phil. Trans. R. Soc. B.* **2009**, *367*, 1587.
[201] Y. Nakahara, M. Mizuguchi, K. I. Miyata, *J. Collid Interface Sci.* **1979**, *68*, 401.
[202] J. A. Thomas, L. Seton, R. J. Davey, C. E. DeWolf, *Chem. Commun.* **2002**, 1072.
[203] G. Hadiko, Y. S. Han, M. Fuji, M. Takahashi, *Mater. Lett.* **2005**, *59*, 2519.
[204] N. Loges, K. Graf, L. Nasdala, W. Tremel, *Langmuir* **2006**, *22*, 3073.

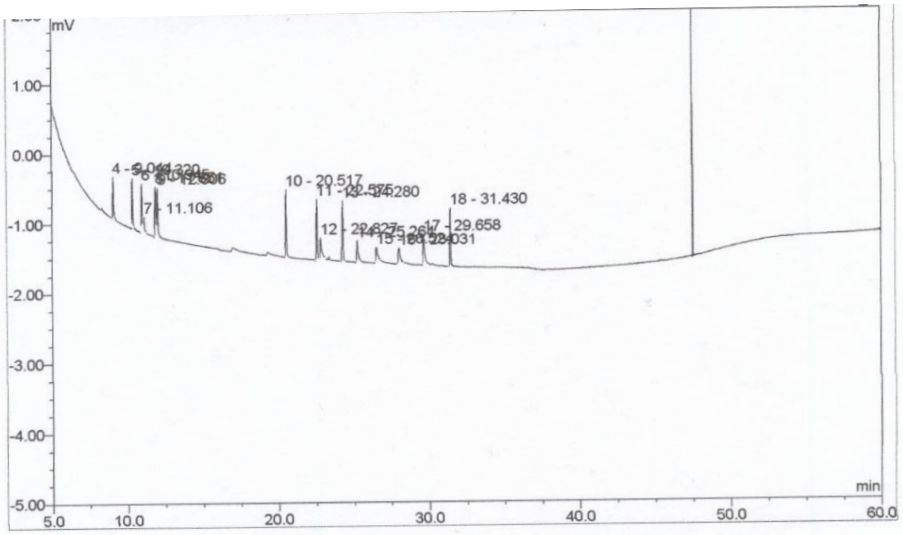
[205] D. Walsh, B. Lebeau, S. Mann, *Adv. Mater.* **1999**, *11*, 324.
[206] Y. S. Han, G. Hadiko, M. Fuji, M. Takahashi, *Chem. Lett.* **2005**, *34*, 152.
[207] F. C. Meldrum, *Int. Mater. Rev.* **2003**, *48*, 187.
[208] D. V. Volodkin, N. I. Larionova, G. B. Sukhorukov, *Biomacromolecules* **2004**, *5*, 1962.
[209] C. J. Cain, A. N. J. Heyn, *Biophys J.* **1964**, *4*, 23.
[210] X. G. Cheng, P. L. Varona, M. J. Olszta, L. B. Gower, *J. Cryst. Growth* **2007**, *307*, 395.
[211] N. Pearnchob, J. Siepmann, R. Bodmeier, *Drug Dev. Ind. Pharm.* **2003**, *29*, 925.
[212] R. G. Mcguire, R. D. Hagenmaier, *Biol. Control* **1996**, *7*, 100.
[213] J. Bai, R. D. Hagenmaier, E. A. Baldwin, *Postharvest Biol. Technol.* **2003**, *28*, 381.
[214] O. L. Lau, *Postharvest Biol. Technol.* **1998**, *14*, 131.
[215] M. Luangtana-anan, S. Limmatvapirat, J. Nunthanid, C. Wanawongthai, *J. Agric. Food Chem.* **2007**, *55*, 687.
[216] C. Limmatvapirat, J. Nunthanid, M. Luangtana-anan, S. Puttipipatkhachorn, *Pharm. Dev. Technol.* **2005**, *10*, 41.
[217] S. Limmatvapirat, C. Limmatvapirat, S. Puttipipatkhachorn, J. Nunthanid, M. Luangtana-anan, *Eur. J. Pharm. Biopharm.* **2007**, *67*, 690.
[218] J. Xue, Z. Zhang, *J. Microencapsulation* **2008**, *25*, 523.
[219] S. Limmatvapirat, C. Limmatvapirat, S. Puttipipatkhachorn, J. Nunthanid, M. Luangtana-anan, P. Sriamornsak, *Eur. J Pharm. Biopharm.* **2008**, *69*, 1004.
[220] H. Lapidus, N. G. Lordi, *J. Pharm. Sci.* **1968**, *57*, 1292.

Appendix

A1. GC Traces for Calibration (Chapter 3, 3.2.3.1)

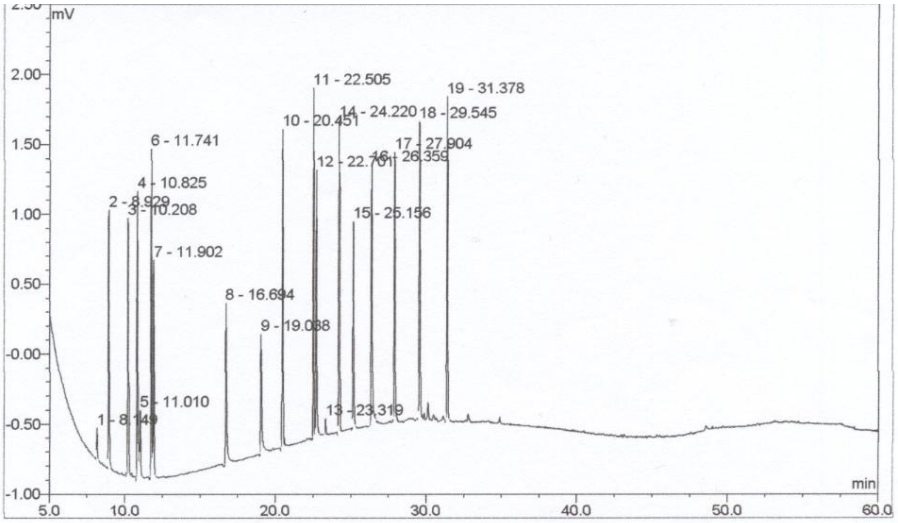
The GC traces for perfume oil with concentrations 1.0, 2.0, 6.0 and 9.0 mg/ml dissolved in hexane are listed below.

Concentration: 1.0 mg/ml



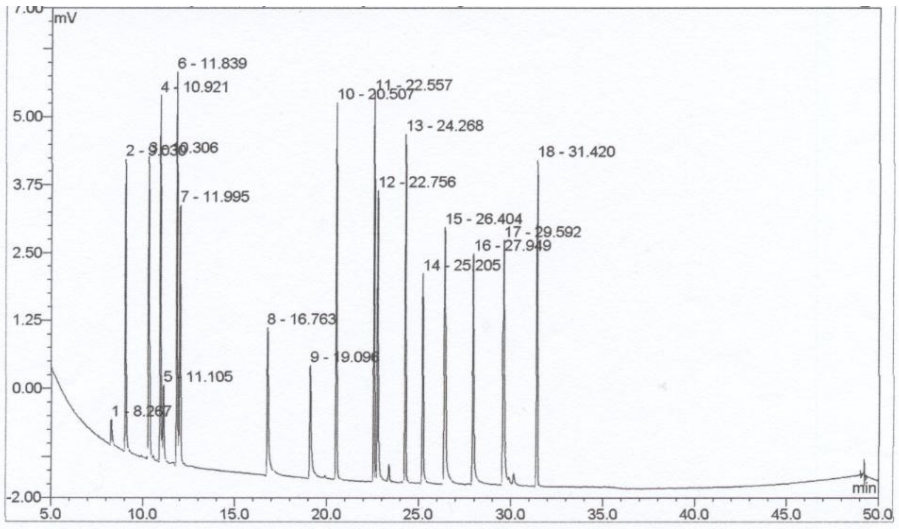
No.	Ret.Time min	Peak Name	Height mV	Area mV*min	Rel.Area %	Amount	Type
1	2.88	n.a.	1245.223	81.179	68.02	n.a.	BM
2	2.91	n.a.	1245.219	17.400	14.58	n.a.	M
3	3.05	n.a.	293.729	20.094	16.84	n.a.	MB
4	9.04	n.a.	0.580	0.034	0.03	n.a.	BMB*
5	10.32	n.a.	0.693	0.043	0.04	n.a.	BMB*
6	10.94	n.a.	0.696	0.054	0.05	n.a.	BM *
7	11.11	n.a.	0.221	0.020	0.02	n.a.	MB*
8	11.85	n.a.	0.701	0.054	0.04	n.a.	BM *
9	12.01	n.a.	0.675	0.046	0.04	n.a.	MB*
10	20.52	n.a.	0.956	0.065	0.05	n.a.	BMB*
11	22.57	n.a.	0.870	0.064	0.05	n.a.	BMb*
12	22.83	n.a.	0.304	0.036	0.03	n.a.	bMB*
13	24.28	n.a.	0.864	0.059	0.05	n.a.	BMB*
14	25.26	n.a.	0.295	0.031	0.03	n.a.	BMB*
15	26.52	n.a.	0.211	0.030	0.03	n.a.	BMB*
16	28.03	n.a.	0.222	0.030	0.03	n.a.	BMB*
17	29.66	n.a.	0.418	0.046	0.04	n.a.	BMB*
18	31.43	n.a.	0.840	0.062	0.05	n.a.	BMB*
Total:			2792.717	119.349	100.00	0.000	

Concentration: 2.0 mg/ml



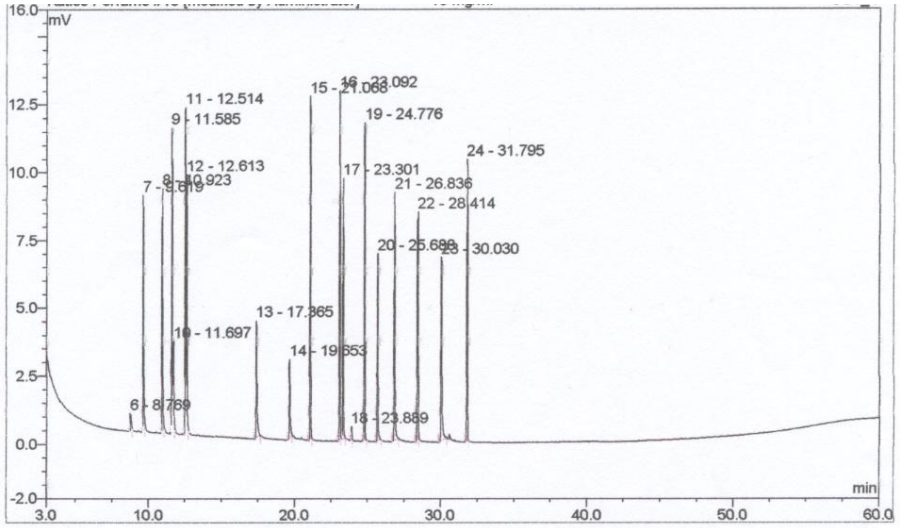
No.	Ret.Time min	Peak Name	Height mV	Area mV*min	Rel.Area %	Amount	Type
1	8.15	n.a.	0.217	0.012	0.55	n.a.	BMB*
2	8.93	n.a.	1.835	0.101	4.84	n.a.	BMB*
3	10.21	n.a.	1.836	0.107	5.16	n.a.	BMB*
4	10.83	n.a.	2.046	0.132	6.32	n.a.	BM *
5	11.01	n.a.	0.477	0.036	1.74	n.a.	MB*
6	11.74	n.a.	2.343	0.136	6.51	n.a.	BM *
7	11.90	n.a.	1.540	0.101	4.83	n.a.	MB*
8	16.69	n.a.	1.146	0.096	4.62	n.a.	BMB*
9	19.04	n.a.	0.841	0.073	3.49	n.a.	BMB*
10	20.45	n.a.	2.278	0.149	7.17	n.a.	BMB*
11	22.51	n.a.	2.493	0.150	7.20	n.a.	BMB*
12	22.70	n.a.	1.897	0.131	6.29	n.a.	BMB*
13	23.32	n.a.	0.115	0.008	0.39	n.a.	BMB*
14	24.22	n.a.	2.236	0.142	6.83	n.a.	BMB*
15	25.16	n.a.	1.463	0.102	4.92	n.a.	BMB*
16	26.36	n.a.	1.858	0.163	7.80	n.a.	BMB*
17	27.90	n.a.	1.902	0.128	6.15	n.a.	BMB*
18	29.55	n.a.	2.127	0.159	7.62	n.a.	BMB*
19	31.38	n.a.	2.310	0.158	7.59	n.a.	BMB*
Total:			30.960	2.083	100.00	0.000	

Concentration: 6.0 mg/ml



No.	Ret.Time min	Peak Name	Height mV	Area mV*min	Rel.Area %	Amount	Type
1	8.27	n.a.	0.439	0.028	0.49	n.a.	BMB*
2	9.03	n.a.	5.344	0.312	5.43	n.a.	BMB*
3	10.31	n.a.	5.513	0.328	5.69	n.a.	BMB*
4	10.92	n.a.	6.713	0.403	7.01	n.a.	BM *
5	11.11	n.a.	1.374	0.103	1.78	n.a.	MB*
6	11.84	n.a.	7.222	0.413	7.17	n.a.	BM *
7	11.99	n.a.	4.748	0.314	5.45	n.a.	MB*
8	16.76	n.a.	2.686	0.237	4.11	n.a.	BMB*
9	19.10	n.a.	2.042	0.185	3.21	n.a.	BMB*
10	20.51	n.a.	6.925	0.446	7.75	n.a.	BMB*
11	22.56	n.a.	7.134	0.441	7.67	n.a.	BMb*
12	22.76	n.a.	5.307	0.358	6.21	n.a.	bMB*
13	24.27	n.a.	6.400	0.402	6.98	n.a.	BMB*
14	25.20	n.a.	3.820	0.274	4.76	n.a.	BMB*
15	26.40	n.a.	4.709	0.417	7.24	n.a.	BMB*
16	27.95	n.a.	4.191	0.296	5.14	n.a.	BMB*
17	29.59	n.a.	4.446	0.381	6.62	n.a.	BMB*
18	31.42	n.a.	5.994	0.419	7.29	n.a.	BMB*
Total:			85.006	5.756	100.00	0.000	

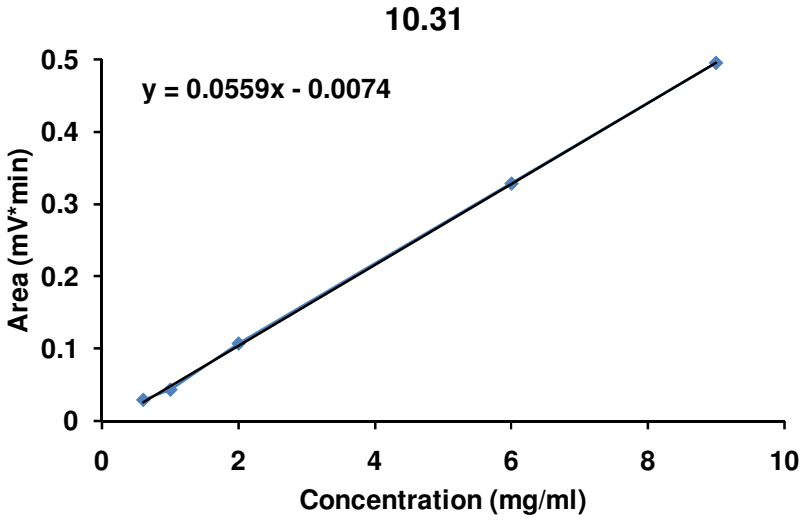
Concentration: 9.0 mg/ml

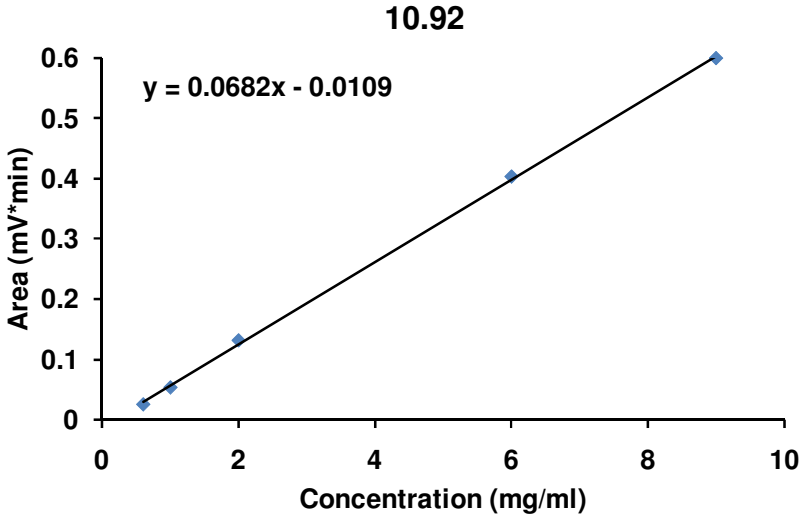


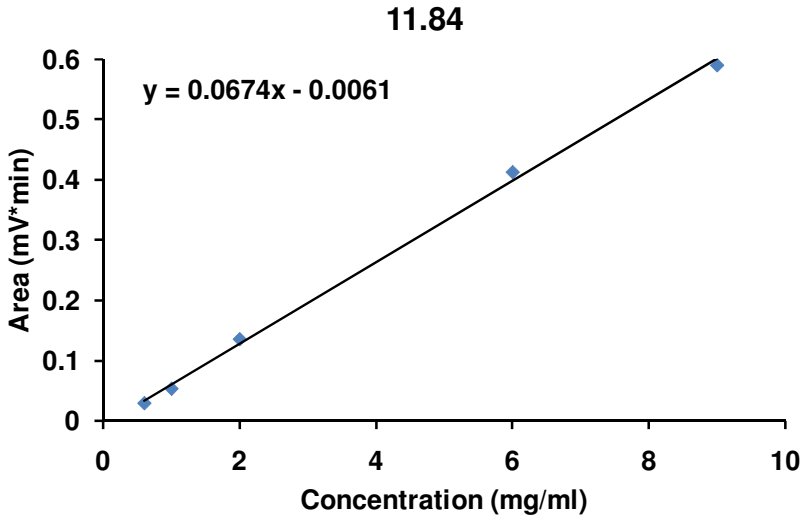
No.	Ret.Time min	Peak Name	Height mV	Area mV*min	Rel.Area %	Amount	Type
1	2.29	n.a.	459.704	9.318	7.55	n.a.	BM
2	2.32	n.a.	98.321	1.182	0.96	n.a.	Ru
3	2.39	n.a.	1240.395	78.327	63.47	n.a.	M
4	2.42	n.a.	1055.392	24.496	19.85	n.a.	MB
5	2.45	n.a.	98.784	1.492	1.21	n.a.	Rd
6	8.77	n.a.	0.656	0.045	0.04	n.a.	BMB*
7	9.62	n.a.	8.715	0.479	0.39	n.a.	BMB*
8	10.92	n.a.	8.935	0.495	0.40	n.a.	BMB*
9	11.59	n.a.	11.253	0.599	0.49	n.a.	BM *
10	11.70	n.a.	3.334	0.202	0.16	n.a.	MB*
11	12.51	n.a.	12.031	0.590	0.48	n.a.	BM *
12	12.61	n.a.	9.509	0.530	0.43	n.a.	MB*
13	17.37	n.a.	4.318	0.330	0.27	n.a.	BMB*
14	19.65	n.a.	2.936	0.220	0.18	n.a.	BMB*
15	21.07	n.a.	12.644	0.678	0.55	n.a.	BMB*
16	23.09	n.a.	12.865	0.657	0.53	n.a.	BMB*
17	23.30	n.a.	9.627	0.522	0.42	n.a.	BMB*
18	23.89	n.a.	0.509	0.029	0.02	n.a.	BMB*
19	24.78	n.a.	11.723	0.604	0.49	n.a.	BMB*
20	25.69	n.a.	6.908	0.413	0.33	n.a.	BMB*
21	26.84	n.a.	9.163	0.604	0.49	n.a.	BMB*
22	28.41	n.a.	8.437	0.462	0.37	n.a.	BMB*
23	30.03	n.a.	6.778	0.524	0.42	n.a.	BMB*
24	31.79	n.a.	10.384	0.611	0.50	n.a.	BMB*
Total:			3103.320	123.410	100.00	0.000	

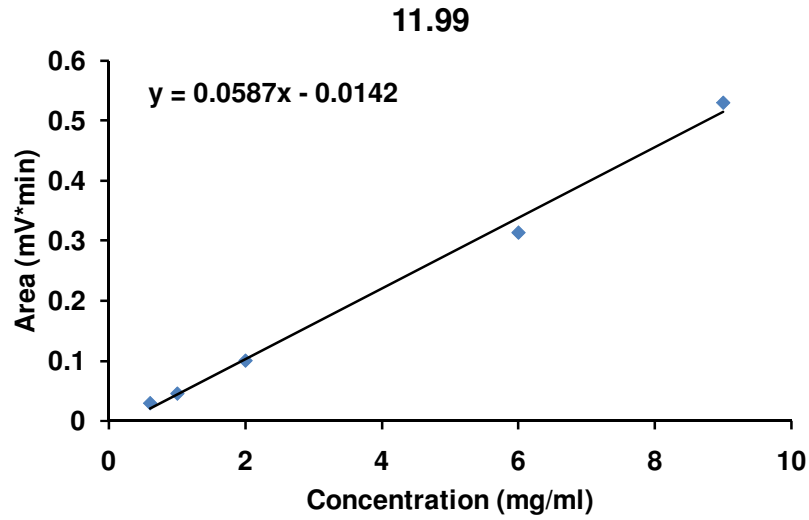
A2. Area vs. Oil Concentration for Calibration (Chapter 3, 3.2.3.1)

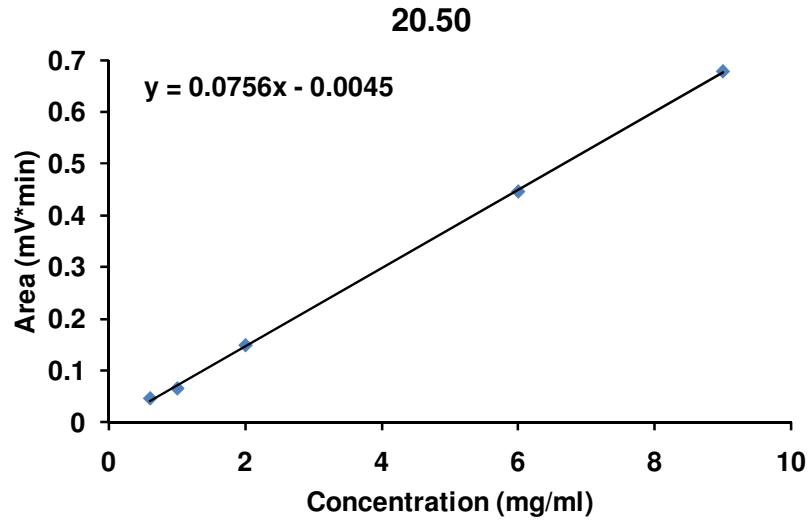
Plots of area vs. oil concentration for retension time 10.31, 10.92, 11.84, 11.99, 20.50, 22.57, 22.76, 24.27 and 25.16.

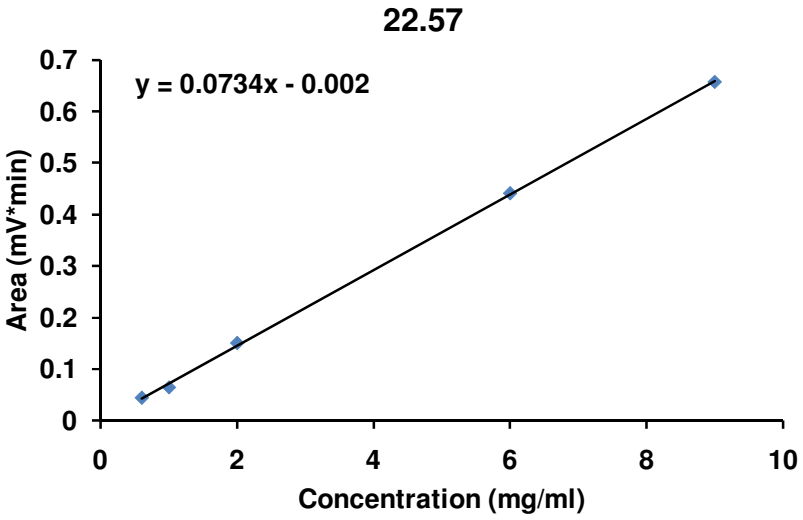


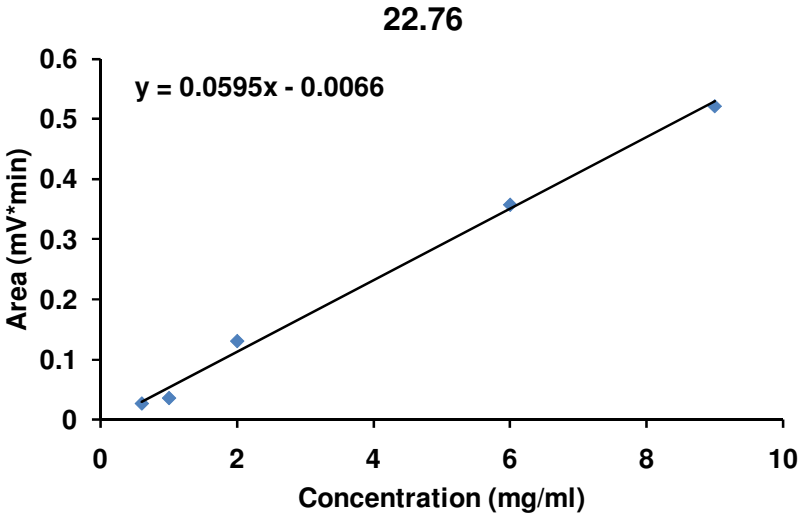


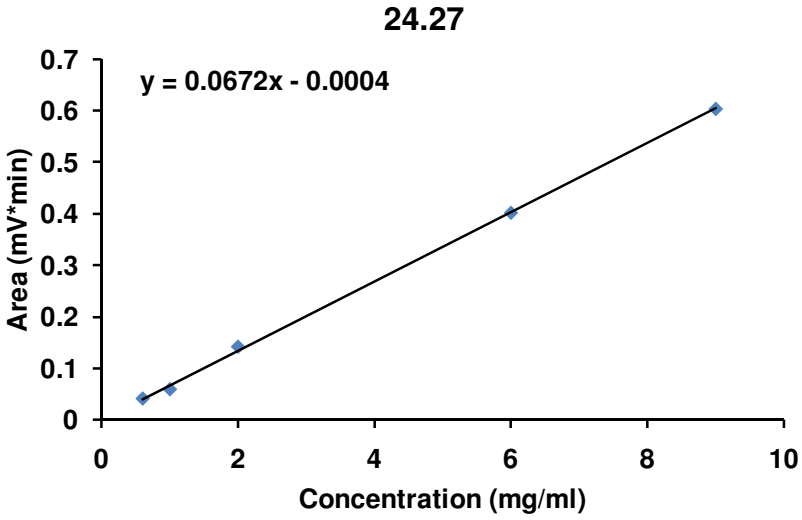

11.84
y = 0.0674x - 0.0061
Area (mV*min)
0.6
0.5
0.4
0.3
0.2
0.1
0
0
2
4
6
8
10
Concentration (mg/ml)

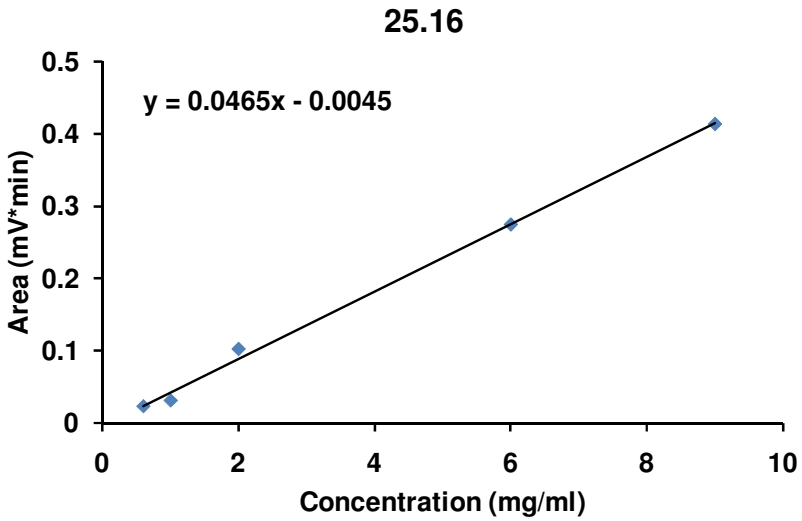

11.99
y = 0.0587x - 0.0142
Area (mV*min)
0.6
0.5
0.4
0.3
0.2
0.1
0
0
2
4
6
8
10
Concentration (mg/ml)


20.50
y = 0.0756x - 0.0045
Area (mV*min)
0.7
0.6
0.5
0.4
0.3
0.2
0.1
0
0
2
4
6
8
10
Concentration (mg/ml)


22.57
y = 0.0734x - 0.002
Area (mV*min)
Concentration (mg/ml)
0
0.1
0.2
0.3
0.4
0.5
0.6
0.7
0
2
4
6
8
10


22.76
y = 0.0595x - 0.0066
Area (mV*min)
Concentration (mg/ml)
0
0.1
0.2
0.3
0.4
0.5
0.6
0
2
4
6
8
10


24.27
y = 0.0672x - 0.0004
Area (mV*min)
Concentration (mg/ml)
0
0.1
0.2
0.3
0.4
0.5
0.6
0.7
0
2
4
6
8
10


25.16
y = 0.0465x - 0.0045
Area (mV*min)
0.5
0.4
0.3
0.2
0.1
0
0
2
4
6
8
10
Concentration (mg/ml)